JANUARY–MARCH 2011 VOL. 3 № 1 (8)

ISSN 2075-8251

ActaNaturae

Molecular and Physiological Mechanisms of Membrane Receptor Systems Functioning

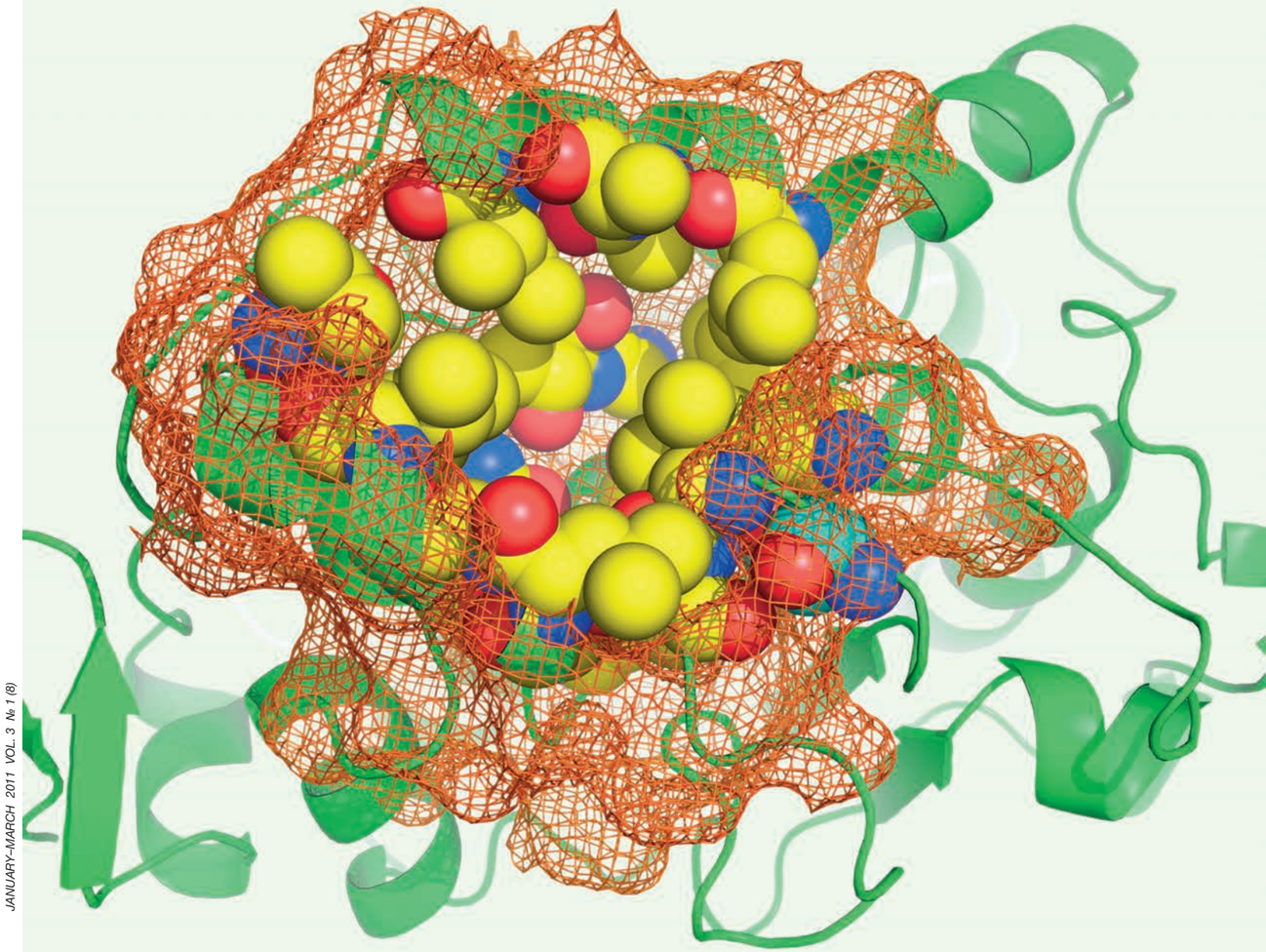

JANUARY–MARCH 2011 VOL. 3 № 1 (8)
ActaNaturae

Letter from the Editors

Dear readers,

We are delighted to bring you the eighth issue of *Acta Naturae* – the first issue of 2011. As you can see, despite the numerous skeptical assessments that greeted the very beginning of our activity, the journal continues to be published, and, moreover, it is carving out a place for itself under the sun in Russia and abroad. The support that is anticipated to come in the nearest future from the Ministry of Education and Science is of crucial importance at this stage.

As usual, this eighth issue opens with review articles devoted to the major issues of life science. The reviews by E.S. Severin and M.V. Savvateeva consider the problems of the functioning of membrane receptor systems, which are crucial in the interaction between a cell and its environment. The design of next-generation drugs is closely connected to the investigation of these systems. The review by T.A. Zdobnova *et al.* deals with the quite urgent problem of tumor diagnostics using quantum dots. Unquestionable success has been achieved in this field; however, a number of problems that raise obstacles in successful application of this method have remained unsolved. The review by D.A. Skvortsov *et al.* contains data on the determination of telomerase activity, which is in many cases a major criterion in assessing malignant cell transformation. The experimental articles deal with different branches of biology. The range of articles is rather broad: medical genetics, cell biology, molecular physiology, and the physicochemistry of proteins. However, the vast majority of these publications are connected to medicine. We believe that the tendency towards "medicinization" represents development in our science.

In the section Forum, the discussion of topical questions of both scientific and science-organizational nature is continued. The report by E.B. Prokhorchuk deals with the results of the 4th Annual Conference of Participants in the International Cancer Genome Consortium, which was held in Australia in December 2010. Work in this direction has been active; it remains to deplore that Russia is not a rightful participant in the Consortium. Vice-chancellor of Moscow State University, Academician A.R. Khokhlov, speculates on the eternal problem of Russian science – the timely and rational renewal of scientific equipment. Finally, the article by I. Sterlingov devoted to the place and role of bibliometry, which is believed to objectively and reasonably assess the current state of things, should be rather interesting to our readers.

We would like to seize this opportunity to invite interested authors to send their articles to our journal.

The Editorial board

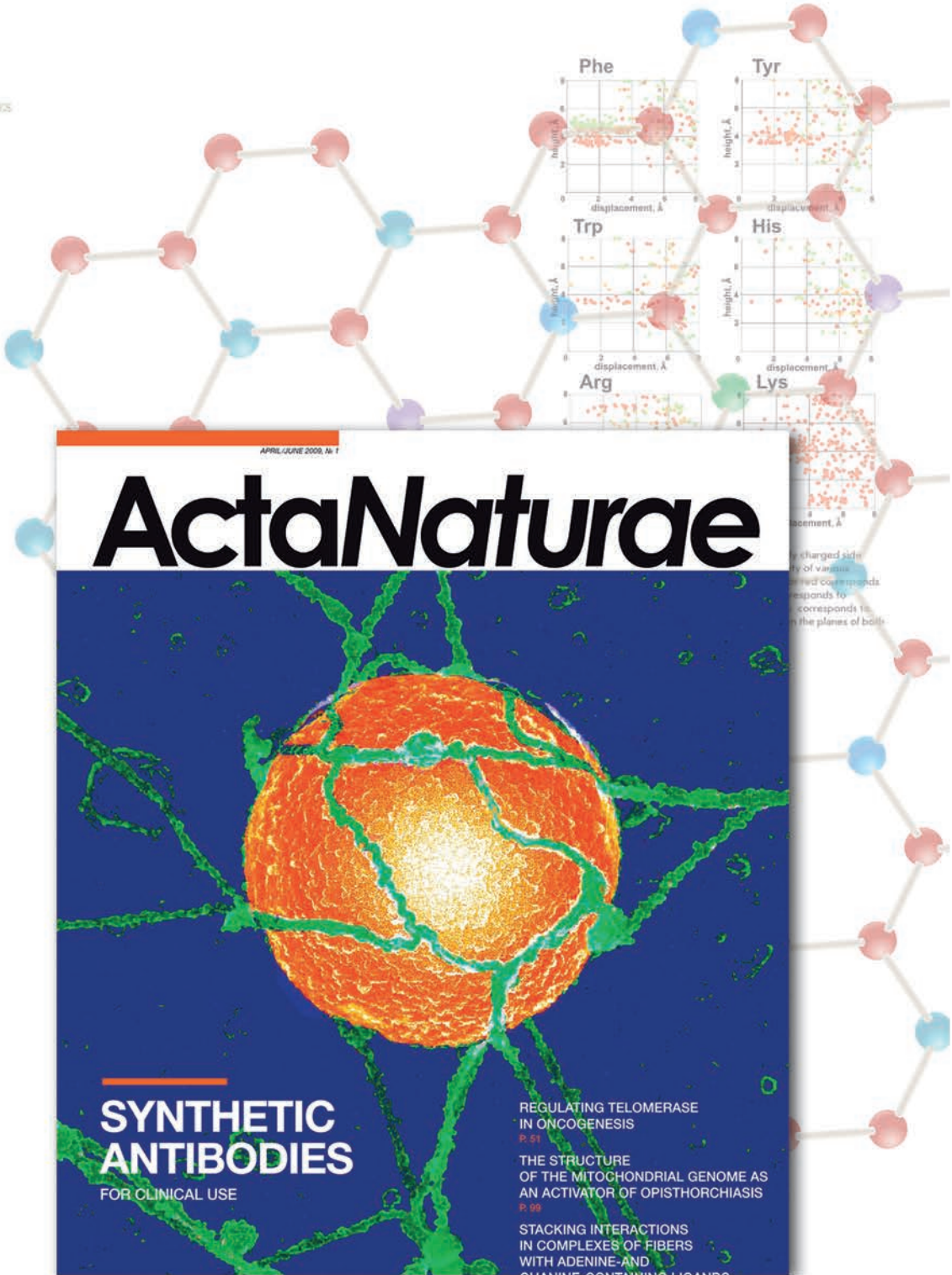

K. D. Nadezhdin, O. V. Bocharova, E. V. Bocharov, A. S. Arseniev

Structural and Dynamic Study of the Transmembrane Domain of the Amyloid Precursor Protein

APPjmtm representative spatial structure with APP residue numbering.

Alzheimer's disease affects people all over the world, regardless of nationality, gender or social status. An adequate study of the disease requires essential understanding of the molecular fundamentals of the pathogenesis. The amyloid β-peptide, which forms amyloid plaques in the brain of people with Alzheimer's disease, is the product of sequential cleavage of a single-span membrane amyloid precursor protein (APP). In the present study, the structure and dynamics of the recombinant peptide corresponding to the APP fragment, Gln686-Lys726, which comprises the APP transmembrane domain with an adjacent N-terminal juxtamembrane sequence, were determined in the membrane mimetic environment composed of detergent micelles using

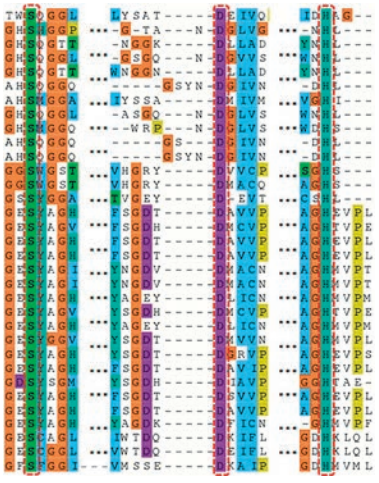

Structural alignment (textual representation) of the active sites of α,β-hydrolase family enzymes.

D. A. Suplatov, V. K. Arzhanik, V. K. Švedas

Comparative Bioinformatic Analysis of Active Site Structures in Evolutionarily Remote Homologues of α,β-Hydrolase Superfamily Enzymes

Comparative bioinformatic analysis is the cornerstone of the study of enzymes' structure-function relationship. The proposed methodology has been used to compare some α,β-hydrolase superfamily enzymes. The insight has revealed a high structural similarity of catalytic site areas, including the conservative organization of a catalytic triad and oxyanion hole residues, despite the wide functional diversity among the remote homologues compared. The methodology can be used to compare the structural organization of the catalytic and substrate binding sites of various classes of enzymes, as well as study enzymes' evolution and to create a databank of enzyme active site structures.

A. V. Safonova, A.N. Petrin, S. D. Arutyunov, V. N. Tsarev, L. A. Akulenko, A. O. Zorina, D. V. Rebrikov, A. V. Rubanovich, S. A. Borinskaya, N. K. Yankovsky

Association of Cytokine Gene Alleles with the Inflammation of Human Periodontal Tissue

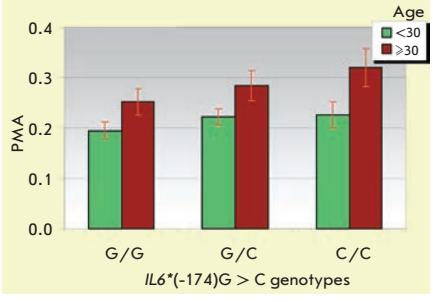

Mean values (± SE) of the PMA index in carriers of different *IL6* (-174) genotypes from two groups: less than 30 years, 215 individuals; and more than 30 years, 70 individuals.

Gingivitis and parodontitis are chronic inflammatory diseases of the periodontal tissue in humans caused by both environmental and genetic factors. The human cytokine genes that regulate the immune response may play an important role in the development of these chronic inflammatory diseases. The aim of this study is to analyze the allele status of eight human cytokine genes and to associate it with the inflammation of periodontal tissue in humans. A total of 296 unrelated males of Russian origin were studied. A significant association of the *IL1B* and *IL6* minor alleles and gingivitis was found. In addition, we found a significant association of the OHI-S index with the *IL18* gene alleles.

ActaNaturae
JANUARY–MARCH 2011, VOL. 3 № 1 (8)

Founders
Ministry of Education and
Science of the Russian Federation,
Lomonosov Moscow State University,
Park Media Ltd

Address: 119991 Moscow, Russia, Leninskiye Gory, Nauchny
Park MGU, vlad.1, stroeniye 75G.
Phone/Fax: +7 (495) 930 80 06
E-mail: knorrevd@gmail.com, enovoselova@strf.ru, biomem@mail.ru

Номер подписан в печать 18 марта 2011 г.
Тираж 200 экз. Цена свободная.
Отпечатано в типографии «МЕДИА-ГРАНД»

CONTENTS

IMAGE ON THE COVER PAGE

Active site area – a substructure of an enzyme consisting of amino acid residues involved in substrate delivery, binding, and orientation (yellow), as well as the amino acid residues of the catalytic machinery (blue) and some surrounding residues selected to benefit the integrity of the fragment (showed as dash). (D.A. Suplatov *et al.*)

94 Steps to Success

Without the use of specialized equipment, it is extremely difficult to achieve results in modern science. Unfortunately, the situation regarding scientific equipment in our country is far from perfect. This concerns not only the quality of instrumental resources in our research institutes and universities, but also the process of purchasing scientific equipment. The vice-chancellor of M.V. Lomonosov Moscow State University, Alexei Khokhlov, in an interview with Konstantin Kiselev, the director of the project Science and Technologies in the Russian Federation, speculates on this eternal problem of the Russian research and design sector.

Alexei Khokhlov

Konstantin Kiselev:
Alexei Removich, to what extent is the quality of scientific equipment and its timely purchase an eternal problem for Russian science?

Alexei Khokhlov:

– I do not think that it is an "eternal" problem. Of course, in Soviet times there used to be similar problems, relating to the prohibition of importing high-technological equipment. Therefore, in some cases we had to design instruments ourselves, and in other cases simply copy the best examples of western scientific equipment. There was definitely a lack of equipment, but it did not result in any catastrophe. Moreover, in a number of fields, such as nuclear physics, low-temperature physics, quantum mechanics, nonlinear optics, and material science, our equipment was unique and was exceptionally advanced. It corresponded to the scientific tasks that were imposed by the economic structure at the time.

After the USSR's collapse, there was a substantial gap in financing of science and technologies for about a decade. During this period, we were more concerned with preserving the institutes and laboratories and paying salaries to our scientists, rather than buying an up-to-date microscope (although we tried our best to do so). It was not until 5 years ago that we had the opportunity to purchase modern, high-quality, expensive equipment for all foreground directions of development of science and technology. More so, centers were established in which unique installations could be shared.

However, I consider it premature to say that our science has been adequately equipped with up-to-date technology. For example, if one compares the equipment in Russian research institutes and that in analogous foreign institutions, such as the Max Planck Institute in Germany, it would be of a much higher standard and more modern in Germany. Foreign laboratories in the leading countries have been better equipped in comparison with Russian ones.

– And does this also mean that German science is ahead of Russian science, in terms of the quality of research?

– Of course, good equipment and results are closely related. Only articles on studies that were carried out on modern equipment are acceptable for publication in scientific journals with good impact factors. The absence of modern equipment means that you will not be able to publish your article in a highly rated journal.

However, the connection is not absolute. Some countries have excellent financial opportunities and equipment, but no scientific schools (such as the Arab oil-producing countries), in which the situation with publications is far from perfect, since these countries lack their own scientific traditions. They may achieve some results thanks to their discipline, diligence, and the

scientific 'stars' they invite to their countries; however, it is difficult for them to catch up, in the absence of their own scientific foundations and the permanent development of the aforesaid. Another factor that has to be taken into consideration is that science is international, and it is possible to pursue one's own ideas on somebody else's equipment.

– Probably this accounts for why foreign scientific organizations (namely American and European) that have modern scientific equipment gladly use theoretical studies made by Russian scientists. Sometimes a series of experiments is carried out using these theories. The results obtained are of global exposure, yet the author of the idea only gets an initial quotation in the article.

– Of course, such situations may occur. However, it is not a tragedy for science and even for the scientist who invented the particularly brilliant theory. In Russia, there never has been a great quantity of good equipment. A similar situation existed in the 21st, as well as the early 20th century. If one peruses the biographies of outstanding Russian scientists of that time, he will discover that the majority of experimental studies by Mechnikov, Vernadskii, and even Mendeleev were carried out when they worked abroad. We are theoreticians rather than practitioners; the theoretical part of Russian science has always been better developed as compared to experimental science.

Modern "Big" science is science of large-scale collaboration. Russian experimentalists partially work on their own equipment and partially implement their hypotheses on the equipment of foreign institutes and universities, in partner laboratories (provided that they possess good ideas).

Meanwhile, in recent times the state has acquired the possibility to purchase modern equipment. In most cases, this equipment comprises the most necessary modern instruments. Starting from 2004, a good deal of new equipment has been purchased for Moscow State University. Today, we purchase it as well, but within the framework of the Program for the Development of MSU.

– Does it cover the entire range of equipment, from an oscilloscope to an expensive force microscope? Do Russian manufacturers cover a certain part of scientific demand?

– Yes, it covers the entire range of equipment – from simple apparatuses and reagents to installations. Some of the equipment is bought from Russian manufacturers and others from foreign ones. However, when it comes to large modern equipment (electron microscopes, chromato-mass spectrometers), we focus on foreign manufacturers. However, there are rival Russian manufacturers producing atomic force microscopes, for example. It all depends on the particular instrument.

– What is the procedure for purchasing expensive equipment at Moscow State University? By the way, what is considered expensive? Is it 100,000 rubles or 30,000,000 rubles?

– According to our legislation, all equipment that costs over 100,000 rubles requires a price quotation and that over 500,000 rubles entails inviting bids or auctions. What is the procedure for purchasing? We announce tenders and purchase equipment within the framework of a tender procedure.

The procedure is neither overly sophisticated nor burdensome; provided that the financing of purchases is made periodically. However, as we receive the money by the very end of the year, we have to perform it in a hurry, which is not good.

– How are the demands formed for scientific equipment at Moscow State University?

– It depends on the particular situation and on the financing source. Money is received by a certain group in the form of either grants or state contracts. There are contracts with firms, with provision of the money for purchasing equipment. In this case, the group decides for itself which equipment it should purchase. Most small equipment is purchased via this channel. There are also the centralized events. Thus, before the 250th Anniversary of Moscow State University, the government of the Russian Federation allocated means aimed at the purchasing of modern equipment. Each department submitted their requests, which were subsequently analyzed and then possibly combined. The university's administration then made the decision regarding which equipment should be purchased. The final decision was left to the rector of the university.

– You mean money plays a crucial role? Does receiving financial support mean that equipment can be purchased?

– Exactly. But in order to receive this support, our rector,V.A. Sadovnichii, expended a great deal of effort. Now, concerning the centers of shared use. The Ministry of Education and Science announced a competition between the centers of shared use, and the university filled out an application enumerating the large equipment that was necessary. The university won this request and subsequently the equipment listed was purchased. Now, the Program of Development of Moscow State University is engaged in it. The committee under the university administration has formulated the priority for the development of Moscow State University. This would be the purchase formation based on the demands of centralized development from research sectors (there are seven in total). Within each sector, the relevant scientists have been (and

are still in the process) of submitting requests for the equipment that they need. Once again, these requests are analyzed and generalized by the leader of the priority sectors; everything is then passed on to the university administration. The administration decides what can and what cannot be purchased, within the framework of the priorities for the current year. The final decision on what is to be purchased belongs to the rector. The requests within the framework of the priorities in development were formulated. The money that was received at the end of 2010 was mostly spent on two mega-projects of Moscow State University: for the modernization of our supercomputer "Lomonosov," the enhancement of its speed to 1.3 petaflops, and for designing the satellite "Lomonosov," which will be launched later this year (in honor of the 300*th* anniversary of M.V. Lomonosov). There is an entire complex of scientific tasks to be studied by this satellite. The remaining money will be spent on other priority directions of development. I think that the majority of the requests submitted in these directions will be implemented this year.

– Will the restructuring of Moscow State University associated with the centralization of management and organizational procedures have an effect on the purchasing of equipment?

– As concerns what I have just said, it will have no effect,since we are speaking about large purchases, which always go through Moscow State University as a single legal entity. Since Federal Act 94 has been adopted, tender procedures have always been fulfilled.

– What about small purchases? Will subdivisions be affected?

– There exists in the law a provision that there are certain nomenclature items of goods. Payment with respect to each item made by a specified legal entity cannot exceed 100,000 rubles. If the limit of the total number of purchases for each item is surpassed, competition procedures kick in . Even if the 100,000 limit was exceeded by 1 kopeck (a computer mouse was bought), it will be difficult to carry out the entire purchase. Since MSU is a very large organization, a problem arises. It is connected with the fact that there will be a need to group and use a competition procedure even for small purchases. We are aware of this problem and are actively searching for solutions so that the performance of scientific groups working in Moscow State University is not hindered. In particular, it is recommended that at the beginning of the year (when no money has yet been allocated), each department announce tenders with step-by-step selection for the maximally wide range of goods and services, according to a specified item of purchase nomenclature.

– How is it performed?

– It can be based on purchases made in the past year. We look through the catalogues and think of everything that may be necessary to us, and we determine the maximum cost of each item. The tender is then announced. Some large supplier wins the tender. They may compete during the tender. But since there is a step-by-step selection, what does it mean? The maximum amount of goods for each item is specified, but we may not select 100% at once. We can select only 80%, during the year, as we need it. When a department needs something, it turns to the winning company: "Kindly supply us with 20 paper packs and with 30 more tomorrow," etc. The company delivers the paper. The delivery time should be agreed upon in advance; the payment is made after delivery, monthly or quarterly.

– Do "miracles" happen at tenders? I mean the cases connected with Federal Act 94.

– Of course. Especially when the crisis struck, many companies appeared and began their destructive activity. The procurement department has methods to fight the companies that were established for such abusive practice.

Undoubtedly, Federal Act 94 is not suitable for the scientific sphere. However, on the other hand, I am going to recount an unpopular viewpoint. Research institutions do not function in a vacuum. When we say that the level of general culture and moral values is rather low in our society, why should the scientific sphere be an exception? Of course, there have been abusive practices. For example, several invoices are made for homogeneous groups of goods; or sometimes goods are purchased by a scientist from a company that is led by the same person. Sometimes such things may occur.

I would put it in another way: the revocation of Federal Act 94 should be conjugated with a general change in procedures and organization of analysis of research projects in the Russian Federation. Unfortunately, our current system is too formal. There are competitions of the Ministry of Education and Science and projects of the Russian Foundation for Basic Research. Of course, the reports are submitted; however, they are very formal. The most important thing is to implement certain items of the performance specification. If you do it, that is all.

– Of course, and it is almost impossible to find faults in it, especially if it is scientific work.

– For scientific work, it should be different. There should be a really good examination of everything that has been done, based on the actual achievements of the group. The achievements can easily be assessed quantitatively: the articles published during the work, in which journals they were published, and

what results were obtained. As soon as these facts are made the cornerstone Federal Act 94 becomes obsolete and wholly unnecessary. But in the existing case, you have committed some trifle; formally complied with all the requirements of the lot, submitted a report — and nobody can find faults against you. Such situations become a good source for various abusive practices. Essentially, the report should include information concerning what has been done. If a scientist has published ten articles in leading journals, which have been well-cited during these years, he is considered a winner. As it is well-known, success is never blamed. He has carte blanche to do as he wishes. He has achieved success. If there is precise control over what a scientist had done, the Federal Act becomes unnecessary. However, if the situation is the same as it is now, formally he did something, but in actuality he did nothing, then the Federal Act is needed. With such a situation as reported in the absence of Federal Act 94, the door is open for a dishonorable figure to pocket the money by creating invoices, each worth 99.9 thousand rubles. This money is usually paid not to his company, but to the one with whom he had already discussed everything.

– Since you hold a certain position in the Russian Academy of Sciences, it may be a suitable time to ask you about the procedure for the procurement of scientific equipment in this system. I understand that there is a special Committee that is responsible for instruments and equipment; a number of requests for scientific equipment are submitted to it.The requests are then analyzed and placed for tender. However, the winner of the tender is always an organization, Akademintorg, which was established by the Academy of Sciences as a unitary enterprise and is entitled to engage in business. There is rumor that Akademintorg marks up the broker's margin way too much, going into a huddle with the suppliers, and so on. Is it not a better idea to give the authority to research institutes of the RAS, since the Act on Science and the statutes of the Academy allow for the decentralization of the procurement of equipment?

– I consider Akademintorg to be an absolutely unnecessary organization. I am not familiar with the procedure of money transfer to the Russian Academy of Sciences. However, if this money can be transferred to an institute which can announce the tender itself (the scientists who actually work will be able to help to do it with due qualification), that would certainly be a preferable variant in comparison with one when a strange tender for a lot of equipment is held. I understand that Akademintorg plays the role of a large supplier. I can understand it when the question is regarding such things as supplying paper, other stationery, and even re-agents. However, when the question is supplying sophisticated equipment, each component being very specific, it would be easier to carry out this procedure in institutes, at a more qualified level. Moreover, the institutes are holding a lot of tenders because they need to purchase the re-agents and other supplies in accordance with Federal Act 94...

– You mean that the argument "There are no specialists in the institutes who can engage in complicated tenders" is unreasonable, since the institutes have already learnt how to do it?

– Yes, they have learnt how to do it, and even do so. There are tender committees in each institute. The argument is absolutely groundless. The equipment can be purchased without Academintorg. Frankly speaking, I do not want to make unsubstantiated statements, but I have information that there are no valuable experts. I do not comment on rumors, nevertheless these rumors do exist. When the question is supplying paper, let supplying companies do it. However, when the question is large equipment, the profit for the companies supplying it is considerable. An additional point is that the representatives of these companies in Russia may be tempted to establish special relations with the purchasing company, when such an opportunity exists...

– I think that it is quite easy to verify whether the rumors are true or not. To do so, an independent committee should be set up. It even could be set up in the Russian Academy of Sciences from other people who are not related to the tender procedure. For instance, to compose it of university professors who are Academy members. I am sure that they are erudite enough to manage to examine the invoices or product catalogues — it would be easier than proving the Newton's binomial formula.

– Of course. However, so far I have known only one case when the Academy of Sciences has asked people who do not belong to the Academy their opinion. It was the program of molecular and cell biology by Academician G.P. Georgiev. In fact, all the information was transparent and clear. Everything could be found online: why the grant was given or why it was not. Also, there is an opportunity to appeal: the calculations or interpretation of facts was incorrect. The appeals committee is mainly composed of professors of Moscow State University (and other institutions of higher education) who do not belong to the Academy of Sciences.

– During the interview, you mentioned the transparency of all procedures on several occasions. When speaking about the purchase

of scientific equipment, does it mean that you are an advocate of any procedure, provided that it is reasonable and verifiable (transparent)?

– You are right — each procedure (lots, projects, purchases...etc) should be subjected to the scrutiny of an external examination. Actually, the world scientific community quite frequently carries out various activities connected with external expertise. This expertise is always performed by people who are outside the system. For instance, I participate quite frequently in committees that inspect the scientific competence or activity of a certain European research institute or foundation.

– What about our foundation? There are inspection committees in the Russian Academy of Sciences, are there not?

– No, it is not very efficient. I participate in the activities of the American National Science Foundation and review the projects. I am frequently invited to the Netherlands, so that the International Expert Panel, rather than Dutch scientists, can evaluate grant applications. Therefore, I believe that it is necessary to integrate more actively into the world scientific community and attract foreign experts so that they can evaluate what is going on here. Probably, Federal Act 94 will become unnecessary in this case. A person would understand that even if he has fulfilled all the requirements of a project, his foreign colleagues will come, and they will see the nonsense that he has done and he will thus be ashamed. Probably, this could be a solution? Of course, an external evaluation of everything should be carried out. Then, it will be possible to eliminate many restrictions. ●

BioBibliometry

Statistics on life sciences publications

Bibliometry is changing how science is organized . The count and examination of published works and references in research journals seem to be a magic wand that enables us to embrace the boundless, allowing us to capture in figures, talent, success and place, both in the history of science and of humanity.

Irrespective of criticism, the number of advocates of the count of references and indices is steadily increasing. According to the project of the official Innovation Strategy of the Russian Federation, by the year 2020, 5% of all new articles in the Web of Science database should be written by Russian authors. This is an indicator of success in scientific reform that has been subscribed to by the Ministry of Economics. However, the current share is approximately 2.5%, while as recently as ten years ago it was 3.5%. It is no coincidence that experts remain skeptical regarding the figures quoted in the Strategy project.

The competition for "megagrants" announced by the Ministry of Education and Science had the same demonstrative force. The officials avow that applicants for the six-figure financial support need to have high Hirsh indices. It has been heard that even in more modest competitions held by the Ministry, participants will need to specify the number of citations of their published works.

This year, the assessment of the effectiveness of the state's civil science organizations is due to start, raising heated debate. This is largely due to the fact that it is quite possible that unsatisfactory bibliometric indices may result in the closure of a number of research institutes. The same indices have been widely used to measure the efficiency of the development of national research and federal universities.

At an organizational level, a number of programs for stimulating those researchers who actively publish their results in authoritative journals have also emerged. The type of incentive depends on the type of organization: in some organizations, the refined index of the effectiveness of scientific activity is forcefully used, while some organizations stipulate their own rules, according to which the salary of researchers who publish their results in *Nature* and *Science* may be five times greater in comparison with their less active colleagues.

It goes without saying that any bibliometrical indices should be interpreted with a great deal of caution. There are a number of factors preventing one from affirming the existence of an unequivocal link between the indices and the actual scientific merits of an individual researcher, organization, or even country. However, many scientists in the world put increasing importance on bibliometry in their careers, and they are guided by figures even in terms of self-rating and planning. Sometimes the situation can be absurd; such as the case when after having gotten married and changed their last names, western female researchers continue using their maiden names, which are already indexed in bibliometric databases, for scientific publications.

It is necessary to concede that biomedicine, molecular biology, bioinformatics, and other cutting-edge disciplines of life sciences better suit publication analysis as compared with mathematics or archaeology due to the large amount of publica-

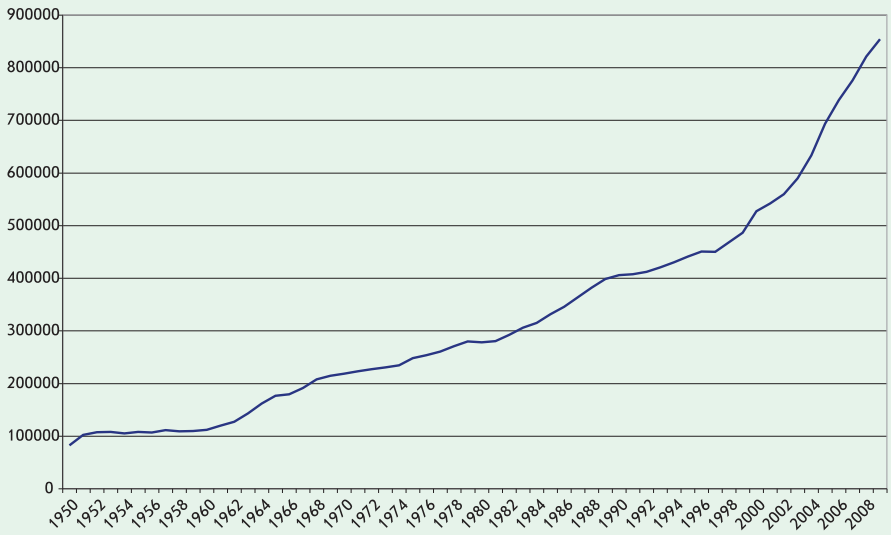

Fig. 1. Publications in MEDLINE database (arranged between the years of 1950 and2009).

tions in biology, the time it takes to publish these works, and the great quantity of citations. An average professor in molecular biology has more articles published than his mathematician colleague; these articles are cited more frequently.

Nevertheless, we consider the assessment of individual researchers and publication of their ratings as being insufficiently proper even in the field of biology. It is much more reliable to refer to the composite indicators with respect to countries and organizations, since large swathes of published data enable to capture actual changes in science. PubMed — the data search system in the MEDLINE database — is the main tool for everyday work

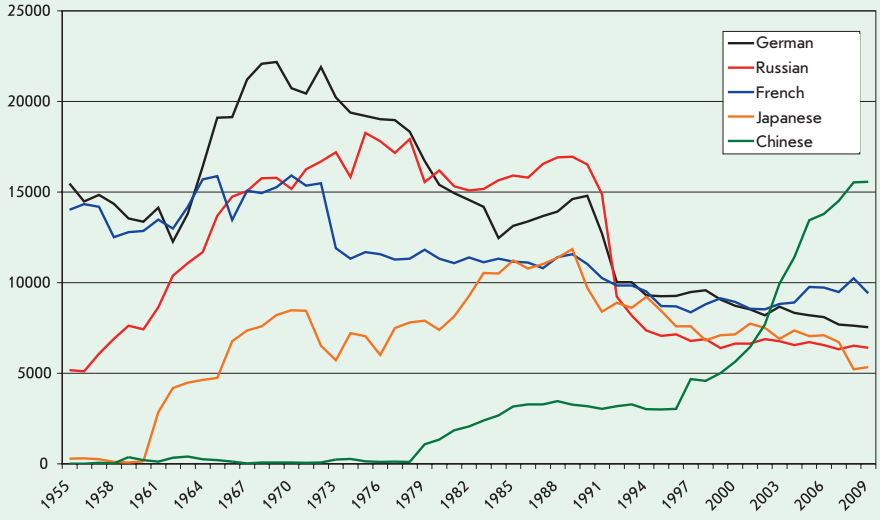

Fig. 2. The major subsidiary languages of science. The number of new publications in the MEDLINE database between the years of 1955 and 2009.

Sergei Kochetkov, Professor, corresponding member of the Russian Academy of Sciences

The article presented should be interesting and extremely useful for the readers of *Acta Naturae* and, indeed, all scientists. Indeed, bibliometry has been assuming a bigger role recently, and this is very likely to continue in the future. I believe that this article will provide an objective and reasonable evaluation of the current state of affairs.

As can be seen from the article, the current state of Russian science is far from excellent; both objective and subjective factors are responsible for this situation. It can be said without fear of exaggeration that the objective reason is the culpable attitude of our authorities toward science over the course of the past two decades. Moreover, such excuses as the recent economic crisis, the tough times during the 1990s, are insufficient. The root cause is a lack of understanding (in the best-case scenario) and a deliberate ignorance (in the worst case) of the role of science in the development of modern economics. As a result, the second-major scientific power in the world became a mere supplier of raw materials to developed countries. I consider measures that were taken recently in an effort to improve the situation to be wholly inefficient (the analysis of the reasons lies beyond the scope of this comment). However, I consider it appropriate to mention that the thoughtless use of bibliometrical indices in order to divide Russian scientists into the categories of "proper" and "improper" may exacerbate this situation.

The subjective reasons for the decrease in the number of publications by Russian scientists in foreign journals is connected with the editorial policies of the journals and, to an increasing extent, with enthusiasm about the bibliometric indices. Indeed, a considerable number of editors of international journals confess in private conversations that Russian publications are not inferior to the corresponding western ones in terms of their quality. However, the endless pursuit of the 'impact factor' of the journal makes the editors reject a considerable number of the articles they receive. Unfortunately, in this case, Russian articles are rejected more frequently, since due to the objective reasons mentioned above, Russian science has not been well integrated into world science. Russian scientists (with several exceptions) are insufficiently acquainted with the international community. Unfortunately, this situation cannot be improved without substantial changes in the state policy towards science. Even provided the corresponding conditions are created, it will take much time to rectify. In this regard, I would like to emphasize , on one hand the absolute necessity for the use of bibliometric indices as the only criteria that objectively describes the situation and, on the other hand, that these indices should not be made a cornerstone. If we compare Russian science to an ill patient, radical treatment should lead to the patient's recovery and not make the problems disappear through his death.

with publications for medics or biologists. This database was created by the National Health Institute (United States) and contains data on published works from approximately 5,000 research journals for the past several decades. Presently, it contains approximately 20 million publications. An increase in the number of articles that are added to MEDLINE each year faithfully represents the general increase in interest in life sciences in our generation (*Fig. 1*).

In the course of the next 3–5 years, the number of new scientific and near-scientific papers in medicine and biology in MEDLINE will pass the threshold of 1 million per year. It is of importance that

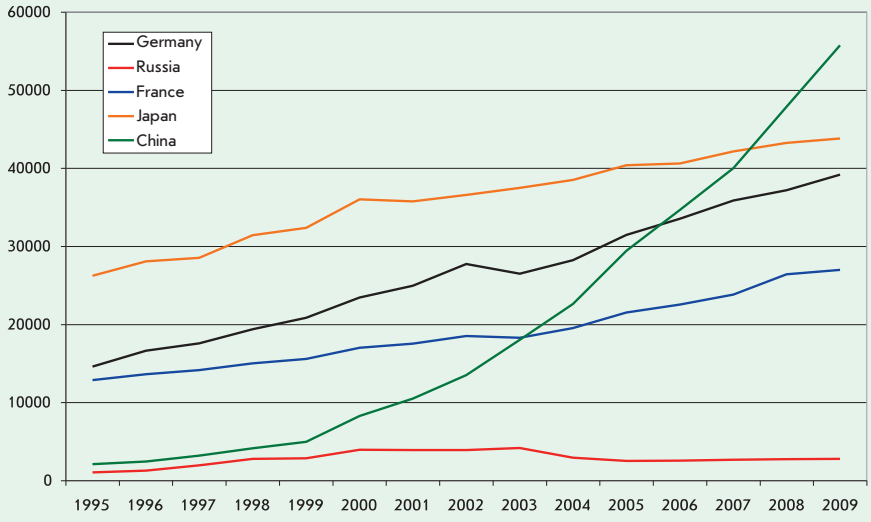

Fig. 3. Publication activity of certain countries. The number of new publications in the MEDLINE database between 1995 and 2009.

Sergei Deyev, Professor, corresponding member of the Russian Academy of Sciences

The drive to assess the results of scientific labor using figures has produced and continues to produce the corresponding criteria. Among the most conspicuous and extensively used is the impact factor devised 50 years ago by Garfield, and a new science-meter indicator that was invented five years ago – the so-called Hirsh index; a quantitative characteristic of a scientist's productivity, based on the number of publications and citations. Each of the aforementioned criteria is less than ideal. Striking examples are available to illustrate that in terms of these formal indices even outstanding scientists can appear like outsiders. Nevertheless, accurate formalized bibliometric indices can and should serve as a basis for the evaluation of a scientist's labor. The subjectivity of such an evaluation for an individual scientist will always be higher than that for research institutions in general. Therefore, these indices are more useful when comparing research institutes and finding the leading ones amongst them. However, these formalized indicators should not be regarded as the one and only determining criteria. Each statistics-based evaluation system has its own drawbacks. Nothing can adequately substitute the expert evaluation given by colleagues. The examination carried out by independent and impartial experts from other departments (ideally, by foreign researchers) would be most efficient and objective. The *a priori* known criteria, transparency and publication of the decisions made as a result of such examinations, minimize errors and inspire respect within the scientific community. The program of the Presidium of the Russian Academy of Sciences "Molecular and Cell Biology" can be given as an example of successful examination organization.

There is an additional factor regarding bibliometry that is worthy of our attention. The difficulties that Russian scientists experience in publishing works in highly rated foreign journals have been widely discussed. The problems are real, valid, and have numerous causes. Therefore, the teams who manage to do it should be given more considerable evaluation. On the other hand, it is an oft-heard argument that Russian science should challenge the West, with a wide range of Russian scientific periodicals. The editors-in-chief and editorial board members make efforts on a heroic scale to enhance the prestige of Russian periodicals. However, the obsolete system of organization of publishing in most Russian journals, coupled with the lack of financial support and subsequent poor translation quality and delayed publication of the English versions of the journals, is a significantly negative factor which prevents the majority of Russian periodicals from having adequate values of impact factors. Unsurprisingly, the authors of the most interesting works strive for publication in foreign journals, thereby limiting the citation of Russian journals and in turn, affecting the impact factors of Russian periodicals.

the processing of texts is available not only for those written in English, but also other commonly used scientific languages. This unique array of data allows one to trace how these languages kept up with English, or how they were left behind (*Fig. 2*).

As we can see, the collapse of the socialist system has had an impact not only on Russian science, but on German science as well. In any case, the lion's share of all texts in MEDLINE is written in English. The percentage of publications written in English increased from 46 to 93% over the period from 1955 to 2009. Based on the increase in general publication activity, almost everyone is using English. We show the distribution of the texts published from 1995 to 2009 according to the authors' countries of origin (regretfully, a large number of articles in MEDLINE do not have the correct country affiliation of authors; therefore, the dynamic is more trustworthy, albeit not absolutely so) (*Fig. 3*).

A lot of interesting facts can be gleaned regarding the content of articles and the changeover of popular topics. We counted the number of articles containing a number of medical terms that are of great social and economic significance, for each year from a period spanning 1951 to 2009. A relative index was used (the number of articles containing this term per 100,000 articles) (*Fig. 4*).

The development of methods and investigation techniques can be traced in the same way (*Fig. 5*).

But let us return to Russian science. The major Russian bibliometric source is the Russian Science Citation Index (RSCI), found within the electronic library of science, eLIBRARY.ru. It was financially backed by the Ministry of Education and Science and comprises data on published works from several thousand Russian research journals. The information on publications by Russian authors in foreign journals from the Scopus database was recently integrated into the RSCI. The total number of publications encompassed with certainty by the index has exceeded 30,000.

Many scientists are critical of the RSCI, both for its focus on Russian journals and for numerous inaccuracies, trivia and errors. However, the number of errors is constantly decreasing, while the inclusion of Scopus data should solve the problem related to publications in foreign journals. Nevertheless, RSCI substantially differs from the most authoritative bibliometric database

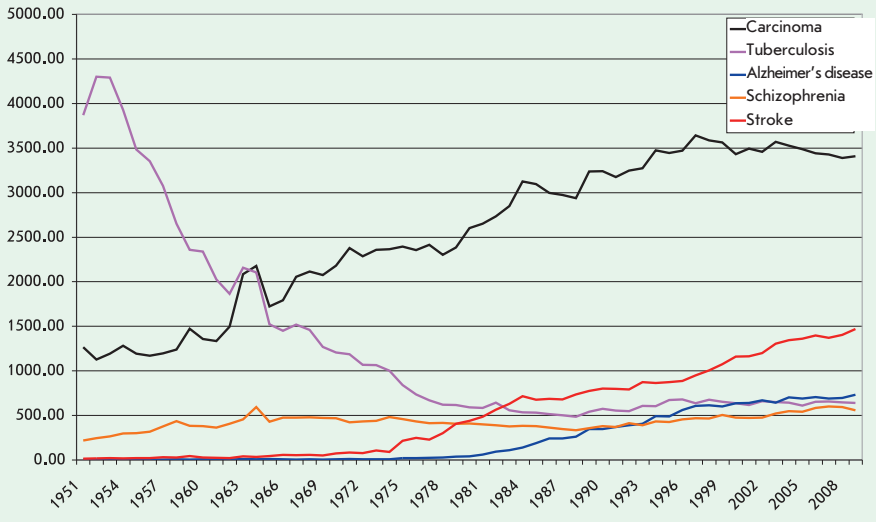

Fig. 4. The relative number of articles devoted to certain biomedical problems (1951–2009, MEDLINE).

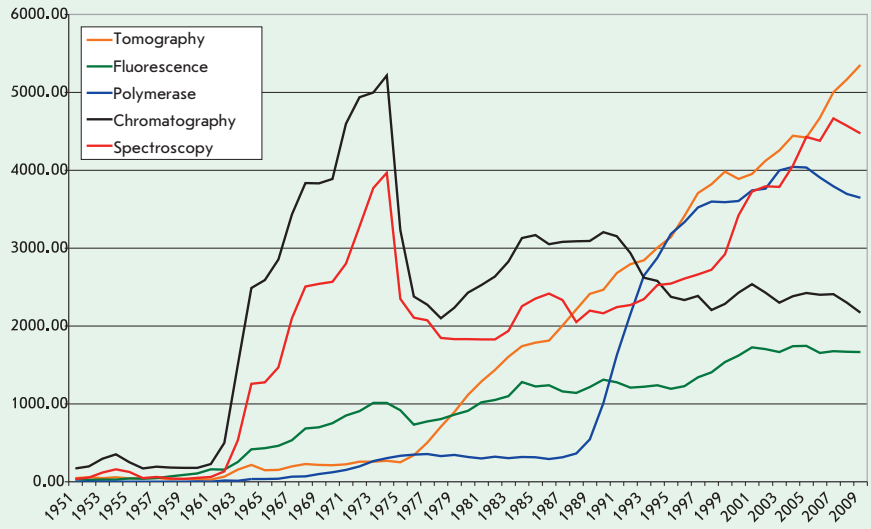

Fig. 5. The relative number of articles mentioning certain experimental and clinical methods (1951–2009, MEDLINE).

Table 1. Impact factors of Russian journals in the sphere of life sciences, 2009, Web of Science Journal Citation Reports

№	Journal	Impact factor
1	Biochemistry (Moscow)	1.327
2	Applied Biochemistry and Microbiology	0.67
3	Microbiology	0.638
4	Molecular Biology	0.57
5	Russian Journal of Genetics	0.501
6	Russian Journal of Plant Physiology	0.5
7	Russian Journal of Bioorganic Chemistry	0.473
8	Russian Journal of Ecology	0.414
9	Zhurnal Obshchei Biologii	0.377
10	Journal of Evolutionary Biochemistry and Physiology	0.267

Table 2. Impact factors of Russian journals in the sphere of life sciences, 2009, RSCI. The self-citation coefficient shows the share of citations from this journal in the total number of citations to the articles published in this journal

№	Journal	Impact factor	The total number of articles in RSCI	Self-citation coefficient, %
1	Microbiology	1.69	1953	No data
2	Biomedical Technologies and Radio Electronics (Biomeditsinskie tekhnologii i radio elektronika)	0.951	135	0
3	Geophysical Processes and Biosphere (Geofizicheskie protsessy i biosphera)	0.852	106	62.5
4	Human Physiology (Fiziologia cheloveka)	0.757	705	27.8
5	Molecular Biology (Molekulyarnaya biologiya)	0.67	1075	17
6	Russian Journal of Gastroentherology, Hepatology, Coloproctology (Rossijskiy zhurnal gastroenterologii, gepatologii, koloproktologii)	0.645	390	20
7	Information Technologies in Medicine (Vrach i informatsionnye tekhnologii)	0.644	376	17.2
8	Biochemistry (Biokhimia)	0.588	1785	27.4
9	Russian Journal of Nematology	0.538	106	н/д
10	Advances in Modern Biology (Uspekhi sovremennoi biologii)	0.514	295	17.6

Table 3. Biological Institutes of the Russian Academy of Sciences in the lead in terms of the citation of works published between 2005 and 2009, RSCI

Organization	Publications (A)	Citation (B)	Financing, thousand rubles (C)	B/A	C/A	C/B
Institute of Bioorganic Chemistry	1337	6103	315617	4.56	236.1	51.7
Institute of Molecular Biology	1078	4035	116096	3.74	107.7	28.8
Institute of Cytology and Genetics, Siberian Branch RAS	1488	3237	No data	2.18	No data	No data
Institute of General Genetics	696	3063	85421	4.4	122.7	27.9
Institute of Biological Instrument Engineering	138	2671	69773	19.4	505.6	26.1
Zoological Institute	1504	2548	117026	1.69	77.8	45.9
Institute of Microbiology	704	2143	51701	3.04	73.4	24.1
Institute of Molecular Genetics	530	1968	74457	3.71	140.5	37.8
Institute of Biochemistry	684	1950	103580	2.85	151.4	53.1
Institute of Ecology and Evolution	1419	2002	215157	1.41	151.6	107.5
Institute of Cytology	726	1871	105806	2.58	145.7	56.6
Institute of Theoretical and Experimental Biophysics	921	1945	127707	2.11	138.7	65.7
Institute of Biochemical Physics	1285	1812	138538	1.41	107.8	76.5
Institute of Protein Research	329	1592	67366	4.84	204.8	42.3
Institute of Chemical Biology and Fundamental Medicine, Siberian Branch RAS	559	1576	No data	2.82	No data	No data

in the world (the Web of Science). For the purpose of illustration, two versions of the top-10 biological journals are provided based on the value of the impact factor (*Tables 1 and 2*).

The projected assessment of the efficiency of the institutes of the Russian Academy of Sciences will be widely based on bibliometry. Even today, the RSCI permits to calculate a number of indices for certain organizations.

We selected 15 research institutes of the Russian Academy of Sciences with a biology profile that are in the lead in terms of the number of citations of articles published between 2005 and 2009 (*Table 3*). The amount of planned financing through the Russian Academy of Sciences is used as an indicator of the size of the organization. It should be noted that the areas of study encompassed by the Zoology Institute and the Institute of Ecology are on average cited less internationally, in comparison with molecular biology and bioinformatics, amongst others. There

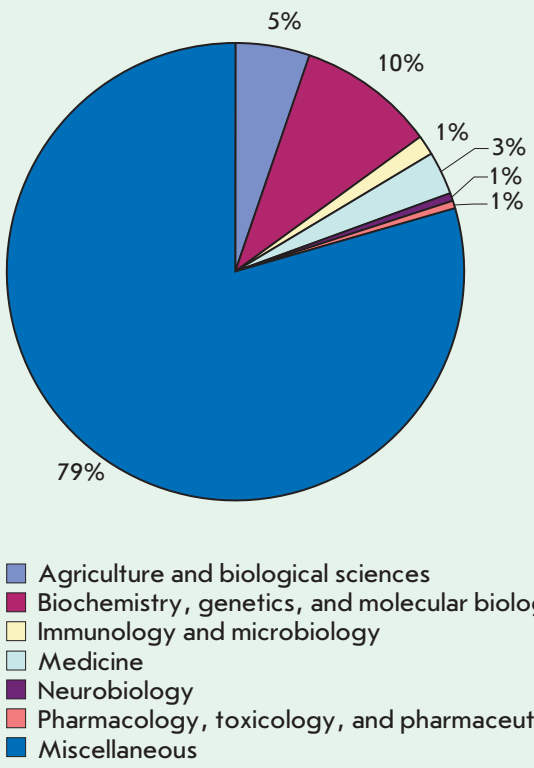

Fig. 6. The weight of the individual life science in the total amount of published works by Russian authors in 2009. Scopus. N = 33,690.

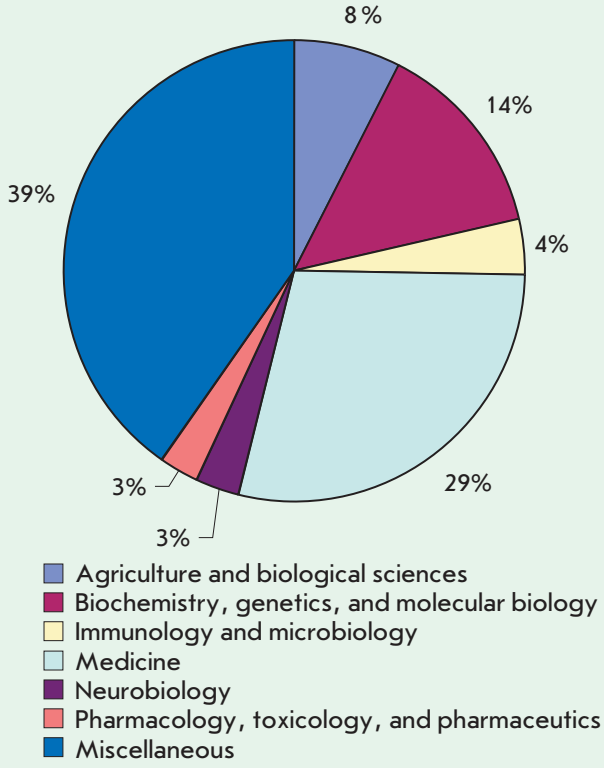

Fig. 7. The weight of the individual life science in the total amount of published works by U.S. authors in 2009. Scopus. N = 415,057.

are many biological and medical organizations in the Russian Federation; however, none of them can engage competitively in terms of citation with physics institutes. If one were to rate all organizations which make up the RSCI in terms of the number of citations, the leading biological institute (the Institute of Biological Chemistry) will only be ranked towards the end of the list of the top 20 organizations.

In order to demonstrate the place of life science in the general scheme of Russian publications, the Scopus database, which indexes 18,000 international journals, is an appropriate tool (*Fig. 6*).

It is enough to compare it with the United States to note a wide difference. As bibliometry attests, life sciences still play second fiddle in Russia (*Fig. 7*).

Taking into account the increased interest in bibliometry and its significance in managing science, we intend to publish the updated indices for life sciences on a regular basis. ●

Ivan Sterligov

The Cancer Genome: What's New?

Based on materials from the 4th Annual Conference of Participants in the International Cancer Genome Consortium: December 1–3, 2010, Brisbane, Australia

E. B. Prokhorchuk
Centre "Bioengineering", Russian Academy of Sciences
E-mail: prokhortchouk@biengi.ac.ru

It's been eight months since the announcement of the establishment of the International Cancer Genome Consortium [1]. The conference was held with the intention of showing that the participants had started successfully. The Consortium was established in 2008 by predominantly European researchers, with the purpose of performing a consolidated and coordinated investigation of the genome of cancer cells. It should be noted that, in the United States, a similar project called TCGA – The Center Genome Atlas (http://tcga.cancer.gov–had been launched several years earlier. An agreement was made that TCGA would become part of ICGC. It is unquestionable that this decision benefited European researchers more, since it provided access to the numerous American databases that had accumulated. The establishment of the ICGC was for the most part stimulated by a technological breakthrough in determining the nucleotide sequence of DNA, enabling it to migrate from the analogue signal on micromatrices to a digital signal on NGS sequencers. At the time this article was being written, twelve countries were participating in the consortium: Italy, Spain, France, Germany, Great Britain, the United States, Canada, India, China, Australia, and Japan. Mexico is also reported to be on the verge of joining. Information on which country is "responsible" for a particular cancer type can be found on the Consortium website http://www.icgc.org. The total budget of the ICGC was announced at the Brisbane Conference. The sum is rather impressive: $500 million. This is the sum of contracts signed between the governments of participating countries and their national research centers, institutes, and universities, ensuring that at least 12,100 cancer genomes will be investigated. So, what is the status of the individual projects today, and what are the participants most concerned with?

One participant in each project (a mini-consortium devoted to a certain cancer type) is tasked with outlining the general state of the specific practice. The structure of almost all investigations appears to be the same. The first stage comprises a collection of clinical material. During this stage, the central role is most frequently played by hospitals, surgeons, and oncologists. They are responsible for collecting and storing material, recording medical history, and selecting the treatment regimen for a patient. A detailed histological description of the clinical material then has to be compiled. For example, three independent oncologists need to anonymously assess the sections of formalin fixed tumors in the Consortium devoted to kidney cancer CA-GEKID (Cancer Genomics of Kidney), supported by the Seventh Framework Program. Only if there is unanimity concerning the homogeneity of the material (at least 90% of cancer cells on the section) and the stage of tumor progression (which can be expressed quantitatively with no more than 5% inaccuracy) can the refrigerated adjacent section be used for the extraction of DNA and RNA. The problem of the heterogeneity of tumor material was mentioned by all speakers. The contamination of samples with stromal cells and the ingress of several tumor foci into the surgical material are the primary reasons why no more than 10% of several hundreds of tumor/control samples live up to the molecular-genetic investigations. Certain laboratories (John McPherson, Canada) have attempted to enrich the cell material using flow cytofluorimetric sorting (but the attempts have not been sufficiently successful) or used xenotransplantants in immune-deficient mice (in this case, increasingly considerable enrichment can be performed). All mini consortia use almost the same methods for analyzing nucleic acids at subsequent stages. The following are the most frequently sequenced by ICGC researchers in a tumor/control pair: 1) genome

with a coverage depth of ×30–×50; 2) transcriptome; 3) exome; 4) repertoire of micro-RNAs; and 5) highly methylated DNAs. On average, all mini consortia (probably, with the exception of the "advanced" TCGA and relatively young consortia, such as the German project "Genomics of prostate cancer") have reached appreciably the same level. In general, the genomes of no more than 10 tumor/control pairs and no more than several tens of transcriptomes or exomes had been successfully sequenced using NGS (Illumina or SOLiD) by December 2010. Neither consortium has provided data on DNA methylation or the repertoire of micro-RNAs. This is not surprising, since most teams only started receiving financial support in the beginning of, or middle of, 2010. However, ahead of the fifth meeting of the ICGC, to be held in June 2011 in Tokyo, almost all teams have promised to approach 30–50 genomes and several hundreds exomes/transcriptomes. Only American researchers of the Consortium have promised to approach 3,000 re-sequenced cancer genomes in two years. To be completely fair, it should be noted that the 3,000 genomes mark emerged in the American program as the joint effort of all institutes on all oncopathologies that they study. The policy of the consortium towards confirmation of the data obtained using NGS attracts significant interest. For example, in the Broad Institute, United States (Gad Getz), the following procedure is used: first, data on 30–40 genomes are accumulated, and mutations in cancer genomes are detected, and only then is the existence of mutations in amplicones attested using bar-coding and alternative methods of sequencing (Sanger sequencing or 454). Finally, the bioinformatics analysis caps these technological chains. This method allows to isolate somatic mutations which have occurred only in tumour cells, but not in the normal tissues adjacent to the tumour/or in blood cells. Databases of these mutations created at the Sanger Institute (Great Britain) – COSMIC (http://www.sanger.ac.uk/genetics/CGP/cosmic/) – have been widely mentioned, as well as the TCGA databases (http://www.broadinstitute.org/tcga/ password: tcga; login: tcga). None of the speakers mentioned a mutation in the intergenic regions or in promoters. On the contrary, more than sufficient data were given on coding regions and the exone-intron junction. On the basis of the preliminary data provided by NGS, it appears that 100 somatic mutations on average emerge in tumor cells (with the threshold value $p = 10^{-5}$); these values being very close in tumors of different etiologies. So, which genes are most frequently subjected to mutation? *TP53* is the absolute leader – from 85 to 96% depending on the tumor type. The following genes were also mentioned: *VHL*, in the case of kidney cancer; *MUC17*, upon gastric cancer; *CTNB1* (β-catenin) upon intestinal cancer, etc. This begs the very reasonable question as to whether it was necessary to spend US$500 million to determine that well-known genes –tumor growth suppressors – are mutated, while oncogenes are either amplified or characterized by an elevated level of transcription. The answer was given in the form of a lecture by Prof. Rob Sutherland, who was the first to propose anti-estrogen therapy for breast cancer. He explicitly stated that the scheme of therapy for each particular patient will be selected depending on the "genotype" of the mutations in his tumor. Herceptin, which is efficient only upon HER2+ malignant neoplasms of the breast, can serve as a striking example. The opposite is also true: mutations may disturb a certain methabolic pathway in tumor cells; therefore, a therapeutic drug, which would block this disturbance, could be found among the drugs that are very unlike those used in oncology. Hence, both concepts ("the right drug for a particular tumor" and "the right tumor for a certain drug") are valid. Such a change in the paradigm of pharmaceutics could considerably accelerate and improve the results in clinical trials of anti-tumor drugs. This means that in the future we are bound to witness a number of experiments devoted to finding the correlation between a whole-genome genotype of mutations in a tumor and the most efficient method for anti-tumor therapy. It is the underlying purpose of the ICGC consortium; namely, a transition to personified therapy for oncology patients. The issues of bioinformatic processing of genetic information were discussed in addition. With a considerable reduction in the cost of genome sequencing, the amount of data generated increases. Increasing computer resources are necessary in order to process, store, and provide access to the results obtained. The costs of computer resources compensate for the fall in prices and make the cost of the entire investigation even higher. Time will tell for how long the pursuit of cancer genomes will continue. Thus far, the amount of investigations is surely on the increase; the consortium is expected to have new participants with new projects. ●

REFERENCES

1. Hudson T.J., Anderson W., Artez A., Barker A.D., Bell C., Bernabé R.R., Bhan M.K., Calvo F., Eerola I., Gerhard D.S., et al. // Nature. 2010. V. 464(7291). P. 993–998.

Molecular and Physiological Mechanisms of Membrane Receptor Systems Functioning

E. S. Severin[1*], M. V. Savvateeva[2]
[1]All-Russia Research Center for Molecular Diagnostics and Therapy
[2]Biology Faculty, Lomonosov Moscow State University
E-mail: e.severin@mail.ru
Received 16.11.2010

ABSTRACT **Molecular physiology is a new interdisciplinary field of knowledge that looks into how complicated biological systems function. The living cell is a relatively simple, but at the same time very sophisticated biological system. After the sequencing of the human genome, molecular physiology has endeavored to investigate the systems of cellular interactions at a completely new level based on knowledge of the spatial organization and functions of receptors, their ligands, and protein-protein interactions. In recent years, the achievements in molecular physiology have centered on the study of sensor reception mechanisms and intercellular data transfer, as well as the immune system physiology, amongst other processes.**
KEYWORDS **molecular physiology, receptor profile, secondary messengers, targeted delivery, epigenetic diagnostics, prostate cancer**
ABBREVIATIONS **BPA - Benign prostatic adenoma, PIN – Prostatic Intraepithelial Neoplasia, PSA – Prostate-specific antigen, PC – prostate cancer, cAMP – cyclic adenosine monophosphate, cGMP – Cyclic guanosine monophosphate, AMACR - Alpha-methylacyl-coenzyme A Racemase, CGI – CpG-island, DAG – Diacylglycerol, DD3 - Differential Display Code 3, EPCA - Early Prostate Cancer Antigen,** *ERG4* **– V-ets Erythroblastosis virus E26 oncogene homolog,** *ETS* **– transcription factor,** *ETV1* **– ETS translocation variant 1, EGFR - Epidermal Growth Factor Receptor, GSTP1 - Glutathione-S-Transferase ϖ1, IP3 - Inositol Trisphosphate,** *RARβ2* **- Retinoic Acid Receptor Beta 2,** *RASSF1A* **- RAS Association Domain Family Protein 1A,** *TMPRSS2* **- Transmembrane Serine Protease 2**

When considering the functioning mechanisms of membrane receptor systems, it is necessary to first highlight the achievements in molecular physiology regarding the process regulation that occurs in the cell, as well as the intracellular transmission of hormonal signals. The concept of secondary messengers (secondary mediators) is considered today fundamental in cellular and physical-chemical biology, as well as in molecular medicine. However, towards the end of the 1950s the discovery of the first biologically active substance with signal-transduction functions – cAMP – had upended concepts regarding biochemical process regulation in the cell and the intracellular mechanisms of signal transduction. It appears that the signal molecules not able to cross through the cellular membrane interact with the specific receptors and enzyme systems located on the membrane's external surface. Thus, through interaction with membrane receptor systems, biologically active substances determine the production of one or several secondary messengers; low-weight biologically active molecules which transmit signals on intracellular effector structures. Currently, more than 10 similar molecules have been described – they are as follows: cyclic nucleotides cAMP and cGMP; inositol exchange products – inositol phosphate (IP3); diacylglycerol (DAG), as well as Ca^{2+} ions; polynucleotide oligoA; nitrogen monoxide (NO); arachidonic acid exchange products; and a number of other substances of lipid-origin (*Fig. 1*).

It appears that key stages in signal transduction mediated by secondary messengers are common to regulation systems: *agonist – receptor- effector protein- secondary messenger- modulating protein component – physiological response.* The main features of secondary messengers are their universality and trigger functions. Furthermore, both various molecular structures (e.g., ion channels) and multistage cascades of enzymatic reactions can act as effectors and their regulation systems.

In the second half of the 20th century, not a single Nobel Prize was awarded for the outstanding achievements in research concerning this group of biologically active compounds. In various years, E. Sutherland, E. Fischer and E. Krebs, F. Gilman and M. Rodbell, F.

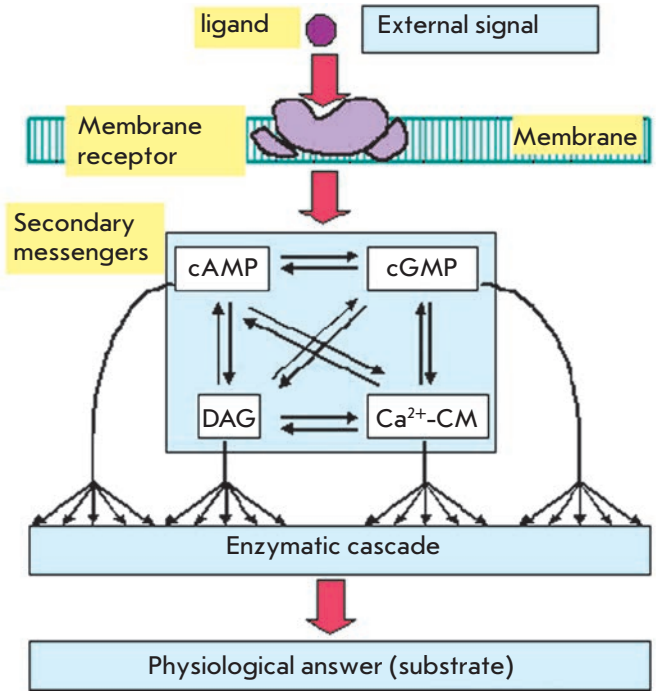

Fig. 1. The main stages of signal transduction mediated by secondary messengers in the cell (cAMP - cyclic adenosine monophosphate, cGMP - cyclic guanosine monophosphate, DG - diacylglycerol).

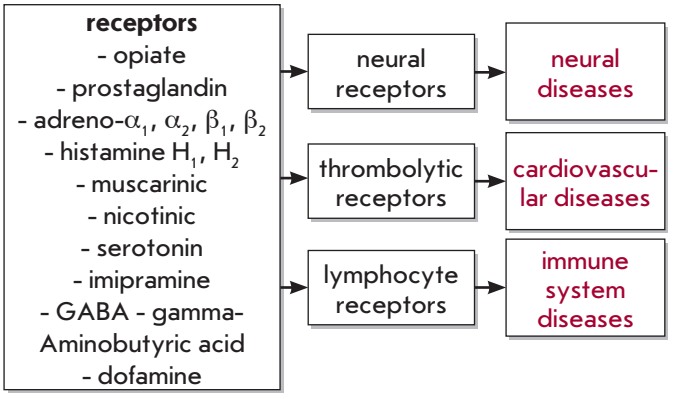

Fig. 2. Relation between the receptor portrait of a cell and the features of systemic pathologies (GABA - γ-aminobutyric acid).

Grignard, L. Ignarro, R. Furchgott and F. Murad *et al.* were awarded Nobel prizes. It should be noted that the main achievements in molecular physiology are in some way linked to cell surface receptors. Studies focusing on central nervous system neurons, neuron junctions, and neural impulse distribution have led to significant improvements in our understanding of cell physiology.

Receptors of the cellular membrane can be subdivided into two basic classes: ionotropic and metabotropic. Ionotropic receptors are membrane channels which open or close after binding with a ligand. Emerging ion streams modulate intracellular ion concentrations, which may cause repeat activation of intracellular mediators. Metabotropic receptors may be directly linked to secondary messenger systems. Conformational changes in a receptor during ligand-binding trigger initiation of a biochemical reaction cascade, leading to changes in the functional state of the cell. Membrane receptors play a significant role in intracellular communications, signal transduction into the cell, neural impulse transduction, and many other cell functions. The variability of receptors to various ligand types represented on the membrane of the exact cell constitutes its receptor profile, which determines the type of physiological activity of that cell (*Fig. 2*).

It should be noted that the study of the functions of a receptor complex not only allows us to understand the 'life' of a normal cell, but can also shed light on the molecular origin of various diseases. On the level of cell receptor system functioning, molecular physiology and molecular medicine are intrinsically linked. P. Erlich's postulate on the selective effects of curing substances on selective targets (1905) served as the starting point for pharmacological science – in particular pharmacokinetics – in which one of the basic goals is to study the receptor mechanisms of curing substance activity. Receptor profiles determine not only the functional activity of a normal cell, but also the specific pathological conditions of the cells and entire organs. In recent years, many studies have been devoted to both the receptor profile and its dependence on pathological processes in precisely targeted organs.

We have defined the parameters of the main human alveolar macrophage receptor systems in both normal and pathological conditions [1]. After estimation of the examples of ligand dissociation constants, it was shown that the physiological constant profiles of pathological and normal conditions are substantially different (*Fig. 3*). We also compared the enzyme activity of phosphorylation systems in normal cells and human tumor cells. It was shown that in normal and tumor cells enzyme activity levels substantially differ; the same tendencies in studies of kinases are observed for different types of tumor cells [2]. An avalanche of experimental data relating to the intracellular "machinery" is being accumulated; specific details of the synapse transduction mechanisms, and knowledge on the structure and functions of normal and defect genes and proteins.

The significance of the membrane receptor functions and their spatial localization makes these mol-

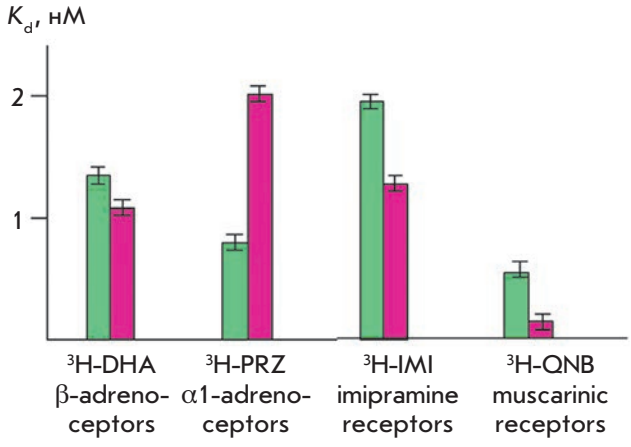

Fig. 3. Binding parameters of various receptors of the human lung alveolar macrophages with ligands in normal and chronic inflammations of the lungs (^{3}H - tritium, DHA, PRZ, IMI, QNB - studied ligands, green shows the values of Kd for the studied ligands in normal lungs; raspberry - chronic inflammation of the lungs).

ecules the main targets for the development of drugs against a wide range of diseases, including oncology. In recent years, one of the brightest achievements in molecular physiology has been the development of target drugs based on "therapeutic" monoclonal antibodies. An example of this is trastuzumab, which is based on humanized monoclonal antibodies to receptor ErbB2 (HER2, HER2/neu) of the epidermal growing factor family (EGFR). The drug is widely used for the treatment of such diseases as breast cancer, amongst others. Humanized monoclonal antibodies specifically bind to the extracellular part of the HER2/neu receptor molecule, and they prevent uncontrolled cell proliferation, causing block age of the cell cycle and suppression of angiogenesis. Furthermore, when monoclonal antibodies bind to the target cell, the activation of cell immunity and apparent antibody-dependent cytotoxicity are observed.

The implementation of a molecular approach, in this particular case the use of target drugs based on monoclonal antibodies, can considerably improve the clinical situation, improve a patient's quality of life, and extend their lifespan. Developing target therapeutic drugs being capable of interacting selectively with targets inside the cell or on its surface is one of the priorities in molecular medicine, since the receptor profile of each cell type is unique. This direction is considered to have great potential, since irregularities in the activity of various enzymes or of their regulation is the basic reason behind metabolic disorders and diseases, as enzymes participate in all biochemical reactions and are likely to determine the course of pathological processes.

Membrane-bound enzymes play a wide range of biological roles, participate in its main processes, such as processing of biologically active molecules, degradation of extracellular matrix components, decomposition or activation of soluble or surface proteins, cell adhesion, and signal transduction into cell. Thus, the activity of different proteases, particularly those localized on the membrane, is believed to be responsible for the events that occur at the early stages of tumor development, because of the disturbances in expression regulation in enzymes belonging to this class [3–6]. We obtained strong evidence of the significance of such an approach in studies of prostate cancer (PC) markers.

Prostate cancer is one of the most widespread tumors in the male population, characterized by a rapid metastasis process [7]. In countries of the European Union, two hundred thousand new cases of prostate cancer are diagnosed annually, with a total of forty thousand deaths occurring [8]. Here, we approach another aspect of molecular physiology and medical intervention – the molecular diagnostics of diseases.

To this date, a large number of genes and their products which are believed to be involved in the development of PC have been detected, and they can reasonably be considered as markers of this disease [9-14]. Changes in prostate tissue during the malignization process affect all basic cell functions and are reflected on different levels of structures and processes, such as cytomorphological changes, changes in the expression of genes and their products, epigenetic changes, etc. The basic molecular markers, indicating prostate tissue malignization, are illustrated in *Fig. 4*.

Malignant tumors in the prostate (including PC) can cause changes in the genome, a very significant occurence. In particular, changes appear in the DNA methylation profile [15–24]. Hypermethylation of the 5`-regulatory regions of several genes leads to their inactivation. These changes in genetic material can be used in the diagnosis of prostate pathological conditions.

Amongst the well known epigenetic anomalies is the change in the *GST1* gene promoter region methylation profile, found within tumor cells. This gene encodes cytoplasm glutation-S-transferase of the 1 class, which participates in apoptosis regulation and xenobiotic utilization. Hence, in normal cells of the prostate, the promoter region of the GST1 gene is non-methylated, whereas upon proliferative inflammatatory atrophy (PIA) the methylation frequency of this region in the *GST1* gene is 6.4%; for highly active prostatic intraepithelial neoplasia (PIN) – 70%; and for prostate adenocarcinoma – 90% [25].

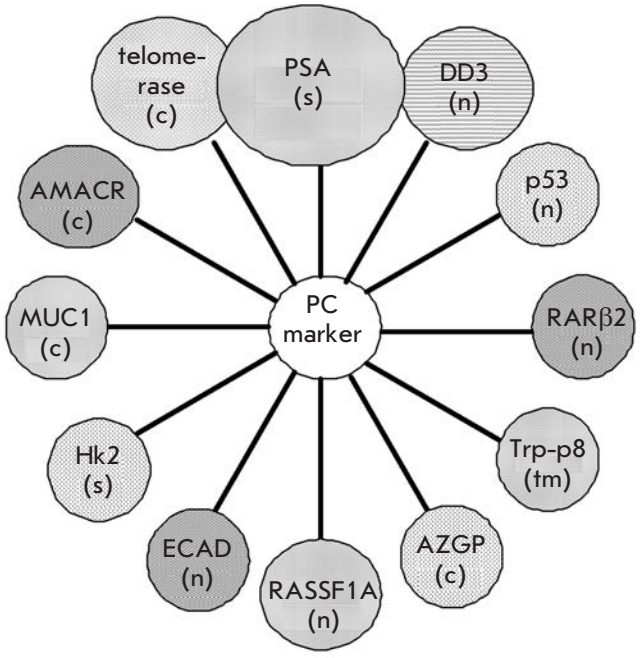

Fig. 4. Some markers of prostate cancer and their localization in the cell (PSA - prostate specific antigen, DD3 - differential display code 3, p53 - protein 53, RARβ2 - retinoic acid receptor beta2, Trp-p8 - transient receptor potential-p8, AZGP - zinc a-2-glycoprotein 1, RASSF1A - RAS association domain family protein 1A, ECAD - E-cadherin, Hk2 - human prostate specific glandular kallikrein, MUC1 - mucin 1, AMACR - a-methylacyl-coenzyme A Racemase, n - nuclear, c - cytoplasmic, s - soluble, tm - transmembrane).

Changes in the methylation status of the 5'-regulatory regions influence not only the *GST1* gene, but also genes the products of which participate in tumor proliferation suppression [26-32]. CGI methylation in the promoter regions of such genes causes inactivation, which is associated with increased risk of development of a malignant tumor: *RAR2* (retinoic acid receptor 2) gene encodes the protein responsible for the receptor-mediated suppression of tumor growth (retinoids are well-known inhibitors of tumor growth and progress). Methylation of the CpG islands in the promoter region of the *RAR2* gene indicates prostate tumor malignization. In healthy pancreatic tissue, methylation of CpG islands is absent [33]. The *RASSF1A* (RAS association domain family protein 1A) gene is also a tumor growth suppressor. Methylation of the CpG islands in the promoter region of this gene was detected upon malignization of various tissue types [34, 35]. The frequency and methylation rate of *RASSF1A* correlate with the tumor's aggressiveness, allowing for an adequate prognosis of the outcome of a disease [36].

A number of studies performed earlier indicate the key role of DNA damage in the development of the malignization process. The most significant among these damages is considered to be the emergence of multiple chromosome rearrangements and mutations in tumor tissues. Genome instability is a common feature of tumor cells which manifests itself on the level of both chromosomes and selected genes. Moreover, each type of tumor is characterized by an assigned set of the most widespread disorders. In the tumor tissue, a high number of structural rearrangements can be found; firstly, translocations and deletions, the quantity of which significantly rises as the tumor progresses.

The level of transcripts consisting of the 5'-untranslated region of the androgen-regulated gene *TMPRSS2* and exones of the genes of the *ETC* (*ERG4* or *ETVI*) family is considerably higher in tumor cells [37]. Rearrangements affecting the *TMPRSS2* gene and genes of the transcription factors ETC (*ERG4, ETVI, ETV4*, etc.) occur in prostate tumor cells. These rearrangements result in the generation of chimera oncogenes [38, 39]. Androgen-dependent promoter elements ensure a high level of expression of such chimera oncogenes [38, 39].

It is necessary to note that there is a positive correlation between the presence of the chimera *TMPRSS2-ETC* gene transcript and disease severity. A high frequency of detection (50 –60%) is characteristic for mRNA of this chimera gene in prostate adenocarcinoma; whereas for PIN, this value is 16%; and in normal tissue, it is 4%.

During the early stages of the disease (when the tumor process is localized), PC is comparably easy to cure; however, as a result of a shortage of diagnosis methods, tumors are usually detected during the final stages of the disease. The current methods are either insufficiently informative or traumatic. Some recent scientific publications reveal losses of some prognostic significance of the basic, presently used biochemical tests for PC – PSA (determination of the prostate-specific antigen concentration in blood). In medical practice false negative and false positive diagnoses based on PSA determination occur frequently. The preliminary diagnosis is confirmed by biopsy; a rather painful procedure with negative consequences for the general condition of the prostate. Thus, the basic goal of a diagnosis is not simply to confirm the disease, but also to reveal the pathogenic process at the earliest possible stage and to determine the stage of the tumor's progression.

Many types of biochemical markers of PC have been described; those originating from serum, urine, semen and prostate tissues. Only a few of these markers can be used in clinical practice, and only one has made it to the clinical trial phase. The markers GSTP1, DD3,

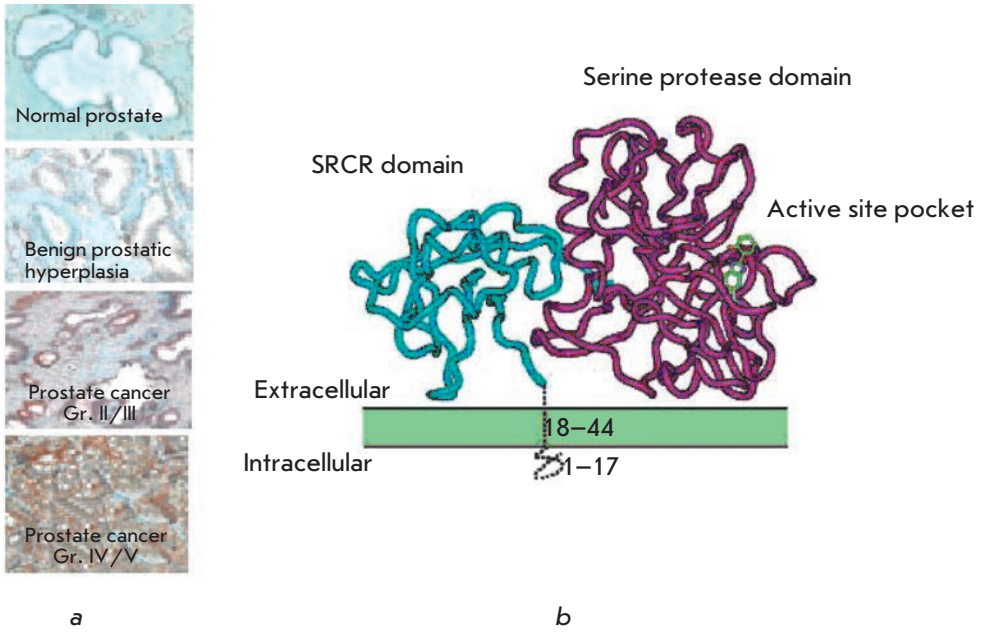

Fig. 5. a - Histochemical staining of sections of prostate tissue from patients with prostate diseases of varying severity with monoclonal antibodies against hepsin (color intensity correlates with the expression level of hepsin on the cell surface). b - Domain structure of hepsin and location of the protein relative to the cell membrane (green shows the plasma membrane and the active center of hepsin; blue - SRCR-domain of hepsin; violet - protease domain of hepsin).

AMACR, EPCA, and hepsin are among those showing the most promise. As previously stated, the expression level of hepsin (limited in a normal cell) rapidly increases in a progressing tumor. It is necessary to note that the specificity of high expression levels of hepsin by tumor cells had attracted attention at the earliest stages of the study of that protein. Expression of this enzyme increases as the tumor progresses and reaches a maximum at terminal stages (*Fig. 5*) [40].

Thus, because of the high specificity of hepsin expression in tumor cells, there is an opportunity to answer the question as to whether the neoplasm in prostate is benign or malignant. Hepsin is preferable to the molecular markers currently being used in clinical practice in terms of several parameters. We propose the following hypothesis: an increase in hepsin proteolytic activity on a cell surface is specific of prostate tumors. For a confirmation of this hypothesis, we obtained a producer strain of recombinant hepsin and found the most specific substrate for it via a process of perfect purification and activation procedures [41]. We proved that it is possible to determine the proteolytic activity in biomaterial samples obtained from males with various pathological conditions of prostate, selected the conditions of this analysis, and we confirmed its specificity in the case of a tumor. The resulting data testifies to the fact that proteolytic activity in a conditionally healthy donor group is similar to that in a group of patients with chronic prostatitis and BPH; but it reliably differed from the proteolytic activity in a group of patients with prostate adenocarcinoma (*Fig. 6*).

This fact confirms the high specificity of the method: whilst chronic prostatitis and the BPH background level of proteolysis activity are constant (as in conditionally healthy patients), the PC progress level of proteolysis activity rapidly increases, and the basic impact includes hepsin, so far as a specific substrate is used for detection [42].

Based on the studies carried out in our laboratory, a PC detection test-kit has been developed. It is based on hepsin activity determination in epithelial cells of the prostate collected with urine after rectal massage (Patent "Prostate cancer detection test-kit and prostate cancer diagnostic method" [Eurasian patent № 011694], diagnostic kit (Registration № FSR 2009/05065)). Such parameters as sensitivity, specificity, prognostic significance of positive and negative results, and diagnostic accuracy of the developed method are not inferior to those of the well-known biochemical tests for PC and other methods currently under development; indeed, it proved better by some parameters (*Fig. 7*).

Besides, the new method has significant advantages in comparison with the currently widely used PSA concentration determination methods.

The method presented by us is better than existing ones, because of the non-invasive character of biomaterial collection; since enzyme activity is measured in urine. To conclude, application of this method, which was developed in conjunction with existing methods, will help to avoid false diagnosis and will have a beneficial impact on the general conditions and quality of life of the patient.

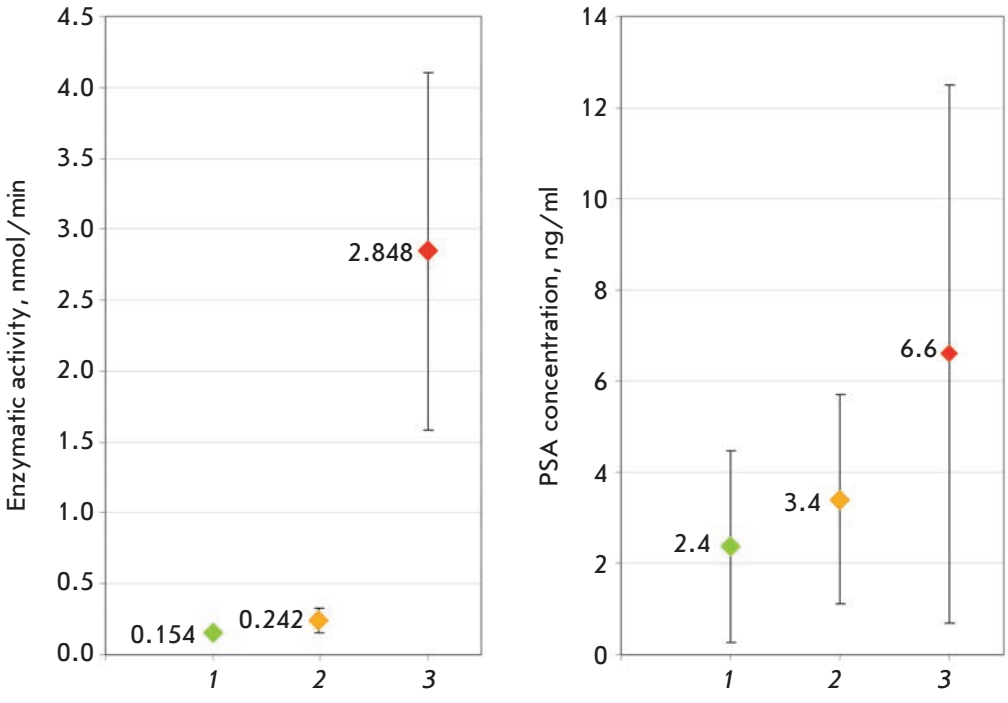

Fig. 6. Comparative analysis of diagnostic indexes for diagnostic methods of prostate diseases by determination of the concentration of PSA in the blood of the patient and determination of hepsin activity using "PHOTO-HEPSIN" (the average values of experimental groups and the spread of values). 1 - a group of healthy donors; 2 – a group of BPH patients; and 3 - a group of patients with prostate cancer.

The results obtained allow to conclude that the new method of malignant neoplasm of prostate diagnostics with determination of hepsin activity has a set of advantages as compared with the currently widely used PSA determination and can be recommended for PC screening studies in clinical laboratory conditions.

Increase of the size of a tumor as a result of increasing, uncontrollable tumor cell proliferation causes them to invade surrounding tissues. This process is followed by the end of any contact both between tumor cells and normal cells; because of the action of various transmembrane proteases, it affects the surrounding territorial matrix, as well.

Serine protease hepsin is one of the enzymes that regulate the process of local invasion of tumor cells [4]. The expression level of hepsin was shown to considerably increase on the surface of prostate adenocarcinoma cells [43-47]. Hepsin was shown to be the key activation factor of the proteolytic processes in tumor tissue, which result in dissemination of tumor cells. In order to better understand the role of hepsin in these processes, it would help to review how the associated membrane proteolysis participates in the tumor's progress. During the pathological process, activity of the membrane-bound proteases causes an uncontrollable proteolysis of the territorial matrix and disorganization of its structure.

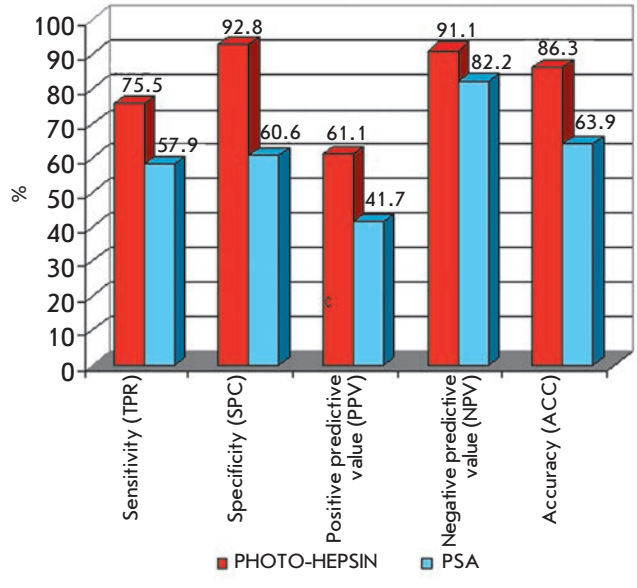

Fig. 7. Comparative analysis of the basic evaluative diagnostic indexes of the methods for prostate diseases diagnosis - determination of the concentration of PSA in the blood of the patient and determination of hepsin activity using "PHOTO-HEPSIN" (red shows the values of "PHOTO HEPSIN" parameters; blue shows the values of the parameters of the method for PSA concentration determination; -PV - negative predictive value; and +PV - positive predictive value).

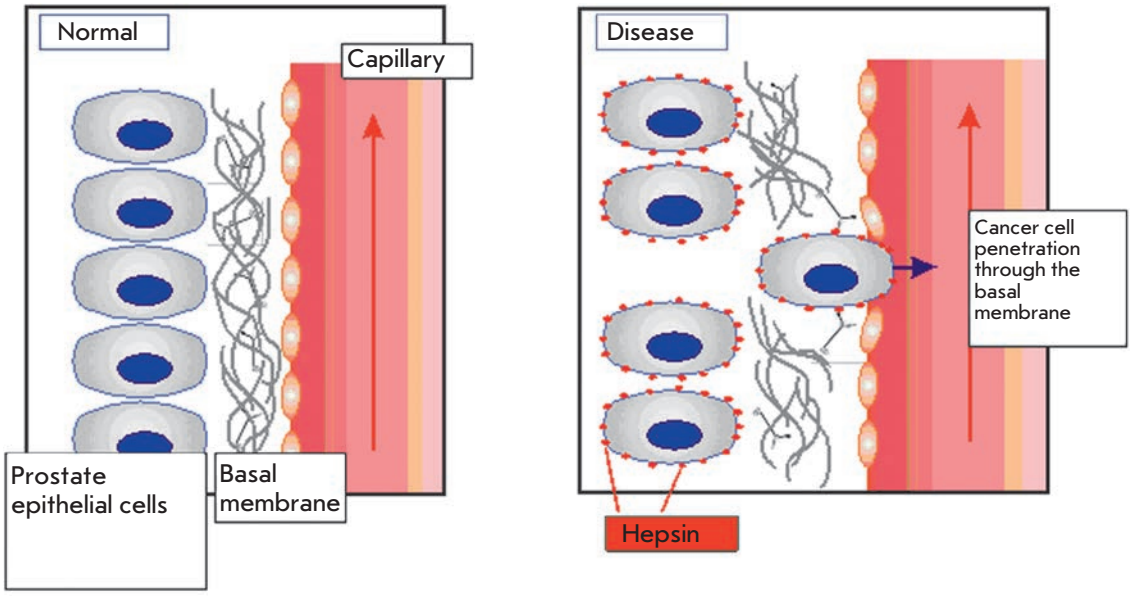

Fig. 8. Invasion of tumor cells through the basement membrane with the participation of hepsin.

The majority of studies devoted to evaluating the role of hepsin in oncopathology have focused on tumors of the prostate. We shall review the basal membrane disorder of this organ from the perspective of molecular physiology and the potential role of hepsin. The basal membrane of the prostate is a specialized extracellular structure separating epithelial and stromal cells from each other and consisting of the matrix proteins produced by these two cell types [48]. Disruption of this structure is necessary for a local invasion in the early metastasis process [49].The molecular mechanisms involving hepsin in the progress of malignant neoplasm has become clear. The set of extracellular matrix components which are potential hepsin substrates have been discovered [4, 50].

Another aspect of hepsin's impacts on the pathological process is the activation of enzymes in inactive form that are also involved in the process of basal membrane degradation [51]. Thus, hepsin can multiply and increase proteolysis on the surface of tumor and stromal cells, which aggravates the damage to the basal membrane and accelerates tumor progress (*Fig. 8*).

This hypothesis confirms the data on the suppression of the tumor cell's invasive growth when hepsin activity is inhibited [52]. This, and other features of hepsin, makes it a convenient target for therapeutic actions. Therefore, studying the inhibition mechanisms is considered promising in the development of antitumor drugs that can be effective in case of tumors for which an elevated expression of hepsin is characteristic. The search for specific hepsin inhibitors is underway, with the purpose of creating targeted drugs and developing PC therapy methods [53]. Hepsin is involved in such phenomena as the increase in cell motility, matrix protein separation and extracellular structure disorganization, and activation of extracellular proteases and their cascades, which underlie tumor progression. Inhibition of the activity of this enzyme may lead to suppression of these processes, and it will positively influence disease outcome.

In 2008, in a screening of the libraries of drugs and various chemical compounds aimed at searching for potential low-molecular-weight inhibitors of hepsin, a set of compounds capable of specifically inhibiting its proteolytic activity were found. Anthralin (anthracene-1,8,9-triol) emerged as one of the most efficient inhibitors of hepsin. Some compounds were dose-dependently shown to suppress the activity of recombinant hepsin and to exhibit no cytotoxic effect on various cell lines, which is significant for therapeutic applications. Among all compounds, anthralin demonstrated the highest inhibiting ability towards hepsin: it inhibited hepsin 5.5 and 85 times more efficiently than trypsin and thrombin, respectively [53].

As was discovered earlier in our laboratory, anthralin inhibits recombinant hepsin. Due to this, we assumed that anthralin may affect the native form of the protein in the same way [41]. The main contribution to proteolytic activity on the surface of prostate adenocarcinoma cells is made by hepsin, since it is its gene that is over-expressed. Therefore, it can be assumed that the impact of a specific hepsin inhibitor will considerably decrease the general proteolytic activity. The introduction of Anthralin into lysated human prostate adenocarcinoma cells caused a 50–70% reduction in the general proteolytic activity, which attests to the fact

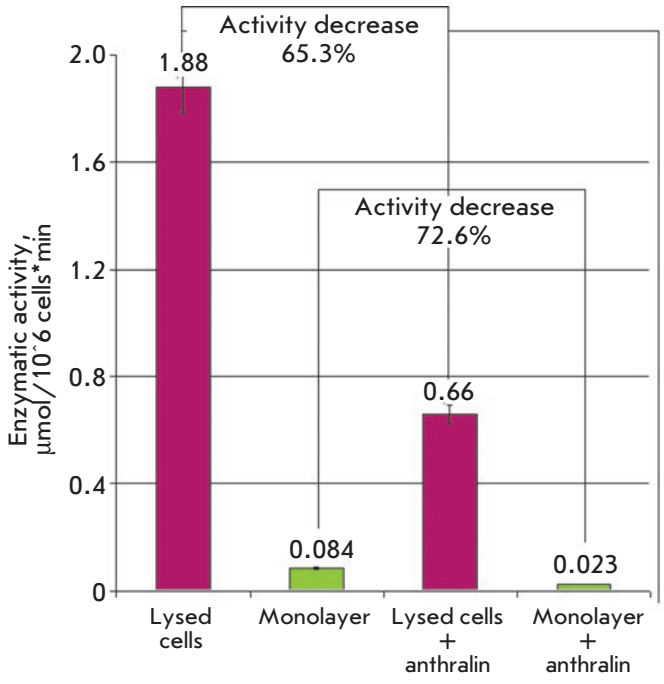

Fig. 9. Comparison of the proteolytic activity of live and lysed LnCap cells in the absence and presence of anthralin (purple shows the data for lysed cells, green shows the data for a monolayer of living cells).

that anthralin has an efficient inhibiting action on native hepsin localized on the membranes of tumor cells. *Figure 9* shows the results of a determination of the proteolytic activity of a LnCap human prostate adenocarcinoma cell line in the presence and absence of anthralin.

The impact on the specified enzyme systems can control the disorders observed, while membrane localization of a number of enzymes is extremely convenient for designing targeted drugs and their application. The controlled enzyme activity typically underlies the approaches that are applied for the treatment of various diseases and the development of new drugs. With account for the abundance of serine proteases and their participation in pathological processes, the search for new inhibitors is of great significance. Even today, some compounds capable of suppressing protease activity are used in tumor therapy. Data confirming elevated expression of some members of the family of transmembrane serine proteases upon various oncopathologies has been published. The inhibition of the activity of enzymes belonging to this family is considered as promising in antitumor therapy.

Transmembrane localization of hepsin makes this enzyme a good target for therapeutic agents, since the localization of the transmembrane domain of this protein on a cell's surface may facilitate drug delivery. Another advantage of hepsin when used as a molecular target is that the negative effects in hepsin suppression would be minimal, whereas the high specificity of its expression by malignant tissue cells can be used for effective and specific antitumor therapy.

In the present paper, we have attempted to summarize the main features of molecular physiology as a new interdisciplinary field of fundamental knowledge on sophisticated biological systems. Molecular physiology has a special place in the variety of contemporary life sciences. This role has to do with the connection of molecular physiology to medicine and the stupendous number of potential medical applications. Furthermore, the role is associated with the conceptual revolution which has been taking place over the past 10–15 years. These factors allow to regard molecular physiology as a common discipline in biology which is located at the border between such sciences as biochemistry, bioorganic chemistry, molecular and cell biology, microbiology, and evolutionary biology. ●

REFERENCES

1. Kondratenko T.Y., Zacharova I.V., Kuzina N.V., Katukov V.Yu., Severin E.S., Kornilova Z.Ch., Perelman M.I. // Biochem. Mol. Biol. Int. 1993. V. 29. № 1. P. 123–130.
2. Petukhov S.P., Chibalin A.V., Kovalenko M.V., Bulargina T.V., Severin E.S. // Biokhimia. 1991. V. 56. № 11. P. 2077-2096.
3. Chang C., Werb Z. // Trends Cell. Biol. 2001. V. 11. P. 37–43.
4. Klezovitch O., Chevillet J., Mirosevich J., Roberts R.L., Matusik R.J., Vasioukhin V. // Cancer Cell. 2004. V. 6. P. 185–195.
5. Andreasen P.A., Kjoller L., Christensen L., Duffy M.J. // Int. J. Cancer. 1997. V. 72. P. 1–22.
6. Dano K., Behrendt N., Hoyer-Hansen G., Johnsen M., Lund L.R., Ploug M., Romer J. // Thromb. Haemost. 2005. V. 93. P. 676–681.
7. Davydov M.I., Axel E.M. // Vestn. N.N. Blokhin RCRC RAMS. 2008. V. 19. № 2. Appl. 1. 154 p.
8. Vasil'eva E.B., Savvateeva M.V., Kuznetsova E.M., Severin S.E., Fiev D.N., Alyaev Yu.G., Vinarov A.Z. // Onkourologia. 2008. № 3. P. 50-53.
9. Yu Y.P., Landsittel D., Jing L., Nelson J., Ren B., Liu L., McDonald C., Thomas R., Dhir R., Finkelstein S., Michalopoulos G., et al. // J. Clin. Oncol. 2004. V. 22. № 14. P. 2790–2799.
10. Popa I., Fradet Y., Beaudry G., Hovington H., Beaudry G., Tetu B. // Modern Pathol. 2007. V. 20. № 11. P. 1121–1127.
11. Furusato B., Gao C.L., Ravindranath L., Chen Y., Cullen J., McLeod D.G., Dobi A., Srivastava S., Retrovics G., Sesterhenn I.A. // Modern Pathol. 2008. V. 21. № 2. P. 67–75.
12. Santinelli A., Mazzucchelli R., Barbisan F., Lopez-Beltran A., Cheng L., Scarpelli M., Montironi R. // Am. J. Clin. Pathol. 2007. V. 128. № 4. P. 657–666.

13. Ananthanarayanan V., Deaton R.J., Yang X.J., Pins M.R., Gann P.H. // Prostate. 2005. V. 63. № 4. P. 341–346.
14. Uetsuki H., Tsunemori H., Taoka R., Haba R., Ishikawa M., Kakehi Y. // J. Urol. 2005. V. 174. № 2. P. 514–518.
15. Baylin S.B., Herman J.G., Graff J.R., Vertino P.M., Issa J.P. // Adv. Cancer Res. 1998. V. 72. P. 141–196.
16. Bird A. // Cell. 1992. V. 70. P. 5–8.
17. Merlo A., Herman J.G., Mao L., Lee D.J., Gabrielson E., Burger P.C., Baylin S.B., Sidransky D. // Nat. Med. 1995. V. 1. P. 686–692.
18. Herman J.G., Umar A., Polyak K., Graff J.R., Ahuja N., Issa J.P., Markowitz S., Willson J.K., Hamilton S.R., Kinzler K.W., et al. // Proc. Natl. Acad. Sci. USA. 1998. V. 95. № 12. P. 6870–6875.
19. Hoque M.O., Topaloglu O., Begum S., Henrique R., Rosenbaum E., van Criekinge W., Westra W.H., Sidransky D. // J. Clin. Oncol. 2005. V. 23. № 27. P. 6569–6575.
20. Cooper C.S., Foster C.S. // Br. J. Cancer. 2009. V. 100. № 2. P. 240–245.
21. Nelson W.G., Yegnasubramanian S., Agoston A.T., Bastian P.J., Lee B.H., Nakayama M., De Marzo A.M. // Front. Biosci. 2007. V. 12. P. 4254–4266.
22. Dobosy J.R., Roberts J.L., Fu V.X., Jarrard D.F. // J. Urol. 2007. V. 177. № 3. P. 822–831.
23. Li L.C. // Front. Biosci. 2007. V. 12. P. 3377–3397.
24. Esteller M. // Nat. Rev. Genet. 2007. V. 8. № 4. P. 286–298.
25. Nakayama M., Bennett C.J., Hicks J.L., Epstein J.I., Platz E.A., Nelson W.G., De Marzo A.M. // Am. J. Pathol. 2003. V. 163. №3. P. 923–933.
26. Henrique R., Costa V.L., Cerveira N., Carvalho A.L., Hoque M.O., Ribeiro F.R., Oliveira J., Teixeira M.R., Sidransky D., Jeronimo C. // J. Mol. Med. 2006. V. 84. № 11. P. 911–918.
27. Henrique R., Jeronimo C., Hoque M.O., Carvalho A.L., Oliveira J., Teixeira M.R., Lopes C., Sidransky D. // DNA Cell Biol. 2005. V. 24. № 4. P. 264–269.
28. Henrique R., Jeronimo C., Hoque M.O., Nomoto S., Carvalho A.L., Costa V.L., Oliveira J., Teixeira M.R., Lopes C., Sidransky D. // Cancer Epidemiol. Biomarkers Prev. 2005. V. 14. № 5. P. 1274–1278.
29. Henrique R., Jeronimo C., Teixeira M.R., Hoque M.O., Carvalho A.L., Pais.I., Ribeiro F.R., Oliveira J., Lopes C., Sidransky D. // Mol. Cancer Res. 2006. V. 4. № 1. P. 1–8.
30. Henrique R., Ribeiro F.R., Fonseca D., Hoque M.O., Carvalho A.L., Costa V.L., Pinto M., Oliveira J., Teixeira M.R., Sidransky D., et al. // Clin. Cancer Res. 2007. V. 13. № 20. P. 6122–6129.
31. Henrique R., Ribeiro F.R., Fonseca D., Hoque M.O., Carvalho A.L., Costa V.L., Pinto M., Oliveira J., Teixeira M.R., Sidransky D., et al. // Clin. Cancer Res. 2007. V. 10. P. 8472–8478.
32. Jeronimo C., Usadel H., Henrique R., SilvaC., Oliveira J., Lopes C., Sidransky D. // Urology. 2002. V. 60. № 6. P. 1131–1135.
33. Meyer H.A., Ahrens-Fath I., Sommer A., Haendler B. // Biomed. Pharmacother. 2004. V. 58. P. 10–16.
34. Aitchison A., Warren A., Neal D., Rabbitts P. // Prostate. 2007. V. 67. № 6. P. 638–644.
35. Krop I., Player A., Tablante A., Taylor-Parker M., Lahti-Domenici J., Fukuoka J., Batra S.K., Papadopoulos N., Richards W.G., Sugarbaker D.J., et al. // Mol. Cancer Res. 2004. V. 2. № 9. P. 489–494.
36. Liu L., Yoon J.H., Dammann R., Pfeifer G.P. // Oncogene. 2002. V. 21. № 44. P. 6835–6840.
37. Tomlins S.A., Rhodes D.R., Perner S., Dhanasekaran S.M., Mehra R., Sun X.W., Varambally S., Cao X., Tchinda J., Kuefer R., et al. // Science. 2005. V. 310. P. 644–648.
38. Tomlins S.A., Rubin M.A., Chinnaiyan A.M. // Annu. Rev. Pathol. 2006. V. 1. P. 243–271.
39. Perner S., Mosquera J.M., Demichelis F., Hofer M.D., Paris P.L., Simko J., Collons C., Bismar T.A., Chinnaiyan A.M., De Marzo A.M., et al. // Am. J. Surg. Pathol. 2007. V. 31. P. 882–888.
40. Xuan J.A., Schneider D., Toy P., Newton A., Zhu Y., Finster S., Vogel D., Mintzer B., Dinter H., et al. // Cancer Res. 2006. V. 66. P. 3611–3619.
41. Raevskaya A.A., Kuznetsova E.M., Savvateeva M.V., Severin S.E. // Biochemistry (Mosc). 2010. V. 75. P. 866–872.
42. Vasil'eva E.B., Savvateeva M.V., Kuznetsova E.M., Severin S.E., Severin E.S., Fiev D.N., Alyasov Yu.G., Vinarov A.Z. // Andrologia i genitalnaya khirurgia. 2008. №3. P. 46-49.
43. Dhanasekaran S.M., Barrette T.R., Ghosh D., Shah R., Varambally S., Kurachi K., Pienta K.J., Rubin M.A., Chinnaiyan A.M. // Nature. 2001. V. 412. P. 822–826.
44. Luo J., Duggan D.J., Chen Y., Sauvageot J., Ewing C.M., Bittner M.L., Trent J.M., Isaacs W.B. // Cancer Res. 2001. V. 61. P. 4683–4688.
45. Magee J.A., Araki T., Patil S., Ehrig T., True L., Humphtey P.A., Catalona W.J., Watson M.A., Milbrandt J. // Cancer Res. 2001. V. 61. P. 5692–5696.
46. Chen Z., Fan Z., McNeal J.E., Nolley R., Caldwell M.C., Mahadevappa M., Zhang Z., Warrington J.A., Stamey T.A. // J. Urol. 2003. V. 169. P. 1316–1319.
47. Yamaguchi N., Okui A., Yamada T., Nakazato H., Mitsui S. // J. Biol. Chem. 2002. V. 277. P. 6806–6812.
48. Nagle R.B., Hao J., Knox J.D., Dalkin B.L., Clark V., Cress A.E. // Am. J. Pathol. 1995. V. 146. P. 1498–1507.
49. Robinson V.L., Kauffman E.C., Sokoloff M.H., Rinker-Schaeffer C.W. // Cancer Treat. Res. 2004. V. 118. P. 1–21.
50. Tripathi M., Nandana S., Yamashita H., Ganasan R., Kirchhofer D., Quaranta V. // J. Biol. Chem. 2008. V. 283. P. 30576–30584.
51. Moran P., Li W., Fan B., Vij R., Eigenbrot C., Kirchhofer D. // J. Biol. Chem. 2006. V. 281. P. 30439–30446.
52. Miyata S., Fukushima T., Kohama K., Tanaka H., Takeshima H., Kataoka H. // Hum. Cell. 2007. V. 20. P. 100–106.
53. Chevillet J.R., Park G.J., Bedalov A., Simon J.A., Vasioukhin V.I. // Mol. Cancer Ther. 2008. V. 7. P. 3343–3351.

Quantum Dots for Molecular Diagnostics of Tumors

T. A. Zdobnova*, E. N. Lebedenko, S.M. Deyev
Shemyakin and Ovchinnikov Institute of Bioorganic Chemistry, Russian Academy of Sciences
*E-mail: t.zdobnova@mail.ru
Received 15.10.2010

ABSTRACT **Semiconductor quantum dots (QDs) are a new class of fluorophores with unique physical and chemical properties, which allow to appreciably expand the possibilities for the current methods of fluorescent imaging and optical diagnostics. Here we discuss the prospects of QD application for molecular diagnostics of tumors ranging from cancer-specific marker detection on microplates to non-invasive tumor imaging *in vivo*. We also point out the essential problems that require resolution in order to clinically promote QD, and we indicate innovative approaches to oncology which are implementable using QD.**
KEYWORDS **quantum dots, fluorescence imaging, multicolor labeling, nanoparticles.**
ABBREVIATIONS **AFP – alpha-fetoprotein; EGF – epidermal growth factor; EGFR - epidermal growth factor receptor; ELISA – enzyme-linked immunosorbent assay; HER2/neu - human epidermal growth factor receptor 2/neu; IGF1R – type 1 insulin-like growth factor receptor; IHC – immunohistochemistry; MAA – mercaptoacetic acid; QDs – quantum dots; PEG – polyethylene glycol; scFv – single-chain variable antibody fragment; PSCA – prostate stem cell antigen; PSMA – prostate-specific membrane antigen; RES –reticuloendothelial system; ROS – reactive oxygen species.**

INTRODUCTION

In recent biomedical studies, much attention has been paid to the search for new methods of noninvasive imaging of the internal structure of biological objects. Instruments with a high spatial resolution have been designed, and, consequently, optical methods for investigation are gaining widespread use. One of the most demonstrable and informative methods among these is the fluorescent diagnostics of pathological foci directly in the organism.

A considerable portion of the methods being developed are directed toward imaging tumors, tissues and organs; studying the molecular structure of tumor cells by auto-fluorescence registration; or by specific staining of the objects under observation with fluorescent contrasting dyes. Methods such as these enable us not only to localize a tumor in the organism, but also to estimate the level of expression of various proteins, as well as the activity of individual cells and the processes that have an impact on tumor behavior and its response to the action of therapeutic agents.

In modern methods of diagnostics, special demands are placed on the contrast agents used. Fluorophores must possess the following properties: small dimensions (1–10 nm); sufficient brightness and a high quantum yield; it is necessary that their excitation and fluorescence in the spectral range correspond to optimum penetration into biological tissues; and chemical stability, photostability, and biocompatibility (stability in biological media and nontoxicity). Moreover, frequently in order to perform biological studies, these fluorophores need to be conjugated with different targeting molecules, so that they can be delivered to particular targets (proteins, compartments, and cells). The conjugates need to specifically interact with the target and do so in a stable manner, whilst possessing a low level of nonspecific binding.

Fluorescent semiconductor nanocrystals, so-called quantum dots (QDs), are a relatively novel class of fluorophores with unique optical and physicochemical properties, atypical of other fluorescent dyes. Two major classes of fluorophores have been conventionally used for diagnostics: organic dyes and fluorescent proteins [1]. These fluorophores were first used in biology and medicine and have subsequently evolved significantly. At this point, a large variety of organic dyes with a small molecular weight and fluorescent proteins, characterized by high brightness, good quantum yield and emission over the entire spectral region from blue to the near-infrared (IR) region, have been designed [2, 3]. However, some of the properties of these fluorophores (in particular, broad emission spectrum and low photobleaching thresholds) still limit their effectiveness in such types of studies as long-term imaging and 'multiplexing' (simultaneous detection of multiple signals) without an additional complex of instrumentation and processing [4].

QDs possess a number of physicochemical features that open wider possibilities in comparison with conventionally used fluorescent labels, making them par-

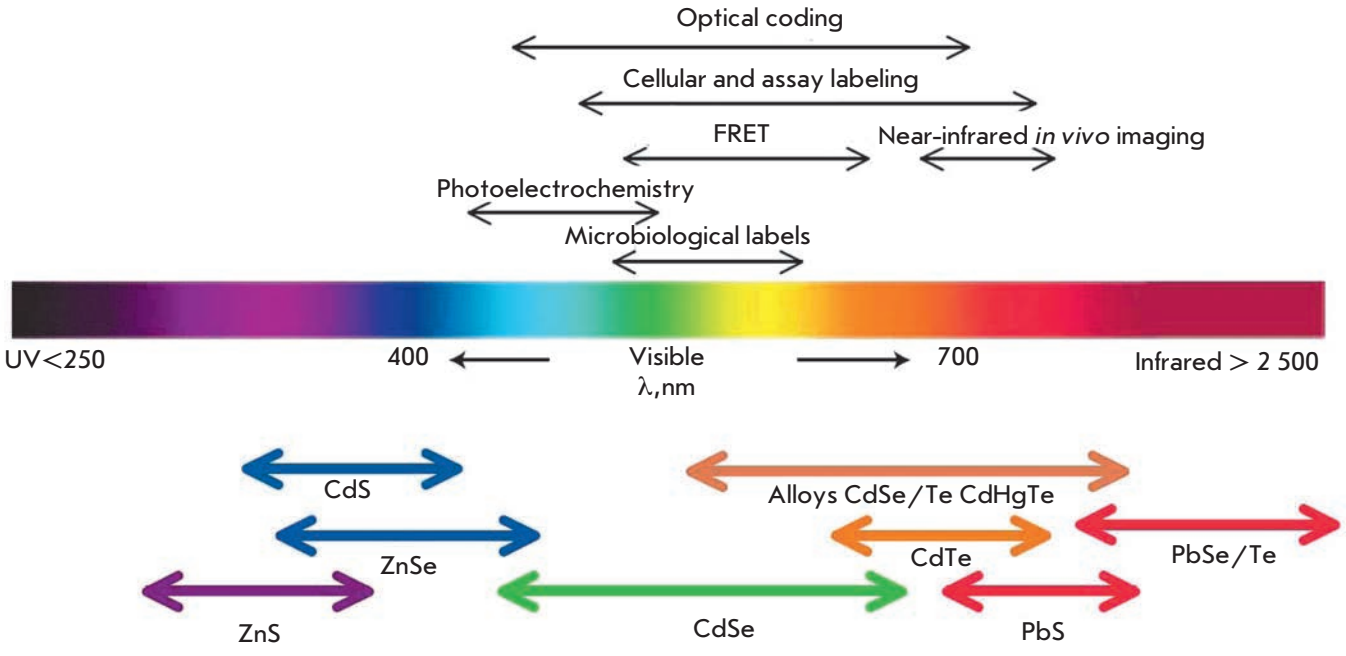

Fig. 1. Representative QD core materials scaled as a function of their emission wavelength superimposed over the spectrum. Representative areas of biological interest are also presented corresponding to the pertinent emission, highlighting how most biological usage falls in the visible – near-infrared region. Reprinted by permission from Macmillan Publishers Ltd.: [Nature Materials] (Medintz I.L., Uyeda H.T., Goldman E.R., Mattoussi H. Nat Mater. 2005 4:435-446), copyright (2005).

ticularly attractive for use in various biological experiments [5, 6].

This review will summarize how QDs can be used for studying the molecular mechanisms of the processes that occur in tumor cells and for both *in vitro* and *in vivo* tumor diagnostics.

1. QD FEATURES PROVIDING ADVANTAGES WHEN USING THEM IN BIOMEDICAL STUDIES

Quantum dots are almost spherical nanocrystals 1–10 nm in diameter, consisting of a small number of atoms (500–10,000) of semiconductor materials of groups II–VI (e.g., CdSe, CdTe, CdS, and ZnSe) or groups III–V (e.g., InP and InAs) of Mendeleev's periodic table. The term "dot" mainly characterizes the extremely small dimension of these objects; while the adjective "quantum" describes the fact that their behavior and properties are described to a significant extent by quantum mechanics, rather than classical mechanics. The decrease in the particle size of the compound to a value smaller than the exciton Bohr radius (e.g., for spherical CdSe particles this diameter is less than 6 nm) results in that the properties of the compound are determined not as much by their chemical composition as by their particle size. In light of this, semiconductor nanocrystals are characterized by their unique optical characteristics and physicochemical properties that distinguish them favorably from other fluorophores that are conventionally used in biology [7].

QDs possess a high molar extinction coefficient (higher than that of organic dyes by a factor of 10–100) and a high quantum yield (up to 90%), which provides to these fluorophores exceptional brightness. QDs are characterized by a broad absorption spectrum, a considerable Stokes shift, and a narrow and symmetrical (without a "tail" in the red region) fluorescence spectrum (peak width ~25–40 nm). In this regard, the emission wavelength is core size-tunable, enabling us to create a wide range of various QDs fluorescing within a spectral range from UV to IR (400–2,000 nm), using the same materials and the same procedures (*Fig. 1*). Furthermore, the broad excitation spectrum typical of these nanoparticles (QDs can be excited by light at any wavelength smaller than their fluorescence wavelength) allows to excite a mixture of different QDs at one wavelength that is considerably remote (> 100 nm) from their fluorescence wavelengths [9]. Such properties of QDs significantly increase their potential use in multicolor labeling and

the simultaneous identification of different biological objects, in comparison with other dyes [6].

High resistance to photobleaching (that is higher than that of organic fluorophores by a factor of 100–1,000) and an exceptional stability towards photo- and chemical degradation [7, 10], which is typical of fluorescent semiconductor nanocrystals, makes it possible for us to use them in long-term experiments on real-time imaging of the processes occurring inside a cell (e.g., endocytosis) [11] or translocation of individual receptor molecules along the living cellular surface and for staining the samples that require long-term storage [13].

A more detailed description of the physicochemical properties of QDs important for their biological application, and a comparative evaluation of their use and that of other fluorophores in biomedical studies, can be found in reviews [4–6].

Physicochemical and optical properties and the features of QDs directly depend on the method of their synthesis. This wide field (not an issue for this review) is still under development. It is increasing the number of QDs used in biomedical studies and enhancing their properties (ref. reviews [4, 5]).

Until recently, two types of water-soluble monodisperse QDs had been in use in biology: the so-called bioinert nanocrystals and nanocrystals conjugated to various biological molecules in order to add certain specificity to them.

Bioinert QDs find application as nonspecific contrast agents for cell staining due to endocytosis, for the contrasting of blood vessels and lymph nodes, and for studying biodistribution, toxicity, and *in vivo* passive delivery of nanoparticles into animal tumors. Water-soluble QDs modified with hydrophilic thiols [14] and encapsulated by silicon or amphiphilic polymers [16] are frequently used as such bioinert particles. Such particles are typically coated with a layer of inert molecules, in order to reduce the nonspecific binding; the manufacturers of commercial QDs usually use polyethylene glycol (PEG) for this purpose.

2. TARGETING OF QDS TO TUMOR CELLS

It is a common requirement when using QDs as fluorophores for tumor imaging that they bind to various targeting molecules, thus ensuring the selective delivery of QDs to tumor cells and their components. The specificity of labeling is provided by the selection of a target that optimally suits each particular case and the corresponding targeting molecule.

The receptor part of signal proteins that are overexpressed on tumor cell membranes is used most often as a specific target. The level of expression of these cellular molecular oncomarkers, determined directly in the tumor tissue, characterizes the molecular profile of each individual tumor and is used to determine the immune status of the tumor and the individualization of therapeutic treatment [17].

Antibodies and their fragments, ligands of specific receptors localized on the tumor cell surface, small molecules (such as peptides and aptamers) with specific affinity for some of the oncomarkers are used as a targeting module, which provides the selective delivery of QDs to tumor cells and their components, depending on the aims and objects of the study.

2.1 Targeting agents

Immynoglobulin (Ig) molecules have been known for a long time, as they are widely used as efficient targeting modules for the specific delivery of diagnostic and therapeutic agents both *in vitro* at the cell and tissue level and *in vivo* at the whole body level. As early as in one of the first studies devoted to using QDs for biological investigations, the potential to obtain complexes of QDs with IgG molecules and the ability of the resulting complexes to bind to specific antispecies polyclonal antibodies and to form precipitates in the solution were illustrated [14]. Later, such complexes were used for the labeling of particular molecules located in various cell compartments (on the membrane surface, in cytoplasm, and in the cellular nucleus) [16].

Regardless of the wide distribution of full-size antibodies in diagnostic systems *in vitro*, their application as targeting agents *in vivo* usually requires the elimination of their effector functions and a radical modification of physicochemical properties [18]. Antibodies of scFv format are those that best meet these requirements [19, 20]. These small antibody fragments do not contain a constant domain. Although this fact has no effect on their targeting properties, it reduces the possibility of the side effects caused by the interaction between the constant domains and receptors of the cells of the immune system and proteins of the complement system [21]. scFv antibodies against surface oncomarkers are widely used as targeting modules for the fluorescent imaging of tumor cells and delivery of therapeutic agents to them [22–24].

At the Nie laboratory, it was demonstrated that QDs conjugated to targeting mini antibodies scFv could be used for tumor imaging, including *in vivo* imaging. Accumulation by tumor cells and efficient internalization of QDs conjugated to a human anti-EGFR-antibody of the scFv format were observed after their intravenous injection into a human pancreatic bearing mouse [25].

The major bottleneck of scFv antibodies as targeting agents is their monovalence, since monovalent binding to an antigen on the cell surface does not ensure the long-term retention of the antibody and results in

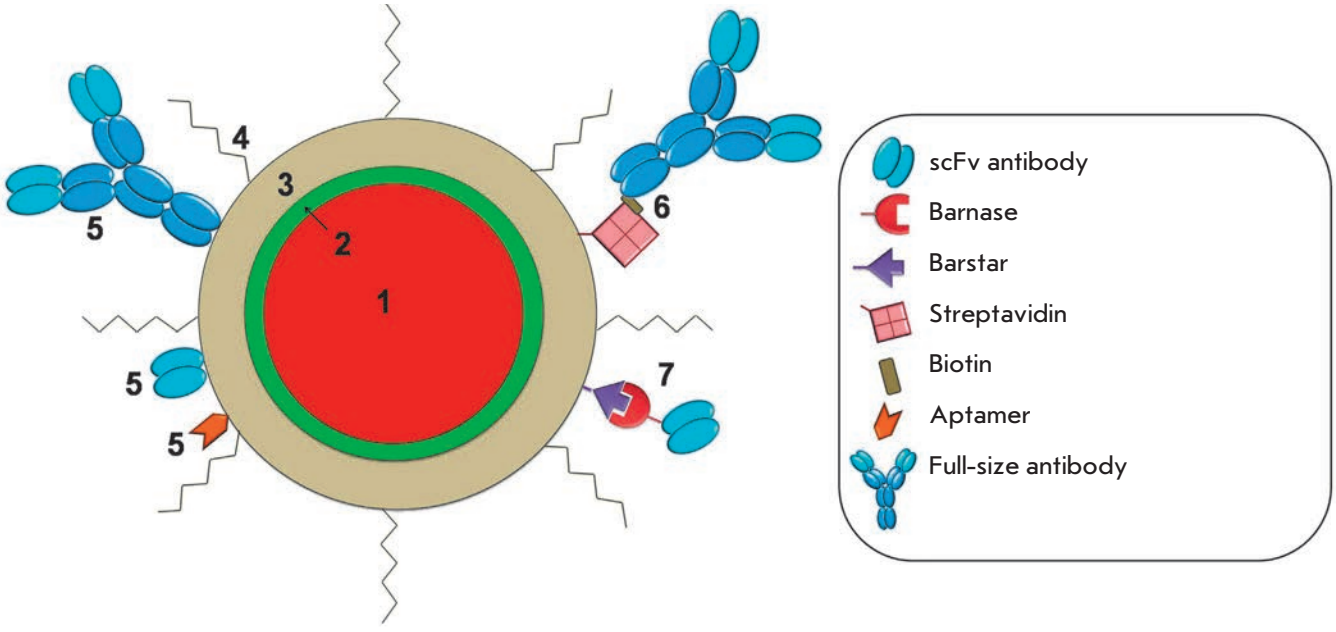

Fig. 2. Design of a current quantum dot for biomedical application. (1) –fluorescent core (usually CdSe or CdTe); (2) - protective shell (usually ZnS); (3) – polymer coating to provide colloidal stability, and direct linkage to biologically active molecules, (4) – PEG, (5) – targeting molecules joined with QD directly or through biotin-streptavidin (6) and barnase-barstar (7) adaptor systems.

its rapid dissociation [26, 27]. Meanwhile, the typically large surface area of QDs makes it possible to attach several scFv molecules to each nanoparticle and create unique multivalent constructions with enhanced properties [28].

Peptides are used as targeting molecules in order to perform specific recognition of certain proteins, with the purpose of imaging cells and their components [29]. The application of this approach in the design of targeted QDs was first demonstrated for short recombinant peptides that were capable of specific recognition of integrin in human neiroblastoma studies [30]. Later, it was proven that this approach could also be used in the specific labeling of the cells of lung endothelium, brain endothelium, and human breast carcinoma both *in vitro* and in living cells [31]. Arginyl-glycyl-aspartic acid (RGD peptide) capable of recognizing integrin has been noted as a good alternative targeting agent for the fluorescing in the IR range QDs during *in vivo* imaging of different tumors in the mouse organism [32].

Another promising targeting agent for the delivery of QDs to tumor cells is aptamers; the specially designed oligonucleotides capable of recognizing certain proteins and cell components and binding to them with high specificity. Various aptamer-based conjugates have been successfully used for cell imaging and recognition, biomarker detection, etc. [33]. Conjugates of QDs with the aptamer specific to the PSMA cancer marker selectively stained immobilized and living prostate tumor LNCaP cells and the same cells in a model medium of collagen matrix [34]. It was shown that the use of aptamers as a targeting agent for imaging prostate tumor cells using QDs was equally efficient as using QDs conjugated to anti-PSMA-antibodies, but considerably less expensive [35]. QD-aptamer conjugates can be used in parallel with other targeting agents, such as peptides, for the simultaneous imaging of several oncomarkers [36]. Moreover, the preparation of biotin-conjugated aptamers, which have the ability to bind to any streptavidin-conjugated QDs, provides the possibility to create universal reagents for the two-stage delivery of QDs to tumor cells [33].

2.2 Methods for binding targeting agents to QDs

In contemporary practice, two major approaches to binding the targeting molecules to QDs are used: direct binding (typically covalent) of protein molecules to active groups on the QD surface and adaptor-mediated binding (*Fig. 2*).

Usually, protein molecules are bound directly to the semiconductor part of a nanocrystal (via the SH group or by metal-affine coordination of histidine residues with the zinc atoms of a nanocrystal shell) or to its hydrophilic coating (by conjugation with carboxyl, amine,

and thiol groups using special catalysts; via electrostatic interaction). These methods were thoroughly described in the reviews [5, 37].

The surface area of a nanocrystal is appreciably large and is accessible for the binding of several biological molecules. A range of 2 to 5 protein molecules and more than 50 small molecules (oligonucleotides or peptides) can be bound to one nanoparticle 4 nm in diameter [38]. It should be noted that the reactivity of certain types of biological molecules after direct conjugation with nanocrystals can vary considerably. In particular, although antibodies retain their specificity after conjugation, they lose their affinity considerably [39]. Moreover, direct conjugation of QDs with antibodies requires that the antibody activity in each new conjugate be checked.

The use of so-called "self-assembling adaptors" (small adhesive molecules that bind to each other with high efficiency and specificity but do not form homodimers) is a more promising approach to QD binding to antibodies. The formation of complexes with these small molecules has no considerable effect on antibody affinity and allows us to simply prepare various combinations of antibodies with different specificities to QDs that fluoresce in different ranges, without any additional modifications. Heterodimerization modules that were previously designed for the preparation of recombinant bispecific and multivalent antibodies and for two-stage delivery of therapeutic agents to the tumor are used as adaptor molecules to bind QDs to antibodies.

The streptavidin–biotin system is the most well-known and broadly used system among these modules; it possesses a high binding affinity $K_a \sim 10^{-14} - 10^{-15}$ M [40]. Streptavidin is attached to QDs covalently or via electrostatic interactions, which allows them to bind to biotin-conjugated targeting agents. Streptavidin-conjugated QDs were first used for imaging of the tumor marker HER2/neu on the surface of human breast tumor SKBR-3 cells through biotin-conjugated anti-human secondary antibodies and humanized anti-HER2/neu antibodies [16]. A similar three-stage system was used for binding QDs to antibody fragments specific to glycyn receptors on a neuron membrane, making it possible to observe the motion of individual receptors in living neurons [41]. The three-stage system based on the biotin–streptavidin affine pair (primary antibodies; biotinilated secondary antibodies; streptavidin-conjugated quantum dots) allows for the use of single streptavidin-conjugated quantum dots for the imaging of a number of various targets without any additional modification, since the labeling specificity is determined by the corresponding primary and biotinilated secondary antibodies.

By using primary antibodies that bind to QDs via a biotin–streptavidin bridge [11], the number of stages in the labeling process can be reduced to two. This approach is not only used for antibodies, but also for many other targeting agents. Thus, QDs conjugated with an integrin-recognizing peptide via a biotine–streptavidin module have been successfully used for labeling the αv-subunit of integrin in human neuroblastoma cells SK-N-SH [27].

Because of its universal nature, the streptavidin–biotin system is now widely used in certain types of immune diagnostic investigations that use QDs. Streptavidin-conjugated QDs and biotin-conjugated antibodies became commercially available recently (e.g., see www.invitrogen.com). However, it is important to note that the application of this system to create site-directed fluorophores for tumor imaging in a human organism *in vivo* is restricted by the presence of a large quantity of endogenous biotin, which can compete with biotinilated components, thus reducing the labeling efficiency.

In order to prepare antibody-conjugated QDs, we propose the use of a barnase–barstar adaptor module, which has shown good results in the preparation of heterodimeric mini-antibodies and their fluorescent derivatives [26, 42, 43]. This adaptor module is based on the ability of ribonuclease barnase from *Bacillus amyloliquefaciens* to form a very stable complex ($K_d \sim 10^{-14}$ M) with its natural protein inhibitor, barstar [26].

Since the binding regions of barnase and barstar are localized outside their N- and C-terminal parts, each of these proteins is accessible for fusion with scFv antibody fragments. Meanwhile, the binding efficiency of module components is retained. The small dimensions of barnase and barstar (110 and 89 a.a., respectively), stability, good solubility, and stability towards proteases allow to produce appreciable quantities of the desired chimeric proteins in bacterial producers. Moreover, barnase, within recombinant proteins, serves as an intramolecular chaperone, ensuring the correct folding of recombinant proteins, which is particularly important when designing structures with targeting antibodies [44].

The small dimensions and extreme stability over a wide range of conditions make it possible to easily form conjugates of both barnase and barstar with active groups on the QD surface. It was also found that the conjugation of QDs with barstar considerably reduces the non-specific binding of QDs to the cellular membrane. Hence, fluorescent nanocrystals, which usually adhere nonspecifically to human ovarian adenocarcinoma SKOV-3 cells and penetrate them (*Fig. 3A*), become virtually neutral with respect to these cells after conjugation with barstar (*Fig. 3B*). At the same time, the barstar located on the QD surface provides

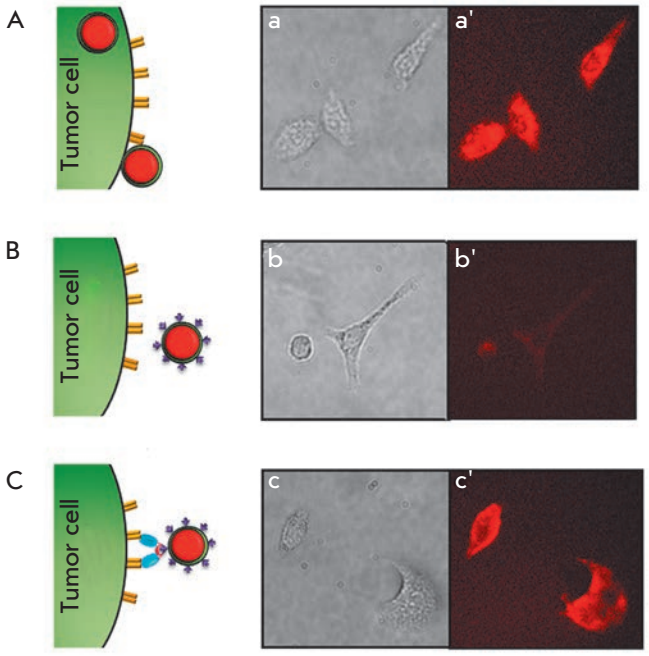

Fig. 3. Non-specific and specific interaction of QDs with tumor cells. Schematics (on the left) and results (on the right) of fluorescent microscopy of SKOV-3 cells after incubation with QD (A), with QD-barstar (B), and with anti-HER-2/neu scFv dimer joined with barnase, following QD-barstar (C). Cell images in visible light (a, b, c) and fluorescent cell images (a', b', c') are shown. Legend see *Fig. 2*.

the additional binding of targeting antibodies using the barnase–barstar adaptor system, ensuring the efficient and specific labeling of cancer cells (*Fig. 3C*).

An important advantage of the barnase–barstar module is the accurate (1 : 1) ratio between the components in the complex and the total absence of self-aggregation, as well as a high interaction affinity, higher than that of all other dimerization systems, with the exception of the streptavidin–biotin system. As opposed to the streptavidin–biotin system, the use of the barnase–barstar system is based on genetic engineering technologies and requires no covalent modifications of antibodies.

The barnase–barstar adaptor system has been successfully used for the preparation of fluorescent complexes for the imaging of tumor cells overexpressing oncomarker HER2/neu, based on 4D5scFv antibodies and QDs of two types 1) QDs modified by mercaptoacetic acid and 2) QDs covered with a polymeric shell [45, 46]. In both of these cases, efficient and selective staining of membranes after the incubation of breast adenocarcinoma cells and human ovarian adenocarcinoma cells with the obtained fluorescent complex was observed.

Furthermore, it was shown that QDs conjugated to targeting antibodies, with the help of adaptors, can be bound to molecules or nanoparticles of a different nature. Thus, they can be regarded as components of a "Molecular Lego kit" [43]. By implementing the conception of such a Lego kit, self-assembling multimodal structures were designed on the basis of the barnase–barstar adaptor module using QDs and magnetic particles. The resulting fluorescent magnetic nanoparticles are supplied with humanized mini-antibodies against the HER2/neu oncomarker and can efficiently and selectively label the corresponding tumor cells [28]. As a result, fluorescence-labeled tumor cells acquire responsiveness to a magnetic field (*Fig. 4*).

2.3 The problem of nonspecific binding of QDs

QD tendency to "adhesion," i.e., nonspecific binding to the cellular membrane, proteins, and components of the extracellular matrix, and their uncontrolled penetration into cells is a significant impediment to selective QD-based fluorescence labeling of biological objects. For example, particles with a strong negative or positive charge containing on their surface carboxyl or amino groups, respectively, were shown to possess a high level of nonspecific binding with cells and tissues [47, 48]. Such nonspecific binding can be explained by the electrostatic interaction between charged groups on the QD surface and the charged regions of proteins and other molecules on the cellular surface.

An additional explanation for the nonspecific binding of QDs with the cellular surface may be the hydrophobic interaction between the lipids in the cellular membrane and the stabilizing agent molecules (e.g., tri-*n*-octylphosphine or oleate anion) that remain on the QD surface after their synthesis due to the incomplete coating of a nanoparticle core with a ligand providing hydrophility, or due to instable binding of this ligand. Thus, it was shown that QDs comprising cysteine, MAA, dihydrolipoic, and other mercapto-carboxylic acids, notable for their dynamic and instable Zn–S bond, exhibit the highest level of nonspecific binding [47].

It was determined that the degree of nonspecific binding strongly depends on the cell type [47, 49], which can be explained by different contents of charged and hydrophobic regions on the membrane of particular cells.

In order to reduce the degree of nonspecific binding, QDs are additionally coated with a layer of inert molecules. One such substances, widely used now, is PEG, a nontoxic hydrophilic polymer commonly used for enhancing the biocompatibility of drugs [48].

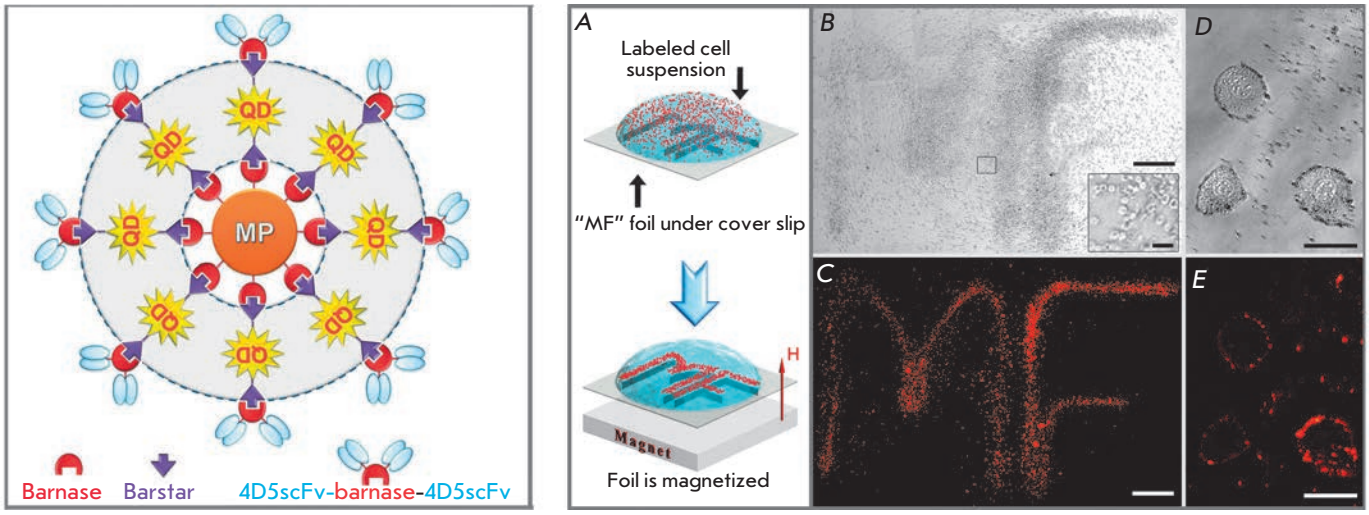

Fig. 4. Superstructures consisting of QDs, magnetic particles (MP), and scFv antibodies. Conceptual design of superstructures based on barnase-barstar adaptor system (on the left), and multifunctionality proving (on the right). Human ovarian cancer SKOV-3 cells labeled by the assembled trifunctional structures were dragged toward the contour of letters "MF" (A). Bright-field (*B* - 100x magnification and D - individual cells) and fluorescent (C - 100x magnification and E - individual cells) photos of the sample. Adapted by permission from the National Academy of Sciences of the United States of America: [Proc. Natl. Acad. Sci. USA] (Nikitin M.P., Zdobnova T.A., Lukash S.V., Stremovskiy O.A., Deyev S.M. Proc Natl Acad Sci USA. 2010 107:5827-5832), copyright (2010).

Quantum dots modified by PEG have a surface charge that is close to neutral and remain colloidally stable under various experimental conditions. Furthermore, PEG reduces the ability of QDs to interact with the cell surface or with the proteins of an extracellular matrix; i.e., it results in the passivation of the QD surface [50].

In the case of PEG-coated QDs, it should be noted that despite the fact that they are successfully used both *in vitro* and *in vivo* experiments, such a modification is not sufficient for some other purposes. Furthermore, PEG-coated particles have a considerably higher hydrodynamic diameter, which impedes their access to biological targets [51].

In order to minimize the nonspecific binding of QDs without increasing their size, a method for coating nanocrystals with a neutral hydroxyl layer was proposed [52]. The hydrodynamic diameter of the resulting nanocrystals is 13–14 nm, which is smaller than the size of PEG-modified nanocrystals by 50%. When using the obtained complexes for HeLa cells imaging, 140-fold and 20-fold reductions of nonspecific binding, in comparison with carboxylated QDs and biotin-conjugated QDs, respectively, were observed. To perform the targeted delivery of such nanocrystals, it is necessary to supply them with targeting molecules, resulting in a partial loss of material and a decrease in the yield of the final product. Meanwhile, it is quite realistic to reduce the nonspecific adhesion of QDs on the cellular membrane and simultaneously provide nonspecific binding of a nanoparticle to certain receptors expressed on the surface of a tumor cell. It was noted that some small neutral molecules, such as peptides or small proteins, enable to reduce the nonspecific binding of QDs [52]. We demonstrated that the component of the adaptor system, barstar, also possesses this property (see above Section 2.2, *Fig. 3*).

3. *In vitro* DIAGNOSTICS

One of the most promising and rapidly developing areas of application of QDs is their usage as fluorescent labels during *in vitro* study of tumor cells: for imaging tumor cells and for localizing the individual molecules expressed in them. The unique properties of QDs, which make it possible to perform multicolor labeling and long-term observation of fluorescence of objects, allow one to considerably broaden the range of conventional methods that are used in this field. *In vitro* diagnostics is now the only application of QDs out of all alternatives of the biomedical use of QDs which can be quickly implemented in clinical practice (as opposed to the *in vivo* use of QDs, which requires long investigations of QD toxicity and further consequences of their introduction into the organism).

The major directions of investigation include: 1) imaging of tumor cells overexpressing certain oncomarkers,

2) staining of tissues and their sections; and 3) observation of individual molecules and cells in real time.

3.1 Imaging of tumor cells

The imaging of tumor cells and identification of the individual oncomarkers within them is of great practical importance. Most of the oncomarkers used for imaging are represented by receptors overexpressed on the membrane surface of tumor cells, and they are almost non-expressed in normal tissues. A high level of expression of such markers correlates with a tumor process in the organism; their detection and quantitative assessment being important for the early diagnostics, classification, and therapy of tumors [51].

Several years after pioneering studies on the design and use of biocompatible QDs were published [14, 15], a few research groups claimed that it was possible to use QD conjugates for the imaging of tumor cells. Thus far, QDs conjugated to various targeting agents (antibodies, ligands, peptides) have been known. They are intended for visualizing the cells of clinically significant human tumors: prostate carcinoma [53], breast adenocarcinoma and ductal carcinoma [21, 54, 55], pancreatic carcinoma [56], glioblastoma [32], and squamous cell carcinoma of the tongue [57].

Efforts in this area have primarily focused on the optimization of the properties of QDs for their application in experiments *in vivo* and at the whole-body level. The preliminary purpose was a good solubility in aqueous solutions, biocompatibility, low toxicity of QDs, and additionally their supplying with targeting molecules providing the specificity of labeling. Over a short period of time, appreciably simple, inexpensive, and well reproducible QD-based methods for the imaging of cancer cells were designed for the diagnostics of clinically significant tumor types and prognosis of the disease's progresson (*Table*). Hence, significant methodical groundwork was laid for implementing these methods in clinical practice and further *in vivo* studies aimed at the imaging of tumors and their metastases directly in the living organism.

3.2 Simultaneous detection of several oncomarkers

Generally, targeting molecules (antigens, peptides, aptamers, etc.) that selectively bind to the surface oncomarker provide a high specificity of labeling of the corresponding tumor cells [17]. At the same time, such a feature of tumor cells as their extreme variability during the development of the disease and response to the action of therapeutic agents raises for researchers the problem of simultaneous imaging of several surface markers (see Section 1).

The fundamental possibility of using QDs for simultaneous multiplex detection was demonstrated on five tumor markers in a human breast tumor cell culture. The simultaneous detection of the receptors ER, PR, EGFR, mTOP, and HER2/neu using QDs fluorescing in different spectrum regions correlates positively with the results of conventional methods; including immunohistochemistry, western blotting, and fluorescence *in situ* hybridization, while it considerably increases the rate of analysis and reduces cost [61].

Simultaneous imaging of two hypothesized cancer markers - integrin $\alpha_v\beta_3$ and nucleolin-using QDs conjugated to the RGD peptide and aptamer AS1411, respectively, enables to compare the localization of these markers in the cell [36]. Internalization of nucleolin and the surface distribution of integrin were confirmed using confocal microscopy, which will probably allow to better understand how they participate in the processes occurring in tumor cells.

The results of these studies demonstrate that QDs conjugated to targeting molecules have a powerful potential as components of novel systems for assessing tumor types, their progression stage, and the metastatic potential on the basis of multiplex imaging.

Fundamental studies of oncological processes, in addition to the detection of the markers that are overexpressed in cancer cells, require that a number of other proteins, frequently characterized by a low-copy number, be revealed. The golden standard today for identifying low-copy number proteins is enzyme-linked immunosorbent assay (ELISA); its sensitivity attains the picomolar value. This method has been widely used; however, it is quite labor-intensive, expensive, time-consuming, and does not allow for multiplexing. The replacement of organic fluorophores and colorimetric reagents in immune enzyme studies by QDs alone does not provide a significant advantage in terms of sensitivity (the sensitivity of the analysis with QDs is ~ 100 pmol) [70]. It is the application of QDs with different spectral characteristics which allows simultaneous detection of several proteins to be performed. Thus, four toxins were simultaneously detected using four different QDs, which emitted between 510 and 610 nm, in a sandwich immunoassay configuration with a single extitation source [70]. Unfortunately, these authors have not managed to carry out the quantitative assessment at this stage; further investigations are required to design a good immunofluorescence test. Another study demonstrated the simplicity and obviousness of the simultaneous detection of two proteins with two spectrally different QDs in a western blot assay [71]. Unquestionably, simultaneous multicolor labeling using QDs is a novel and powerful method that will allow us to solve both conventional and fundamentally new problems that previously could not be solved or were extremely labor-intensive when conventional approaches were used.

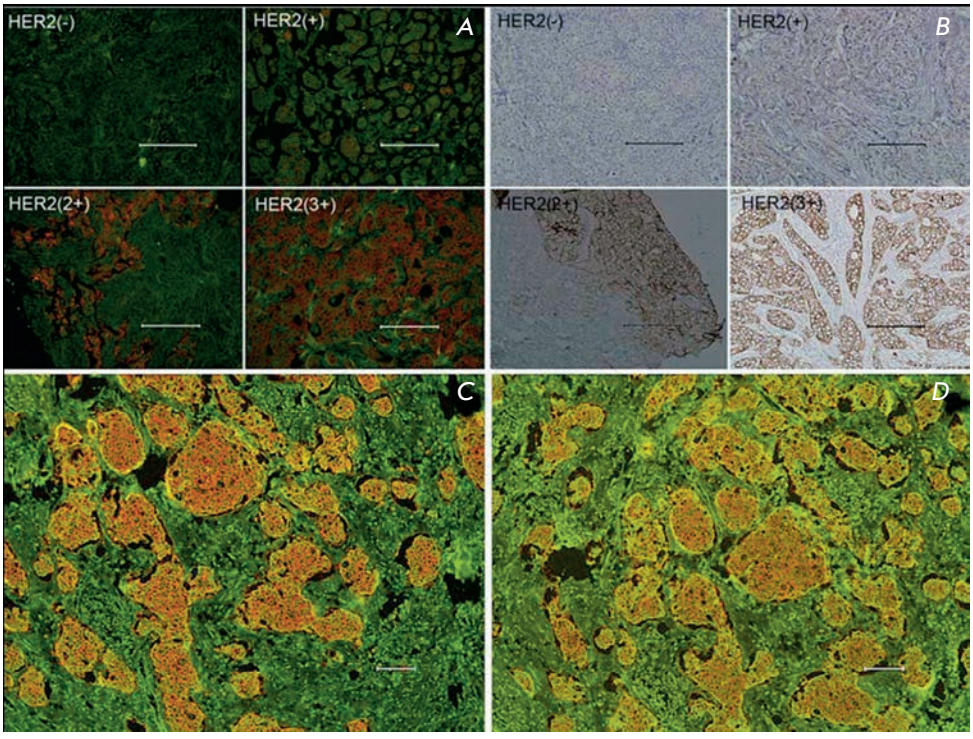

Fig. 5. Advantages of QDs for immunohistochemical assays. A – Specimens with different HER2 IHC scores detected by QD-IHC (A) and by conventional IHC using peroxidase (B). Preservation of QD fluorescence and photobleaching on day 2 (C) and day 75 (D). *Scale bar* 100 μm. Adapted by permission from Elsevier: [Biomaterials] (Chen C, Peng J, Xia H, Yang G, Wu Q, Chen L, Zeng L, Zhang Z, Pang D, Li Y. Biomaterials. 2009 30:2912-2918), copyright (2009).

Simultaneous multiplex labeling using QDs with different spectral characteristics also provides indisputable advantages in studies requiring high-performance screening of molecules. QDs are successfully used for the analysis of various components of cell systems using microarray technology and for the parallel analysis of the genome and proteome content of healthy and affected cells [72]. The brightness and stability of QDs significantly increase the sensitivity and the possibility of parallel detection of the components of complex mixtures. The results obtained can help better understand the signal paths in cells, as well as be used in the design of new therapeutic approaches.

3.3 Immunohistochemical assay

Immunohistochemical assay (IHC) is the method for tumor diagnostics most widely used in clinical practice. This method of morphological study is based on imaging and microscopic evaluation of the results of the antigen–antibody reaction in biopsied tissue sections and allows not only to detect the presence and intensity of a signal, but also to evaluate signal distribution over the cell (staining of the membrane, cytoplasm, nucleus, and other structural elements). Immunochemical staining of formaldehyde-fixed and paraffin-embedded tissue sections of tumor biopsy samples is a complicated task because of high tissue autofluorescence and the reduction of the amount of antigen during the fixation and paraffin embedding.

QDs appeared very well-suited for the resolution of this problem. Images of fixed sections of human skin basal carcinoma [60], mouse breast tumor overexpressing the human receptor HER2/neu [16], and basal-squamous cell carcinoma of human skin [73] were obtained using QDs. It was also demonstrated by the example of the human breast tumor that QD-based probes can be designed for quantitative and highly sensitive detection of the low expression of cancer surface markers, in particular, oncomarker HER2/neu [74]. Researchers have also noted the excellent photostability of QD-stained samples: their fluorescence intensity remains intact for 9–75 days [74] (*Fig. 5*).

The combination of conventional IHC procedures with QD-based fluorescent dyes allows one to considerably improve the resolution and sensitivity of the method (see review [17]) and provides a possibility of simultaneous imaging of several markers [75]. Moreover, the application of QDs makes the IHC method much more illustrative (*Fig. 5*).

3.4 Real-time detection of molecular processes and cells

The high resistance of QDs to photobleaching and their high level of brightness enable us to use them for imaging of the processes occurring in cells, including trac-

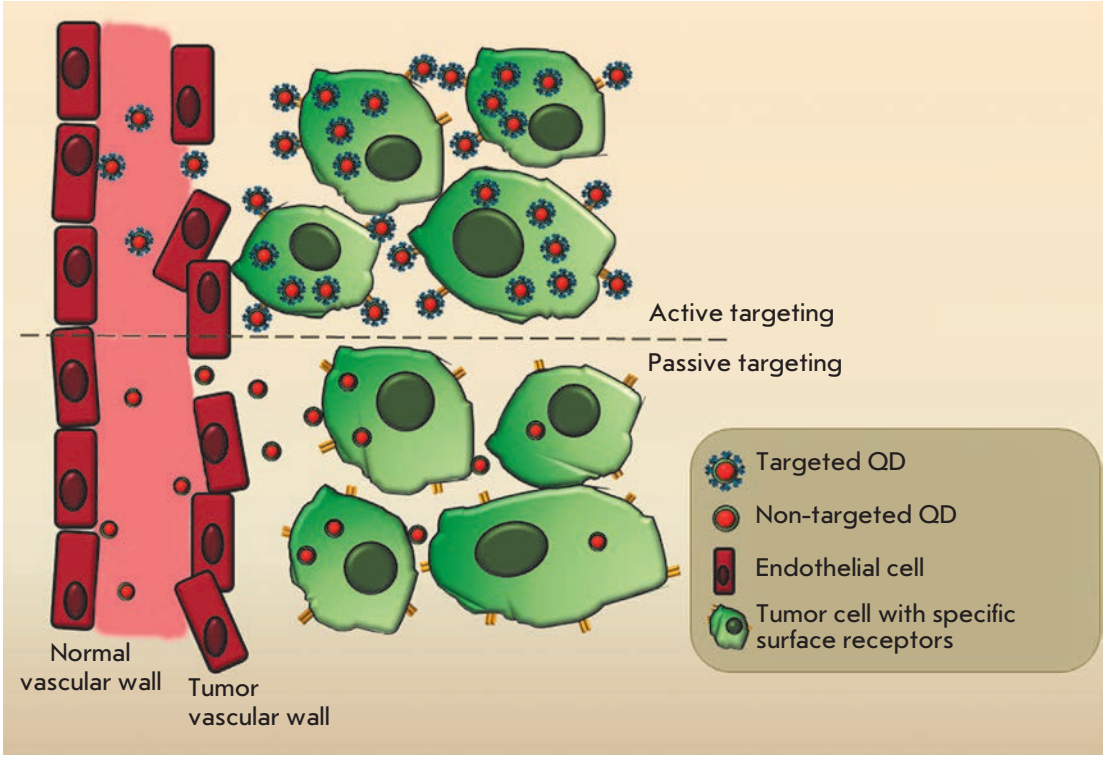

Fig.6. Schematic illustration of passive and active tumor-targeting after system administration of QD.

ing the dynamics of individual molecules [41]. Certain membrane proteins are of special interest; the investigation of their localization and dynamics is crucial in understanding such processes as chemotaxis and inter- and intracellular signal transduction. Thus, QDs conjugated with the corresponding targeting ligands have been successfully used for imaging of the dynamics of the receptors of glycine [12] and γ-amino butyric acid [76] in a neuron cell culture.

Since a vast number of significant oncomarkers are represented by proteins which have regulatory functions in normal cells and which participate in signal transduction, study of the functioning of these proteins is important for understanding the nature and mechanisms of the malignization process. QDs conjugated with an epidermal growth factor (EGF) were used to study the mechanisms of EGF internalization and signal transduction pathways with the participation of proteins from the erbB1/2/3 family of transmembrane tyrokinase receptors [11].

It was demonstrated that QDs can be used to study the motility of tumor cells with the purpose of determining their invasive potential [77]. Use of QDs as markers for imaging of the trajectory of cell motion is less laborious and allows to obtain more reliable data as compared with the conventional Boyden's chamber assay.

These novel and extremely interesting directions of study have as yet not found application in clinical diagnostics; however, they will undoubtedly be developed as a domain of fundamental science and will help to obtain new knowledge on tumor pathogenesis.

4. *In vivo* ANIMAL IMAGING

During the past five years, considerable progress has been made in the application of QDs as fluorophores in experiments on cells and fixed tissues. Meanwhile, the use of these nanoparticles for imaging in multicellular organisms, especially in such highly organized ones as mammals, is only in the early stages of development.

Two major problems emerge during fluorescent labeling at the whole-body level: 1) signal attenuation due to the increased size of the organism and tissue thickness, and 2) the difficulty of delivering fluorophores to the target cells and tissues.

A significant obstacle is the depth of fluorescence penetration, since biological tissues absorb most of the signals that are used for imaging; furthermore, they are characterized by a considerable autofluorescence in the green region of the spectrum. However, in the IR region there exists the so-called "optical window" (650–1300 nm), in which light absorption by living tissues is minimal. The existence of such a window results from the fact that the minimum level of absorption of the major chromophores in mammals (blood, flavins, vitamins, and NAD(P)H) lies in this region [78]. That is why for *in vivo* imaging, QDs fluorescing in the near-

IR region (700–800 nm) are used, allowing to improve the brightness of the resulting signal and to reduce the background.

Fluorophore delivery to target cells in the organism of a mammal is complicated and consists of multiple stages, since the substances being delivered need to penetrate through a number of structural and physiological barriers, including the vascular endothelium, the immune barrier, and the metabolic degradation of the introduced substances. Moreover, after system administration the fluorophore can be delivered via the blood stream into non-target organs and organism tissues and accumulate there, thus reducing the contrast and increasing the possibility of false-positive signals and the manifestation of a toxic effect. Therefore, the excess fluorophore that has not bound to the target cells should be quickly and completely removed from the organism.

4.1 Tumor detection using QDs

In a living organism, accumulation of QDs injected intravenously in tumor tissue for its subsequent imaging is possible through two mechanisms: 1) a passive mechanism, which is typical of particles of a certain size, and 2) an active mechanism, using the targeting agent [53] (*Fig. 6*).

In the case of the passive mechanism, nanometer-sized particles accumulate preferentially at tumor site due to its structural features. Such particles can penetrate into a tumor with ease, due to the increased permeability of vascular walls, and remain there as a result of the impaired lymphatic drainage therein. It has been demonstrated that the capillary permeability of the endothelial barrier in newly vascularized tumors is considerably higher than that in normal tissues. Normal blood vessels are lined with a unfenestrated endothelium; hence, the penetration of macromolecules and nanoparticles into the tissue is impeded. Blood vessels formed during the tumor-induced angiogenesis are characterized by a nontypical structure and wide endothelial pores. These pores are so large that molecules up to 400 nm in size can leave the vessels and accumulate in tumor tissue [79]. Moreover, there is almost no lymphatic drainage in tumor tissue; therefore, macromolecules stay there for a considerable amount of time. The described enhanced permeability and retention effect (EPR) is used for the delivery of therapeutic and diagnostic agents based on latexes, liposomes, and other particles into tumors [80]. In the case of the passive delivery, nontargeted PEG-coated QDs that possess a minimal level of nonspecific binding with proteins and blood cells are used [53].

To provide active delivery of QDs to tumors, they are supplied with targeting molecules capable of binding to the specific receptors exposed on the tumor cell surface (see Section 2.1).

The possibility of intravital labeling of tumors with quantum dots was first demonstrated on mouse models. It was demonstrated that after intravenous administration, QDs conjugated to peptides specific to various types of tumors and their vessels are selectively accumulated in the tumor vasculature [31].

The first progress in the *in vivo* application of QDs has stimulated a large number of studies devoted to the intravital imaging of human model tumors in animal organisms using QDs targeted at different tumor markers. Full-size antibodies and their fragments, specific peptides, and natural ligands were used as targeting ligands with equal success (*Table*). The results of these studies demonstrate that the use of the mechanism of active targeting, as compared with that of passive targeting, considerably enhances QD accumulation in the tumor regardless of the type of QDs employed and of the type of the targeting agent (*Fig. 7*). The use of targeted QDs as fluorophores, in combination with modern optical imaging methods, allows to perform imaging of not only solid tumors, but also metastases in organs [65] and bone tissue [58] and to reveal micrometastases at the early stages of the disease [81]. It should be noted that in all cases, along with successful labeling of tumors *in vivo* using both the active and passive mechanisms, nonspecific accumulation of QDs in different organs of model animals was observed, primarily, in the liver, spleen, and lymph nodes (*Fig. 7*).

In addition, locally introduced QDs can also be of great diagnostic significance. Thus, it was demonstrated that QDs of different colors injected into the peripheral areas of the body were located in different lymph nodes, giving different coloration to them [82]. In recent times, a significant number of studies have been devoted to the imaging of sentinel lymph nodes, along which the metastatic spread typically occurs [83, 84]. Intraoperative imaging of the primary tumor, along with sentinel lymph nodes, provides the possibility of determining the size of the surgery field and the necessity of lymphodissection [85].

The size of QDs and their ability to induce two-photon excitation have prompted researchers to investigate the potential of these particles as promising contrast agents for angiography; possible alternatives to the fluorescent dextrane conventionally used for these purposes. Because of the large cross-section of two-photon absorption (larger than that of conventional organic dyes by 2–3 orders of magnitude), QDs can be excited in the IR range. This fact allows to attain a higher resolution at a great tissue depth (since long waves are less scattered than short waves) and reduce the level of phototoxicity (the exciting photons in the IR region of

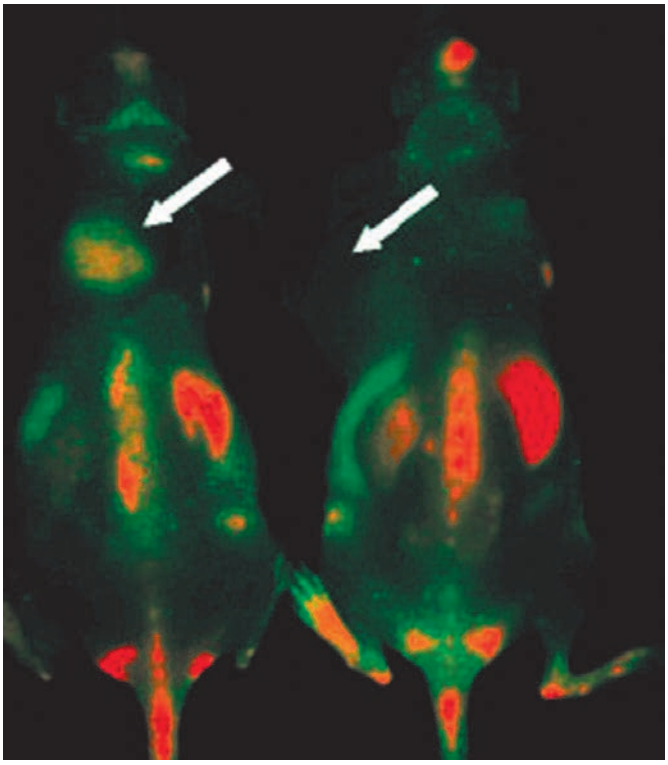

Fig. 7. *In vivo* fluorescence imaging of U87MG tumor-bearing mice (left shoulder, indicated by white arrows) injected with targeted (left) and nontargeted QD (right). The mice autofluorescence is color-coded green, while the unmixed QD signal is color-coded red. Prominent uptake in the liver, bone marrow, and lymph nodes was also visible. Reprinted by permission from the American Chemical Society: [Nano Letters] (Cai W, Shin D.W., Chen K, Gheysens O, Cao Q, Wang S.X., Gambhir S.S., Chen X. Nano Lett. 2006 6:669–676), copyright (2006).

the spectrum possess a lower energy; therefore, they are less destructive for the tissue under investigation) [86]. Indeed, the use of two-photon excitation of QDs for contrasting the blood vessels of tumor cells considerably enhances the imaging contrast, in comparison with conventional methods [87].

Thus, the results of intravital imaging of tumors presented above demonstrate that, due to the high level of absorption by organs of the reticuloendothelial system (RES) and the absence of complete removal from the organism (see Section 5.2 of this review), the clinical application of QDs as contrast agents for *in vivo* imaging is accompanied by certain difficulties. At the same time, the exceptional brightness, high quantum yield, and large cross section of two-photon absorption, which determines the fluorophore brightness in multiphoton microscopy, allow to successfully utilize QDs as imaging agents for the study of the anatomy and pathophysiology of tumors on animal models. The use of QDs considerably improves the existing methods of intravital microscopy of tumors and their microenvironment. The combination of the exceptional spectral properties of QDs and modern technologies that allow us to obtain *in vivo* images with high resolution may result in a considerable breakthrough in the understanding of tumor biology.

4.2 QD biodistribution and pharmacokinetics

The key success factor of *in vivo* diagnostics of tumors are: high fluorophore content in a tumor, in comparison with that found in normal tissues and blood, and the absence of false-positive signals. In addition, it is essential that diagnostic agents be capable of rapid excretion from the organism.

It was demonstrated *in vitro* that the action and biological fate of QDs in the cell depends to a considerable extent on the size and chemical properties of the surface of these particles [88, 89]. The same parameters were assumed to play a significant role in the distribution of QDs in the organism, as well.

When studying the biodistribution of QDs in the organism of model animals, it turned out that all QDs were completely cleared from the bloodstream to accumulate in organs and tissues [90], mostly in RES organs (liver, spleen and lymph nodes). Similar results were obtained in tumor imaging: along with label accumulation in tumor, some QDs also remained in RES organs [25, 31, 32, 53, 65]. Almost in all cases, no QDs were detected in the lung, heart, muscle, or brain tissues; in a number of studies, a small amount of QDs was found in the kidneys. Contrary to expectations, such distribution was independent of surface properties and the type of targeting agent (or the absence of it) conjugated with QD, while the presence of PEG on the particle surface resulted in a slight increase in its blood half-life but did not completely prevent accumulation in these organs. The QD blood half-life varied from several minutes to several tens of hours and depended to a large extent on their hydrodynamic diameter [91], as well as the surface charge and structure [92].

In this context, direct comparison of QDs and the standard organic dye Alexa Fluor 680, both conjugated with anti-IGF1R-antibodies in experiments *in vivo* on model animals, is of interest [55]. It was shown that both fluorophores can allow specific imaging of breast tumor; however, QDs are considerably poorer excreted from the organism, accumulating in RES organs.

The initial results of the investigation of the effect of the size and dimensions of the QD surface on their distribution in the organism after intravenous administration are quite controversial. It was shown in a series of studies that the surface coating [93, 93] and size

[94] have a significant effect on the pharmacokinetics and biodistribution of the particles. Conversely, in the systematic study [95] performed in view of all factors that may have an effect on biodistribution, no significant differences were observed for QDs of different sizes, different charges, and those with the presence or absence of different molecules (albumin, PEG) on the surface – all QDs mostly accumulated in the liver and spleen.

QDs can be excreted from the organism via two paths: via the kidneys and the liver [93, 96]. The excretion path to the largest extent depends on two parameters of the particle: their size and surface coating, which determines the tendency towards adsorption of the proteins of the blood serum [78]. The investigation of the excretion from the organism of specially designed series of QDs of different sizes and with different coatings [59] demonstrated that one of the required condition for the full excretion of nanoparticles from the organism via the kidneys is a value of the hydrodynamic diameter of a QD less than 5.5 nm (i.e., below the renal filtration threshold). Currently, all synthesized QDs with fluorescence in red and near-IR ranges that are used for *in vivo* imaging possess a higher size value (approximately 10 nm) and cannot be removed from the organism via the kidneys. Moreover, these QDs are coated with a polymer to improve stability and contain charged functional groups and PEG on their surface, which further increases their size. Thus, the hydrodynamic diameter of popular commercial QDs (Invitrogen) is 15–19 nm [82]. There is only a single excretion path for such non-biodegradable QDs: via the liver, with bile. This process is very slow and inefficient; and the long-term stay of nanoparticles in RES organs increases the possibility of QD shell degradation and the rise of a toxic effect. Thus, although QDs are ideally suitable for *in vivo* imaging of tumors in terms of their parameters, with the exception of their hydrodynamic diameter, their accumulation in the liver, spleen, and other RES organs is inevitable. Interestingly, a number of authors mention the renal accumulation of QDs with a hydrodynamic diameter significantly higher than the renal filtration threshold [95, 97]. In the absence of additional studies, it is difficult to say whether these data are an artifact or attest to some other unstudied mechanisms of interaction between nanoparticles and the living organism. Either way, the complicated excretion from the organism remains one of the major impediments to the use of QDs in the human organism.

5. RISKS IN USING QDS IN BIOLOGICAL AND MEDICAL STUDIES

The unique physicochemical properties of QDs make them extremely attractive fluorophores for the *in vivo* imaging of living objects. The pioneering studies in this field began quite recently (less than 10 years ago); in fact the search for a design of QD optimal for these purposes is ongoing. In this regard, QDs that are used by different laboratories strongly differ in such parameters as their size, shape, charge, concentration, oxidation-reduction properties, surface coating, and physical stability. A wide range of these parameters, in combination with various experimental conditions (treatment time, selection of the model cell lines and media, using the same concentration units, the presence or absence of a targeting agent) make it considerably more difficult to compare the published data on QD biosafety and to get a broad outline. Despite this fact, in a field of extremely diverse and controversial information, a number of regularities have been revealed [90, 98].

5.1 QD citotoxicity

The cytotoxic effect of QDs is largely determined by four main factors: the presence of heavy metal ions in their composition, the ability to generate reactive oxygen species (ROS), colloidal instability, and nonspecific interaction with biological molecules [90, 98].

First-generation QDs, consisting only of the fluorescent core (CdTe or CdSe) and stabilized by thiol ligands (e.g., cysteine or MAA), can easily be subjected to oxidation and degradation to release toxic cadmium ions [99] and are capable of inducing ROS formation [100]. Such particles are extremely toxic for culture cells even in small concentration; hence, they are not suitable for investigations on living objects. Second-generation QDs are coated with a shell made of an inert zinc sulfide in order to prevent non-radiative energy dissipation. Moreover, it was found that such a shell actually impedes oxidation and degradation of the fluorescent core and hinders the release of cadmium ions, considerably reducing cytotoxicity. Meanwhile, insufficient colloidal stability is typical of QDs stabilized by an inexpensive and simple method using small thiol ligands [99]. The deposition of such QD aggregates on the cell surface, even without penetration of the cell, may lead to physical damage, functional abnormalities, and as a result, cell death [89]. In principle, second-generation QDs can be used for short-term investigations on cell cultures; however, a significant risk exists when they are used in organisms.

Today, third-generation QDs are used in most biological studies; they are represented by CdSe/ZnS particles coated by a polymeric or silicon shell. These QDs possess a much higher colloidal, chemical, and optical stability as compared with their analogues coated with small ligands. The third-generation QDs manifest some toxicity in cell cultures only under extreme conditions or when used at concentrations that exceed the con-

Human cancer cells imaging using quantum dots

Tumor type	Cell line (model)	Target/ oncomarker	Targeting module	Quantum dots	Imaging method	Comments	Reference
Prostate cancer	C4-2	PSMA	J591 (full-size monoclonal antibody)	CdSe/ZnS core-shell QD coated amphiphilic polymer	Fluorescent microscopy of cells and tissue sections, whole-body *in vivo* imaging using macro-illumination system	Passive and active QD tumor targeting were compared.	[53]*
	LNCaP (carcinoma)		A10 RNA aptamer	Carboxyl core-shell CdSe/ ZnS QD (EviTag)	Confocal microscopy of cells	Authors report the first example of multifunctional nanoparticles (QD-doxorubicin conjugates) for targeted cancer imaging and therapy.	[35]
	C4-2B (bone metastatic carcinoma)		J591	Qdot® 800 Antibody Conjugation Kit (Invitrogen)	Whole-body *in vivo* imaging using IVIS Imaging System	Targeted QD were used successfully for bone metastases detection.	[58]*
	LNCaP		GPI peptide	Cysteine-coated CdSe/ ZnCdS core-shell QD, PEGylated	Fluorescent microscopy of cells, intraoperative fluorescent *post mortem* imaging of internal organs	Small IR QDs for in vivo imaging were created.	[59]*
		$\alpha_v\beta_3$ integrin	RGD peptide				
Breast cancer	MDA-MB-435 (ductal carcinoma)	Endothelium of tumor blood vessels	GFE and LyP-1 peptides	MAA-coated CdSe/ZnS core-shell QD	Confocal microscopy of cells and tissue sections	Authors postulated that QD PEGylation prevents nonselective accumulation of QD in RES.	[31]*
	SKBR-3 (adenocarcinoma)	HER2/neu	Trastuzumab/ Herceptin® (humanized monoclonal full-size antibody)	Carboxyl CdSe/ZnS core-shell QD stabilized with amphiphilic polymer (Quantum Dot Corporation)	Fluorescent microscopy of fixed cells	QDs were used to label different types of targets at different subcellular locations and with different types of specimens (cultured live cells, fixed cells, and tissue sections).	[16]
	MCF-7	p-glycoprotein	Anti-p-glycoprotein primary antibody and QD-conjugated anti-mouse polyvalent goat secondary antibody	Cysteine-modified CdSe/ ZnS core-shell QD coated with polymer bearing surface amino group	Confocal microscopy of cells, fluorescent IHC	Higher photostability of QD as compared with organic dyes was demonstrated.	[60]
	MDA-MB-435	$\alpha_v\beta_3$ integrin	RGD peptide	Qdot® 705 ITK™ amino (PEG) quantum dots» (Invitrogen)	Fluorescent microscopy of cells	——	[32]
	MCF-7 (adenocarcinoma a), BT-474 (ductal carcinoma)	EGFR, HER2/ neu	Full-size monoclonal antibody	Qdot® Antibody Conjugation Kit (Invitrogen)	Fluorescent microscopy of tissue section	IHC detecting of five tumor markers labeled with QD.	[61]
	KPL-4	HER2/neu	Trastuzumab/ Herceptin®	Qdot® Antibody Conjugation Kits (Invitrogen)	*In vivo* fluorescent microscopy	*In vivo* real-time tracking of single QD after i.v. injection.	[54]*
	SK-BR-3, MCF-7/HER2	HER2	scFv antibody fragment	Carboxyl CdSe/ZnS core-shell polymer-coated QD (Invitrogen)	Fluorescent microscopy and flow cytometry of cells, *in vivo* whole-body imaging using macro-illumination system	Creation of multifunctional structures based on immunoliposome and QD.	[62]
	KPL-4	HER2/neu	Trastuzumab/ Herceptin®	Qdot® 800 Antibody Conjugation Kit (Invitrogen)	*In vivo* fluorescent microscopy	In vivo real-time tracking of single QD after i.v. injection.	[63]*
	MCF-7	IGF1R	AVE-1642 (humanized monoclonal antibody)	Qdot® Antibody Conjugation Kits (Invitrogen)	Fluorescent microscopy, flow cytometry	Detection of expression level of cell surface receptor.	[55]

Liver cancer	HCCLM6 (hepatocellular carcinoma)	AFP	Mouse anti-human AFP monoclonal antibody	CdSe/ZnS core-shell QD modified thioglycolic acid	*In vivo* spectroscopy imaging and *post mortem* confocal microscopy of tumor	Passive and active QD tumor targeting were compared.	[64]*
			Mouse anti-human AFP monoclonal antibody	CdSe/ZnS core-shell QD modified thioglycolic acid	Whole-body in vivo imaging, serum biochemical examination, confocal microscopy of tissue sections, tissue distribution of Cd and Se using ICP-MS quantitative assessment	*In vivo* visualization of tumor and metastases. Cytotoxicity *in vitro*, the acute toxicity *in vivo*, the hemodynamics and quantitative tissue distribution were estimated.	[74]*
Pancreatic cancer	MIA PaCa-2 (carcinoma)	Claudin-4, PSCA	Full-size monoclonal antibody	InP/ZnS core-shell QD modified mercaptosuccinic acid	Whole-body imaging using Maestro macro-illumination system, confocal microscopy of tissue sections	Imaging by non-cadmium-based nontoxic QD	[56]
	MIA PaCa-2	EGFR	scFv antibody fragment	CdSe/ZnS core-shell QD coated amphiphilic polymer with PEG	Confocal microscopy of tissue sections	Tissue distribution of targeted and non-targeted QD was investigated	[25]*
Colorectal cancer	HCT166	EGFR	EGF	Qdot® 800 ITK™ amino (PEG) quantum dots (Invitrogen)	Whole-body *in vivo* imaging using IVIS system, *ex vivo* fluorescent imaging of organs	Three distinct phases of tumor influx, clearance and equilibration of accumulation of targeted and non-targeted QD were observed	[66] *
Cervical cancer	HeLa (adenocarcinoma)	p-glycoprotein	4E3 (full-size monoclonal antibody)	DHLA- modified CdSe/ZnS core-shell QD	Fluorescent microscopy of live nonfixed cells	Long-time preservation of QD fluorescence were demonstrated	[67]
Brain-growth	U-87 MG (glioblastoma)	$\alpha_v\beta_3$ integrin	RGD peptide	Qdot® 705 ITK™ amino (PEG) quantum dots (Invitrogen)	Confocal microscopy of cells and tissue sections. Whole-body *in vivo* imaging using Maestro macro-illuminating system.	Passive and active QD tumor targeting were compared	[32]*
Tongue cancer	Tca8113 (squamous cell carcinoma)	p- glycoprotein	Anti-p-glycoprotein primary antibody, biotinylated anti-mouse polyclonal secondary antibody, streptavidin, biotin-conjugated QD	CdTe core QD modified with thioglycolic acid	Fluorescent microscopy	Imaging using water-synthesized QD	[57]
Ovarium cancer	A431 (squamous cell carcinoma)	EGFR	EGF	QD-streptavidin conjugates (Invitrogen)	Confocal microscopy and flow cytometry of cells	Single-molecule fluorescent imaging using QD	[11]
					Fluorescent microscopy, FRET, AFM		[68]
Naso-pharyngeal cancer	KB (squamous cell carcinoma)	Folate receptor	Folic acid	InP/ZnS	Confocal and two-photon microscopy	Targeted imaging by non-cadmium-based nontoxic QD	[69]

* - whole-body *in vivo* imaging

centration required for staining and imaging of cell targets by an order of magnitude [89, 101]. These QDs are the most promising for use in the organism. However, it should be taken into consideration when designing them that QDs are not molecules but nanoparticles, and that the physicochemical properties of their surface, rather than their composition, are more important factors in toxicity manifestation (the same is true for other nanoparticles). Some bioinert nanoparticles (gold, carbon) have the same toxic effect on cells as QDs. For example, gold nanoparticles and QDs coated with an amphiphilic polymer shell caused the same physical damages to a mammary cell culture and induced detachment from the substrat [89]. Thus, although the additional, secondary stable shell prevents oxidation and degradation of a QD, it may itself contribute to the overall toxicity of the particles [102].

In summary, it should be noted that since the appearance of the first colloidal QDs for biological applications, significant work has been carried out to reduce their toxicity, mainly by using various shells, and the groundwork has been laid for their *in vivo* application.

5.2 *In vivo* toxicity

In vitro investigation of cytotoxicity is an important and necessary stage in the design of QD-based agents for diagnostics and therapy, since it allows accelerating and standartizing the process of selection of particles for *in vivo* application . However, these studies are usually insufficient for QD use in clinical practice. When using QDs for whole-body imaging, it is necessary to take into account not only the colloidal nature and physicochemical properties of the surface of these particles, but also their interaction with the immune system and the possibility of physicochemical damage occurring under aggressive conditions in the organism, with the release of toxic elements from their fluorescent core.

To this point, data on the interaction between the immune system and certain types of nanoparticles (liposome, carbon, gold, magnetic) have been obtained [103]. After intravenous administration, nanoparticles were shown to become rapidly subjected to opsonization and subsequent phagocytosis by the cells of the immune system. Moreover, their injection into the blood may result in thrombocyte aggregation, activation of the complement system, and stimulation or suppression of the immune system [103]. With regard to QDs, there has been very little experimental data collected on this topic. It could be assumed that the interaction between QDs and the immune system cells is similar to the interaction that is typical of other nanoparticles. Indeed, it was shown by Japanese researchers [104] that QDs both *in vitro* and *in vivo* do not induce an increase in cytokine production by $CD4^+$ T lymphocytes, but that they stimulate cell proliferation in the immune system.

The data obtained in the first systematic study of the toxicity and biodistribution of QDs in the organism were published quite recently [95]. Short-term (up to 7 days) and long-term (more than 80 days) biological effects of QDs with different polymeric shells were studied in rat models. The standard clinical biochemical and hematological tests were carried out, as well as histological studies of organs. Contrary to expectations, after intravenous administration of QDs containing carboxyl groups, PEG, or bovine serum albumin on their surface (at a total dosage of 60 nmol/animal introduced within a period of four weeks), no pronounced toxicity was observed for either particle variant.

The researchers studying QD biodistribution in the organism and the possibility of tumor imaging *in vivo* have also repeatedly observed the absence of indicators of acute toxicity in animals, the absence of necroses, and the retention of tissue morphology during experiments [86, 93, 96]. However, the possibility of QD accumulation and degradation in the organism does not exclude their latent toxicity and delayed effect.

QD stability inside RES tissues and organs is the subject of intense debate. Some authors have demonstrated that polymer-coated QDs retain their morphology and fluorescent properties in tissues over a long period of time (up to 4 months) without degradation and following the release of potentially toxic constituent elements of QDs [96, 97]. At the same time, the degradation of such particles in the organism, which results in fluorescence variation, was observed in some cases [53]. This process appears quite real, since it was shown in experiments *in vitro* that some ROS sources, such as oxygen peroxide and hypochlorous acid, always present in the cell in small quantities, can pass through the polymeric shell and cause a degradation of the fluorescent core [105]. It is also possible that only a part of QDs is subjected to degradation in the organism, while the other part remains intact; the ratio between these parts is just a matter of time (months or even years) [95].

Thus, no apparent toxicity of QDs in model organisms has been shown. However, the existence of numerous risk factors, insufficiency of data, and the absence of long-term studies prevents us from drawing a final conclusion on whether it is safe to use QDs in the organism. The separate, fragmentary and controversial data on QD toxicity found in studies devoted to the biodistribution of these particles emphasize the necessity of wide investigations that would deal with different systems of organs for an adequate assessment of the risks in the use of QDs *in vivo*.

CONCLUSIONS: PROBLEMS AND POTENTIALS

Quantum dots are a relatively new class of compounds with seemingly immense potential for use in various types of tumor diagnostics, from the microplate assay for oncomarker detection to noninvasive *in vivo* imaging of tumors. The unique physicochemical properties of QDs, easily tunable fluorescence spectra, a high quantum yield (particularly, in the IR region), the possibility of excitation over a wide range of wavelengths and narrow emission fluorescence peaks, large section of two-photon absorption, and resistance to photobleaching, make possible a considerable broadening of the capabilities of modern methods of fluorescence imaging and optical diagnostics. These fluorophores allow one to solve problems that are difficult to overcome using conventional dyes; e.g., simultaneous detection of several markers, long-term real-time observation of molecular processes, and taking images of tumors deep in tissues. However, when performing a number of routine tasks, the problems associated with the colloidal nature of QDs outweigh the advantages provided by their optical properties.

The relatively large surface area of QDs that is accessible for chemical modifications, coupled with the possibility of binding to other molecules and particles, allows to prepare various QD-based multimodule constructions that contain particles of different nature (gold, magnet, diamond, liposome, etc.) in addition to the QDs (*Fig. 3*) [28, 106] and simultaneously possess targeting, diagnostic, and therapeutic properties [107]. These multifunctional nanodevices are intended for simultaneous delivery of an active agent to the tumor whilst monitoring this process [35, 62]. The further optimization of biocompatible QDs will facilitate the development of such innovative approaches in oncology as image-guided surgery, molecular profiling of tumors, as well as personalized diagnostics and therapy [108].

The success of the realization of the high potential of the QD method and its implementation in *in vivo* diagnostics depends on achieving solutions to the following important problems. The first such problem is the necessity of long-term toxicological studies and careful investigation of the delayed effect of QD introduction. Coatings based on polymeric materials have already been designed. They considerably enhance QD bioinertness and appreciably reduced their toxicity. However, because QDs accumulate in reticuloendothelial system organs, their removal from the organism being very slow, how safe it is to use them in a living organism still requires further study. In light of this, two other tasks can be formulated: firstly, the necessity to design a new generation of QDs that would be rapidly removed from the organism, and secondly the study of the effects of a possible introduction of QDs into the environment, whilst ensuring ecological safety upon wide application. Presumably, solving these tasks will lead to the development of new materials and technologies for constructing fluorescent nanoparticles. ●

The studies carried out in the S.M. Deyev's laboratory including development of oligomeric supramolecular complexes for cancer diagnostics and therapy, particularly with use of QDs, were supported by the Russian Foundation for Basic Research (grant № 09-04-01201-a), the Federal Target Program "Research and Developments of the Priority Directions of Scientific and Technological Complex in Russia in 2007–2012", and programs of the Presidium of the Russian Academy of Sciences "Molecular and Cellular Biology" and "Fundaments of Basic Research of Nanotechnologies and Nanomaterials".

REFERENCES

1. Giepmans B.N., Adams S.R., Ellisman M.H., Tsien R.Y. // Science. 2006. V. 312. № 5771. P. 217–224.
2. Chudakov D.M., Lukyanov S., Lukyanov K.A. // Trends Biotechnol. 2005. V. 23. № 12. P. 605–613.
3. Shcherbo D., Murphy C.S., Ermakova G.V., Solovieva E.A., Chepurnykh T.V., Shcheglov A.S., Verkhusha V.V., Pletnev V.Z., Hazelwood K.L., Roche P.M., Lukyanov S., Zaraisky A.G., Davidson M.W., Chudakov D.M. // Biochem. J. 2009. V. 418. № 3. P. 567–754.
4. Wang C., Gao X., Su X. // Anal. Bioanal. Chem. 2010. V. 397. № 4. P. 1397–1415.
5. Oleinikov V.A., Sukhanova A.V., Nabiev I.R. // Nanotechnologies in Russia. 2007. V. 2. № 1-2. P. 160-173.
6. Resh-Genger U., Grabolle1 M., Cavaliere-Jaricot S., Nitschke R., Nann T. // Nat. Methods. 2008. V. 5. № 9. P. 763–775.
7. Alivisatos P. // Nature Biotechnol. 2004. V. 22. № 1. P. 47–52.
8. Medintz I.L., Uyeda H.T., Goldman E.R., Mattoussi H. // Nat. Mater. 2005. V. 4. № 6. P. 435–446.
9. Dabbousi B.O., Rodriguez-Viejo J., Mikulec F.V., Heine J.R., Mattoussi H., Ober R., Jensen K. F., Bawendi M.G. // J. Phys. Chem. B. 1997. V. 101. № 46. P. 9463–9475.
10. Parak W.J., Gerion D., Pellegrino T., Zanchet D., Micheel C., Williams S.C., Alivisatos A.P., Boudreau R., Le Gros M.A., Larabell C.A. // Nanotech. 2003. V. 14. № 7. R15–R27. doi: 10.1088/0957-4484/14/7/201.
11. Lidke D.S., Nagy P., Heintzmann R., Arndt-Jovin D.J., Post J.N., Grecco H.E., Jares-Erijman E.A., Jovin T.M. // Nat. Biotechnol. 2004. V. 22. № 2. P. 198–203.
12. Dahan M., Levi S., Luccardini C., Rostaing P., Riveau B., Triller A. // Science. 2003. V. 302. № 5644. P. 442–445.
13. Tholouli E., Hoyland J.A., Di Vizio D., O'Connell F., Macdermott S.A., Twomey D., Levenson R., Yin J.A., Golub T.R., Loda M., Byers R. // Biochem. Biophys. Res. Commun. 2006. V. 348. № 2. P. 628–636.

14. Chan W.C., Nie S. // Science. 1998. V. 281. № 5385. P. 2016–2018.
15. Bruchez M.Jr., Moronne M., Gin P., Weiss S., Alivisatos A.P. // Science. 1998. V. 281. № 5385. P. 2013–2016.
16. Wu M.X., Liu H., Haley K.N., Treadway J.A., Larson J.P., Ge N., Peale F., Bruchez M. // Nat. Biotechnol. 2003. V. 21. № 1. P. 41–46.
17. Smith A.M., Dave S., Nie S., True L., Gao X. // Expert Rev. Mol. Diagn. 2006. V. 6. № 2. P. 231–244.
18. Deyev S.M., Lebedenko E.N. // Acta Naturae. 2009. V. 1. № 1. P. 32–50.
19. Bird R.E., Hardman K.D., Jacobson J.W., Johnson S., Kaufman B.M., Lee S.M., Lee T., Pope S.H., Riordan G.S., Whitlow M. // Science. 1988. V. 242. № 4877. P. 423–426.
20. Pack P., Plückthun A. // Biochemistry. 1992. V. 31. № 6. P. 1579–1584.
21. Wu A.M., Yazaki P.J. // Q. J. Nucl. Med. 2000. V. 44. № 3. P. 268–283.
22. Edelweiss E., Balandin T.G., Ivanova J.L., Lutsenko G.V., Leonova O.G., Popenko V.I., Sapozhnikov A.M., Deyev S.M. // PLoS ONE. 2008. V. 3. № 6. P. e2434.
23. Balandin T.G., Edelweiss E., Andronova N.V., Treshalina E.M., Sapozhnikov A.M., Deyev S.M. // Invest. New Drugs. 2009. DOI 10.1007/s10637-009-9329-2.
24. Serebrovskaya E.O., Edelweiss E.F., Stremovskiy O.A., Lukyanov K.A., Chudakov D.M., Deyev S.M. // Proc. Natl. Acad. Sci. USA. 2009. V. 106. № 23. P. 9221–9225.
25. Yang L., Mao H., Wang Y.A., Cao Z., Peng X., Wang X., Duan H., Ni C., Yuan Q., Adams G., Smith M.Q., Wood W.C., Gao X., Nie S. // Small. 2009. V. 5. № 2. P. 235–243.
26. Deyev S.M., Waibel R., Lebedenko E.N., Schubiger A.P., Plückthun A. // Nat. Biotechnol. 2003. V. 21. № 12. P. 1486–1492.
27. Deyev S.M., Lebedenko E.N. // Bioessays. 2008. V. 30. № 9. P. 904–918.
28. Nikitin M.P., Zdobnova T.A., Lukash S.V., Stremovskiy O.A., Deyev S.M. // Proc. Natl. Acad. Sci. USA. 2010. V. 107. № 13. P. 5827–5832.
29. Zhou M., Ghosh I. // Biopolymers. 2007. V. 88. № 3. P. 325–339.
30. Winter J.O., Liu T.Y., Korgel B.A., Schmidt C.E. // Adv. Mater. 2001. V. 13. № 22. P. 1673–1677.
31. Akerman M.E., Chan W.C., Laakkonen P., Bhatia S.N., Ruoslahti E. // Proc. Natl. Acad. Sci. USA. 2002. V. 99. № 20. P. 12617–12621.
32. Cai W., Shin D.W., Chen K., Gheysens O., Cao Q., Wang S.X., Gambhir S.S., Chen X. // Nano Lett. 2006. V. 6. № 4. P. 669–676.
33. Zhang J., Jia X., Lv X.J., Deng Y.L., Xie H.Y. // Talanta. 2010. V. 81. № 1–2. P. 505–509.
34. Chu T.C., Shieh F., Lavery L.A., Levy M., Kortum R.R., Korgel B.A., Ellington A.D. // Biosens. Bioelectron. 2006. V. 21. № 10. P. 1859–1866.
35. Bagalkot V., Zhang L., Levy-Nissenbaum E., Jon S., Kantoff P.W., Langer R., Farokhzad O.C. // Nano Lett. 2007. V. 7. № 10. P. 3065–3070.
36. Ko M.H., Kim S., Kang W.J., Lee J.H., Kang H., Moon S.H., Hwang D.W., Ko H.Y., Lee D.S. // Small. 2009. V. 5. № 10. P. 1207–1212.
37. Smith A.M., Duan H., Mohs A.M., Nie S. // Adv. Drug. Deliv. Rev. 2008. V. 60. № 11. P. 1226–1240.
38. Chan W.C., Maxwell D.J., Gao X., Bailey R.E., Han M., Nie S. // Curr. Opin. Biotechnol. 2002. V. 13. № 1. P. 40–46.
39. Pathak S., Davidson M.C., Silva G.A. // Nano Lett. 2007. V. 7. № 7. P. 1839–1845.
40. Green N.M. // Methods Enzymol. 1990. V. 184. P. 51–67.
41. Dahan M. // Histochem. Cell Biol. 2006. V. 125. № 5. P. 451–456.
42. Lebedenko E.N., Balandin T.G., Edelweiss E.F., Georgiev O., Moiseeva E.S., Petrov R.V., Deyev S.M.// Dokl Biochem Biophys. 2007. V. 414. P. 120-123.
43. Deyev S.M., Lebedenko E.N. // Russian Journal of Bioorganic Chemistry. 2009. V. 35. № 6. P. 685-701.
44. Martsev S.P., Tsybovsky Y.I., Stremovskiy O.A., Odintsov S.G., Balandin T.G., Arosio P., Kravchuk Z.I., Deyev S.M. // Protein Eng. Des. Sel. 2004. V. 17. № 1. P. 85–93.
45. Zdobnova T.A., Dorofeev S.G., Tananaev P.N., Vasiliev R.B., Balandin T.G., Edelweiss E.F., Stremovskiy O.A., Balalaeva I.V., Turchin I.V., Lebedenko E.N., Zlomanov V.P., Deyev S.M. // J. Biomed. Opt. 2009. V. 14. № 2. P. 021004.
46. Zdobnova T.A., Dorofeev S.G., Tananaev P.N., Zlomanov V.P., Stremovskiy O.A., Lebedenko E.N., Balalaeva I.V., Deyev S.M., Petrov R.V. // Dokl. Biochem. Biophys. 2010. V. 430. P. 41-44.
47. Bentzen E.L., Tomlinson I.D., Mason J., Gresch P., Warnement M.R., Wright D., Sanders-Bush E., Blakely R., Rosenthal S.J. // Bioconjug. Chem. 2005. V. 16. № 6. P. 1488–1494.
48. Duan H., Nie S. // J. Am. Chem. Soc. 2007. V. 129. № 11. P. 3333–3338.
49. Belyaeva T.N., Salova A.V., Leontieva E.A., Mozhenok T.P., Kornilova E.S., Krolenko S.A. // Cell and Tissue Biology. 2009. V. 3. № 6. P. 551-558.
50. Kelf T.A., Sreenivasan V.K., Sun J., Kim E.J., Goldys E.M., Zvyagin A.V. // Nanotechnology. 2010. V. 21. № 28. e285105.
51. Xing Y., Chaudry Q., Shen C., Kong K.Y., Zhau H.E., Chung L.W., Petros J.A., O'Regan R.M., Yezhelyev M.V., Simons J.W., Wang M.D., Nie S.M. // Nat. Protoc. 2007. V. 2. № 5. P. 1152–1165.
52. Kairdolf B.A., Mancini M.C., Smith A.M., Nie S. // Anal. Chem. 2008. V. 80. № 8. P. 3029–3034.
53. Gao X., Cui Y., Levenson R.M., Chung L.W., Nie S. // Nat. Biotechnol. 2004. V. 22. № 8. P. 969–976.
54. Tada H., Higuchi T.M., Wanatabe N., Ohuchi N. // Cancer Res. 2007. V. 67. № 3. P. 1138–1144.
55. Zhang H., Sachdev D., Wang C., Hubel A., Gaillard-Kelly M., Yee D. // Breast Cancer Res Treat. 2009. V. 114. № 2. P. 277–285.
56. Yong K.-T., Ding H., Roy I., Law W.-C., Bergey E.J., Maitra A., Prasad P.N. // ACS Nano. 2009. V. 3. № 3. P. 502–510.
57. Li Z., Wang K., Tan W., Li J., Fu Z., Ma C., Li H., He X., Liu J. // Anal. Biochem. 2006. V. 354. № 2. P. 169–174.
58. Shi C., Zhu Y., Xie Z., Qian W., Hsieh C.L., Nie S., Su Y., Zhau H.E., Chung L.W. // Urology. 2009. V. 74. № 2. P. 446–451.
59. Choi H.S., Liu W., Liu F., Nasr K., Misra P., Bawendi M.G., Frangioni J.V. // Nat. Nanotechnol. 2010. V. 5. № 1. P. 42–47.
60. Sukhanova A., Devy J., Venteo L., Kaplan H., Artemyev M., Oleinikov V., Klinov D., Pluot M., Cohen J.H., Nabiev I. // Anal. Biochem. 2004. V. 324. № 1. P. 60–67.
61. Yezhelyev M.V., Al-Hajj A., Morris C., Marcus A.I., Liu T., Lewis M., Cohen C., Zrazhevskiy P., Simons J.W., Rogatko A., Nie S., Gao X., O'Regan R.M. // Adv. Mater. 2007. V. 19. № 20. P. 3146–3151.
62. Weng K.C., Noble C.O., Papahadjopoulos-Sternberg B., Chen F.F., Drummond D.C., Kirpotin D.B., Wang D., Hom Y.K., Hann B., Park J.W. // Nano Lett. 2008. V. 8. № 9. P. 2851–2857.
63. Takeda M., Tada H., Higuchi H., Kobayashi Y., Kobayashi

M., Sakurai Y., Ishida T., Ohuchi N. // Breast Cancer. 2008. V. 15. № 2. P. 145–152.
64. Yu X., Chen L.D., Li K.Y., Li Y., Xiao S., Luo X., Liu J., Zhou L., Deng Y.L., Pang D.W., Wang Q.Q. // J. Biomed. Opt. 2007. V. 12. № 1. P. 014008.
65. Chen L.D., Liu J., Yu X.F., He M., Pei X.F., Tang Z.Y., Wang Q.Q., Pang D.W., Li Y. // Biomaterials. 2008. V. 29. № 31. P. 4170–4176.
66. Diagaradjane P., Orenstein-Cardona J.M., Colón-Casasnovas N.E., Deorukhkar A., Shentu S., Kuno N., Schwartz D.L., Gelovani J.G., Krishnan S. // Clin. Cancer Res. 2008. V. 14. № 3. P. 731–741.
67. Jaiswal J.K., Mattoussi H., Mauro J.M., Simon S.M. // Nat. Biotechnol. 2003. V. 21. № 1. P. 47–51.
68. Kawashima N., Nakayama K., Itoh K., Itoh T., Ishikawa M., Biju V. // Chemistry. 2010. V. 16. № 4. P. 1186–1192.
69. Bharali D.J., Lucey D.W., Jayakumar H., Pudavar H.E., Prasad P.N. // J. Am. Chem. Soc. 2005. V. 127. № 32. P. 11364–11371.
70. Goldman E.R., Clapp A.R., Anderson G.P., Uyeda H.T., Mauro J.M., Medintz I.L., Mattoussi H. // Anal. Chem. 2004. V. 76. № 3. P. 684–688.
71. Makrides S.C., Gasbarro C., Bello J.M. // Biotechniques. 2005. V. 39. № 4. P. 501–506.
72. Rousserie G., Sukhanova A., Even-Desrumeaux K., Fleury F., Chames P., Baty D., Oleinikov V., Pluot M., Cohen J.H., Nabiev I. // Crit. Rev. Oncol. Hematol. 2010. V. 74. № 1. P. 1–15.
73. Estrada C.R., Salanga M., Bielenberg D.R., Harrell W.B., Zurakowski D., Zhu X., Palmer M.R., Freeman M.R., Adam R.M. // Cancer Res. 2006. V. 66. № 6. P. 3078–3086.
74. Chen C., Peng J., Xia H., Yang G., Wu Q., Chen L., Zeng L., Zhang Z., Pang D., Li Y. // Biomaterials. 2009. V. 30. № 15. P. 2912–2918.
75. Fountaine T.J., Wincovitch S.M., Geho D.H., Gargield S.H., Pittaluga S. // Mod. Pathol. 2006. V. 19. № 9. P. 1181–1191.
76. Bouzigues C., Lévi S., Triller A., Dahan M. // Methods Mol. Biol. 2007. V. 374. P. 81–91.
77. Parak W.J., Boudreau R., Gros M.L., Gerion D., Zanchet D., Micheel C.M., Williams S.C., Alivisatos A.P., Larabell C.A. // Adv. Mater. 2002. V. 14. № 12. P. 882–885.
78. Frangioni J.V. // Curr. Opin. Chem. Biol. 2003. V. 7. № 5. P. 626–634.
79. Jain R.K. // J. Control. Release. 2001. V. 74. № 1–2. P. 7–25.
80. Maeda H., Wu J., Sawa T., Matsumura Y., Hori K. // J. Control. Release. 2000. V. 65. № 1–2. P. 271–284.
81. Mahmoud W., Sukhanova A., Oleinikov V., Rakovich Y.P., Donegan J.F., Pluot M., Cohen J.H., Volkov Y., Nabiev I. // Proteomics. 2010. V. 10. № 4. P. 700–716.
82. Kobayashi H., Hama Y., Koyama Y., Barrett T., Regino C.A., Urano Y., Choyke P.L. // Nano Lett. 2007. V. 7. № 6. P. 1711–1716.
83. Luciani A., Itti E., Rahmouni A., Meignan M., Clement O. // Eur. J. Radiol. 2006. V. 58. № 3. P. 338–344.
84. Ravizzini G., Turkbey B., Barrett T., Kobayashi H., Choyke P.L. // Wiley Interdiscip. Rev. Nanomed. Nanobiotechnol. 2009. V. 1. № 6. P. 610–623.
85. Kim S., Lim Y.T., Soltesz E.G., De Grand A.M., Lee J., Nakayama A., Parker J.A., Mihaljevic T., Laurence R.G., Dor D.M., Cohn L.H., Bawendi M.G., Frangioni J.V. // Nat. Biotechnol. 2004. V. 22. № 1. P. 93–97.
86. Larson D.R., Zipfel W.R., Williams R.M., Clark S.W., Bruchez M.P., Wise F.W., Webb W.W. // Science. 2003. V. 300. № 5624. P. 1434–1436.
87. Stroh M., Zimmer J.P., Duda D.G., Levchenko T.S., Cohen K.S., Brown E.B., Scadden D.T., Torchilin V.P., Bawendi M.G., Fukumura D., Jain R.K. // Nat. Med. 2005. V. 11. № 6. P. 678–682.
88. Lovric J., Cho S.J., Winnik F.M., Maysinger D. // Chem. Biol. 2005. V. 12. № 11. P. 1227–1234.
89. Kirchner C., Liedl T., Kudera S., Pellegrino T., Javier A.M., Gaub H.E., Stolzle S., Fertig N., Parak W.J. // Nano Lett. 2005. V. 5. № 2. P. 331–338.
90. Pelley J.L., Daar A.S., Saner M.A. // Toxicol. Sci. 2009. V. 112. № 2. P. 276–296.
91. Choi H.S., Liu W., Misra P., Tanaka E., Zimmer J.P., Itty Ipe B., Bawendi M.G., Frangioni J.V. // Nat. Biotechnol. 2007. V. 25. № 10. P. 1165–1170.
92. Campbell R.B., Fukumura D., Brown E.B., Mazzola L.M., Izumi Y., Jain R.K., Torchilin V.P., Munn L.L. // Cancer Res. 2002. V. 62. № 23. P. 6831–6836.
93. Fischer H., Liu L., Pang K.S., Chan W. // Adv. Funct. Mater. 2006. № 10. V. 16. P. 1299–1305.
94. Schipper M.L., Iyer G., Koh A.L., Cheng Z., Ebenstein Y., Aharoni A., Keren S., Bentolila L.A., Li J., Rao J., Chen X., Banin U., Wu A.M., Sinclair R., Weiss S., Gambhir S.S. // Small. 2009. V. 5. № 1. P. 126–134.
95. Hauck T.S., Anderson R.E., Fischer H.C., Newbigging S., Chan W.C. // Small. 2010. № 1. V. 6. P. 138–144.
96. Ballou B., Lagerholm B.C., Ernst L.A., Bruchez M.P., Waggoner A.S. // Bioconjug. Chem. 2004. V. 15. № 1. P. 79–86.
97. Yang R.H., Chang L.W., Wu J.P. // Environ. Health. Perspect. 2007. V. 115. № 9. P. 1339–1343.
98. Hardman R. // Environ. Health Perspect. 2006. V. 114. № 2. P. 165–172.
99. Aldana J., Wang Y.A., Peng X. // J. Am. Chem. Soc. 2001. V. 123. № 36. P. 8844–8850.
100. Haram S.K., Quinn B.M., Bard A.J. // J. Am. Chem. Soc. 2001. V. 123. № 36. P. 8860–8861.
101. Zhang T., Stilwell J.L., Gerion D., Ding L., Elboudwarej O., Cooke P.A., Gray J.W., Alivisatos A.P., Chen F.F. // Nano Lett. 2006. V. 6. № 4. P. 800–808.
102. Rzigalinski B.A., Strobl J.S. // Toxicol. Appl. Pharmacol. 2009. V. 238. № 3. P. 280–288.
103. Dobrovolskaia M.A., McNeil S.E. // Nat. Nanotechnol. 2007. V. 2. № 8. P. 469–478.
104. Hoshino A., Hanada S., Manabe N., Nakayama T., Yamamoto K. // IEEE Trans. Nanobioscience. 2009. V. 8. № 1. P. 51–57.
105. Mancini M.C., Kairdolf B.A., Smith A.M., Nie S. // J. Am. Chem. Soc. 2008. V. 130. № 33. P. 10836–10837.
106. Kim J., Piao Y., Hyeon T. // Chem. Soc. Rev. 2009. V. 38. № 2. P. 372–390.
107. Biju V., Mundayoor S., Omkumar R.V., Anas A., Ishikawa M. // Biotechnol. Adv. 2010. V. 28. № 2. P. 199–213.
108. Zrazhevskiy P., Gao X. // Nano Today. 2009. V. 4. № 5. P. 414–428.
109. Generalova A.N., Sizova S.V., Zdobnova T.A., Zarifullina M.M., Artemyev M.V., Baranov A.V., Oleinikov V.A., Zubov V.P., Deyev S.M. // Nanomedicine. 2011. V. 6. № 2. P. 195–209.

Assays for Detection of Telomerase Activity

D. A. Skvortsov, M. E. Zvereva, O.V. Shpanchenko, O. A. Dontsova
Faculty of Chemistry, Lomonosov Moscow State University
*E-mail: skvorratd@mail.ru
Received 02.11.2010

ABSRACT **Progressive loss of the telomeric ends of chromosomes caused by the semi-conservative mechanism of DNA replication is an important timing mechanism which controls the number of cells doubling. Telomerase is an enzyme which elongates one chain of the telomeric DNA and compensates for its shortening during replication. Therefore, telomerase activity serves as a proliferation marker. Telomerase activity is not detected in most somatic cells, with the exception of embryonic tissues, stem cells, and reproductive organs. In most tumor cells (80–90%), telomerase is activated and plays the role of the main instrument that supports the telomere length, which can be used for the diagnostics of neoplastic transformation. This is the primary reason why assays regarding the development of telomerase activity have attracted the attention of researchers. Telomerase activity testing may be useful in the search for telomerase inhibitors, which have the potential to be anti-cancer drugs. Moreover, telomerase activation may play a positive role in tissue regeneration; e.g., after partial removal of the liver or cardiac infarction.**

All telomerase activity detection assays can be divided into two large groups: those based on direct detection of telomerase products, and those based on different systems of amplification of the signals from DNA that yield from telomerase. The methods discussed in this review are suitable for testing telomerase activity in different samples: in protozoa and mammalian cells, mixed cellular populations, and tissues.

KEYWORDS **telomerase, telomerase activity assay, tumor diagnostics, physicochemical methods, polymerase activity assay, DNA determination.**

WHAT IS TELOMERASE AND WHY DO WE NEED TO DETERMINE ITS ACTIVITY?

In 1961, Hayflick and Moorhead demonstrated that a somatic cell culture has a limited life period (the Hayflick limit) [1]. In 1973, Olovnikov postulated that the number of cell divisions can be determined by the shortening of the telomeric ends of chromosomes [2], which play the role of a timing mechanism in cells. Telomeres protect the cell genome against degradation and participate in the meiotic pairing of chromosomes and the regulation of the transcription of the genes located in the pretelomeric region [3, 4]. Present in immortalized cells (with the ability of infinite division) is a mechanism that compensates for telomere shortening. In 1985, Blackburn and Greider discovered telomerase, an enzyme that elongates one of the telomere chains [5].

Telomerase is an RNA–protein complex; its main components are an RNA-matrix for telomere synthesis (TERC), which also has a structural function, and reverse transcriptase (TERT) [6]. The telomerase complex (telomerase) binds with a telomere or an oligonucleotide, the sequence of which may differ from the telomere sequence (telomere-imitating oligonucleotide), and synthesizes a short DNA fragment (in mammals, GTTAGG). Next, telomerase moves to the telomeric end (translocation) and again synthesizes a DNA fragment (*Fig. 1*). Telomerase activity is proportional to the total amount of DNA that it synthesizes, while the processivity is in proportion to the length of the fragments synthesized.

Telomerase activity is a marker of the proliferative activity of cells. Telomerase components may perform functions that are independent of the arrangement of the active complex. For example, hTERT (human TERT), regardless of the presence of hTERC (human TERC), may function as an RNA-dependent RNA-polimerase [7]. An enhancement of hTERC expression does not necessarily coincide with the emergence of telomerase activity [8]. hTERC inhibits protein kinase ATR, the targets of which are the known tumor growth suppressor p53 and CHK1 protein kinase at a checkpoint control, which is part of the system of signal transmission from the damaged DNA. A decrease in the hTERC level leads to stoppage of the cell cycle at G1 and G2 phases as a result of the activation of the p53 protein and CHK1 protein kinase. However, the mechanism of this activity has yet to be revealed [9].

Telomerase activity has not been detected in the vast majority of normal human cells; however, it manifests

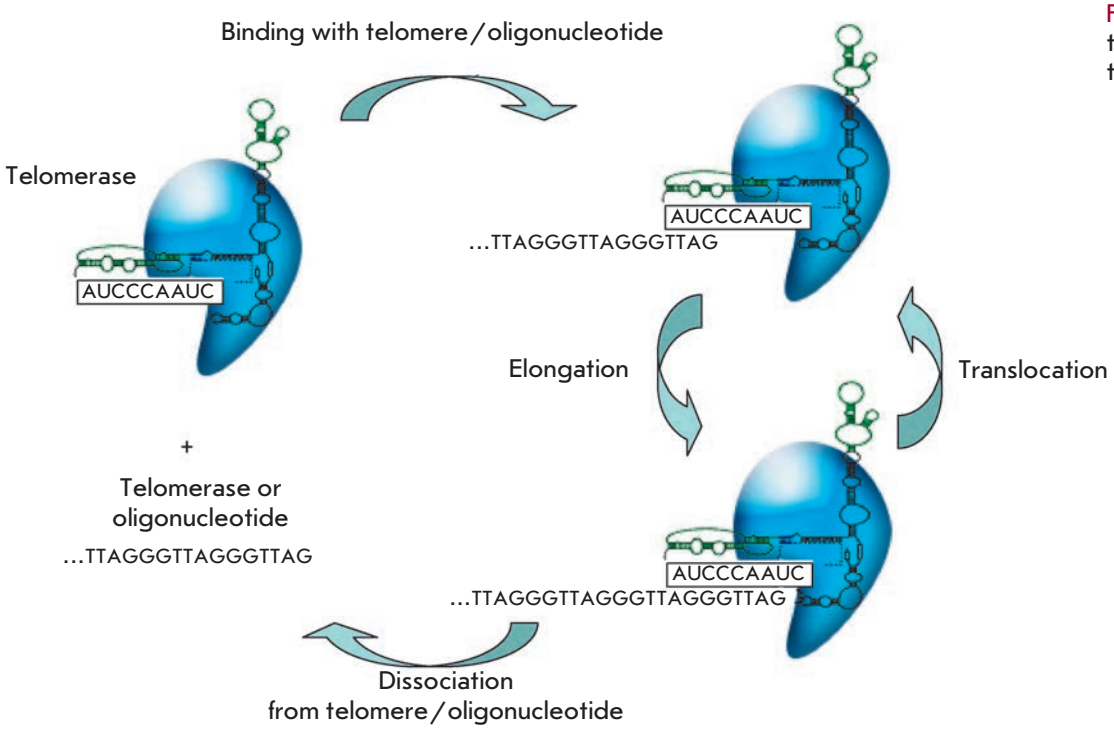

Fig. 1. General functional scheme of the telomerase complex.

itself in reproductive organs and embryonal tissues. Thus, the enzyme is active in stem cells and some rapidly regenerating tissues, such as the intestinal epithelium; however, in this case telomerase activity is usually lower than it is in tumor cells (*Fig. 2*). Telomerase activity is more typical of malignant tumors, its activity and detection frequency being noticeably lower in benign tumors [10]. Detection of telomerase activity is used for both tumor diagnostics and in the search for potential anti-tumor drugs that would act as telomerase inhibitors. Furthermore, telomerase participates in tissue regeneration after the partial removal of the liver or cardiac infarction. In addition, the role of telomerase in the ageing process, in connection with the telomere's function as a cell-timing mechanism, attracts a significant degree of interest.

METHODS COMPRISING THE AMPLIFICATION OF TELOMERASE-SYNTHESIZED DNA (TRAP)

The most common methods for detecting telomerase activity are TRAPs (telomeric repeat amplification protocols) [11], which allow one to perform semi-quanti-

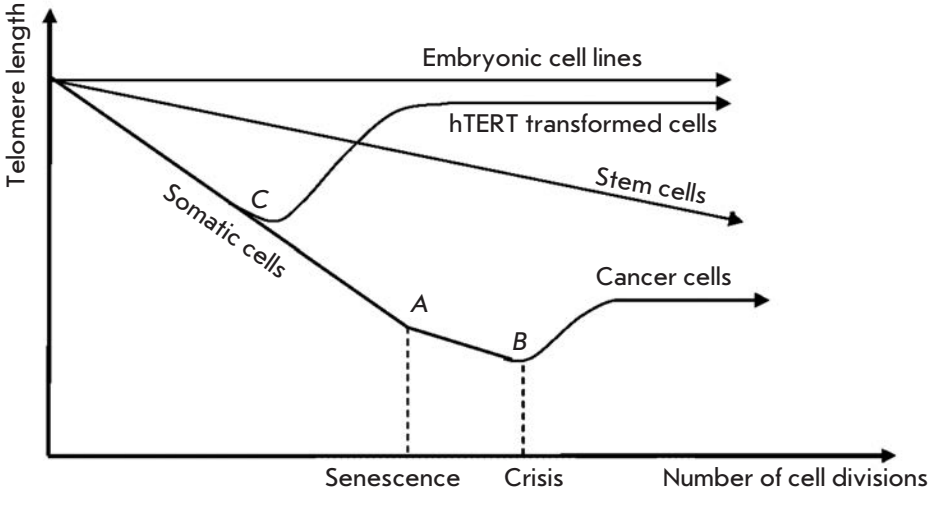

Fig. 2. Dependence of telomere length on the number of cell divisions in different cell types: embryonic cell lines, somatic cells, hTERT-transformed cells. A– Hayflick limit, B – crisis with subsequent apoptosis or tumor transformation, C – cell transformation by *hTERT* gene.

Table 1. Some oligonucleotides that are used in different TRAP modifications

Oligonucleotide name	Oligonucleotide sequence
TS	5'-AATCCGTCGAGCAGAGTT-3'
CX	5'-$(CCCTTA)_3$CCCTAA-3'
ACX	5'-GCGCGG$(CTTACC)_3$CTAACC-3'
RP	5'-TAGAGCACAGCCTGTCCGTG-3'
RPC3	5'-TAGAGCACAGCCTGTCCGTG$(CTAACC)_3$-3'
TSG4	5'-GGGATTGGGATTGGGATTGGGTT-3'

tative and quantitative analyses, using some of their modifications. Such modifications include: increase of the analysis rate, replacement of the radioactive label by nonlabeled compounds, the reduction of the amount of side products, etc. Among these methods are the scintillation proximity assay, hybridization protection assay, transcription amplification assay, and the magnetic bead-based extraction assay [12]. Some modifications even enable to detect telomerase activity within a single cell [13].

The telomeric repeat amplification protocol can be subdivided into three main stages: primer elongation, amplification of telomerase-synthesized DNA, and thirdly, its detection. At the elongation stage, telomeric repeats are added to the telomere-imitating oligonucleotide (TS, *Table 1*) by telomerase present in the cell extract. Then, PCR-amplification of telomerase-synthesized DNA is carried out with the use of specific primers (telomere-imitating and reverse primers). At this stage, different labels can be incorporated into the telomerase-synthesized DNA, such as radioactive, fluorescent, or affine labels. This stage is then followed by detection (in the original method, it comprises electrophoretic separation of PCR products and photographing) (*Fig. 3*).

The original TRAP method has several drawbacks. Initially, the CX oligonucleotide, which complementarily overlaps with TS for several bp, is used in the amplification of PCR products. It results in the dimerization of primers and products that emerge due to the interaction between primers. Even when using the optimal ACX primer with the noncomplementary TS end, a background signal may emerge during the analysis of concentrated extracts from tumor tissues [14]. An additional problem is encountered when using reverse primers which completely correspond to telomeric repeats. The primers are not annealed at the matrix edges during PCR (as a result of periodicity in telomeres), and hence false signals emerge. This problem is typically solved by adding regions that are noncomplementary to telomeres (*Table 1*) with a 5'-end nontelomeric "appendix" made of 6 bp to the primer ends. In order to reduce

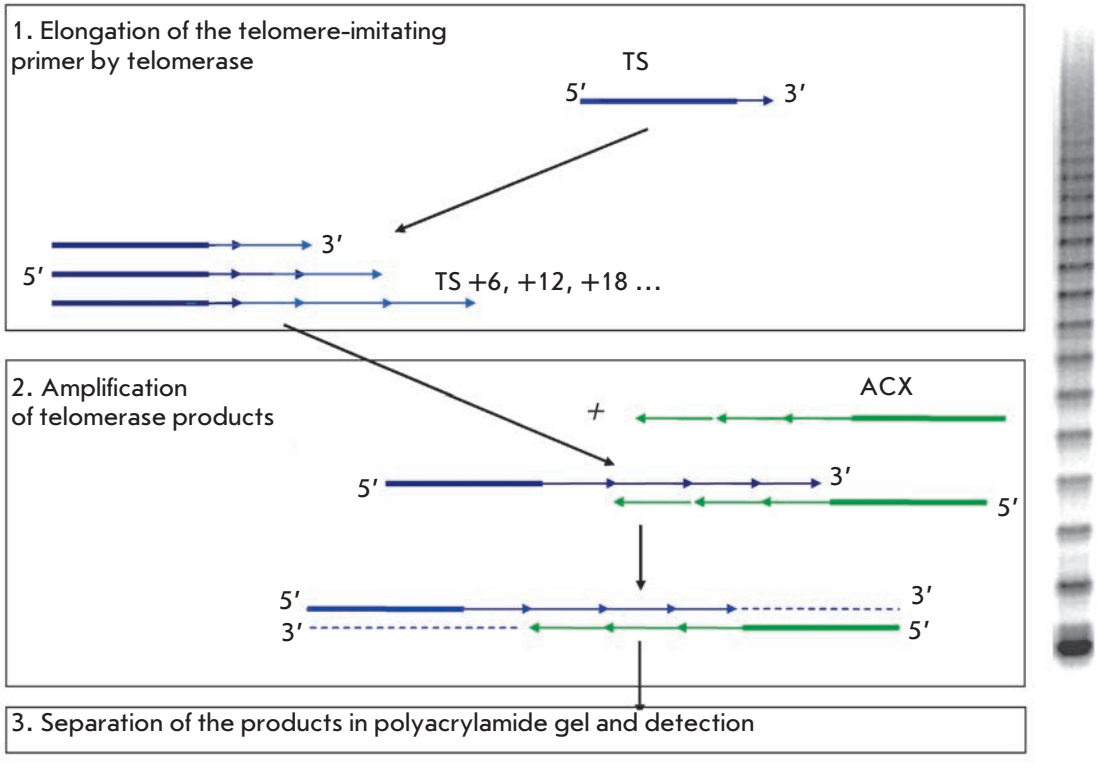

Fig. 3. Telomeric repeat amplification protocol (TRAP).

nonspecific signals, it is possible to use a combination of several primers that are used as reversed ones (more information on the two-primer system is given below, primers RP and RPC3 are given in *Table 1*). Oligonucleotide TSG4 (*Table 1*) can also be added to the TRAP mixture in order to assess the effect of duplex-stabilizing inhibitors; this oligonucleotide does not require the synthesis of several repeats by telomerase before the inhibitor begins its action [15]. The advantages and drawbacks of the various nucleotides used in TRAP were discussed more thoroughly in [12]. Moreover, in the case when PCR is used for signal amplification, the PCR inhibitors contained in the specimen can impact the results of telomerase activity detection.

Originally, in the TRAP method, PCR products were detected in polyacrylamide gel (PAAG) on account of the radioactive label, which was introduced using a radioactively labeled primer or incorporated into the DNA during the reaction. The method allows to perform a qualitative assessment of the activity and processivity of telomerase in cell and tissue extracts; however, as previously stated this requires radioactive specimens.

PCR at the second stage of TRAP allows to obtain an amount of DNA sufficient for gel staining, e.g., using ethidium bromide [16] (an appreciably strong mutagen with a low sensitivity), silver nitrite [17] (its sensitivity is equal to that when using the radioactive label; however, the method is more laborious and relatively expensive), and Sybr Green [18] and its analogs (its sensitivity is equal to that when using the radioactive label [19], while mutagenicity is considerably higher than that in ethidium bromide, although it is an intercalating dye, as well). Fluorescent labeling of the nucleotides employed in TRAP can also be used [20].

Purification of telomerase-synthesized DNA and TRAP efficiency

It is appreciably simple to obtain extracts of tumor cells or cell lines and detect telomerase activity in them, even though the tissues are composed of several cell types and may contain compounds that have an effect on the quantitative and even qualitative assessment of telomerase activity. Therefore, false-positive or false-negative results can be obtained, and they may affect the validity of the diagnosis and prognosis of a disease. The features of biopsic specimens, such as large volumes of fluid (blood, etc.) or presence of numerous normal cells, may complicate the detection of telomerase activity, as well. In these cases, the extraction of telomerase-synthesized DNA can be carried out using modified magnetic beads. During this procedure, PCR inhibitors are removed or strongly diluted. The TRAP method involving this extraction consists of three main stages: the elongation of the substrate-imitating oligonucleotide by telomerase, the extraction of telomerase-synthesized DNA using modified magnetic beads, and amplification.

During the extraction stage, telomerase-synthesized DNA is hybridized with the C-rich biotin-conjugated primer $(CCCTAA)_2$ and isolated from the extraction mixture using the magnetic beads coated with streptavidin-coated magnetic beads. Then, the telomerase-synthesized DNA is released from the complex by heating, and PCR is carried out. The sensitivity of this modification towards PCR inhibitors is lower by an order of magnitude as compared with the standard TRAP method; its efficiency is slightly higher during the analysis of tissue and other complex specimens [21]. Phenol-chloroform extraction can be used instead of the biotin-conjugated primer and magnetic beads [16], although in this case it becomes more difficult to remove the impurities that are more soluble in water than in organic solvents.

Internal standards for TRAP

Internal standards (amplified with the same primers as telomerase-synthesized DNA) allow for the presence of Taq polymerase inhibitors (e.g., gem-containing compounds) in the specimens to be taken into consideration, and for the performing of the total control of PCR. They can also be used for the standardization of the amount of telomerase-synthesized DNA. There are two most common standards, with the length of 36 and 150 bp. The 36 bp standard is excessively amplified if the specimens have a low telomerase activity, competes with the telomerase-synthesized DNA, and provides a false-negative signal [18]. The 150 bp standard is more sensitive towards the Taq polymerase inhibitors present in the reaction mixture. The standards can be used in TRAP with real-time PCR and primers in which the fluorescent label differs from that in primers for the amplification of telomerase-synthesized DNA [22].

TRAP with an additional specific reverse primer ("two-primer" TRAP)

Two-primer TRAP is a modification of the standard TRAP which is used to reduce false signals (*Fig. 4*).

In this TRAP version, no electrophoretic analysis of PCR products is carried out. Instead, the total radioactivity is assessed as a criterion of telomerase activity. The telomerase-synthesized DNA is amplified using two reverse primers with lengths of 20 (RP) and 38 (RPC3) nucleotides (*Table 1*), in the presence of [^{3}H]TTP or [α-^{32}P]dCTP; the amount of the longer primer added is 50 times lower than that of the shorter primer. After the PCR, the two-chain DNA is isolated by deposition and filtration. The advantage of this method is that,

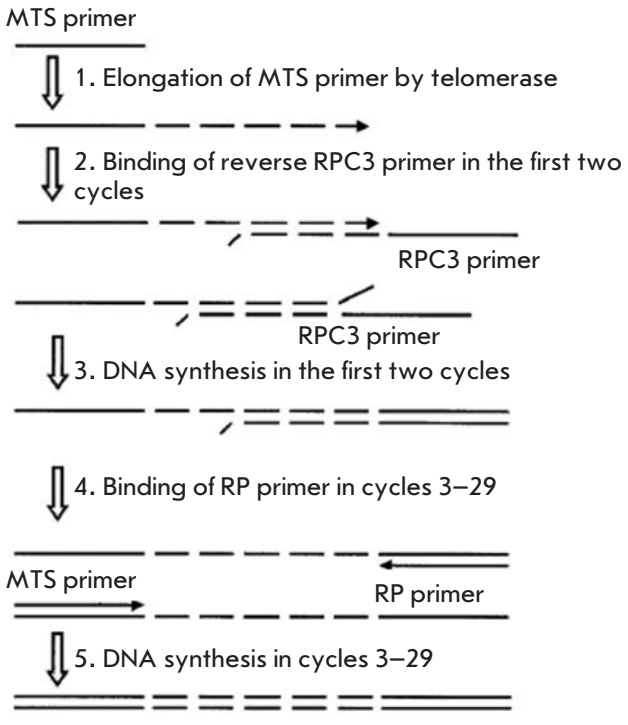

Fig. 4. "Two-primer" TRAP scheme [23, 24].

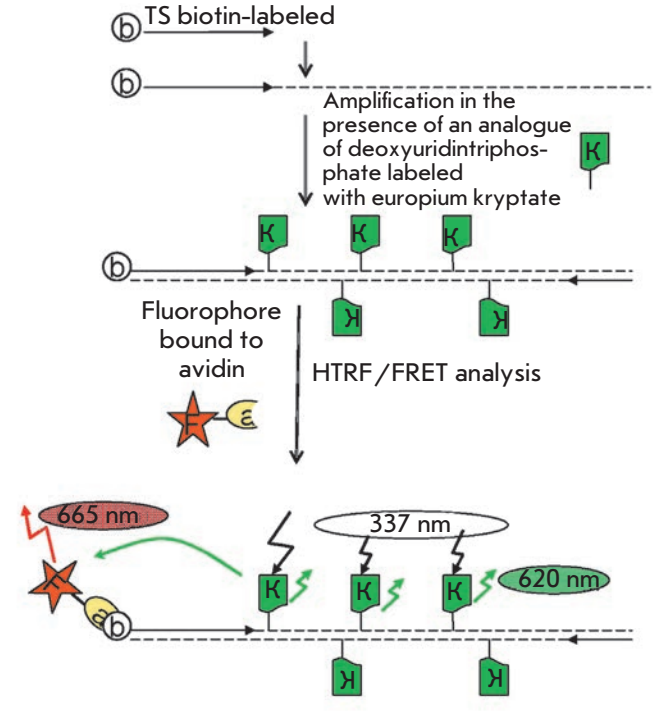

Fig. 5. Scheme of the TRAP method with time-resolution fluorescence energy resonance transfer [26]. F – fluorophore, a – avidin, b –biotin, and K – analog of deoxyuridintriphosphate labeled with europium kryptate.

due to the low concentration of the RPC3 primer, the amount of products of interaction between the primers is reduced, while the presence of standard amounts of the RP primer ensures a significant degree of amplification of the telomerase-synthesized DNA [23, 24]. This method makes it possible to qualitatively determine telomerase activity in extracts of tissues and cell lines. The sensitivity threshold of this method is the 10-cell extract of the telomerase-positive cell line.

TRAP with fluorescence resonance energy transfer (FRET)

One of the alternatives to DNA staining in the TRAP method is to use primers with energy transfer (amplifluors). Amplifluors are characterized by their unique hairpin structure, which contains a donor (fluorescein) and acceptor (4'-dimethylaminophenyl-azobenzoic acid). Fluorescence manifests itself only in the case when a primer incorporates into PCR products; i.e., the necessity for using radioisotopes disappears, and the volume of post-PCR analysis considerably decreases. The replacement of the telomerase substrate and reverse primer by amplifluors allows to achieve an increasingly high intensity of the fluorescent signal. The primers that are used for amplification of the internal standards need to have a donor-acceptor pair with a fluorescence wavelength that differs from that of the primers used for amplification of telomerase-synthesized DNA [22].

The method involving the use of the time-resolution fluorescence resonance energy transfer (HTRF) combines the standard FRET technique and a long-lived fluorescent donor. The method is based on the use of europium or terbium cryptate complexes. These lanthanides are characterized by a long fluorescence decay period, whereas the complexation of macrocyclic compounds yielding cryptate complexes additionally enhances their stability [25]. A deoxyuridin triphosphate labeled with europium cryptate was used to assess the amount of DNA in TRAP with biotin-conjugated oligonucleotide TS. After the allophycocyanin–streptavidin, a conjugate was added and the FRET signal of DNA in TRAP was observed [26] (*Fig. 5*). This method allows a semi-quantitative detection of telomerase activity in tissue and cell line extracts. The sensitivity threshold of this method is the 10-cell extract of the telomerase-positive cell line.

TRAP with detection using the scintillation proximity assay

Another means for the detection of the DNA amplified in TRAP without PAAG is the scintillation proximity assay. When used in combination with the traditional

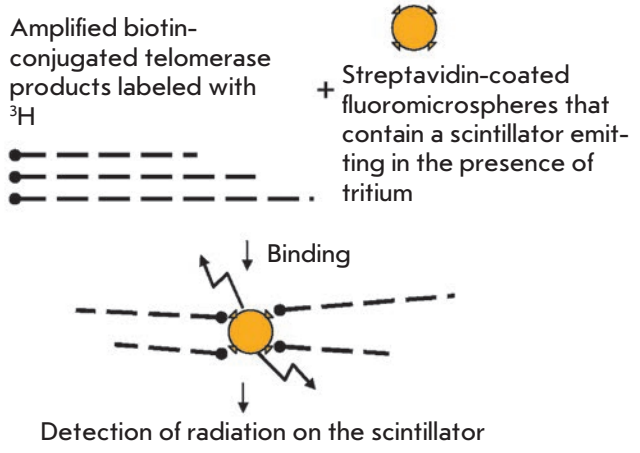

Fig. 6. Scheme for TRAP with scintillation proximity assay.

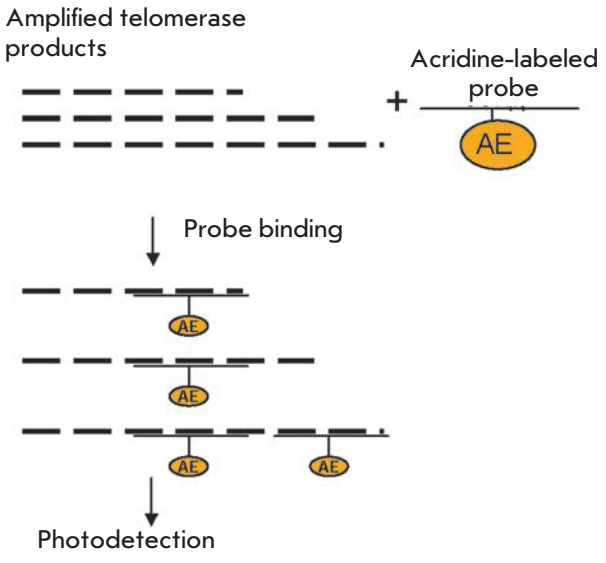

Fig. 7. Scheme for TRAP with hybridization protection assay.

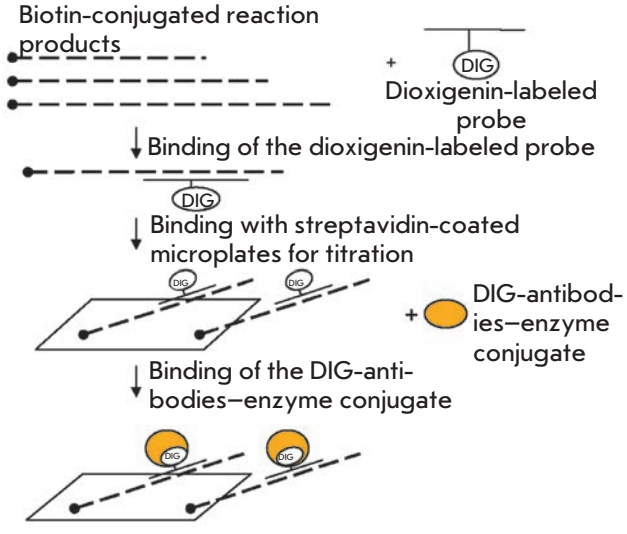

Fig. 8. Scheme for ELISA detection of PCR products in TRAP-ELISA (or detection of telomerase reaction products in direct ELISA).

TRAP, it helps increase the rate of detection of telomerase activity. 5'-Biotin-conjugated oligonucleotides act as substrates in this method; the amplification takes place in the presence of [^{3}H]TTP. Biotin-conjugated ^{3}H-labeled DNA binds with streptavidin-coated fluoromicrospheres, which contain a scintillator that emits in the presence of tritium (*Fig. 6*). Thus, instead of separating DNA in a gel followed by photo-detection, the yield of PCR products is assessed on a scintillation counter, which allows to reduce the assay time after the PCR to 1 h and semi-quantitatively determine telomerase activity in large series of tissue and cell line extracts. The sensitivity threshold of this method is the 10-cell extract of the telomerase-positive cell line. The major drawback of this method is the use of tritium. Furthermore, like most methods for detecting TRAP products without PAAG, it is sensitive to PCR artifacts [27].

TRAP with detection using the hybridization protection assay

TRAP modification in which the hybridization protection assay (Hybridization protection assay-TRAP) is used is a safer modification. Probes labeled with covalently bound acridine [28] are used in this method for detecting DNA after the amplification (*Fig. 7*). The same detection scheme is used in the transcription scheme of telomerase repeat amplification. This method allows for semi-quantitative determination of telomerase activity in tissue and cell line extracts. The sensitivity threshold of this method is the 10-cell extract of the telomerase-positive cell line.

TRAP combined with enzyme-linked immunosorbent assay (ELISA)

In the TRAP-ELISA method, DNA after the amplification is determined colorimetrically, facilitating the qualitative and semi-quantitative assessment of telomerase activity. Biotin-conjugation of the TS primer allows for the binding of the amplified DNA to streptavidin-coated microplates (*Fig. 8*). The amplified DNA denatures and is hybridized with digoxigenin (DIG)-labeled probes, which demonstrate specificity towards telomeric repeats, and binds to the microplates due to the streptavidin–biotin interaction. This complex can

be detected using polyclonal sheep antibodies to DIG conjugated to horseradish peroxidase; the activity of the latter is determined colorimetrically [29, 30]. This method differs from the hybridization version by the emergence of a second step of signal amplification due to the enzymatic reaction.

One of the drawbacks of the TRAP-ELISA method is the complexity in separating the telomerase-positive and telomerase-negative controls, which may result from the absence of internal controls and two steps of signal amplification. Nevertheless, the TRAP-ELISA method is faster as compared with TRAP, which is based on the separation of the amplified DNA in gel. This fact makes it possible to use the TRAP-ELISA method in screening studies. The method is suitable for semi-quantitative determination of telomerase activity in tissue and cell line extracts. The sensitivity threshold of this method is the 10-cell extract of the telomerase-positive cell line.

TRAP with electrochemical detection

After the PCR, the nonreacted nucleotide triphosphates can be separated, followed by treatment of the remaining products with 3 M HCl. In the method under consideration, dGMP, one of the products of the complete hydrolysis of the amplified DNA, is determined electro-chemically [31]. The method makes it possible to semi-quantitatively determine telomerase activity in tissue and cell line extracts. The sensitivity threshold of this method is the 10-cell extract of the telomerase-positive cell line. The method has no special advantages over other methods in which no gel-electrophoresis or radioactive labeling are used. However, the method is more laborious.

TRAP with real-time PCR

Real-time PCR is used for simultaneous DNA amplification and measurement of the amount of products obtained after each amplification cycle. Standard TRAP, combined with real-time PCR, allows to obtain quantitative results [32, 33]. This method is suitable for studying telomerase inhibitors and analyzing large specimen series [12]. When comparing it with the conventional TRAP, it can be noted that over-estimation of telomerase activity and leveling of small differences in the activity is possible without the assessment of the amount of real-time PCR products, due to saturation of the PCR reaction in the final stages. Moreover, the possibility of dimerization of primers resulting in the emergence of a false-positive signal causes an additional problem. This problem can be made more acute when using the reverse anchor-primer, which will impede dimerization, reduce the number of primers and number of cycles, resulting in dimerization of primers to occur mostly at late stages of the program (35–39 cycles); in the meantime, the number of cycles is 28 in the standard TRAP. This problem is also mitigated when measuring fluorescence in the early exponential phase of PCR [32]. The method makes it possible to quantitatively determine telomerase activity in tissue and cell line extracts. The sensitivity threshold of this method is 10 to 50 cell extracts of the telomerase-positive cell line.

Similar to the standard TRAP with gel-electrophoresis, TRAP with real-time PCR has several variants of detection, e.g., using the probes which are specific to the telomerase-synthesized DNA amplified in the PCR and fluoresce only as a component of a duplex. Otherwise, these probes will form the nonfluorescent hairpin structure [34]. The advantages of this method include a high rate of detection of telomerase-synthesized DNA upon flow analysis and enhanced specificity due to the use of corresponding probes [35]. The method allows semi-quantitative determination of telomerase activity in tissue and cell line extracts. The sensitivity threshold of this method is the 10-cell extract of the telomerase-positive cell line.

TRAP on microchips

TRAP on microchips is the combination of the two-primer TRAP and binding of PCR products on chips, followed by probe hybridization and detection. Various fluorescent labels are used to determine telomerase-synthesized DNA and the internal standard; e.g., Cy3 for the telomerase-synthesized DNA being amplified and Cy5, for the standard.

In situ TRAP

Telomerase activity is typically analyzed in a cell extract. If cell lines are homogeneous, the result represents the telomerase activity in cells. When the extracts of tumor tissue specimens are investigated, it is reasonable to consider only the mere fact of the presence or absence of telomerase activity, since the content of tumor cells in such specimens varies from 3 to 90% and more. In this case, the results obtained reveal nothing about the level of telomerase activity in various types of cells constituting the tissue or on the differences between tumor and normal cells within the same tissue (e.g., an increase in telomerase activity in blood is associated with the emergence of activated leukocytes or degeneration of certain blood cells). In order to overcome this drawback, the *in situ* TRAP method was designed, in which FITC-labeled direct and reverse primers are used [36]. In this method, the cell suspension specimens are immobilized onto silane-coated glasses and dried with cold air. The reaction mixture for TRAP

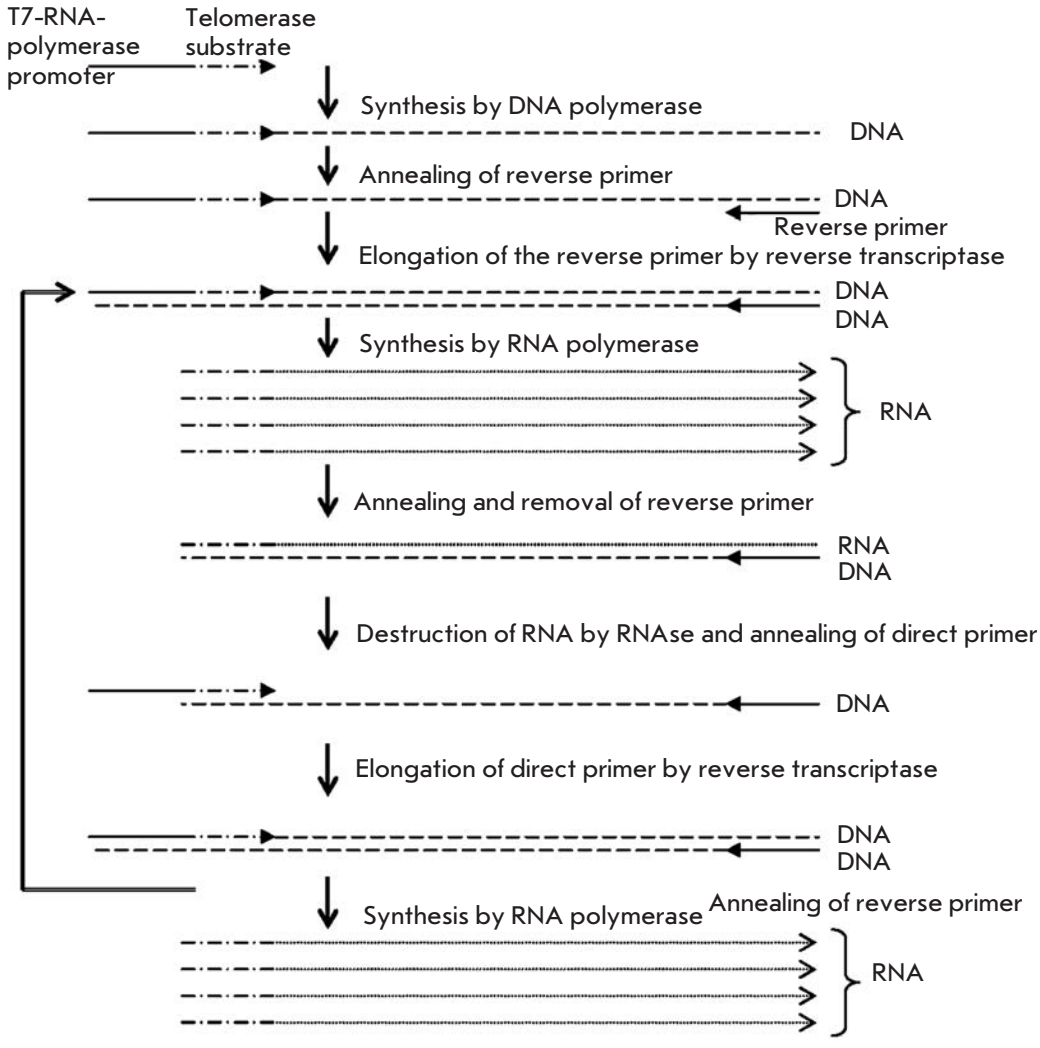

Fig. 9. Scheme of telomerase activity detection with the PCR amplification of telomerase products for transcriptional amplification [12, 42].

is then applied onto each specimen, followed by incubation. Telomerase is inactivated via heating, the reverse primer with polymerase is added, and *in situ* PCR is performed. Upon completion of the reaction, the glasses are analyzed on a fluorescence microscope; cell types are identified by the staining procedure. The fluorescence intensity and its localization (nucleus/cytoplasm) are used to determine telomerase activity in separate cell types within the mixture. High telomerase activity in urogenital and bronchial lavages manifests itself through bright fluorescence of the nuclei of malignant (but not benign) cells [37, 38]. A comparison with the conventionally stained specimens points to association between the fluorescence in the nucleus with malignant cells, whereas the signal from cytoplasm is detected in granulocytes and macrophages [39]. A similar correlation was found during the analysis of pleural effusion [40]. Moreover, *in situ* TRAP has been successfully used not only for the cell suspension specimens, but also on tissue sections (in particular, for diagnostics of liver cancer) [41]. The method allows for a semi-quantitative determination of telomerase activity and its localization in isolated cells of tissues and cell suspensions.

Transcription amplification of telomerase-synthesized DNA

In order to increase the amount of telomerase-synthesized DNA, PCR is replaced by transcription amplification. Combined with "hybridization protection," this method allows to determine the telomerase activity as quickly as after 4 hours. The primer, which acts as a substrate for telomerase, contains the site of T7-RNA-polymerase binding, along with the telomere-imitating sequence. The telomerase-synthesized DNA acts as a substrate for hybridization of the reverse primer, which contains an additional sequence that is noncomplementary to the telomeric repeats. Due to this sequence, the reverse primer binds with the end of the telomerase-synthesized DNA, and the completion of the double-chain DNA takes place at the next

stage. T7-RNA-polymerase uses this DNA as a matrix to synthesize RNA. This RNA is used by the reverse transcriptase to synthesize a new DNA chain. RNA is then removed by RNase; the second DNA chain of the single-chain DNA is completed with the aid of the direct primer (*Fig. 9*).

Using this scheme, telomerase-synthesized DNA can be amplified at 40°C for 75 min in amounts comparable with PCR. The subsequent reactions may be carried out in the same tube as those in which amplification takes place. The method's sensitivity allows to detect telomerase activity in specimens consisting of 1–1,000 cells. The method is sensitive towards the presence of RNases [12, 42]. The major advantage of this method over TRAP with PCR amplification is that no heating of a specimen is required upon amplification and that the specific Taq polymerase inhibitors are neglected. This method makes it possible to semi-quantitatively determine the telomerase activity in tissue and cell line extracts. The sensitivity threshold of this method is the 10-cell extract of a telomerase-positive cell line.

DIRECT DETECTION OF TELOMERASE-SYNTHESIZED DNA

Detection of telomerase activity using direct incorporation of a radioactively labeled substrate

The method is based on the ability of telomerase to elongate oligonucleotides in the presence of dNTP. If an oligonucleotide or one of the dNTP (typically, dGTPl, since telomerase-synthesized telomeres are enriched in guanine residues) contains a radioactive label, telomerase activity can be electrophoretically assessed by its incorporation into DNA [43]. The major drawbacks of this method include the use of large amounts of radioactive isotopes and insufficient sensitivity (in many cases), which is conditioned by a low telomerase content in cells and tissues.

The first method used for telomerase activity detection was a method in which radioactive labeling was used without any additional amplification. This method is still employed today for the thorough investigation of telomerase-synthesized DNA and quantitative measurements. The method allows for qualitative determination of the activity and processivity of telomerase in cell line extracts; however, it is characterized by low sensitivity (10,000 cells of telomerase-positive cell line).

Determination of telomerase-synthesized DNA by changes in surface plasmon resonance

Surface plasmon resonance (SPR) manifests on a metal's surface under conditions of total internal reflection and is characterized by a nonspecific angle of reflection and, therefore, the refraction index. As this effect manifests itself on the surface of a metal film, it propagates deep into the solution with exponential damping as a distance function. The interactions between the molecules change the damped wave, which has an effect on the characteristics of the surface plasmon and manifests itself in the variation of the resonance angle and the refraction index in the near-surface layer. The interaction between bio-molecules is judged by the alteration of the refraction index (*Fig. 10A*).

SPR can be used to determine telomerase activity as the corresponding elongation of a telomere-imitating oligonucleotide, using a biosensor.

5'-Biotin-conjugated oligonucleotides, which contain telomeric repeats, are *in situ* immobilized on the surface of a dextrane sensor pretreated with streptavidin on a BIACORE instrument. They are then treated with a cell extract. If the extract contains telomerase, binding of telomerase takes place and the oligonucleotide is elongated, which is determined by SPR after proteins are removed with a sodium dodecyl sulfate solution (*Fig. 10B*). The degree of oligonucleotide elongation depends on specimen concentration and reaction time. The results of the analysis of tumor and cell line extracts using this method, as well as the results of testing telomerase inhibitors, correlate with the data obtained by the TRAP method [44]. The signal intensity can be increased by treating the sensor with telomerase-synthesized DNA with antisense oligonucleotides with respect to the telomeres that are covalently bound with streptavidin and gold nanoparticles [45].

This method allows to quantitatively determine telomerase activity in tissue and cell line extracts and collect data on the kinetics of the reaction, demonstrating the binding and dissociation of telomerase from the substrate. The sensitivity threshold of this method is the 50-cell extract of the telomerase-positive cell line.

Determination of telomerase activity using oligo-modified magnetic particles and NMR

This method is based on the use of magnetic particles of an iron oxide which are modified with oligonucleotides that are complementary to telomeric repeats. These particles bind to the telomerase-synthesized repeats due to complementary interactions and form extended linear structures (MRS complexes) (*Fig. 11A*). The effect of this hybridization is determined by the spin-spin relaxation time. During the formation of an organized nanoparticle ensemble, there is a noticeable change in the magnetic relaxation time of the surrounding water molecules, which can be measured in a relaxometer (the relaxometer measures both the spin-spin relaxation times of the nuclear magnetization of proton-bearing liquids in multi-component systems and the content of components with different

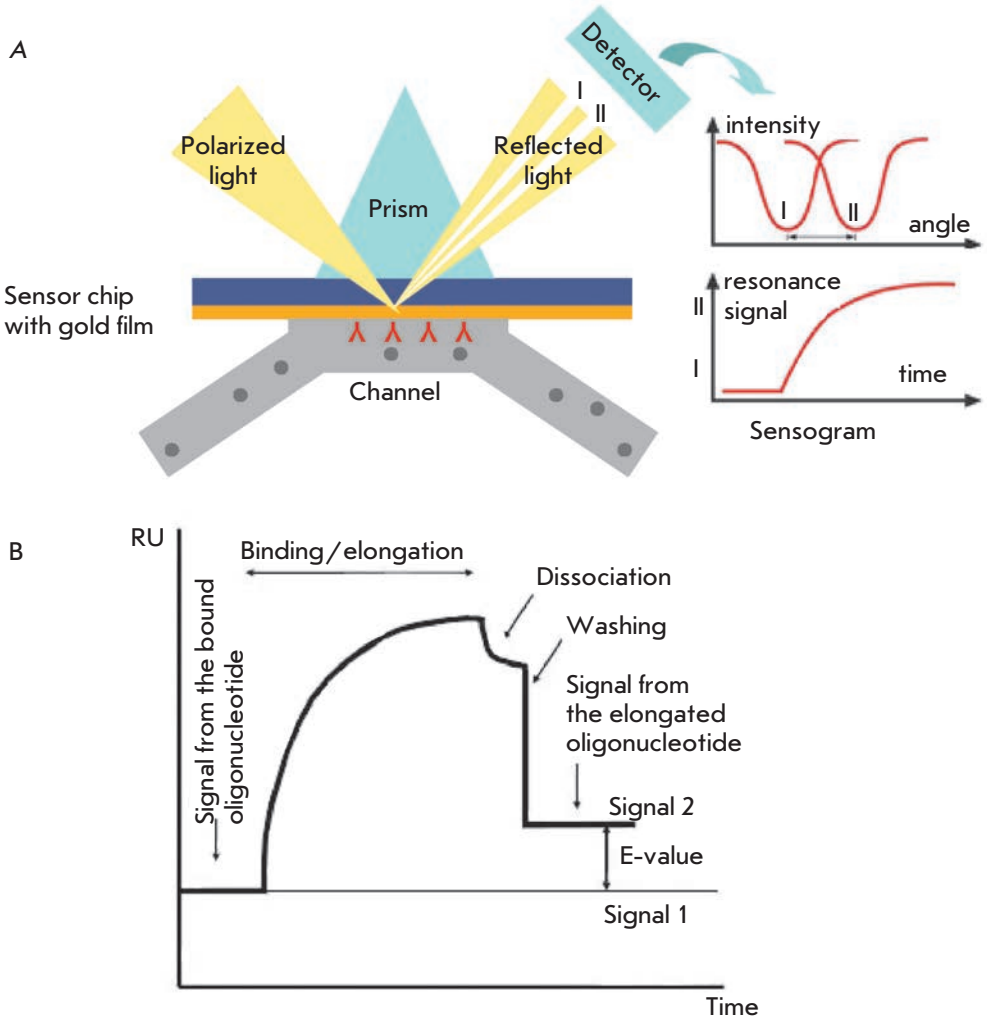

Fig. 10. Scheme of the use of surface plasmon resonance (SPR) for detecting macromolecules; (A) sensogram corresponding to the general scheme and (B) SPR sensogram for telomerase activity detection. RU – resonance units. The difference between signals 1 and 2 represents DNA that was synthesized by telomerase [44].

relaxation times). The magnetic switching occurs rapidly, attaining half of the maximum change after 30s and reaching a plateau after 40–60 min (*Fig. 11B*). The magnetic switching has been confirmed by magnetic force microscopy and by correlation of the magnetic switching and the size of the nanoensembles being formed. The local distortion of the magnetic field increases on nanoparticles in ordered ensembles, whereas the nonordered nanoparticles provide a considerably lower magnetic effect [46].

The relaxation time was measured in a volume of 200–500 μl in an NMR spectrometer at a magnetic induction of 0.47 T. For the magnetic resonance scanning of 384 well plates with 50 μl of the mixture at 1.5 T, the spin-spin relaxation (T2) and spin-lattice relaxation (T1) times were assessed. The adaptation to the flow treatment using magnetic resonance scanning made it possible to analyze several hundred specimens as quickly as in several tens of minutes with high sensitivity [46]. The method allows for the quantitative determination of telomerase activity in tissue and cell line extracts using the high-performance microplate format. In addition to the common instruments and reagents, these analyses require a plate NMR-spectrometer and a specimen of oligonucleotide-modified nanoparticles. The sensitivity threshold of this method is the 10-cell extract of the telomerase-positive cell line.

Determination of telomerase activity using the quartz crystal microbalance technique

An Au-quartz resonator can be used for a microgravitometrical analysis of telomerase activity, according to the quartz crystal microbalance technique. Quartz crystals possess a piezoelectric effect. Alternation of the current imposition results in the emergence of oscillations in a quartz crystal; in specially curved crystals, a current of a certain frequency may lead to the formation of a stationary wave. Its resonance frequency can be quite accurately determined. The wave changes upon ligand binding on the crystal's surface. The quartz

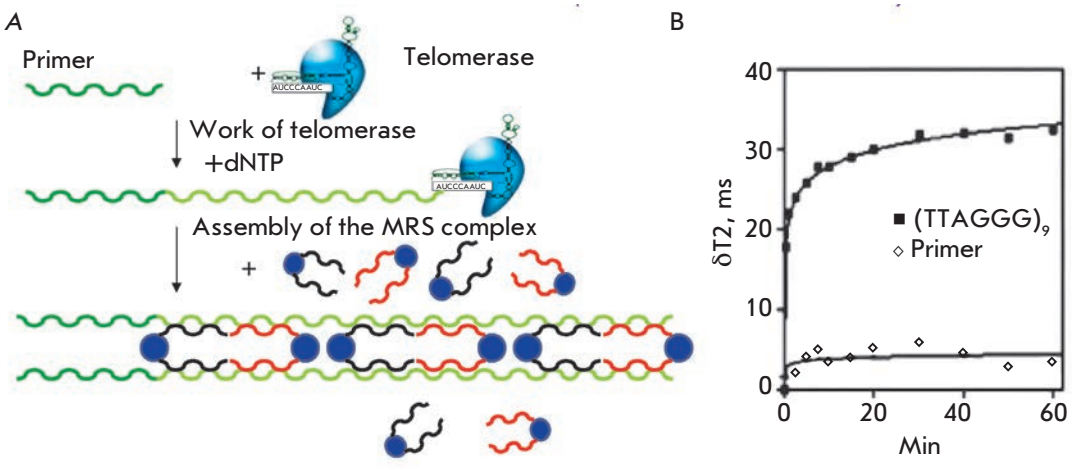

Fig. 11. Telomerase magnetic nanosensor. A - Complex assembly between the synthesized telomere repeats and oligonucleotide magnetic nanoparticles conjugated with antitelomere. B - Induced magnetic T2 changes as a function of time after adding an oligonucleotide consisting of either a 54-bp telomeric repeat or the primer [46].

crystal microbalance technique in liquids is utilized to determine the affine binding of molecules (in particular, proteins) on surfaces that contain the corresponding recognition sites.

In this method, the telomere-imitating oligonucleotide is bound to the sensor's surface, elongated by telomerase. Next, the synthesized DNA chain is hybridized with a biotin-conjugated oligonucleotide (*Fig. 12A*). An alternative variant includes the elongation of the telomere-imitating oligonucleotide that is bound to the sensor in the presence of a biotin-labeled NTP (*Fig. 12B*). Next, the sensor's surface is treated with an avidin–alkaline phosphatase conjugate and a solution of alkaline phosphatase substrate – 5-bromo-4-chloro-3-indolylphosphate, which upon hydrolysis yields an insoluble product on the sensor's surface. When determining telomerase activity through a decrease in the resonance frequency of the crystal, it is possible to observe the steps of oligonucleotide elongation, binding with the telomerase-synthesized DNA of the avidin–alkaline phosphatase conjugate, and the deposition of products of the reaction catalyzed by the alkaline phosphatase on the crystal's surface [47]. The method allows for the quantitative determination of the telomerase activity in tissue and cell line extracts. The sensitivity threshold of this method is the 3,300-cell extracts of the telomerase-positive cell line at a high rate. A frequency analyzer and an Au-quartz crystal are needed in this method. Moreover, the identification of artifact signals is complicated.

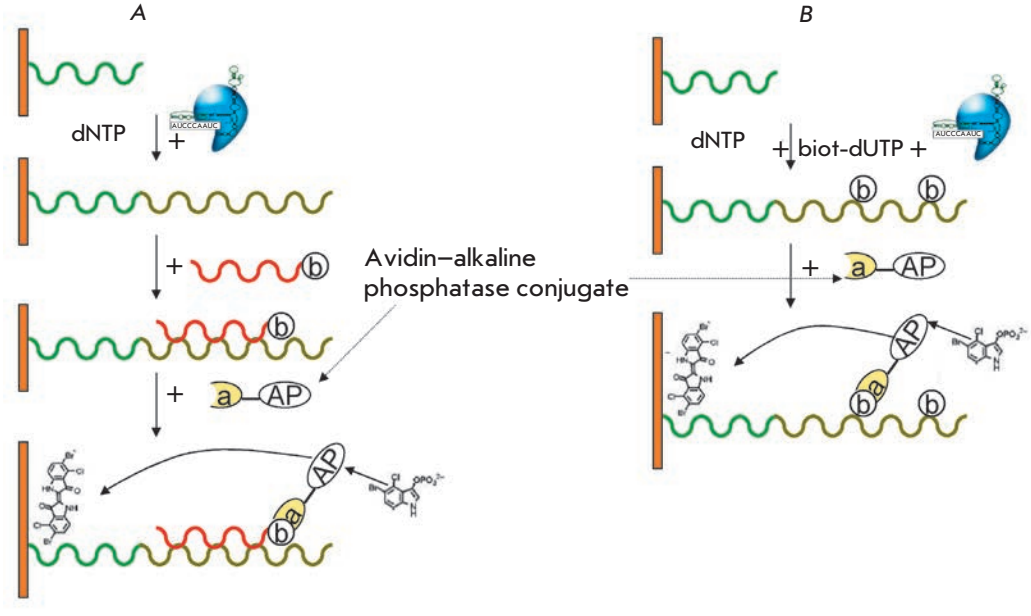

Fig. 12. Processes on the sensor in quartz crystal microbalance and electrochemical methods. A - Insertion of a biotin-labeled dUTP into the telomerase-synthesized DNA. B - Hybridization of biotin-labeled oligonucleotide with telomerase-synthesized DNA [47]. b – biotin as a component of the oligonucleotide, a-AP –avidin–alkaline phosphatase conjugate, dUTP – mixture of nucleoside triphosphates, biot-dUTP – biotin-labeled dUTP.

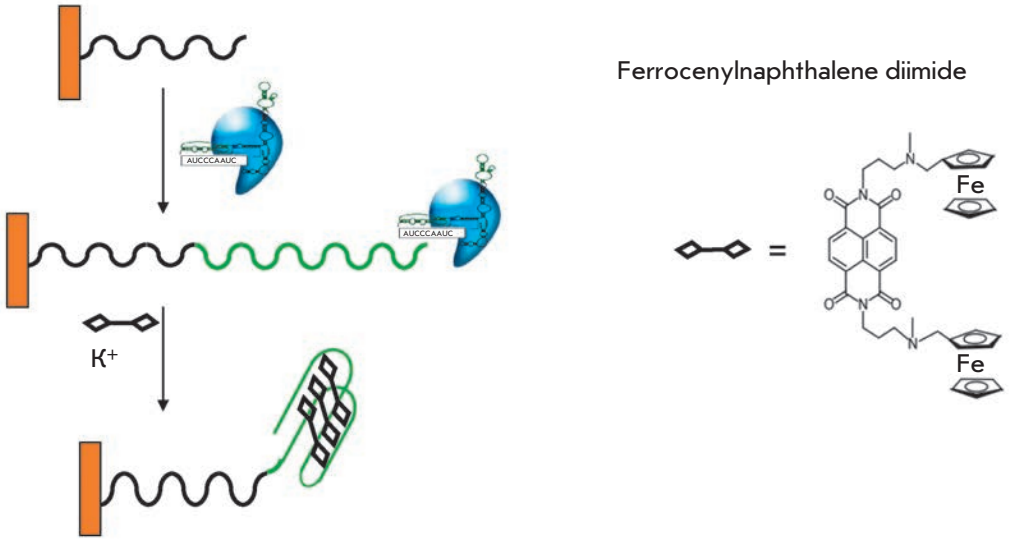

Fig. 13. Assembly on the electrochemically detectable complex upon telomerase activity detection with ferrocenylnaphthalene diimide [48].

Electrochemical detection of telomerase activity with ferrocenyl naphthalene diimide

This method is based on the ability of telomeric repeats to form G-quadruplexes. Telomerase elongates an oligonucleotide that is immobilized on an electrode. The synthesized telomeric then repeats when there is a high concentration of potassium ions, forming quadruplexes; while ferrocenyl naphthalene diimide can stoichiometrically bind with DNA quadruplexes under these conditions and stabilize their structure (*Fig. 13*). In turn, the bound ferrocenyl naphthalene diimide can be detected using electrochemical methods. In this method, the quantities of DNA fragments that are folded into a quadruplex are assessed. This number depends not only on the total number of repeats, but also, to an unpredictable degree, on the length and position of individual DNA fragments, which can be considered a drawback. The sensitivity of the method is sufficient to detect the telomerase-synthesized DNA without amplification [48] (100–1,000 cells of the telomerase-positive cell line); however, this method has not as yet been tested on a tumor tissue extract.

Biobarcode assay for telomerase activity detection

Today, the most sensitive method for direct detection of telomerase activity without amplification of the telomerase-synthesized DNA is based on the biobarcode system. In the original biobarcode system, magnetic particles bind to a target, which in turn binds to nanoparticles covalently modified with an oligonucleotide due to antigen-antibody interactions. These nanoparticles serve as a biological barcode. The resulting "sandwich" is isolated from the reaction mixture in the magnetic field and denatured; the result is determined by the released DNA fragments. In the system of telomerase activity detection, the telomerase-synthesized DNA is recognized using complementary DNA fragments. DNA nanoparticles consist of gold nanoparticles and oligonucleotides of two types; one of these can form a duplex with the telomerase-synthesized DNA, whereas the second cannot. Because of this, the probability of binding another DNA-target to the same nanoparticle is reduced (*Fig. 14*). The electroactive complex $[Ru(NH_3)_6]^{3+}$, which is capable of binding to negatively charged DNA chains due to electrostatic interactions, is used for detection [49]. The method allows to quantitatively detect telomerase activity in cell line extracts; however, it has not been tested on tumor tissue extracts yet. The sensitivity threshold of this method is the 10-cell extract of the telomerase-positive cell line.

Telomerase activity detection using optical biosensors

The principle of this method is to a certain extent similar to that of SPR. The method is based on the fact that upon binding of a target, the refraction index on the sensor's surface changes in proportion to the amount of bound targets. A cassette consisting of three oligonucleotides helps to avoid steric impediments. Phosphate groups covalently interact with the surface via the 5'-end of an oligonucleotide. Then, an oligonucleotide containing a short noncomplementary region on its 3'-end complementarily binds to the immobilized DNA. The prominent 3'-end of the DNA is modified with phosphorothioate, which enhances the affinity of telomerase-primer binding by a factor of 10 [50]. After treatment with a telomerase-containing extract, the

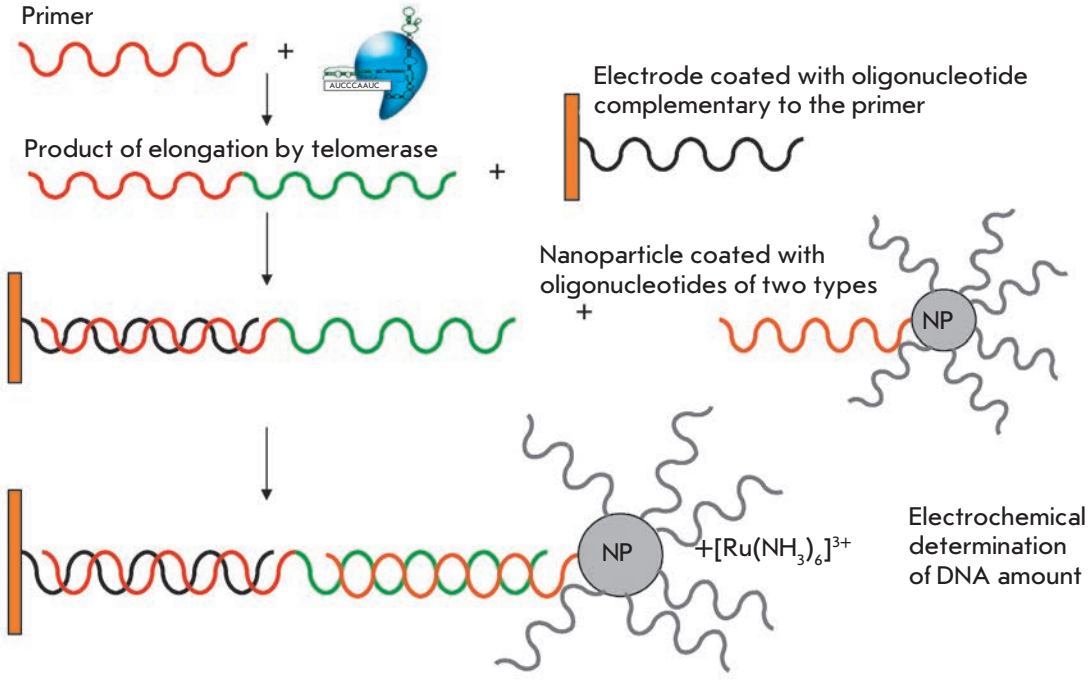

Fig. 14. Biobarcode-based electrochemical telomerase detection [49]. NP – nanoparticles.

enzyme is removed from the sensor's surface by proteinase K in the presence of dNTP (*Fig. 15A*).

Telomerase activity was assessed in this case by the sensogram of the surface charge (ng/mm^2, determined by the change in the refraction index) (*Fig. 15B*). The method allows to quantitatively detect the telomerase activity in cell line extracts; however, it cannot be used for tumor tissue extracts, since its sensitivity threshold is the 10^5-cell extract of the telomerase-positive cell line. In addition, phosphorothioate-modified oligonucleotides and a special optosensor are used in this method.

The system of telomerase activity detection based on quantum dots

A quantum dot is a conductor or semiconductor fragment that is limited along all three spacial dimensions and contains conductivity electrons. The dot has to be quite small in order to produce considerable quantum effects. This can be achieved if the kinetic energy of an electron $E = \hbar^2/md$ (d is the characteristic dimension of a dot, m is the effective mass of an electron on the dot) conditioned by the uncertainty of its momentum is considerably higher than that of all other energy scales, primarily, higher than the temperature expressed in energy units. Any appreciably small piece of the metal or semiconductor can serve as a quantum dot. In this microcrystal, an electron feels as if in a three-dimensional potential well; it has many bound energy levels with a characteristic distance between them (the accurate expression for the energy levels depends on the shape of a dot). Like upon transition between the energy levels of an atom, a photon can be emitted upon transition between the energy levels of a quantum dot. Unlike in atoms, the transition frequencies can be easily controlled by varying the crystal's dimensions.

A telomere-imitating oligonucleotide modified at its end with the thio group is attached to a nanoparticle (quantum dot). This quantum dot is capable of fluorescing by absorbing a quantum with a wavelength of λ1 (400 nm) and emitting a quantum with a wavelength of λ1' (560 nm). If a modified fluorescent oligonucleotide TR-dUTP (dUTP labeled with Texas Red) is incorporated into DNA upon telomerase-elongation of an oligonucleotide attached to a quantum dot, a fluorescence energy transfer occurs (*Fig. 16A*), which is accompanied by a decrease in emission with a wavelength of λ1' and the beginning of emission with a wavelength of λ2 (610 nm) (*Fig. 16B*). The method allows for a quantitative assessment of the telomerase activity. The sensitivity threshold is approximately 10,000 HeLa cells [51], which is not enough for an analysis of clinical materials.

Instead of incorporating TR-dUTP, it is possible to use the ability of telomeric repeats to fold into G-quadruplexes and bind hemin. In this case, an energy transfer takes place between a quantum dot and the G-quadruplex–hemin complex with corresponding fluorescence quenching. The sensitivity of this method is 270 T293 cells [52].

Telomerase activity detection using an on-chip nanowire sensor

A sensor chip is a transistor comprising antibody-coated silicon nanowires with aldehydes groups on their

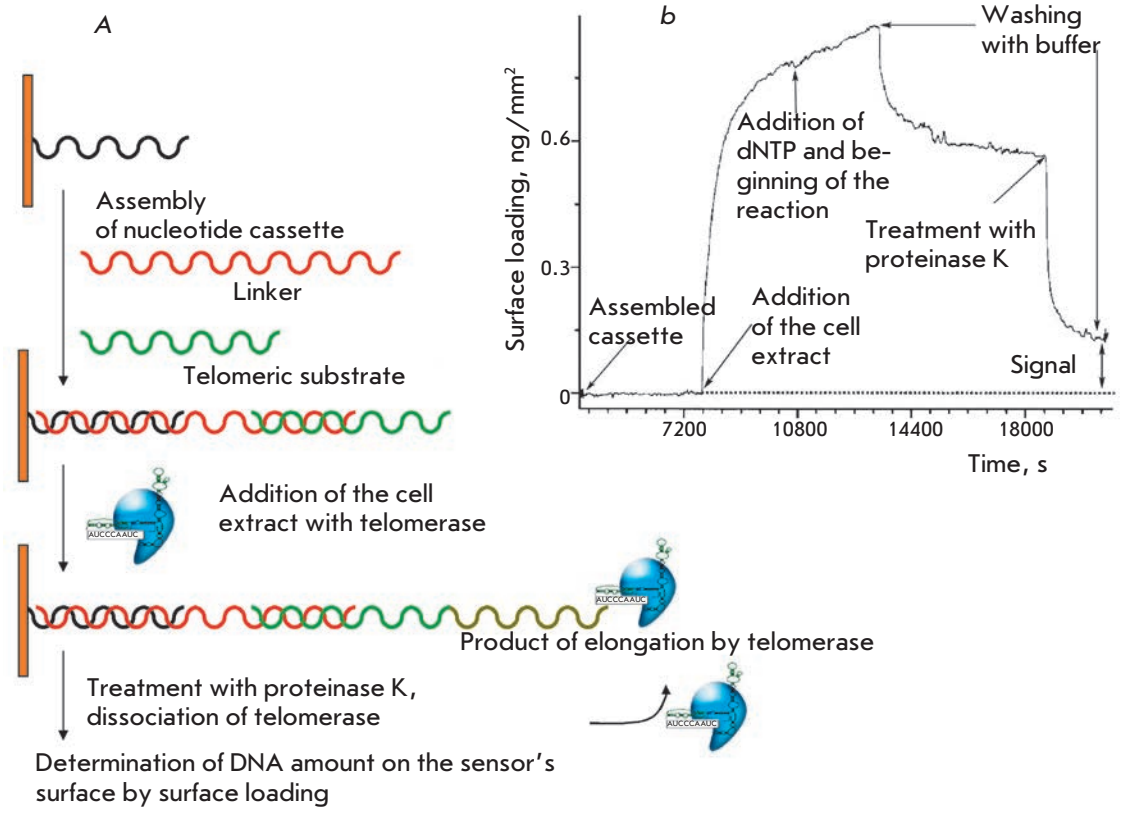

Fig. 15. A - The scheme of formation of telomerase-synthesized DNA on the sensor surface. B - Sensogram for determination of the surface loading on the optical sensor [50].

surface, to which monoclonal antibodies can be linked. The conductivity of the antibody-coated nanowire varies depending upon the binding of antigens, which is detected.

When using a sensor chip to determine telomerase activity, the transistor nanowire is modified by telomere-imitating oligonucleotides instead of antibodies. After the introduction of telomerase and dNTP, the oligonucleotides bound on the surface elongate, which results in change in the conductivity of the transistor to which the oligonucleotides are bound [53]. The sensitivity of this method is 100 HeLa cells.

A similar method is based on using an ion-selective field-effect transistor. In the presence of certain chemical agents, a potential emerges on the shutter of these transistors. It opens the conductivity channel of the transistor; i.e., current starts flowing through it. The current's intensity is proportional to the concentration of the desired component. The Al_2O_3-shutter of the transistor is modified with a telomerase substrate. As a primer is elongated by telomerase, the potential on the shutter also changes. The method allows to determine telomerase activity in cell line extracts (this method has not been tested on clinical materials). Its sensitivity is 65 T293 cells [54]. The major advantage of the method is that a large number of different analyses of one specimen can be carried out on a single chip, which can be a

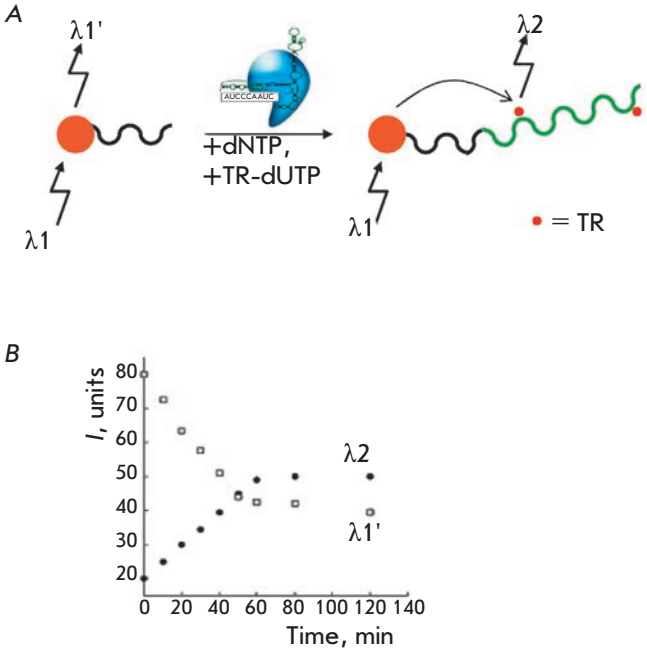

Fig. 16. A - Telomerization of the oligonucleotide bound with CdSe-ZnS by a quantum dot with the incorporation of Texas Red-labeled dUTP. B - Switching from the wavelength of quantum dot fluorescence (λ1) to Texas Red fluorescence (λ2) upon telomerization of the nucleotide bound with CdSe-ZnS by a quantum dot with the incorporation of TR-dUTP [51]. TR – Texas Red.

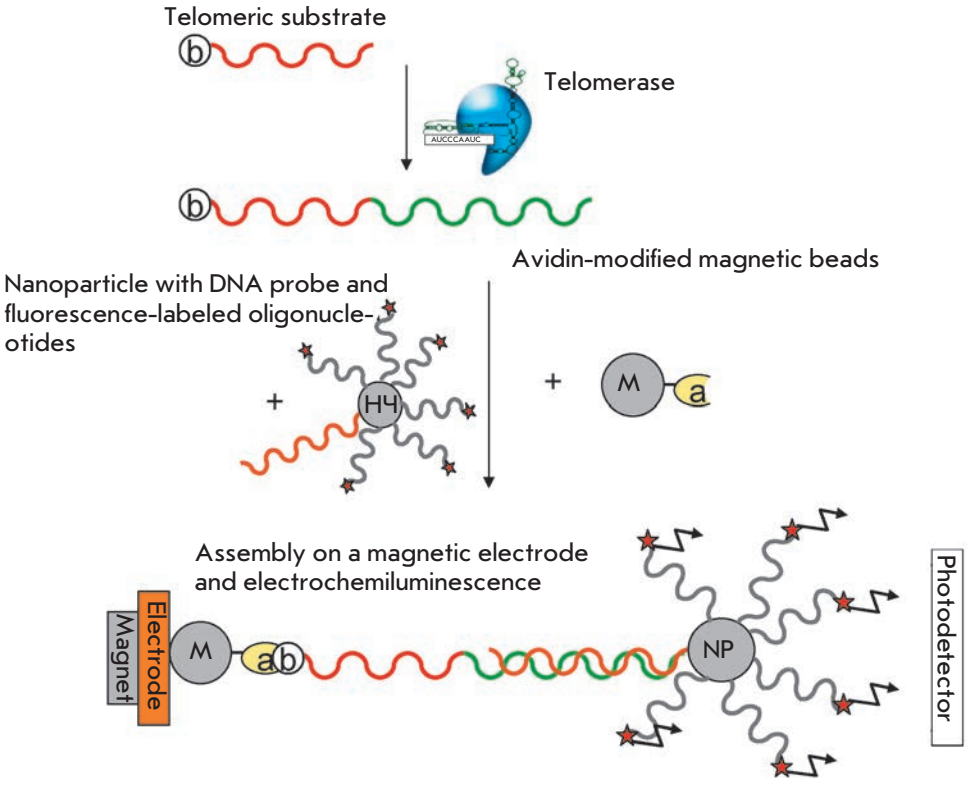

Fig. 17. Electrochemiluminescence method for telomerase activity detection [54].

set of sensors with respect to various markers. Moreover, the stages of telomerase binding and dissociation can be observed.

Bioluminescence method to determine telomerase activity

Determination of telomerase activity using the bioluminescence method is based on the fact that the telomerase-catalyzed elongation of the telomere-imitating oligonucleotide is accompanied by the cleavage of pyrophosphate; its amount is determined luminometrically. In the presence of adenosine-5'-phosphosulfate, ATP-sulfurylase converts pyrophosphate into ATP; its content is determined using the luciferin/luciferase method. According to [55], the sensitivity and specificity of the method is comparable with the sensitivity of TRAP-ELISA. This method allows quantitative determination of the telomerase activity in cell line and tissue extracts (having been tested on lung tumors). The advantage of the method is the linear dependence of the signal on the amount of telomerase-synthesized DNA, combined with high efficiency.

Electrochemiluminescence method to determine telomerase activity

Telomerase activity can also be determined by electrochemiluminescence (luminescence upon electrolysis). In this method, the 5'-biotin-conjugated primer is elongated by telomerase followed by incubation with a suspension of magnetic beads modified with avidin. The DNA immobilized on magnetic beads is hybridized with an electrochemiluminescence sample (modified with a ruthenium-bis(2,2'-bipyridine)(2,2'-bipyridine-4,4'-bicarbonate)-N-hydroxysuccinimide ester oligonucleotide that is covalently bound to a gold nanoparticle). These ternary complexes (magnetic bead–telomeric sample–electroluminescence sample) are washed and injected into a reaction cuvette in which they are magnetized to the working electrode and begin to luminesce under voltage (*Fig. 17*). This method allows for the quantitative determination of telomerase activity in samples that contain at least 500 HeLa cells [56]. It provides an appreciably high signal/noise ratio due to the stage of magnetic bead extraction; however, it has not been tested on clinical materials.

Telomerase activity detection by FRET and total internal reflection fluorescence microscopy

The FRET-based method is intended to distinguish the single-letter synthesis (a nonprocessive method of synthesis) and the beginning of synthesis of the second DNA repeat (a conditionally processive method of synthesis) by individual complexes of *Tetrahymena thermophila* telomerase. FRET was determined using the total internal reflection fluorescence microscopy that is based on the phenomenon of reflection of electromagnetic waves

from the interface of two transparent media. The transparent media emerge under the condition that a wave comes from the medium with a higher refraction index, at an angle that exceeds the angle of total reflection. The intensity of the radiation penetrating into the second medium decreases in accordance with the exponential law, which allows to reveal the fluorescent objects that are excited by this radiation within an ~100-nm thick boundary layer with a resolution of up to 10 nm.

Biotin-conjugated primers $(TG)_8T_2G_4T_2$ were bound on streptavidin-coated quartz slides and treated with a telomerase-containing extract in the presence of dGTP and ddTTP; the latter ceasing the synthesis at the second repeat. As a result, detectable products of two types were formed. The slides with the reaction products were treated with a Cy3-labeled oligonucleotide (Cy3-$(CA)_8$) in order to stain each primer bound to the slide with Cy3 because of complementary interaction with a nontelomeric region of the oligonucleotide $(TG)_8$. Then, the system was treated with a Cy5-labeled detecting oligonucleotide (Cy5-$C_2A_2C_3$), which was complementary to the telomeric sequence. This nucleotide can be more effectively bound with the longer telomerase product. The FRET signal is recorded between Cy3 and Cy5 [57] (*Fig. 18*). The method allows to identify individual signals from the elongation of the primer by telomerase.

In order to verify and normalize the system, primers of three types labeled with Alexa Fluor-488 were used: those corresponding to the sites without synthesis; to single-letter synthesis; and to the synthesis of the second repeat ($(TG)_8T_2G_4T_2$, $(TG)_8T_2G_4T_2G$, $(TG)_8T_2G_4T_2G_4T$) with 5'-end biotin, which were bound with streptavidin-coated quartz slides. Fluorophore Alexa Fluor-488 makes it possible to determine the density and localization of the primers bound to the slide [57].

The determination of telomerase activity using FRET and total internal reflection fluorescence microscopy allows to detect the elongation of individual primers by telomerase and can be combined with FRET-based methods of investigation of the telomerase structure. This method can be used to determine only the first 1.5 telomerase-synthesized repeats; i.e., it does not reveal total telomerase activity. The method has been tested only on *T. thermophila* telomerase and has been aimed only at solving research problems so far.

DETERMINATION OF TELOMERASE ACTIVITY BY ELISA SIGNAL AMPLIFICATION

Determination of telomerase activity using digoxigenin-labeled oligonucleotides complementary to telomeres

The determination of telomerase-synthesized DNA by ELISA is appealing, since it is an isotope-free method. This method is based on hybridization of telomerase-synthesized DNA with a digoxigenin-labeled oligonucleotide and determination of the resulting complex by ELISA, using a dioxigenin antibody–alkaline phosphatase conjugate (*Fig. 8*). The sensitivity threshold of the method is 10 amol of the product, which is typical for digoxigenin systems. When using T293 cell extracts, the sensitivity level was 37,500 cells [58], which is insufficient for the analysis of clinical materials. The method for determining telomerase-synthesized DNA by ELISA is far from being the most sensitive; however, it has been completely automated and optimized for the search for telomerase inhibitors.

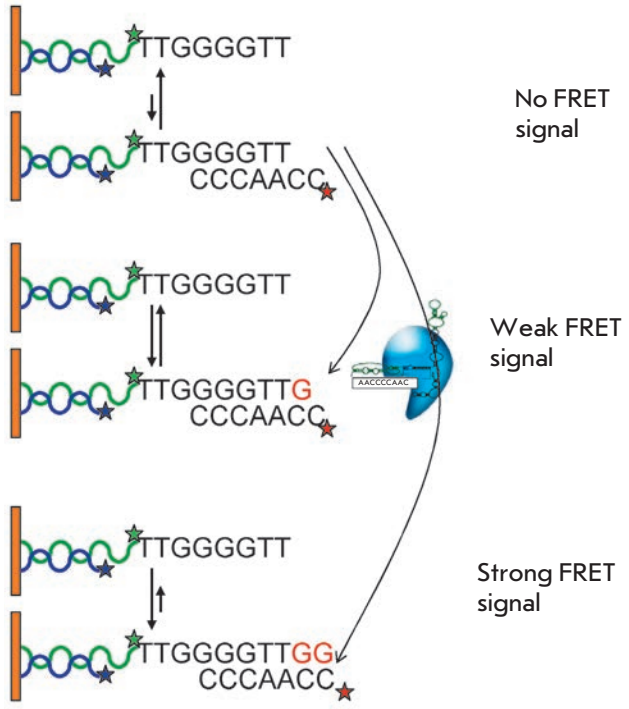

Fig. 18. Telomerase activity detection using FRET and total internal reflection fluorescence [57].

Electrochemical determination of telomerase activity using avidin–alkaline phosphatase conjugates

This method is based on ELISA signal amplification with electrochemical detection. A thiolized oligonucleotide substrate, which is covalently attached to a gold electrode, is elongated by telomerase in the presence of NTP. ELISA is then carried out (similar to the method in which a quartz crystal microbalance is applied), yielding an insoluble product on the electrode's surface, which is detected electrochemically (*Fig. 12*). Chronopotentiometry (the method based on measuring the variation of the electrode potential E in time under a controlled (constant) value of the electrolysis current) is used for the detection. The larger the deposit

Table 2. Brief comparison of the methods for telomerase activity detection

Method for telomerase activity detection	Sensitivity*	Advantages	Drawbacks**	Reference
Direct incorporation of a radioactively labeled substrate	10^5–10^6	The absence of artifacts associated with PCR. The telomerase-synthesized DNA can be immediately observed in the gel. Its size and amount can be estimated.	Low sensitivity, the necessity of working with large amounts of a radioactive label, long-term exposition.	[43]
Determination of telomerase-synthesized DNA by the changes in surface plasmon resonance	20–100	The absence of artifacts associated with PCR. No radioactive label and PAAG. Information on the reaction's kinetics. The possibility of signal detection against 1,000-fold excess of telomerase-negative cells. Telomerase binding and dissociation can be observed.	The BIACORE system and biotin-conjugated primers are required.	[44, 54]
Using oligo-modified magnetic particles and NMR	10	The absence of artifacts associated with PCR. No radioactive label and PAAG. A very high performance microplate format.	A NMR spectrometer and a sample of nanoparticles covalently bound to oligonucleotides are required.	[46]
Using the quartz crystal microbalance technique	3300	The absence of artifacts associated with PCR. High sensitivity. Rapid procedure.	A frequency analyzer and a Au-quartz crystal are required. Identification of artifact signals (in case of emergence) is difficult.	[47]
Electrochemically, using ferrocenyl naphthalene diimide	100–1000	The absence of artifacts associated with PCR. High sensitivity. Rapid procedure.	The number of structures folded into the quadruplex is assessed, which depends not only on the total number of repeats, but also is unpredictably dependent on the length and position of individual DNA fragments.	[48]
Using a biobarcode	10	One of the most sensitive methods today for direct telomerase activity detection without amplification of the telomerase-synthesized DNA	A modified electrode and nanoparticles coated with oligonucleotides of two types are required.	[49]
Using optical biosensors	10^5	No radioactivity, no PAAG, no PCR.	Phosphorothioate-modified oligonucleotides and a special optosensor are required. The sensitivity is insufficient for clinical materials.	[50]
Based on quantum dots	10,000/270	No radioactivity, no PAAG, no PCR.	Oligonucleotides covalently bound to quantum dots are required. The sensitivity is insufficient for clinical materials.	[51]
Using an on-chip nanowire sensor	100	It is possible to carry out a large number of different analyses of one specimen on a single chip. Telomerase binding and dissociation can be observed.	A transistor chip and the equipment to analyze it are required.	[53]
Bioluminescent method	5	Linear dependence of the signal on the amount of the telomerase-synthesized DNA. No radioactivity, no PAAG, no PCR. High-efficiency format.	The luciferase system for bioluminescence detection and a luminometer are required.	[55]
Electrochemiluminescence method	500	A high signal/noise ratio due to purification by modified magnetic bead extraction. High sensitivity.	It is difficult to synthesize a sample, requirements to the equipment.	[56]
Using FRET and total internal reflection fluorescence microscopy	1	Extremely high sensitivity – it is possible to detect the elongation of individual primers by telomerase. Possibility of combining this method with FRET-based methods for investigating the telomerase structure.	The method determines only the first 1.5 telomerase-synthesized repeats. It was tested only for *Tetrahymena thermophila* telomerase.	[57]
Using digoxigenin-labeled oligonucleotides complementary to telomeres (ELISA)	37,500	Quantitative determination; the method has been automated.	The sensitivity is insufficient for clinical materials.	[58]
Electrochemically, using avidin–alkaline phosphatase conjugates	3,300	The absence of artifacts associated with PCR. High sensitivity. Rapid procedure.	A specially prepared electrode is needed. It is difficult to identify artifact signals if they emerge.	[47]
Using a fluorimetric optosensor	10^6–10^7	No radioactivity, no PAAG, no PCR.	Phosphotioate-modified oligonucleotides and an optic fiber system for fluorescence detection are required. The sensitivity is insufficient for analyzing clinical materials.	[59]

Using DNAzyme-labeled oligonucleotides	1,000	No radioactivity, no PAAG, no PCR. Simple procedure and short analysis time.	The specificity of the method is not very high; a background signal is present.	[61]
On the basis of the telomerase substrate that refolds in DNAzyme	10,000	No radioactivity, no PAAG, no PCR. A very simple procedure and short analysis time.	The sensitivity and specificity of the method are not very high; a background signal is present.	[60]
TRAP	10	Amplificates of telomerase-synthesized DNA can be observed. PAAG makes it possible to identify some PCR artifacts. High specificity.	Working with the radioactive label, necessity of using PAAG. PCR artifacts are possible.	[11]
TRAP from a single cell	1	High sensitivity. PAAG makes it possible to identify some PCR artifacts and qualitatively judge the processivity.	Working with the radioactive label, working with individual cells, necessity of using PAAG. PCR artifacts are possible.	[13]
TRAP with fluorescent primers	100	No radioactive labeling. PAAG makes it possible to identify some PCR artifacts and qualitatively judge the processivity.	Necessity of fluorescently labeled primers, necessity of using PAAG. PCR artifacts are possible.	[20]
TRAP with fluorescent staining of DNA in gel	10	No radioactive labeling. PAAG makes it possible to identify some PCR artifacts and qualitatively judge the processivity.	Necessity of using PAAG. PCR artifacts are possible. Most intercalating fluorescent dyes are mutagenic.	[16, 18]
TRAP with DNA staining with silver nitrite in gel	10	No radioactive labeling. PAAG makes it possible to identify some PCR artifacts and qualitatively judge the processivity.	Necessity of using PAAG. Possibility of PCR artifacts. High labor input.	[17]
TRAP with analyzing by scintillation proximity assay	10	No radioactivity, no PAAG. Highly efficient microplate format. Simple estimation of the amounts.	Necessity of using [^{3}H]TTP and biotin-conjugated primers. Working with tritium. PCR artifacts are possible.	[27]
TRAP with detection by “hybridization protection”	10	No radioactivity, no PAAG. Highly efficient microplate format. Simple estimation of the amounts.	Acridine-labeled samples are required. PCR artifacts are possible.	[28]
TRAP with amplifluore primers	10-50	No radioactivity, no PAAG. Highly efficient microplate format. Quantitative assessment. Different labeling of amplificates by the telomerase-synthesized DNA and PCR control.	PCR artifacts are possible. Amplifluores are required.	[22]
TRAP combined with ELISA	10	No radioactivity, no PAAG. Highly efficient microplate format.	PCR and ELISA artifacts are possible.	[29]
TRAP with primers with fluorescence resonance energy transfer (FRET)	10	No radioactivity, no PAAG. Highly efficient microplate format.	Unequal consideration of the first and subsequent repeats synthesized by telomerase when carrying out the quantitative assessment. PCR artifacts are possible. Special fluorophores are required.	[26]
TRAP on microchips	10	No radioactivity, no PAAG. Small reaction volumes. Highly efficient microplate format. Simple estimation of the amounts.	Chips and an instrument to read them are necessary.	[35]
TRAP with real-time PCR	50	No radioactivity, no PAAG. Highly efficient microplate format. Simple estimation of the amounts. Different labeling of amplificates of the telomerase-synthesized DNA and PCR control with amplifluores is possible.	An amplifier for real-time PCR is required. The identification of PCR artifacts is complicated.	[32, 33]
In situ TRAP	1	The method provides information on the telomerase activity in individual cells and some information on endocellular localization of the activity.	A complicated procedure. Low efficiency. A fluorescence microscope is required. The method has been optimized only for analyzing clinical samples and cell lines.	[36]
TRAP with transcriptional amplification	10	Isothermal amplification, no PCR artifacts, PAAG-free detection, highly efficient format.	Acridine-labeled samples are required. Artifacts of transcriptional amplification are possible. Higher requirements of purity (absence of RNases) because of the transcriptional amplification.	[42]

* The minimum number of cells of telomerase-positive cell lines for which activity can be detected.

** In PAAG-free methods (with the exception of determination of telomerase activity using FRET and total internal reflection fluorescence microscopy), polymerase activity (but not processivity) is assessed.

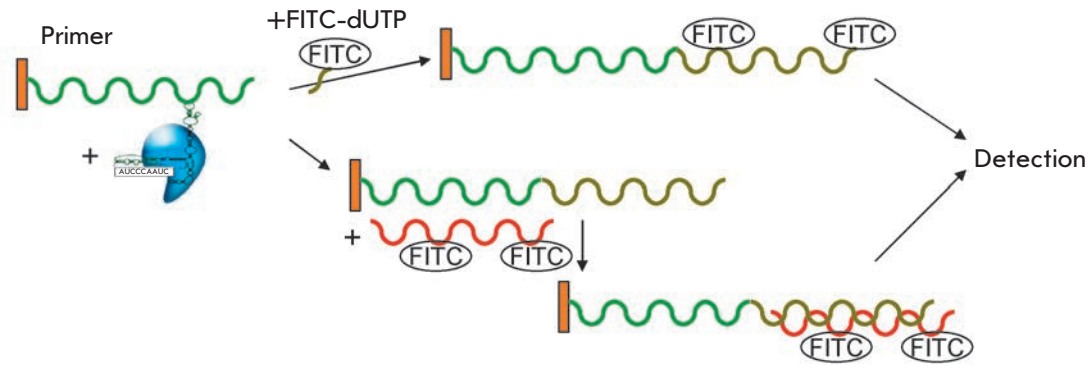

Fig. 19. Scheme of formation of fluorescence-labeled telomerase-synthesized DNA detection by a fluorimetric optical sensor [59].

on the electrode's surface, the stronger the variation of the potential. This method allows for the quantitative determination of telomerase activity in tissue and cell line extracts at a high rate [47]. The sensitivity of this method is sufficient for determining telomerase activity in an extract corresponding to 1,000 HeLa cells.

Determination of telomerase activity using a fluorimetric optosensor

This optical sensor is based on fluorimetry (in fact, it is a fluorimeter with an optical fiber used in the excitation and detection systems). The oligonucleotide, the telomerase substrate, is modified at the 3'-end by phosphotioate in order to enhance the affinity of the telomere-oligonucleotide binding region of hTERT and, therefore, the rate of the telomerase reaction. This primer covalently binds to the surface of an optical biosensor; its elongation by telomerase is traced in real time by incorporation of dUTP labeled with a isothiocyanate fluorescein derivative (FITC), or the elongated chain is determined by hybridization of the FITC-labeled complementary DNA sample ($(CCAATC)_4$-FITC) (*Fig. 19*). No PCR amplification or additional purification stages are required in this method [59]. Furthermore, the efficiency of the telomerase function was compared in the presence of regular dNTP and in the presence of FITC-labeled dUTP. In order to achieve this, telomerase-synthesized DNA, in the presence of FITC-labeled dUTP, was labeled with a FITC-labeled complementary DNA sample. It turned out that telomerase was less efficient in the presence of FITC-labeled dUTP [59]. This method allows for the quantitative determination of telomerase activity; however, its sensitivity does not exceed 10^6–10^7, which is insufficient for analyzing clinical materials. In addition, this method uses the custom-built system of fluorescence detection.

Determination of telomerase activity using DNAzymes

DNAzymes are DNA fragments with enzymatic activity.

There are several ways in which DNAzymes can be used when analyzing telomerase. First, a telomerase substrate may have a hairpin at its 5'-end, which refolds as the substrate elongates, thus forming a catalytic structure (*Fig. 20A*). In doing so, one chain of the original hairpin forms a duplex with the *de novo* synthesized telomeric repeats, while the second hairpin in the presence of a hemin molecule forms a quadruplex with an incorporated hemin molecule with peroxidase activity. This complex catalyzes the oxidation of 2,2'-azino-bis(3-ethylbenzthiazoline)-6-sulfonic acid (ABTS) in the presence of H_2O_2, which results in the accumulation of a colored product (*Fig. 20*). The sensitivity of this method is approximately 10,000 HeLa cells, with a duration of the analysis of approximately 8 min [60]. The slow change in coloration of the extract from the control cells after the thermal treatment should be noted. These authors believe that this is associated with the nonspecific hemin sorption on the reaction mixture components. This method represents the number of elongated substrate molecules; however, it does not take into account the length of the chain synthesized by telomerase.

Similarly, a DNAzyme that is covalently linked with the antisense oligonucleotide can be used for the telomerase-synthesized DNA [61] (*Fig. 20B*). It is virtually similar to ELISA in which an enzyme has already been covalently linked to the probe. The sensitivity of this modification is approximately 1,000 HeLa cells upon a lower background. The drawbacks of the method include low sensitivity and specificity, as well as the presence of a background signal.

CONCLUSIONS

At the time of publication of this article, there were a number of methods for the determination of telomerase activity in various specimens: extracts of cells, tissues, and mixed cell populations. All the aforementioned methods can be divided into two groups: those with direct detection of telomerase-synthesized DNA and those with various amplification schemes; each method

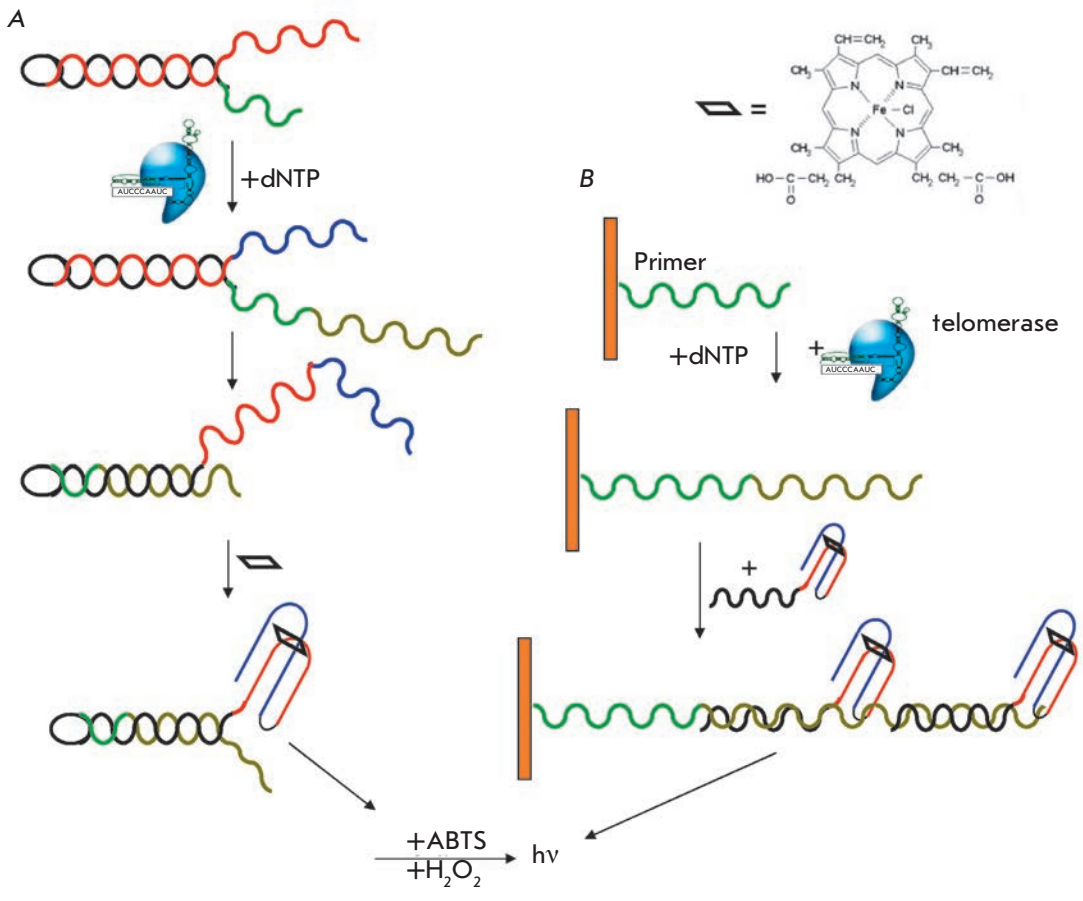

Fig. 20. (A, B) Two schemes for telomerase activity detection with DNAenzymes [60, 61].

has its advantages and drawbacks. A comparison of all these methods is provided in *Table 2*.

After the consideration of all the methods, a number of new systems can be singled out which are comparable in terms of sensitivity with the TRAP method, the most commonly used method at the moment. They do not have artifacts associated with amplification; the analysis is carried out at a high rate with high sensitivity. Meanwhile, they have a number of drawbacks, including high requirements to the specific supplies and equipment. Therefore, the selection of a technique in each particular case can be determined by the availability of the equipment and reagents. In a number of methods, it is difficult to distinguish between the specific and nonspecific signals. Most methods assess only telomerase activity, but not its processivity. They frequently provide no information on the length distribution of the telomerase-synthesized DNA. Some methods are highly specialized; e.g., the method in which telomerase-synthesized DNA is determined using dioxigenin-labeled oligonucleotides that are complementary to telomeres (ELISA) without PCR is far from being the most sensitive method; however, it has been completely automated and optimized for the search for telomerase inhibitors. The determination of telomerase activity by FRET and total internal reflection fluorescence microscopy makes it possible to detect the elongation of individual primers by telomerase, which can be combined with FRET-based methods for investigating the telomerase structure; however, it allows detection of only the first 1.5 telomerase-synthesized repeats and is intended for research purposes. ●

This work was supported by Government Contract № 02.74.11.0706, the Russian Foundation for Basic Research (grant № 08-04-01220-a), and the Federal Agency for Education (contracts № P1390 and P800).

REFERENCES

1. Hayflick L., Moorhead P.S. // Exp. Cell Res. 1961. V. 25. P. 585–621.
2. Olovnikov A.M. // J. Theor. Biol. 1973. V. 41(1). P. 181–190.
3. Blackburn E.H. // Cell. 2001. V. 106(6). P. 661–673.
4. Pandita T.K., Hunt C.R., Sharma G.G., Yang Q. // Cell Mol. Life Sci. 2007. V. 64(2). P. 131–138.
5. Greider C.W., Blackburn E.H. // Cell. 1985. V. 43(2). P. 405–413.
6. Blackburn E.H. // Nature. 1991. V. 350(6319). P. 569–573.

7. Maida Y., Yasukawa M., Furuuchi M., Lassmann T., Possemato R., Okamoto N., Kasim V., Hayashizaki Y., Hahn W.C., Masutomi K. // Nature. 2009. V. 461(7261). P. 230–235.
8. Pasrija T., Srinivasan R., Behera D., Majumdar S. // Eur. J. Cancer. 2007. V. 43(9). P. 1476–1482.
9. Kedde M., le Sage C., Duursma A., Zlotorynski E., van Leeuwen B., Nijkamp W., Beijersbergen R., Agami R. // J. Biol. Chem. 2006. V. 281(52). P. 40503–40514.
10. Skvortsov D.A., Rubtsova M. P., Zvereva M. E., Kisseljov F. L., Dontsova O. A.// Acta Naturae, 2009. V. 1(1). P. 51-67.
11. Kim N.W., Piatyszek M.A., Prowse K.R., Harley C.B., West M.D., Ho P.L., Coviello G.M., Wright W.E., Weinrich S.L., Shay J.W. // Science. 1994. V. 266(5193). P. 2011–2015.
12. Saldanha S.N., Andrews L.G., Tollefsbol T.O. // Anal. Biochem. 2003. V. 315(1). P. 1–21.
13. Wright W.E., Shay J.W., Piatyszek M.A. // Nucl. Acids Res. 1995. V. 23(18). P. 3794–3795.
14. Skvortsov D. A., Gasparyan N. M., Rubtsova M. P., Zvereva M. E., Fedorova M. D., Pavlova L. S., Bogdanov A. A., Dontsova O. A., Kisseljov F. L. // Doklady Akademii Nauk, 2006. V. 408(4). P. 556-559.
15. Gomez D., Mergny J.L., Riou J.F. // Cancer Res. 2002. V. 62(12). P. 3365–3368.
16. Gan Y., Lu J., Johnson A., Wientjes M.G., Schuller D.E., Au J.L. // Pharm. Res. 2001. V. 18(4). P. 488–493.
17. Dalla Torre C.A., Maciel R.M., Pinheiro N.A., Andrade J.A., De Toledo S.R., Villa L.L., Cerutti J.M. // Braz. J. Med. Biol. Res. 2002. V. 35(1). P. 65–68.
18. Holt S.E., Norton J.C., Wright W.E., Shay J.W. // Methods Cell. Sci. 1996. V. 18. P. 237–248.
19. Skvortsov D.A., Zvereva M. E., Pavlova L. S., Petrenko A.A., Kisseljov F. L., Dontsova O. A. // Vestn. MSU, 2010. V. 65(3). P. 165-169.
20. Aldous W.K., Grabill N.R. // Diagn. Mol. Pathol. 1997. V. 6(2). P. 102–110.
21. Gollahon L.S., Holt S.E. // Cancer Lett. 2000. V. 159(2). P. 141–149.
22. Uehara H., Nardone G., Nazarenko I., Hohman R.J. // Biotechniques. 1999. V. 26(3). P. 552–558.
23. Szatmari I., Tokes S., Dunn C.B., Bardos T.J., Aradi J. // Anal. Biochem. 2000. V. 282(1). P. 80–88.
24. Szatmari I., Aradi J. // Nucl. Acids Res. 2001. V. 29(2). P. E3.
25. Bazin H., Preaudat M., Trinquet E., Mathis G. // Spectrochim. Acta A Mol. Biomol. Spectrosc. 2001. V. 57(11). P. 2197–2211.
26. Gabourdes M., Bourgine V., Mathis G., Bazin H., Alpha-Bazin B. // Anal. Biochem. 2004. V. 333(1). P. 105–113.
27. Savoysky E., Akamatsu K., Tsuchiya M., Yamazaki T. // Nucl. Acids Res. 1996. V. 24(6). P. 1175–1176.
28. Hirose M., Abe-Hashimoto J., Ogura K., Tahara H., Ide T., Yoshimura T. // J. Cancer Res. Clin. Oncol. 1997. V. 123(6). P. 337–344.
29. Mayfield M.P., Shah T., Flannigan G.M., Hamilton Stewart P.A., Bibby M.C. // Int. J. Mol. Med. 1998. V. 1(5). P. 835–840.
30. Hoos A., Hepp H.H., Kaul S., Ahlert T., Bastert G., Wallwiener D. // Int. J. Cancer. 1998. V. 79(1). P. 8–12.
31. Chen L., Huang J., Meng F., Zhou N. // Anal. Sci. 2010. V. 26(5). P. 535–538.
32. Hou M., Xu D., Bjorkholm M., Gruber A. // Clin. Chem. 2001. V. 47(3). P. 519–524.
33. Elmore L.W., Forsythe H.L., Ferreira-Gonzalez A., Garrett C.T., Clark G.M., Holt S.E. // Diagn. Mol. Pathol. 2002. V. 11(3). P. 177–185.
34. Kong D., Jin Y., Yin Y., Mi H., Shen H. // Anal. Bioanal. Chem. 2007. V. 388(3). P. 699–709.
35. Heller-Uszynska K., Kilian A. // Biochem. Biophys. Res. Commun. 2004. V. 323(2). P. 465–472.
36. Ohyashiki K., Ohyashiki J.H., Nishimaki J., Toyama K., Ebihara Y., Kato H., Wright W.E., Shay J.W. // Cancer Res. 1997. V. 57(11). P. 2100–2103.
37. Yahata N., Ohyashiki K., Ohyashiki J.H., Iwama H., Hayashi S., Ando K., Hirano T., Tsuchida T., Kato H., Shay J.W., et al. // J. Natl. Cancer Inst. 1998. V. 90(9). P. 684–690.
38. Ohyashiki K., Yahata N., Ohyashiki J.H., Iwama H., Hayashi S., Ando K., Aizawa T., Ito T., Miki M., Ebihara Y. // Cancer. 1998. V. 83(12). P. 2554–2560.
39. Dejmek A., Yahata N., Ohyashiki K., Kakihana M., Hirano T., Kawate N., Kato H., Ebihara Y. // Cancer. 2000. V. 90(2). P. 117–125.
40. Dejmek A., Yahata N., Ohyashiki K., Ebihara Y., Kakihana M., Hirano T., Kawate N., Kato H. // Diagn. Cytopathol. 2001.V. 24(1). P. 11–15.
41. Youssef N., Paradis V., Ferlicot S., Bedossa P. // J. Pathol. 2001. V. 194(4). P. 459–465.
42. Hirose M., Abe-Hashimoto J., Tahara H., Ide T., Yoshimura T. // Clin. Chem. 1998. V. 44(12). P. 2446–2452.
43. Blackburn E.H., Greider C.W., Henderson E., Lee M.S., Shampay J., Shippen-Lentz D. // Genome. 1989. V. 31(2). P. 553–560.
44. Maesawa C., Inaba T., Sato H., Iijima S., Ishida K., Terashima M., Sato R., Suzuki M., Yashima A., Ogasawara S., et al. // Nucl. Acids Res. 2003. V. 31(2). P. E4–4.
45. Rad'ko S.P., Voronina S.A., Gromov A.V., Gnedenko O.V., Bodoev N.V., Ivanov A.S., Yarygin K.N. // Bull. Exp. Biol. Med. 2009. V. 147(6). P. 746–749.
46. Grimm J., Perez J.M., Josephson L., Weissleder R. // Cancer Res. 2004. V. 64(2). P. 639–634.
47. Pavlov V., Willner I., Dishon A., Kotler M. // Biosens. Bioelectron. 2004. V. 20(5). P. 1011–1021.
48. Sato S., Kondo H., Nojima T., Takenaka S. // Anal. Chem. 2005. V. 77(22). P. 7304–7309.
49. Li Y., Liu B., Li X., Wei Q. // Biosens. Bioelectron. 2010. V. 25(11). P. 2543–2547.
50. Schmidt P.M., Matthes E., Scheller F.W., Bienert M., Lehmann C., Ehrlich A., Bier F.F. // Biol. Chem. 2002. V. 383(10). P. 1659–1666.
51. Patolsky F., Gill R., Weizmann Y., Mokari T., Banin U., Willner I. // J. Am. Chem. Soc. 2003. V. 125(46). P. 13918–13919.
52. Sharon E., Freeman R., Willner I. // Anal. Chem. 2010. V. 82(17). P. 7073–7077.
53. Zheng G., Patolsky F., Cui Y., Wang W.U., Lieber C.M. // Nat. Biotechnol. 2005. V. 23(10). P. 1294–1301.
54. Sharon E., Freeman R., Riskin M., Gil N., Tzfati Y., Willner I. // Anal. Chem. 2010. Sep 17. [Epub ahead of print]
55. Xu S.Q., He M., Yu H.P., Wang X.Y., Tan X.L., Lu B., Sun X., Zhou Y.K., Yao Q.F., Xu Y.J., et al. // Clin.Chem. 2002. V. 48(7). P. 1016–1020.
56. Zhou X., Xing D., Zhu D., Jia L. // Anal. Chem. 2009. V. 81(1). P. 255–261.
57. Wu J.Y., Stone M.D., Zhuang X. // Nucl. Acids Res. V. 38(3). P. e16.
58. Kha H., Zhou W., Chen K., Karan-Tamir B., San Miguel T., Zeni L., Kearns K., Mladenovic A., Rasnow B., Robinson M., et al. // Anal. Biochem. 2004. V. 331(2). P. 230–234.
59. Schmidt P.M., Lehmann C., Matthes E., Bier F.F. // Biosens. Bioelectron. 2002. V. 17(11–12). P. 1081–1087.
60. Xiao Y., Pavlov V., Niazov T., Dishon A., Kotler M., Willner I. // J. Am. Chem. Soc. 2004. V. 126(24). P. 7430–7431.
61. Pavlov V., Xiao Y., Gill R., Dishon A., Kotler M., Willner I. // Anal. Chem. 2004. V. 76(7). P. 2152–2156.

Structural and Dynamic Study of the Transmembrane Domain of the Amyloid Precursor Protein

K. D. Nadezhdin, O. V. Bocharova, E. V. Bocharov*, A. S. Arseniev
Shemyakin and Ovchinnikov Institute of Bioorganic Chemistry, Russian Academy of Sciences
*E-mail: bon@nmr.ru
Received 28.10.10

ABSTRACT **Alzheimer's disease affects people all over the world, regardless of nationality, gender or social status. An adequate study of the disease requires essential understanding of the molecular fundamentals of the pathogenesis. The amyloid β-peptide, which forms amyloid plaques in the brain of people with Alzheimer's disease, is the product of sequential cleavage of a single-span membrane amyloid precursor protein (APP). More than half of the APP mutations found to be associated with familial forms of Alzheimer's disease are located in its transmembrane domain. The pathogenic mutations presumably affect the structural-dynamic properties of the APP transmembrane domain by changing its conformational stability and/or lateral dimerization. In the present study, the structure and dynamics of the recombinant peptide corresponding to the APP fragment, Gln686-Lys726, which comprises the APP transmembrane domain with an adjacent N-terminal juxtamembrane sequence, were determined in the membrane mimetic environment composed of detergent micelles using NMR spectroscopy. The structure obtained in dodecylphosphocholine micelles consists of two α-helices: a short surface-associated juxtamembrane helix (Lys687-Asp694) and a long transmembrane helix (Gly700-Leu723), both connected via a mobile loop region. A minor bend of the transmembrane α-helix is observed near the paired residues Gly708-Gly709. A cholesterol-binding hydrophobic cavity is apparently formed under the loop region, where the juxtamembrane α-helix comes into contact with the membrane surface near the N-terminus of the transmembrane α-helix.**

KEYWORDS: **Alzheimer's disease, amyloid precursor protein, transmembrane domain, NMR spectroscopy, spatial structure, dynamics.**

ABBREVIATIONS: **APP – amyloid precursor protein; Aβ –amyloid β-peptide; TM – transmembrane; JM – juxtamembrane, APPjmtm – $APP_{686-726}$ fragment; DPC – dodecylphosphocholine; DSA – doxyl stearic acid; NOE – nuclear Overhauser effect; NOESY – NOE spectroscopy; HSQC – heteronuclear single-quantum correlation.**

INTRODUCTION

Over a century ago, the German physician A. Alzheimer described the degenerative brain disease that manifests itself in selective neural degeneration in the regions of the brain cortex responsible for cognitive perception and memory [1]. This disease can be inherited or appear sporadically; the inherited form (the so-called familial forms of Alzheimer's disease) appears earlier in the life of a subject. Despite the considerable progress achieved in the study of the molecular fundamentals of the pathogenesis of Alzheimer's disease [2], currently available therapy can only slow down the development of the disease, not cure it. During the progressive stages of the disease, the amyloid β-peptide (Aβ) accumulates at neuron contact sites outside nerve cells and aggregates into ordered bundles or fibrils, forming the so-called amyloid plaques [1]. The presence of hydrophobic protein aggregates leads to failure of nerve impulse transmission [1, 3, 4]. Aβ is a product of the sequential cleavage of the membrane glycoprotein, which is an amyloid precursor protein (APP), by β- and γ-secretases [1, 5]. Aβ was recently shown to possess powerful antimicrobial activity and, possibly, to be a component of innate immunity in the human nervous system [6]. Aβ is naturally produced in small amounts with a length of 38 to 43 amino acids; indeed, the most widespread isoforms have a length of 40 and 42 amino acids [1, 3, 4]. Normally, the ratio $Aβ_{1-42}/Aβ_{1-40}$ of peptides is low and amounts to 1/9, but with Alzheimer's disease it increases significantly, leading to the formation of amyloid plaques; the structural changes in Aβ underlie their formation process [1, 3, 4]. At the same time, some experimental data show that oligomeric forms of Aβ (including intracellular) display a potential neurotoxic effect even before the formation of fibrils and plaques [1, 3, 4].

While it dimerizes in plasmolemma, APP has the multidomain structure of an bitopicmembrane pro-

tein [7]. More than half of all familiar APP mutations of Alzheimer's disease fall on its transmembtrane (TM) domain and juxtamembrane regions [8, 9]. It is currently believed that these pathogenic mutations affect the lateral dimerization of the APP in the membrane, changing the conformation of the dimer and/or its stability. This is considered to be a possible cause behind the alternative APP cleavage by γ-secretase in the membrane and the domination of the pathogenic $A\beta_{1-42}$ form over $A\beta_{1-40}$ [9–11]. Meanwhile, it has been demonstrated that the APP-TM domain and its juxtamembrane regions specifically interact with the membrane environment, particularly with cholesterol and Cu^{2+} and Zn^{2+} cations, which may have an effect on the structural-dynamic properties and APP dimerization [12–15]. Thus, to understand better the molecular fundamentals of the pathogenesis of Alzheimer's disease, it is necessary not only to determine the spatial structure of Aβ peptides and their aggregates, but also of the APP protein and its TM domain. Despite some progress in structural-dynamic studies of Aβ amyloid peptides, only theoretical spatial models of the APP-TM domain and its mutant pathogenic forms exist to date. In the present study, the spatial structure is solved by heteronuclear NMR spectroscopy in a membrane mimetic environmet, and the dynamics of the APP-TM domain with a juxtamembrane (JM) region, which was incorporated as a monomer into detergent micelles, is described.

EXPERIMENTAL

Preparation of NMR samples of the APP-TM domain in a membrane mimetic environmet

The necessary for NMR amount of ^{15}N and ^{13}C labeled sample of the recombinant peptide APPjmtm, which corresponded to the APP fragment Gln686–Lys726 with the additional N-terminal residues Gly–Ser that remained after the hybrid protein had been cleaved by thrombin, were prepared according to the procedure described in [16]. The sample's purity was checked using the $^{1}H/^{15}N$-HSQC spectra of the isotope-labeled APPjmtm dissolved in 500 μl of a 5 : 5 : 1 chloroform–methanol–water mixture with a peptide concentration of 0.3 mM. Based on a screening of the composition of the membrane mimetic environment, detergent dodecylphosphocholine (DPC) micelles were selected for the subsequent structural NMR studies of APPjmtm [16]. Dry APPjmtm and DPC samples were dissolved in a 1 : 1 trifluoroethanol–water mixture, kept for several minutes in an ultrasound bath, lyophilized, and dissolved in a 20 mM acetate buffer (pH 5.0, 5% D_2O). In order to prevent bacterial contamination, 0.05 mM NaN_3 was added to the samples; 1 mM EDTA was also added for phospholipase inhibition. To attain a higher uniformity of the micelle size, several freeze–thaw cycles (heating to 40–45°C) were carried out, followed by storage in an ultrasound bath in order to achieve complete transparency of the solution. All samples were prepared on the basis of 0.3–1 mM of APPjmtm in 400 μl of the micelle solution with a peptide–detergent molar ratio of 1 : 70, which ensured that the peptide content was one per micelle. Accordingly, the DPC concentration was higher than the critical micelle concentration (~1 mM). The prepared samples were placed into Shigemi NMR ampoules by means of a glass plunger. The sample's quality was assessed using the 2D NMR spectra $^{1}H/^{15}N$-HSQC. The variation of pH and temperature demonstrated that the best NMR spectra of APPjmtm solubilized in DPC micelles (in terms of signal resolution) are obtained at pH 4.3–5.3 and at a temperature of 40–50°C.

NMR spectroscopy of the APP-TM domain in a membrane-like milieu

The NMR spectra of APPjmtm solubilized in DPC micelles at pH 4.6 and a temperature of 45°C were obtained on AVANCE III spectrometers (Bruker BioSpin, Rheinstetten, Germany) equipped with cryoprobes, with proton operating frequencies of 600 and 800 MHz. The spectra were processed with TOPSPIN 3.0 software (Bruker BioSpin, Rheinstetten, Germany). The NMR spectra were analyzed using CARA software [17]. To assign the ^{1}H-, ^{13}C-, and ^{15}N-resonances of the peptide and obtain the structural data (assignment and integration of cross peaks in NOE), we used an asset of two- and three-dimensional spectra: $^{1}H/^{15}N$-HSQC, $^{1}H/^{13}C$-HSQC; $^{1}H/^{13}C/^{15}N$-HNCA, $^{1}H/^{13}C/^{15}N$-HN(CO)CA, $^{1}H/^{15}N$-HNHA, $^{1}H/^{13}C/^{15}N$-HNCO, $^{1}H/^{15}N$-NOESY-HSQC, $^{1}H/^{13}C$-TOCSY-HSQC, and $^{1}H/^{13}C$-NOESY-HSQC [18]. The data on the intramolecular dynamics of the peptide were obtained via an analysis of the ^{15}N-relaxation data. For that purpose, the values of the heteronuclear $^{15}N\{^{1}H\}$ NOE, longitudinal (T_1) and transverse (T_2) relaxation times, and the rotational correlation time (τ_R) for the ^{15}N-labeled APPjmtm sample were measured based on the procedure described in [19]. The values of the times of exchange of the amide protons of the backbone peptide chain for deuterium of the solvent were assessed according to the changes in the signal intensities in the set of $^{1}H/^{15}N$-HSQC spectra, which had been sequentially accumulated after 1, 2, 4, 6, 8, 10, 14, 18, and 24 h for the pre-lyophilized APPjmtm sample that was dissolved in D_2O and incorporated into the micelles. The degree of spatial remoteness of an amino acid residue from the micelle surface and center were determined based on the broadening of the signals from the

amide groups of APPjmtm in $^{1}H/^{15}N$-HSQC spectra, after 5- and 16-doxyl stearine acids (5- and 16-DSAs) were sequentially added as paramagnetic spin labels in ratios of 0.5, 1, and 2 labels per DPC micelle, respectively. The APPjmtm residues, which take part in cholesterol binding, were identified by analyzing the changes in the generalized chemical shifts $\Delta\delta_{[HN]}$ (which were calculated as a square root of the sum of the squared changes in the chemical shifts of the signals ^{1}H ($\Delta\delta_{1H}$) and ^{15}N ($\Delta\delta_{15N}/5$) [13]) of the cross peaks belonging to the amide groups in $^{1}H/^{15}N$-HSQC spectra; these peaks being induced by the introduction of cholesteryl hemisuccinate (cholesterol analog) on the basis of one hemisuccinate molecule per DPC micelle.

Calculation of the spatial structure of the APP-TM domain

The APPjmtm spatial structure was obtained using the standard procedure [18]. The calculation of the spatial structure using NMR spectroscopy data was carried out with CYANA 2.1 [20] software using the method of molecular dynamics in torsion-angle space and the simulated annealing algorithm. The restrictions imposed on the interproton distances that are used during structure calculation were obtained from the volumes of NOE crosspeaks in the $^{1}H/^{15}N$-NOESY-HSQC and $^{1}H/^{13}C$-NOESY-HSQC spectra accumulated with a mixing time t_m = 80 ms. The restrictions on the dihedral angles were obtained from the values of the ^{1}H, ^{15}N, and ^{13}C chemical shifts of the NH-, CαH-, and CO-groups of APPjmtm with TALOS software [21]. The restrictions on hydrogen bonds were added after preliminary calculation of the structure, by analyzing the spatial proximity of the amide protons and oxygen atoms of the backbone chain of APPjmtm according to the angle criterion 140° < NHO < 180° and 130° < COH < 170°, and the distance criterion 1.9 Å ≤ d(O, H^N) ≤ 2.3 Å, 3.0 Å ≤ d(O, N) ≤ 3.4 Å, 3.2 Å ≤ d(C, H^N) ≤ 3.6 Å [22]. As a result, a set of 100 APPjmtm structures were calculated based on the upper limits for the interproton distances, dihedral angles φ, ψ, and χ^1, hydrogen bonds with consideration of the stereospecific assignment of peptide groups; 20 structures with the minimal target function parameter value were selected as the representative ones. Analysis and visualization of the calculated APPjmtm structures were carried out using CYANA and MOLMOL software [23].

RESULTS AND DISCUSSION

The recombinant peptide APPjmtm containing the APP-TM domain with the adjacent N-terminal juxtamembrane sequence was studied by heteronuclear NMR spectroscopy in a membrane mimetic invironmet - in the form of an aqueous suspension of DPC micelles

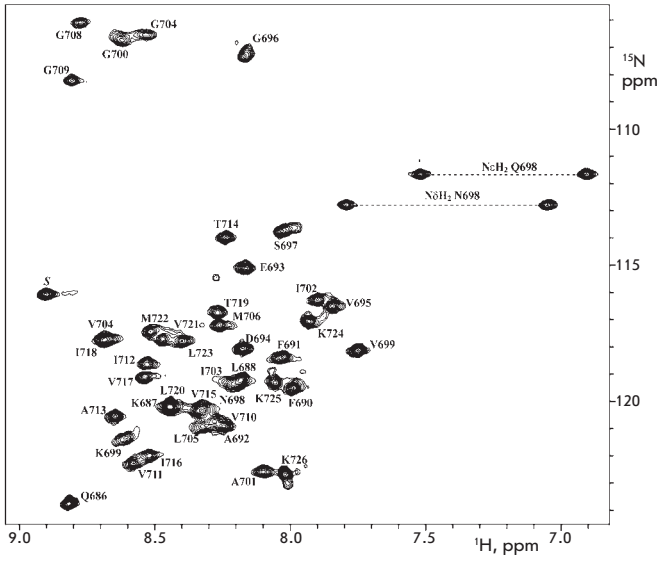

Fig. 1. Heteronuclear NMR spectrum $^{1}H/^{15}N$-HSQC of recombinant uniformly $^{13}C/^{15}N$-labeled peptide APPjmtm solubilized in an aqueous suspension of DPC micelles with a peptide/detergent ratio of 1:70, pH 4.6, 45 °C. The ^{1}H-^{15}N side chain and backbone resonance assignments are shown.

with a 1 : 70 peptide : detergent molar ratio (which corresponded approximately to one peptide per micelle) at pH 4.6 and a temperature of 45°C. It is of interest that APP undergoes cleavage in cell endosomes at a pH value of approximately 5 [13]. The samples of APPjmtm in DPC micelles remained stable at 45°C for a month, which is acceptable for NMR structural studies. The total amount of cross peaks from the amide groups in the $^{1}H/^{15}N$-HSQC spectrum (*Fig. 1*) coincided with the one estimated based on the primary structure of APPjmtm. This fact points to the absence of a slow (at the NMR scale) conformational exchange, and the content of protein impurities is less than 5%. A standard set of two- and three-dimensional heteronuclear NMR spectra was accumulated to sequentially identify the ^{1}H-, ^{13}C-, and ^{15}N-resonances of APPjmtm and obtain the structural-dynamic data (ref. the Experimental section).

It follows from an analysis of the combination of the NMR data obtained that the APPjmtm peptide contains two structured helix regions. The characteristic for the helices *i*- and *i*+3 NOE contacts (*Fig. 2a*), positive secondary chemical shifts of the $^{13}C\alpha$ signals (*Fig. 2c*), and small values of the temperature coefficients of the chemical shifts of $^{1}H^N$ signals (*Fig. 2b*) are observed here. In the $^{1}H/^{15}N$-NOESY-HSQC and $^{1}H/^{13}C$-NOESY-HSQC spectra, no NOE crosspeaks between the protons of amino acid residues from two helix regions were detected, which likely attests to the absence of interhelix

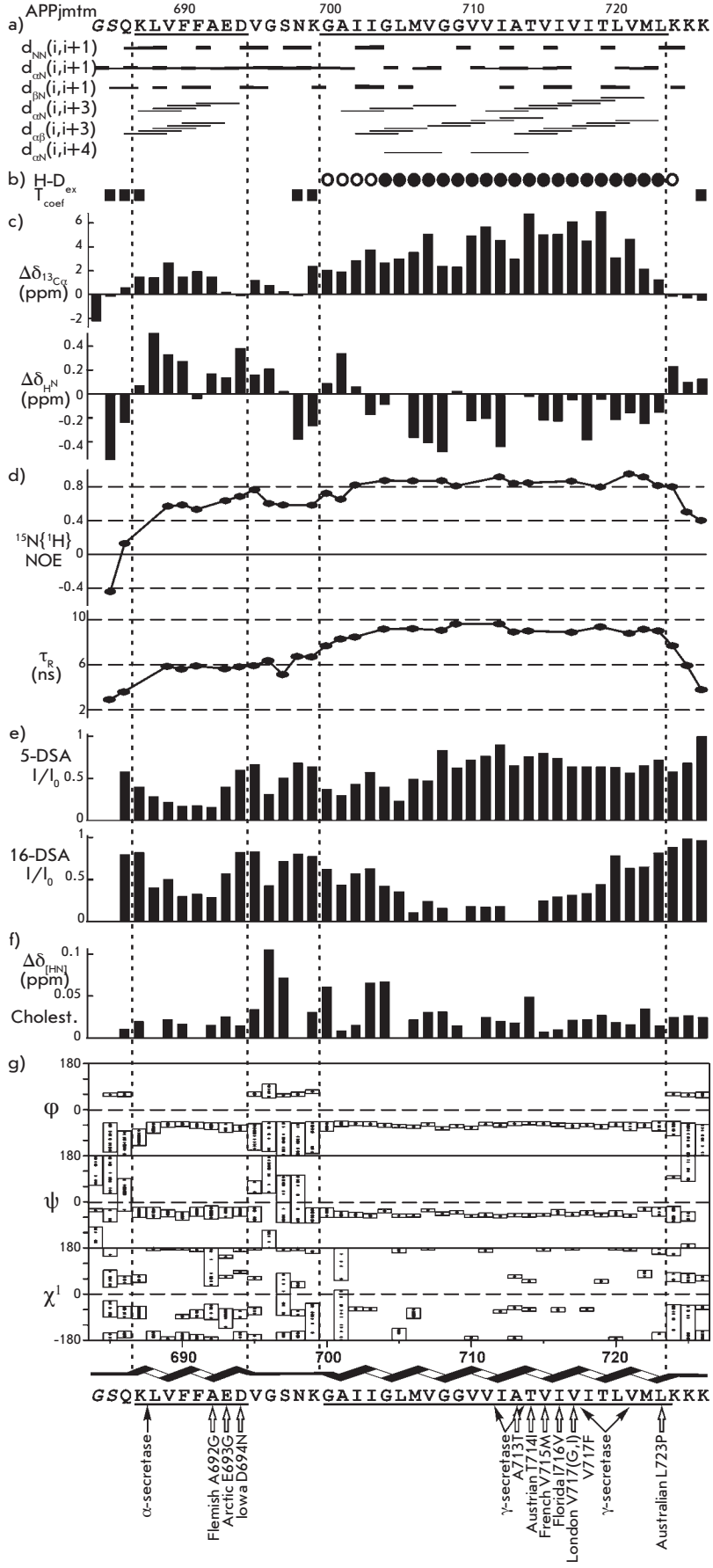

Fig. 2. Structural-dynamic NMR data for APPjmtm. *a* - Interproton NOE connectivities observed in the $^1H/^{15}N$-NOESY-HSQC and $^1H/^{13}C$-NOESY-HSQC spectra acquired with 80-ms mixing times. *b* - Water accessibility of the amide groups of APPjmtm solubilized in a DPC micelle aqueous suspension. Slowly hydrogen-deuterium exchanging amide groups of APPjmtm are presented *at the top* according to estimated half-exchange times: $t_{1/2}>2$ h (*solid box*); $1\leq t_{1/2}\leq 2$ h (*open box*); for the other residues $t_{1/2}<1$ h. APPjmtm residues having a temperature dependence of the amide proton chemical shift of more than 3 pbm on 1 °C are marked *at the bottom* by squares, indicating water accessibility to the amide groups. *c* - $^{13}C\alpha$ and $^1H^N$ secondary chemical shifts shown *at the top* and *bottom*, respectively, for the APPjmtm residues are given by the difference between the actual chemical shift and typical random-coil chemical shift for a given residue. Pronounced positive or negative $\Delta\delta_{13C\alpha}$ values indicate a helical structure or an extended conformation (including β-structure) of a protein [18]. The $\Delta\delta_{HN}$ value aside from others strongly depends on the length of a hydrogen bond in which the amide proton participates; thus, the local increase in $\Delta\delta_{H^N}$ is specified in the shortening of the given hydrogen bond [24]. *d* - ^{15}N-relaxation data for the APPjmtm amide groups are presented: *at the top*, steady-state $^{15}N\{^1H\}$ NOE; *at the bottom*, effective rotation correlation times τ_R of Brownian tumbling calculated from a ratio of ^{15}N longitudinal T_1 and transverse T_2 relaxation times. *e* - Amide signal broadening in the $^1H/^{15}N$-HSQC spectra of APPjmtm caused by the addition of 5- and 16-DSA (in a ratio of one spin-label on DPC micelle) tending mainly to be distributed near the surface and the micelle center, respectively. *f* - Variation of the generalized chemical shift $\Delta\delta_{[HN]}$ of amide crosspeaks in the $^1H/^{15}N$-HSQC spectra of APPjmtm caused by the addition of one cholesteryl hemisuccinate molecule in the DPC micelle. *g* - Distribution of backbone and side chain torsion angles φ, ψ and χ^1 in a representative set of 20 NMR structures of APPjmtm. APP α- and γ-cleavage sites and mutations associated with familial forms of Alzheimer's disease [8, 10] are indicated by arrows *at the bottom* of the APPjmtm amino acid sequence.

Structural characteristics for a representative set of 20 NMR structures of APPjmtm incorporated into DPC micelles

NMR data for structural calculation	Statistics
The total amount of NOE restrictions	318
Intraresidual	111
Interresidual	207
sequential (|i−j|=1)	132
medium range (1<|i−j|<4)	75
long range (|i-j|>4)	0
Restrictions on hydrogen bonds (upper/lower) between the atoms of the backbone chain (24 bonds) between the atoms of the backbone and side chains (0 chains)	72/72 0/0
Restrictions on dihedral angles	74
Angle φ of the backbone chain	30
Angle ψ of the backbone chain	30
Angle χ1 of the side chain	14
Quality of calculation and structural statistics	
Target function of CYANA software (Å^2)	0.38 ± 0.03
Violations of restrictions	
on distances (>0.2 Å)	1
on dihedral angles (>5^0)	0
Pairwise root-mean-square deviation between the structures (Å)	
Juxtamembrane α-helix, Lys687−Asp694 residues	
on atoms of the backbone chain	0.23 ± 0.09
on all heavy atoms	1.59 ± 0.28
TM α-helix, Gly700−Leu723 residues	
on atoms of the backbone chain	0.14±0.05
on all heavy atoms	0.55±0.10
Analysis of the Ramachandran map (% residues)	
in favorable regions	84.6
in additional, allowed regions	13.5*
in fundamentally allowed regions	1.5*
in forbidden regions	0.4*

* Residues from mobile and nonstructured APPjmtm regions.

interactions. It was confirmed from a calculation of the spatial structure using the experimental data listed in *Table* that APPjmtm in DPC micelles consists of two α-helices: Lys687−Asp694 and Gly700−Leu723 (*Fig. 3*), which are connected via a mobile loop region, Val695-Lys699. The relative orientation of the two helices in the resulting set of APPjmtm structures has not been determined (*Fig. 3a*). The structure of each α-helix was calculated with a high level of accuracy (*Table, Figs. 2g, 3a,b*). Let us note that the conformation of the backbone and side chains was determined more accurately for the α-helix of Gly700-Leu723.

In order to determine the topology of the α-helices of APPjmtm in a DPC micelle, we analyzed the broadening of the signals from the backbone amide protons of a peptide, which was conditioned by their spatial proximity to the paramagnetic spin labels of 5- and 16-DSA, which were mainly distributed near the micelle surface and center, respectively. Based on the pattern of intensity variation in the crosspeaks in the $^1H/^{15}N$-HSQC spectrum after the spin labels were added (*Fig. 2e*) and on data on the slow exchange of the protons of amide groups for the deuterium of the solvent (*Fig. 2b*), we concluded that the α-helix of Lys687−Asp694 (hereinafter JM-helix) lies in the region of hydrated polar DPC groups, whereas the α-helix of Gly700−Leu723 (hereinafter TM-helix) transpierces the hydrophobic part of the micelle. The amphiphility of the short JM-helix also indicates that it is located along the micelle surface, approximately perpendicular to the TM-helix, as shown in *Fig. 3d*. The sequence of weakly polar and hydrophobic amino acid residues at the Gly700−Leu723 region forms an extensive ~40 Å TM-segment. The positively charged amino acids of the side chains Lys699 and Lys724, which flank the TM-helix, presumably interact with the negatively charged phosphate groups of detergent heads. The observed (i+4) periodicity of the secondary chemical shift of the signals from $^1H^N$ protons (*Fig. 2c*) points to the periodic variation of the lengths of the hydrogen bonds $H^N\cdots O^C$ along the TM-helix [24]. The amide groups of the residues Leu705, Gly709, Ala713, and Val715 located on one side of the TM-helix (*Fig. 3c*) form shorter hydrogen bonds $H^N\cdots O^C$ as compared with the residues on the opposite side of the helix. Thus, the TM-helix has a small concavity with a weakly polar surface near the paired residues Gly708−Gly709.

The existence of two independent helix regions in the APPjmtm structure is also confirmed by ^{15}N-relaxation data. The JM- and TM-helices of APPjmtm have different characteristic values of the effective correlation time of the rotational correlation time τ_R (~6 and ~9 ns, respectively), which are calculated from the T_1/T_2 ratio (*Fig. 2d*). The mass of the supramolecular complex estimated from the value $<\tau_R> \approx 8$ ns averaged over the helix regions, according to empirical dependence [25], is estimated at 27 kDa; this value corresponds to the APPjmtm monomer surrounded by approximately 57 detergent molecules (the typical composition of a DPC micelle [26]). A significant difference (~3 ns) in $<\tau_R>$ values for residues of the JM- and TM-helices is partially accounted for by the APPjmtm topology with a perpendicular relative arrangement of α-helices in an anisotropically rotating micelle. In addition, APPjmtm rotation inside the micelle and an enhanced lateral mobility of the JM-helix (as compared with the TM-

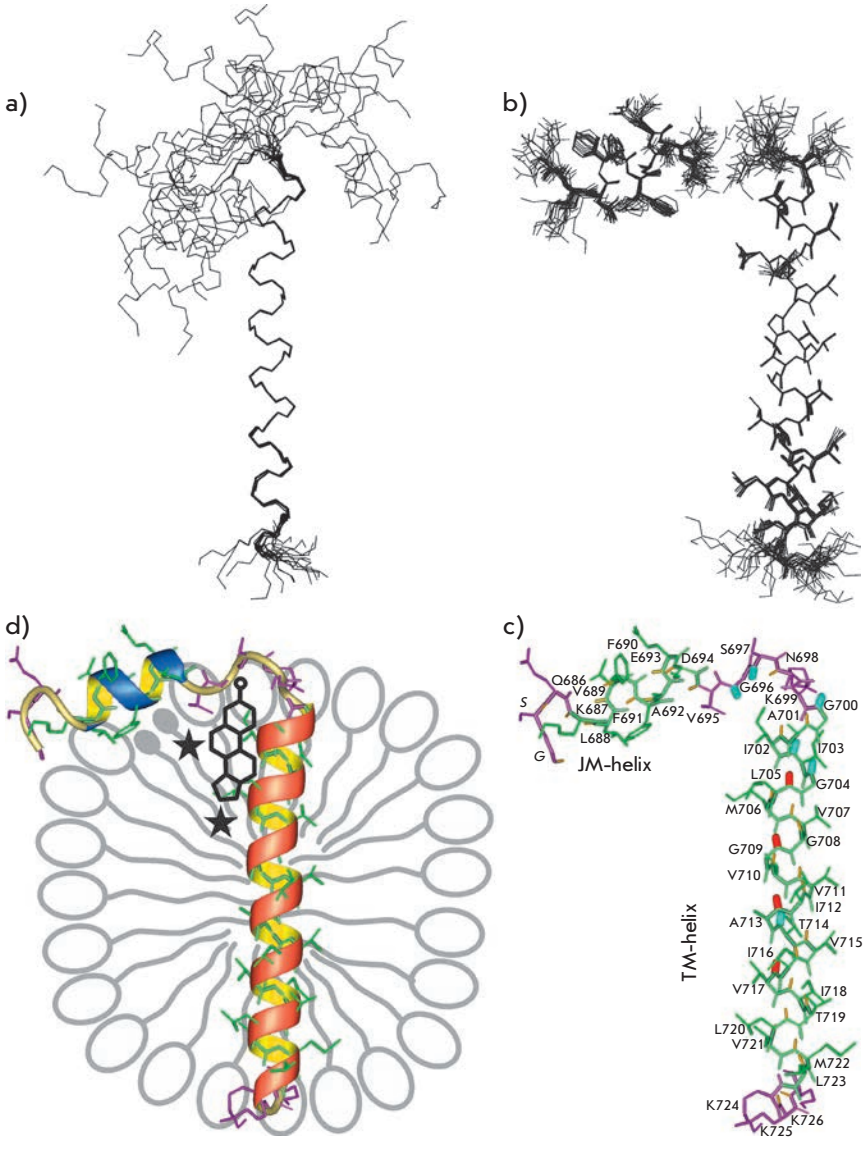

Fig. 3. APPjmtm spatial structure. *a* - Set of 20 NMR-derived structures of APPjmtm after superposition of the backbone atoms of the α-helix Gly700-Leu723. Only backbone bonds are shown. *b* - Set of 20 NMR-derived structures of APPjmtm superposed separately on the backbone atoms of α-helices Gly700-Leu723 (JM-helix) and Gly700-Leu723 (TM-helix). Because of uncertainty in the mutual arrangement of the α-helices, the calculated APPjmtm structures are presented with a gap between residues Gly696 and Ser697 from the flexible interhelical loop region. Only heavy atom bonds are shown. *c* - APPjmtm representative spatial structure with APP residue numbering. Heavy atom bonds of helical and unfolded regions are shown in *green* and *violet*, respectively. Amide groups are highlighted in *red* for the residues showing maximum local values of the $^{1}H^{N}$ secondary chemical shift ($\Delta\delta_{H^N}\approx 0$) along the TM-helix (*Fig. 2, c*). Amide groups displaying a significant variation of the [$^{1}H^{15}N$] generalized chemical shift ($\Delta\delta_{[HN]}>0.04$) upon addition of the cholesterol analogue to the micelles with embedded APPjmtm (*Fig. 2, f*) are highlighted in *blue*. Other amide bonds are shown in *yellow*. *d* - Schematic representation of the supramolecular system of the APPjmtm monomer associating with DPC micelle. The JM- and TM-helices of APPjmtm are colored in *blue* and *red*, respectively. Presumable rarefaction of detergent polar heads under the JM-helix are shown with the embedded spin-labels 5- and 16-DSA, the paramagnetic groups of which are depicted by asterisks situated near the surface and centre of the micelle, respectively. The APP cholesterol-binding site apparently formed under the interhelical loop near the N-terminus of the TM-helix is schematically indicated.

segment) due to the mobile-connecting loop Val695–Lys699 is also possible. A local decrease in the effective correlation time of the rotational correlation time τ_R for Ser697 attests to the mobility of the loop region as compared with α-helices. In turn, it follows from the distribution of the values of heteronuclear $^{15}N\{^{1}H\}$ NOE (*Fig. 2d*) that the N-terminus half of the JM-helix and the connecting loop in Val695–Lys699 are mobile in the pico-nanosecond range ($0.6\leq{}^{15}N\{^{1}H\}$ NOE ≤ 0.8), unlike the rigid TM-helix ($^{15}N\{^{1}H\}$ NOE ≥ 0.8). The increased mobility is responsible for the fact that the conformation of the JM-helix was confirmed less accurately (*Table, Figs. 2g and 3b*) and that the structure of the loop region was not determined at all.

The structural-dynamic data obtained in this work corresponds to the results of recent NMR studies [13] of the secondary structure and dynamics of the longer APP fragment – Asp672–Asn770, the so-called C99 peptide, which represents the C-terminus part of APP after it is hydrolyzed by β-secretase. The boundaries of the helix regions of Val689–Asp694 and Asn698–Lys724 and the C99 peptide were determined; they correspond to the α-helices – the short juxtamembrane and long transmembrane ones being connected by a

mobile loop. However, the spatial structure of the C99 peptide has not been calculated. Based on the titration data of the C99 peptide in LMPG micelles with a water-soluble cholesterol analog, β-CHOLBIMALT, the ability of APP to function as a cholesterol sensor in the neural membrane was assumed. Indeed, APP is known to accumulate in the human organism in cholesterol-rich microdomains, the so-called lipid rafts [27, 28]. Besides, enzymatic hydrolysis by β-secretase, which results in the formation of β-amyloid, takes place primarily in lipid rafts [28]. It has been also confirmed that non-amyloidogenic hydrolysis by α-secretase occurs outside cholesterol-rich clusters; the enzyme being inactivated as a substrate binds with the lipid rafts [28]. In this work, we studied the binding between APP and a cholesterol analog, cholesteryl hemisuccinate, which incorporates into the micelle. The most significant changes in the generalized chemical shift $\Delta\delta_{[HN]}$ observed near the residues Gly695, Ser696, Gly700, Ile701, Ile703, and Thr713 (*Fig. 2e*) point to the site of incorporation of cholesteryl hemisuccinate into the interhelix loop region (*Figs. 3c,d*), which agrees closely with earlier obtained data on the specific interaction between the C99 peptide and another cholesterol analog [13].

The data on APPjmtm titration in micelles with paramagnetic spin labels (*Fig. 2e*) provides indirect evidence pointing to the fact that there is a hydrophobic cavity near the JM-helix and N-terminus of the TM-helix, which is intended for APP interaction with cholesterol. If the distribution of the 5- or 16-DSA spin labels was uniform, there would have been an equal broadenings of the signals located at the same distance from the DPC micelle center. However, different broadening of the signals of the residues located at different ends of the transmembrane α-helix are recorded in both cases (*Fig. 2e*). There are several reasons which could account for this phenomenon. First, the distribution of spin labels over a micelle can be nonuniform due to the specific structure and properties of the APP-jmtm incorporated into it. Secondly, the length and size of the side chains in contact with the labels of amino acid residues have an impact on the degree of screening of amide protons (in all likelihood, it is pronounced to the largest extent at G700–Leu705 and Ile718–Leu723 regions). Meanwhile, the considerable broadening of signals at the Leu688–Ala692 region during the titration with the 16-DSA spin label directly points to a local change in the micelle structure under the near-surface juxtamembrane α–helix, which presumably "pushes away" the polar DPC heads (of the lipids), resulting in the formation of a "hydrophobic pocket." The two spin labels that have small polar groups are incorporated into this "pocket" with some selectivity (*Fig. 3d*).

Modification of the ambient conditions and surroundings of APP in the cell membrane may impact the changes in the conformation of the interhelix loop region. This should result in a variation of the mutual orientation of JM- and TM-helices, with a changing size of the cholesterol-binding "hydrophobic" pocket. In turn, it can play a role in simulation of the APP function. The Gly708–Gly709 tandem in the center of the APP–TM helix can, to some extent, compensate for the thickness of the lipid bilayer, which varies depending on the composition of the cell membrane, among other factors; due to cholesterol in the composition of lipid rafts. It is important to note that familial mutations associated with the early progression of Alzheimer's disease are concentrated not only near the TM-sites of the APP cleavage by γ-secretase, but also at the C-terminus of the JM-helix, where ionogenic Asp693 and Glu694 residues are located (*Fig. 2, bottom*). Therefore, the determination of the spatial structure of the APP-TM domain with a cholesterol-binding juxtamembrane region in a membrane mimetic environment by heteronuclear NMR spectroscopy is a necessary step in uncovering the molecular mechanism of the alternative APP cleavage, which is associated with the pathogenesis of Alzheimer's disease. ●

This work was supported by the Russian Foundation for Basic Research, the Federal Target Program Research and Development in the Priority Fields of Science and Technology in Russia for 2007–2012, and the Molecular and Cell Biology Program of the Presidium of the Russian Academy of Sciences.

REFERENCES

1. Grigorenko A.P., Rogaev E.I. // Mol. Biol. (Mosk). 2007. V. 41. P. 331–345.
2. Duce J.A., Tsatsanis A., Cater M.A., James S.A., Robb E., Wikhe K., Leong S.L., Perez K., Johanssen T., Greenough M.A., et al. // Cell. 2010. V. 142. P. 857–867.
3. Rauk A. // Dalton Trans. 2008. V. 14. P. 1273–1282.
4. Selkoe D.J. // Nature. 2003. V. 426. P. 900–904.
5. Steiner H., Fluhrer R., Haass C. // J. Biol. Chem. 2008. V. 283. P. 29627–29631.
6. Soscia S.J., Kirby J.E., Washicosky K.J., Tucker S.M., Ingelsson M., Hyman B., Burton M.A., Goldstein L.E., Duong S., Tanzi R.E., Moir R.D. // PLoS One. 2010. V. 5. P. e9505.
7. Thinakaran G., Koo E.H. // J. Biol. Chem. 2008. V. 283. P. 29615–29619.
8. Wiley J.C., Hudson M., Kanning K.C., Schecterson L.C., Bothwell M. // J. Neurochem. 2005. V. 94. P. 1189–1201.
9. Gorman P.M., Kim S., Guo M., Melnyk R.A., McLaurin J., Fraser P.E., Bowie J.U., Chakrabartty A. // BMC Neuroscience. 2008. V. 9. P. 17–27.

10. Munter L.M., Voigt P., Harmeier A., Kaden D., Gottschalk K.E., Weise C., Pipkorn R., Schaefer M., Langosch D., Multhaup G. // EMBO J. 2007. V. 26. P. 1702–1712.
11. Kienlen-Campard P., Tasiaux B., van Hees J., Li M., Huysseune S., Sato T., Fei J.Z., Aimoto S., Courtoy P.J., Smith S.O., et al. // J. Biol. Chem. 2008. V. 283. P. 7733–7744.
12. Marenchino M., Williamson P.T., Murri S., Zandomeneghi G., Wunderli-Allenspach H., Meier B.H., Krämer S.D. // Biophys. J. 2008. V. 95. P. 1460–1473.
13. Beel A.J., Mobley C.K., Kim H.J., Tian F., Hadziselimovic A., Jap B., Prestegard J.H., Sanders C.R. // Biochemistry. 2008. V. 47. P. 9428–9446.
14. Curtain C.C., Ali F., Volitakis I., Cherny R.A., Norton R.S., Beyreuther K., Barrow C.J., Masters C.L., Bush A.I., Barnham K.J. // J. Biol. Chem. 2001. V. 276. P. 20466–20473.
15. Bokvist M., Lindstrom F., Watts A., Grubner G. // J. Mol. Biol. 2004. V. 335. P. 1039–1049.
16. Bocharova O.V., Nadezhdin K.D., Bocharov E.V., Arseniev A.S. // Bioorg. Khim. 2010. V. 36. P. 105-111.
17. Keller R.L.J. The Computer Aided Resonance Assignment Tutorial., Goldau, Switzerland: CANTINA Verlag, 2004. 81 p.
18. Cavanagh J., Fairbrother W.J., Palmer A.G., Skelton N.J. Protein NMR spectroscopy: principles and practice. 2nd ed. San Diego, CA, USA: Acad. Press, 2007. 886 p.
19. Bocharov E.V., Korzhnev D.M., Blommers M.J., Arvinte T., Orekhov V.Y., Billeter M., Arseniev A.S. // J. Biol. Chem. 2002. V. 277. P. 46273–46279.
20. Güntert P. // Prog. Nucl. Magn. Reson. Spectrosc. 2003. V. 43. P. 105–125.
21. Cornilescu G., Delaglio F., Bax A. // J. Biomol. NMR. 1999. V. 13. P. 289–302.
22. Baker E.N., Hubbard R.E. // Prog. Biophys. Molec. Biol. 1984. V. 44. P. 97–179.
23. Koradi R., Billeter M., Wüthrich K.J. // Mol. Graphics. 1996. V. 14. P. 51–55.
24. Wagner G., Pardi A., Wüthrich K. // J. Am. Chem. Soc. 1983. V. 105. P. 5948–5949.
25. Daragan V.A., Mayo K.H. // Prog. Nucl. Magn. Reson. Spectrosc. 1997. V. 31. P. 63–105.
26. Lazaridis T., Mallik B., Chen Y. // J. Phys. Chem. B. 2005. V. 109. P. 15098–15106.
27. Vetrivel K.S., Thinakaran G. // Biochim. Biophys. Acta. 2010. V. 1801. P. 860–867.
28. Beel A.J., Sakakura M., Barrett P.J., Sanders C.R. // Biochim. Biophys. Acta. 2010. V. 1801. P. 975–982.

A *In Vitro* and *In Vivo* Study of the Ability of NOD1 Ligands to Activate the Transcriptional Factor NF-kB

A.I. Tukhvatulin[1*], D.Y. Logunov[1], I.I. Gitlin[2] , M.M. Shmarov[1], P.V. Kudan[1], A.A. Adzhieva[1], A.F. Moroz[1], N.N. Kostyukova[1], L.G. Burdelya[2], B.S. Naroditsky[1], A.L. Gintsburg [1], A.V. Gudkov[2]
[1]Gamaleya Research Institute of Epidemiology and Microbiology, Russian Academy of Medical Sciences
[2]Roswell Park Cancer Institute, Elm & Carlton Streets, Buffalo, New York, USA
[*]E-mail: amir_tuhvatulin@yahoo.com
Received 31.01.2011

ABSTRACT Pattern-recognition receptors (PRR) play a crucial role in the induction of the defense reactions of the immune system against pathogenic bacterial and viral infections. The activation of PRR by specific, highly conserved pathogen-associated molecular patterns (PAMPs) induces numerous immune reactions related both to innate and adaptive immunity. In addition to the well-studied Toll-like receptors, pathogens can be recognized by the receptors belonging to the other PRR families; including NOD-like receptors (NLR). Stimulation of members of NOD-like receptors (NOD1, 2) and Toll-like receptors results in the activation of the transcriptional factor NF-kB regulating gene expression in numerous molecules implicated in the development of proinflammatory reactions. As opposed to Toll-like receptors, the NF-kB-activating ability of NLRs has not been fully studied. In this work, we examine the ability of one member of the NLR family – NOD1 – to activate the main proinflammatory transcriptional factor NF-kB. We also compare the NF-kB-activating ability of NOD1 ligands of a different structure with TLR4,5 ligands *in vitro* and *in vivo*.
KEYWORDS pattern-recognition receptors, Toll-like receptors, NOD1-receptor, transcriptional factor NF-kB, peptidoglycan of gram-negative bacteria.
ABBREVIATIONS NF-kB – nuclear factor kappa-light-chain-enhancer of activated B cells); AP-1 – activator protein 1; TLR – Toll-like receptor; PAMPs pathogen-associated molecular patterns; DAMPs – damage-associated molecular patterns; PRR – pattern recognition receptor; TNF-α – tumor necrosis factor alpha; RT-PCR – reverse transcription polymerase chain reaction; IRF – interferon regulatory factor; NRL – NOD-like-receptor; RLR – RIG-like receptors; LPS – lipopolysaccharide.

INTRODUCTION

Until recently, both the mechanisms of recognition of infectious agents by macro-organism cells, as well as the molecular mechanisms of innate and adaptive immunity as a response to the developing infection, had not been subjected to adequate study.

An important step in the understanding of these mechanisms occurred twenty years ago, with the discovery of the first representatives of the pattern recognition receptors (PRR) of innate immunity: TOLL-like receptors (TLR). Today, seven PRR families are known: Toll-like receptors, NOD (nucleotide-oligomerization domain)-like receptors (NLR), RIG-like receptors (RLR), lectin-like receptors, etc. [2]. Representatives of these families can recognize a set of highly conservative fragments of exogenous pathogen-associated molecular pattern (PAMP) molecules, as well as some endogenous damage-associated molecular pattern (DAMP) molecules; each receptor having its specific set. The binding of intrinsic ligands with pattern-recognition receptors triggers intracellular signaling cascades, resulting in the activation of a number of transcriptional factors (AP-1, NF-kB, IRF 1, 3, 5, 7, etc.) which regulate the development of particular immune responses.

NF-kB is the primary pro-inflammatory factor that regulates the expression in a number of molecules which can participate in the development of reactions of both innate and adaptive immunity, such as the secretion of pro-inflammatory cytokines and chemokines, synthesis of antimicrobial peptides, induction of phagocytic activity of the microphages, dendritic cell maturation, etc. [3].

Toll-like receptors and the representatives of the fairly recently discovered subfamily of NOD-like re-

ceptors, NOD1,2, belong to pattern-recognition receptors, the activation of which results in an NF-kB induction.

Toll-like receptors are transmembrane proteins that are localized on the surface of the plasma membrane of cells and within intracellular compartments (endosomes). Such molecules of a different chemical nature, such as lipopolysaccharides (LPS), flagellin, bacterial lipopeptides, bacterial and viral DNA, etc., may serve as ligands of Toll-like receptors. Abundant data characterizing the ability of TLR ligands to activate NF-kB both *in vitro* and *in vivo has* been collected [4]. The mediated NF-kB ability of TLR ligands to initiate different reactions of the immune system allows to use ligands as immediate protection agents against pathogens, molecular adjuvants, etc. [5–7].

Members of another PRR family – NOD receptors – are located directly in the cell cytoplasm and can recognize various molecules, which are fragments of peptidoglycan of gram-positive and gram-negative bacteria. It has been shown that NOD receptors participate in the recognition of bacteria capable of escaping the endosomal space and penetrating the cell cytoplasm and which can trigger specific immune responses [8]. In contrast to TLR ligands, the properties of NOD receptor ligands, including their ability to activate NF-kB, have been studied considerably less.

This work focused on a comparative in *vitro* and *in vivo* analysis of the NF-kB-activating ability of ligands of one representative of NOD receptors, NOD1, as well as TLR 4 and 5 ligands.

EXPERIMENTAL

Cell lines

The NF-kB-activating ability of ligands of the NOD1 and Toll-like receptor 5 *in vitro* was studied using HEK293 cell lines (human embryonic kidney epithelial cells) and HCT116 (human colon carcinoma cells) expressing NOD1 in humans. The cells were cultivated in a DMEM medium with 10 vol % of fetal bovine serum (ref. number SV30160.03, Hyclone,United States); 1 mg/ml glutamine (ref. number F032, PanEco, Russia); 50 U/ml penicillin; and 50 μg/ml streptomycin (ref. number A065, PanEco, Russia) was added at 37°C, in an atmosphere containing 5% CO_2. The cells were seeded at a ratio of 1 : 6 on day 2, after the monolayer had been obtained.

Ligands of NOD1 and Toll-like receptors

The chemically synthesized NOD1 ligands, represented by samples of dipeptide *D*-Glu-mDAP (iE-DAP), tripeptide *L*-Ala-*D*-Glu-*L*-mDAP (Tri-DAP), the tripeptide covalently bound to a monosaccharide MurNAc-*L*-Ala-*D*-Glu-*L*-mDAP (M-Tri-DAP), and the molecule that contained the lauric acid fragment, Lauroyl-γ-*D*-Glu-*D*-mDAP (iE-DAP-C12), in addition to the minimal recognition sequence, were purchased from Invivogen, United States (ref. numbers: tlrl-dap, tlrl-tdap, tlrl-c12dap). Ligand TLR4 – LPS – was purchased from Sigma-Aldrich, United States (ref. number L3024). Ligand TLR5 –flagellin was prepared according to the procedure described in [9].

Extraction and Purification of Molecule GlcNAc-MurNAc-*L*-Ala-*D*-Glu-*L*-mDAP – the fragment of peptridoglycane of *Neisseria meningitidis* serogroup B – NOD1 receptor ligand

Primary cultivation of *N. meningitidis* (wild-type strain 591 belonging to serogroup B was isolated from the cerebrospinal fluid of a meningitis patient in Moscow in 1985. Phenotype: B : NT : P1.1,2) was carried out at a temperature of 37°C in the presence of 5% CO_2 in the Thayer Martin medium (ref. number M413, Himedia, India). In order to add selective properties to the medium, a set of antibiotics V.C.N.T. Supplement (ref. number FD024, Himedia, India) was introduced. The preparative growth of the bacterium was carried out in a Brain Heart Infusion broth (ref. number 211059, Difco, United States) with 10 vol % of equine serum at 37°C added upon rocking (160 oscillations/min). The ligand of a NOD1 receptor was extracted and chromatographically purified according to the earlier published procedure [10], which include the preliminary thermal inactivation of bacteria at 65°C for 1 h and phenol-chloroform extraction upon heating and mixing of the phenol–water mixture at 70°C for 30 min. The aqueous phase containing peptidoglycan fragments was subjected to tangential-flow ultra filtration (Millipore, United Stated) through a filter with a pore diameter of 30 kDa. The filtrate was purified via three sequential methods of reversed-phase high-performance liquid chromatography (HPLC) on a Bio-alliance 2796 chromatograph (Waters, United States). The first two stages of the purification procedure were carried out using a Symmetry C18 Column with a particle diameter of 5 μm, 4.6 × 75 mm (Waters, United States). During the final stage of purification, a Synergi Hygro-RP 80 Å column (particle diameter of 4 μm, 250 × 3 mm (Phenomenex, United States)) was used.

Chromatographic separation of the compounds was performed on a spectrophotometric detector 2487 (Waters, United States, λ 205, 260, and 280 nm). A Q-STAR Elite mass spectrometer with Turbo Spray and Nano Spray ion spray ionization sources (Applied Biosystems/MDS SCIEX, United States) was used as a detector at the final (third) stage of purification. The resulting sample containing a mass spectrometrically

pure substance underwent mass spectrometric analysis in order to determine the primary structure of the molecule under study. At the first stage of analysis, the accurate molecular mass of the substance, equal to 850.353 Da, was determined. The molecules of the substance subjected to study were then fragmented in an ion spray ionization source for further determination of the sequence of amino acids comprising the molecule, using Protein Pilot software (Applied Biosystems, United States). The non-protein part of the molecule was identified by pseudo-MS3 (studying the products of the secondary fragmentation of ions obtained by predecomposition of an analyzed molecule in the ionization source). The final brutto formula of the analyzed molecule was determined by a study of the decomposition paths of the decomposition of its ion.

The comparative analysis of the fragmentation spectra of different control substances (including N-acetylglucosamine) and the analyzed compound under identical conditions made it possible to identify the primary structure of the molecule: GlcNAc-MurNAc-*L*-Ala-*D*-Glu-*L*-mDAP.

The same experiment was performed on the samples of the bacterial culture medium (negative control) in order to verify the results obtained. Furthermore, the biological activity of the sample containing the substance under study, i.e., its ability to activate NF-kB in cells via the Toll-independent mechanism, was measured following each chromatographic stage of purification.

Measurement of β-galactosidase activity

Twenty-four hours after the study samples were added to the cells, the culture medium was removed and the cell lysis buffer with β-galactosidase substrate (1 mM $MgCl_2$; 0.25 M Tris-HCl, pH 7.4; 0.02% NP40; 2 g/l *o*-nitrophenyl-β-*D*-galactopyranoside (ref. number 102473, MP Biomedicals, United States)) was added. The level of activity of β-galactosidase was determined spectrophotometrically (414 nm) on the basis of substrate (*o*-nitrophenyl-β-*D*-galactopyranoside) conversion into the colored product *o*-nitrophenol.

Determination of bioluminescence intensity in HCT116 and HEK293 line cells containing the luciferase reporter gene under expression control of the NF-kB-dependent element

At the preliminary stage, HCT116 and HEK293 line cells were infected with a lentiviral vector containing the luciferase reporter gene under expression control of the NF-kB-dependent promoter. A day before the bioluminescence was to be determined, the cells were seeded into a 96-well plate with a confluence of 2×10^4 per well. The following day, the samples of PRR ligands were added to the cells, and after 8 more h, the lysis buffer containing luciferin Bright-Glo™ Luciferase Assay System (ref. number E2620, Promega, United States) was also added. The buffer volume (100 μl) was equal to the volume of the culture medium. The level of activity of luciferase was determined on the basis of the fluorescence intensity by means of a Wallac 1420 plate reader (Perkin Elmer, United States).

Determination of bioluminescence intensity in the samples of organ homogenates of BalB/C transgenic mice

PRR ligands (LPS or iE-DAP-C12) were intramuscularly introduced into BalB/C transgenic mice containing the luciferase gene, under control of the NF-kB-dependent promoter, after which the organs were collected at intervals of 1, 3, and 5 h. The organs were homogenized in a Reporter Lysis 5x Buffer (ref. number E3971, Promega, United States) with inhibitors of cell proteases added. The level of activity of the transcriptional factor NF-kB in the samples of mouse organ homogenates was determined by the bioluminescence intensity in the samples, normalized with respect to protein content (10 mg) using a Wallac 1420 plate reader (Perkin Elmer, United States).

Determination of expression of NOD1 receptor by RT-PCR

The total RNA from HCT116 and HEK293 cells was isolated using a Trizol reagent (ref. number 15596026, Invitrogen, United States), in accordance with the manufacturer's procedure. A Superscript III kit (ref. number 18080200, Invivogen United States) was used for cDNA synthesis. The amount of cDNA encoding the NOD1 receptor was normalized with respect to the amount of GAPDH cDNA. Thirty-five PCR cycles were performed with the use of primers specific to the nucleotide sequence of the cDNA sequence that encodes human NOD1 – NOD1-forw: ctt-ctg-gtc-act-cac-atc-cgc-a, NOD1-rev: tgg-gca-tag-cac-agc-acg-aac. The primer annealing temperature was measured at 62°C.

Real-time measurement of bioluminescence intensity in the organism of BalB/C transgenic mice

The activity of the NF-kB factor in the organism of BalB/C transgenic mice containing the luciferase reporter gene in their genome, under expression control of the NF-kB-dependent promoter, was measured in real time on the basis of the bioluminescence intensity at intervals of 1, 3, and 5 h after PRR ligands (LPS or iE-DAP-C12) were introduced. Five minutes prior to obtaining the images, 1.5 mg of *D*-luciferin (Caliper Life Sciences) was injected into the mice. The bioluminescence intensity was determined on an IVIS Im-

aging System 100 instrument (Xenogen Corp., United States).

Laboratory animals

Female transgenic mice of the BALB/c-Tg(NFkB-RE-luc[Oslo])-Xen line (Caliper Life Sciences, United States) with a weight range of 18–20 g containing the reporter gene of firefly luciferase in their genome (from pGL3-Basic Vector, Promega, United States), under expression control of the NF-kB-dependent promoter consisting of three NF-kB-binding regions in the promoter of the Igκ light chain gene, were used for the purposes of this experiment.

The mice were given free access to water and food. LPS (5 μg/mouse) and iE-DAP-C12 (200 μg/mouse) solutions were injected intramuscularly into the mice.

RESULTS AND DISCUSSION

Comparison of the NF-kB-activating ability of NOD1 receptor ligands under *in vitro* conditions

Dipeptide *D*-Glu-mDAP is known as the key sequence necessary and sufficient to inactivate the NOD1 receptor upon the decomposition of gram-negative bacteria and penetration of peptidoglycan fragments inside eukaryotic cells [10]. The participation of other amino acids and monosaccharides, the components of the structural molecules of peptidoglycan of gram-negative bacteria, in the recognition by the NOD1 receptor has yet to be described thoroughly (*Fig. 1*).

It thus follows that the study of the dependence of NOD1-mediated NF-kB-activating ability of various peptidoglycan fragments on their structure seems of importance.

In this context, we carried out a screening experiment at a preliminary stage to select the cell model in which the expression of the NOD1 receptor by different cell lines was determined. According to the RT-PCR data, expression of the NOD1 receptor was detected in both the HEK293 cell line (human embryonic kidney epithelial cells) and the HCT116 cell line (human colon carcinoma cells). TLR5 was also expressed in this cell line [11], whereas in H1299 and A549 cell lines the expression of the NOD1 receptor could not be detected under the selected RT-PCR conditions (*Fig. 2*).

Considering that HEK293 line cells do not express TLR (their presence may result in the additional activation of NF-kB when using NOD1 receptor ligands containing the impurities of TLR ligand molecules), this cell line served as a model for studying the ability of NOD1 receptor ligands possessing different structures to activate NF-kB.

Using the lentiviral vector, the gene of the β-galactosidase reporter protein under the transcriptional control of the NF-kB-dependent promoter and the marker of resistance to blasticidin S were introduced into the genome of HEK293 cells. The principle of use of the resulting cell line is based on the ability of the NOD1 receptor after its interaction with specific ligands to activate the kinase cascade (RIP2, IKKα,β), which results in the activation of the NF-kB factor, followed by its translocation into the nucleus, where this factor binds with the intrinsic regulatory element which controls the galactosidase gene. Hence, the activ-

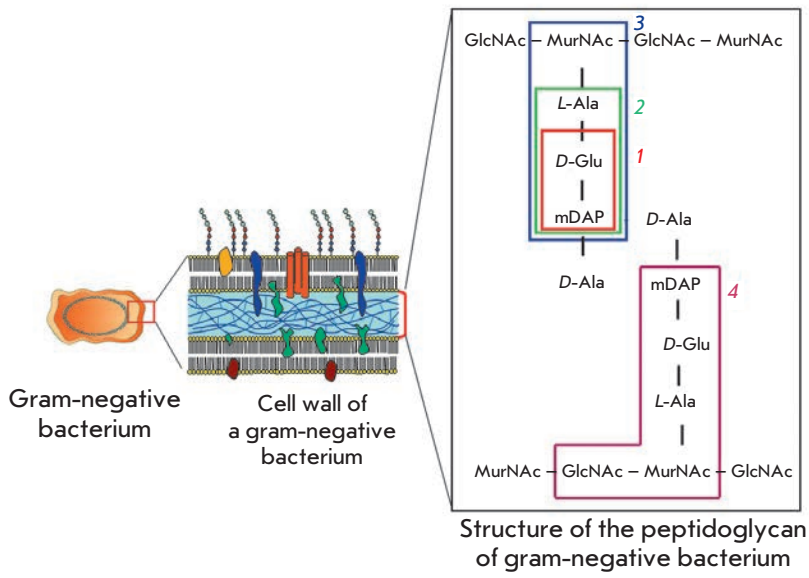

Fig. 1. NOD1 ligands in the peptidoglycan structure of Gram-negative bacteria. *1 – D-Glu-mDAP* (iE-DAP), *2 – L-Ala-D-Glu-L-mDAP* (Tri-DAP), *3 – MurNAc-L-Ala-D-Glu-L-mDAP* (M-Tri-DAP), and *4 – GlcNAc-MurNAc-L-Ala-D-Glu-L-mDAP* (GM-Tri-DAP). *GlcNAc* – N-acetylglucosamine, *MurNAc* – N-Acetylmuramic acid, *L-Ala* – L-alanin, *D-Glu* – *D*-Glutamic acid, *L-mDAP* – L-meso-Diaminopimelic acid.

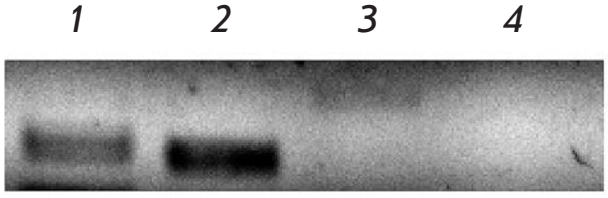

Fig.2. Expression levels of NOD1 receptor detected by RT-PCR with specific primers in *1* – human colon carcinoma cells HCT116, *2* – human embryonic kidney cells HEK293, *3* – non-small cell lung carcinoma cells H1299, and *4* – human lung carcinoma cells A549.

ity of NF-kB in cells can be quantitatively determined on the basis of the staining reaction for galactosidase by registering the interaction between the NOD1 receptor and the intrinsic ligands.

In order to measure the NF-kB activity, NOD1 receptor ligands with a different structure were added to HEK293 line cells: dipeptide *D*-Glu-mDAP (iE-DAP), tripeptide *L*-Ala-*D*-Glu-*L*-mDAP (Tri-DAP), and tripeptide MurNAc-*L*-Ala-*D*-Glu-*L*-mDAP (M-Tri-DAP) covalently bound with a monosaccharide. Furthermore, in our work we used the covalently bound with disaccharide tripeptide GlcNAc-MurNAc-*L*-Ala-*D*-Glu-*L*-mDAP (GM-Tri-DAP), prepared from *N. meningitidis* serogroup B and purified to mass spectrometrical purity using the earlier described method [10]. We additionally used a chemically synthesized molecule which contained the lauric acid fragment Lauroyl-γ-*D*-Glu-*D*-mDAP (iE-DAP-C12) capable of changing the physicochemical properties of this molecule, in addition to the minimal recognition sequence.

As can be seen in *Fig. 3*, a reliable increase in the NF-kB-dependent activation of the β-galactosidase gene expression was attained only at maximum concentrations (1–10 μg/ml) of the *D*-Glu-mDAP dipeptide added, whereas derivatives of this dipeptide with a higher molecular weight (Tri-DAP, M-Tri-DAP, and GM-Tri-DAP) than those that can be found as components of peptidoglycan of gram-negative bacteria induced a reliable increase in NF-kB-dependent β-galactosidase gene expression at lower concentrations (from 0.5 μg/ml). The maximum NOD1-mediated ability of NF-kD activation was shown by the chemically synthesized molecule iE-DAP-C12. The minimum concentration of this molecule, which was capable of inducing the NF-kB-dependent activation of β-galactosidase gene expression, is equal to 20 ng/ml. Such a significant increase in the NF-KB-activating ability (by a factor of approximately 1,000 as compared with *D*-Glu-mDAP) can be explained by the presence of the hydrophobic component of lauric acid, which is likely to facilitate the penetration of iE-DAP-C12 molecule through the plasma membrane and binding to the NOD1 receptor located in the cell cytoplasm.

This experiment thus demonstrated that an increase in the amino acid sequence in the structure of the NOD1 receptor ligand results in a reliable increase in the NF-kB-activating ability of the molecule as compared with the NF-kB-activating minimal sequence *D*-Glu-mDAP, whereas the presence of monosaccharide residues within the ligand molecule does not further increase the activity.

This phenomenon can be explained as follows. For an optimally efficient recognition by the NOD1 recep-

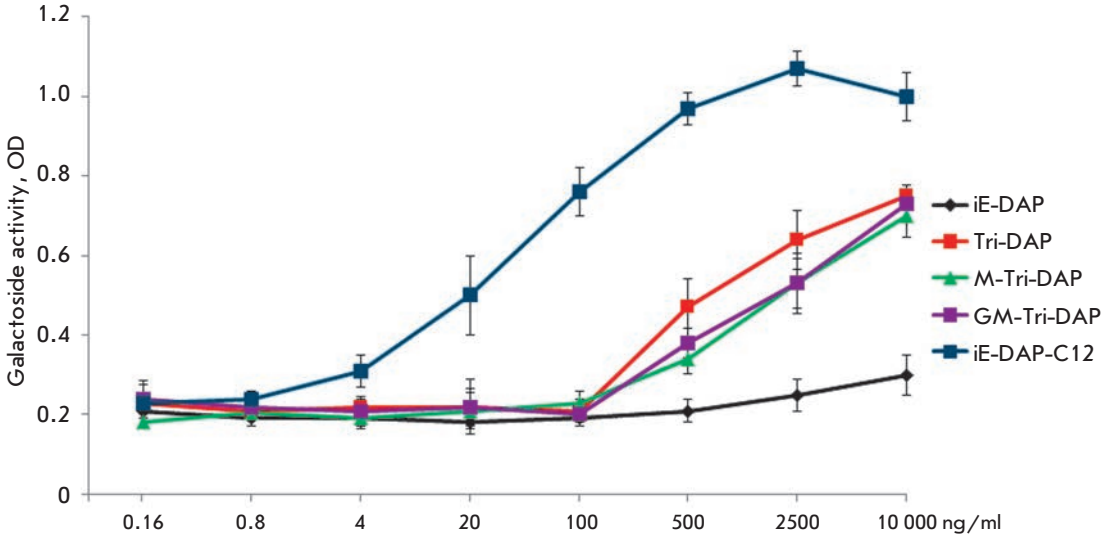

Fig. 3. Activity of NF-kB in HEK293, expressing NOD1. NF-kB-dependent β-galactozidase activity was detected by spectrophotometric measurement (wavelength 414nm) of optical density of colored solution containing the converted specific substrate ortho-Nitrophenyl-β-galactoside (ONPG). The concentration of NOD1 receptor ligands is plotted along the X axis.

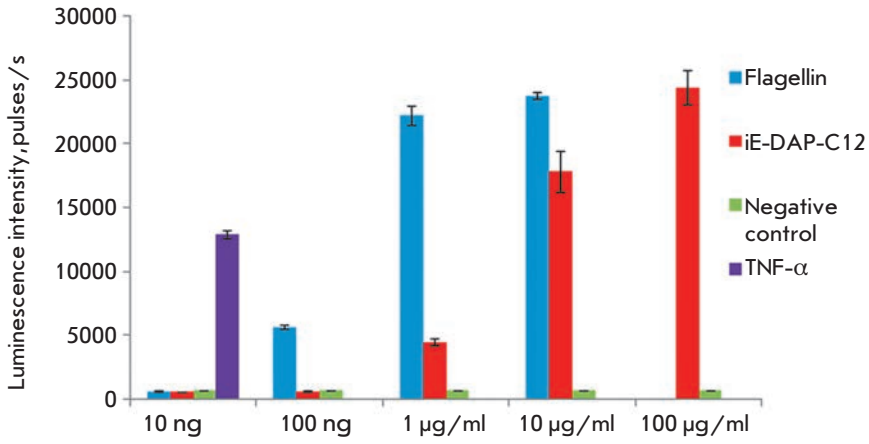

Fig. 4. NF-kB activity in HCT116 expressing NOD1 and TLR5. ■ – cells treated with TLR5 ligand – flagellin; ■– cells treated with NOD1 ligand – iE-DAP-C12; ■ – control intact cells; ■ – cells treated with TNF-α (concentration 10 ng/ml). NF-kB-dependent luciferase activity was detected by spectrophotometric measurement of bioluminescence after addition of specific substrate - luciferin. Y-direction – luminescence intensity units (CPS).

tor (in order to penetrate into the "pocket" of its ligand-recognizing domain), a ligand molecule has to contain at least three covalently bound amino acids, whereas the additionally introduced saccharide molecules do not participate in the direct formation of the ligand-receptor complex. Moreover, the NF-kB-activating ability of the NOD1 receptor ligand can be significantly increased (by a factor of approximately 1,000) by the enhanced hydrophobicity of the molecule, as a result of binding with a fatty acid residue. In all likelihood, such a modification allows to speed up the process, ensuring the necessary ligand concentration near the receptor in the cytoplasm, because its penetration through the cell plasma membrane is made easier.

The iE-DAP-C12 ligand of the NOD1 receptor, which exhibited the highest activity, was selected for further studies.

Comparison of the NF-kB-activating ability of NOD1 and TLR5 ligands in human colon carcinoma cells HCT116

In order to compare the NF-kB-activating ability of NOD1 and TLR5 ligands under *in vitro* conditions, the HCT116 cell line was selected as a model. This cell line expresses both the NOD1 receptor and TLR5, in which the bacterial flagellar protein flagellin serves as a ligand.

The NF-kB activity was measured on the basis of the expression of the luciferase gene, which was introduced into the cell genome under the transcriptional control of the NF-kB-dependent element.

TNF-α was used as positive control of NF-kB activation. This cytokine stimulates NF-kB activation and induces the expression of proinflammatory factors after its interaction with the intrinsic receptor.

The experimental results demonstrate (*Fig. 4*) that the most active NOD1 receptor–ligandiE-DAP-C12–has an effect on NF-kB that can be compared with that of flagellin, but in concentrations that are higher by a factor of 10–100 than those of flagellin. In light of the results of this experiment, a conclusion can be drawn that NOD1 receptor ligands activate NF-kB to a lesser degree than TLR5 ligand; at least for the delivery path that was used. This phenomenon can be explained by a number of reasons: the fact that the NOD1 receptor ligands need to overcome additional barriers, such as the plasma membrane and the cytoplasmic space; a different affinity of TLR and NOD receptors to the intrinsic ligands; and the differences in the lower-lying signaling cascades, resulting in the activation of the transcriptional factor NF-kB.

The ability of NOD1 receptor ligands to induce specific immune responses upon a weaker NF-kB activation in eukaryotic cells as compared with TLR could be an indication that the level of NF-kB activity may determine the development of particular specific immune responses and control their intensity.

The established ratio between the concentrations of NOD1 and TLR ligands which activate NF-kB was taken into consideration to the same extent when carrying out the subsequent studies in *in vivo* conditions.

Studying the NF-kB-activating ability of the NOD1 receptor ligand under *in vivo* conditions

It has been shown that the level of NF-kB activation may differ in different organs of laboratory animals into which TLR ligands has been injected [12, 13]. However, to date there has been no data that clearly shows the ability of the ligands of other PRR–NOD receptors to induce NF-kB activation under *in vivo* conditions. We investigated this question by determining the major activation parameters (the kinetics and intensity of activation in different organs) upon introduction of the NOD1 receptor ligand iE-DAP-C12, which exhibited

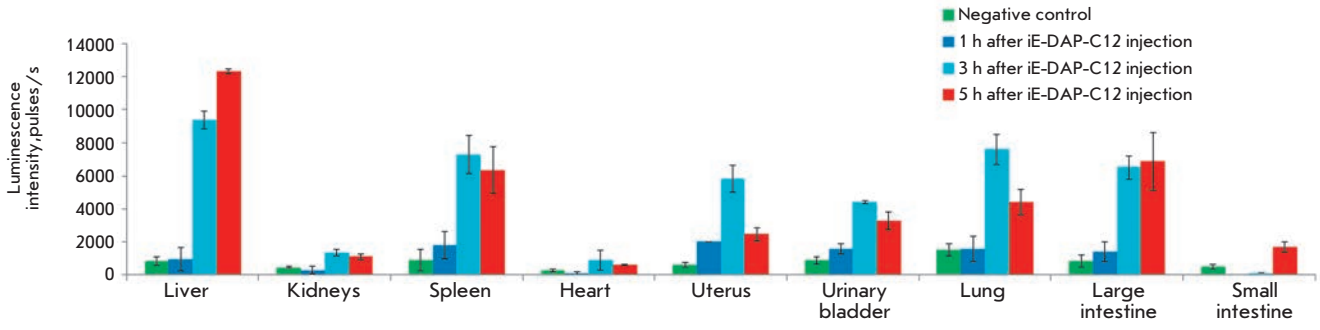

Fig. 5. NF-kB activity in mouse organ homogenates 1,3,5 h after iE-DAP-C12 administration. Samples were normalized with respect to concentration of total protein (10mg/ml). ■ –NF-kB activity in organs of control intact mice 3 h after PBS injection. ■ – NF-kB activity in organs of mice 1 h after iE-DAP-C12 injection (200 μg/animal). ■ – NF-kB activity in organs of mice 3 h after iE-DAP-C12 injection (200 μg/animal). ■ – NF-kB activity in organs of mice 5 h after iE-DAP-C12 injection (200 μg/animal). NF-kB-dependent luciferase activity was detected by spectrophotometric measurement of bioluminescence after addition of specific substrate - luciferin. Y-direction – luminescence intensity units (CPS).

the highest activity in *in vitro* experiments. Furthermore, we compared the NF-kB-activating abilities of NOD ligands and those of TLR4, the thoroughly studied Toll-like receptor, under *in vivo* conditions upon intramuscular injection.

To this end, we used BalB/C transgenic mice with the luciferase reporter gene incorporated into their genome, under the control of a NF-kB-depending promoter. Such a system allows to measure the degree of NF-kB activation in different mouse organs, on the basis of luminescent glowing upon the introduction of PRR ligands [14].

In order to compare the parameters of the NF-kB activation that is observed upon the introduction of iE-DAP-C12, we selected LPS, the ligand of the Toll-like receptor that has been best studied under *in vivo* conditions [13, 15, 16].

The amounts of NOD1 and TLR4 ligands were selected based on the data on the NF-kB-activating ability of these ligands under *in vitro* conditions (200 μg/mouse and 5 μg/mouse, respectively).

It was demonstrated (*Fig. 5*) that upon the intramuscular introduction of iE-DAP-C12, the highest relative and absolute inductions of NF-kB activation (over 12 times) take place in the liver. Moreover, in the liver and the small intestine the highest degree of NF-kB activation is attained 5 h after the introduction of a ligand, whereas a decrease in the level of NF-kB activation was observed at that time in other organs. In three out of nine organs of laboratory animals (kidneys, heart, and small intestine), the introduction of the NOD1 ligand resulted in a minimum increase in the NF-kB activation, as compared with the level of NF-kB activation in the control group.

At the final stage, we compared the levels of NF-kB activation in different organs of mice which received intramuscularly iE-DAP-C12 and LPS 3 h after the introduction of the ligands (maximum NF-kB activation point).

As can be seen in *Figs. 6a and 6b*, the introduction of LPS results in a stronger NF-kB activation in a number of organs (liver, spleen, uterus, and small intestine), when compared with iE-DAP-C12. In the large intestine, lungs, and urinary bladder, the introduction of NOD1 and TLR4 ligands induced a comparable level of NF-kB activation. In other organs such as kidneys and the heart, no reliable increase in the level of NF-kB activation was observed as a response to the introduction of both iE-DAP-C12 and LPS.

Thus, according to the results of the study of the ability of NOD1 ligands to activate NF-kB under *in vivo* conditions, a conclusion can be drawn that the intensity and kinetics of NF-kB activation in response to the introduction of these ligands differ in different mouse organs. Furthermore, differences in the intensity of NF-kB activation in mouse organs after the introduction of NOD1 and TLR4 ligands in the selected concentrations were detected.

After summarizing the data obtained, a conclusion can be drawn that the NF-kB factor activation induced by the interaction between the NOD1 receptor with intrinsic ligands differs from that upon stimulation of TLR representatives (kinetics and intensity of activation) in the same organ, which could be essential for the development of the subsequent immune responses. Moreover, the demonstrated tissue- and organ-specificity of NF-kB upon the introduction of Toll- or NOD receptor ligands into the organism of an animal may lead to the development of different local immune responses in a particular organ or tissue (e.g., differences

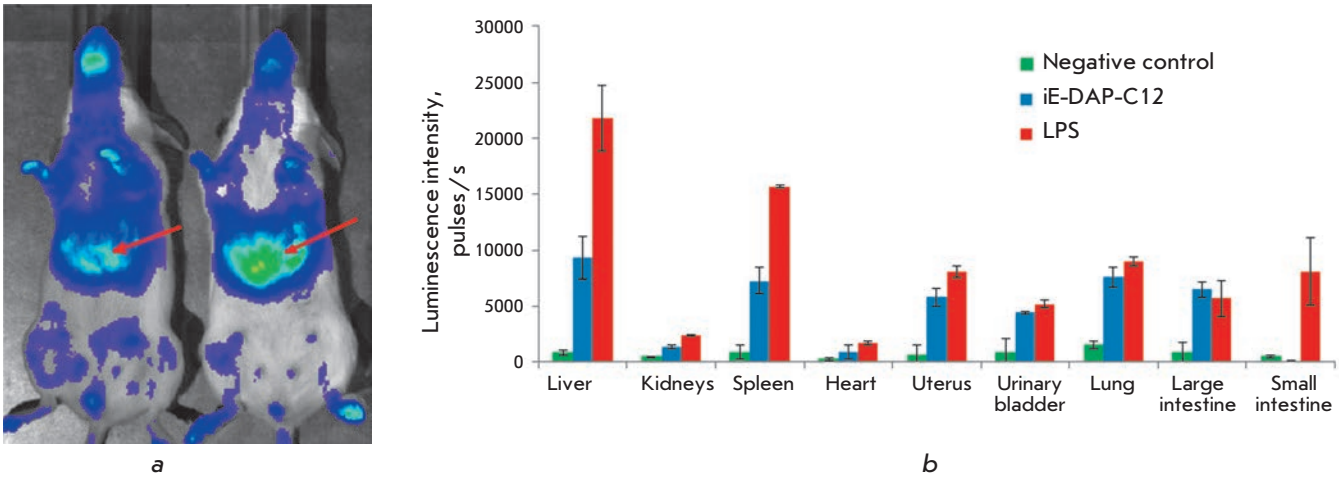

Fig.6.a - Real-time *in vivo* imaging of NF-kB activity in mouse organism after administration of iE-DAP-C12 (left) and LPS of *E. coli* (right). Red arrows point to the maximal bioluminescence intensity detected in liver after PRR ligands exposure. b - NF-kB activity in mouse organ homogenates 3 h after iE-DAP-C12 and LPS administration. Samples were normalized with respect to the concentration of total protein (10 mg/ml). ■ – NF-kB activity in organs of control intact mice 3 h after PBS injection. ■ – NF-kB activity in organs of mice 3 h after iE-DAP-C12 injection (200 μg/animal). ■ – NF-kB activity in organs of mice 3 h after LPS injection (5 μg /animal). NF-kB-dependent luciferase activity was detected by spectrophotometric measurement of bioluminescence after addition of the specific substrate - luciferin. Y-axis – luminescence intensity units (CPS).

in the spectra of secreted cytokines may be observed). The development of some immune responses can be accounted for by the distinctions in differentiation and cell types representing a tissue in which the induction of NF-kB activation took place.

The ability of NOD1 receptor ligands to activate the NF-kB factor under *in vivo* conditions can be used for creating new molecular adjuvants which are characterized by a lower reactogenecity in comparison with some TLR ligands (e.g., LPS). Such adjuvants could be used together with vaccine antigens for protection against different pathogens, including intracellular ones. In order to bolster this hypothesis further, a detailed analysis of the individual immune responses that are initiated by the activation of NOD receptors is required. ●

REFERENCES

1. Medzhitov R., Janeway C. Jr. // Trends Microbiol. 2000. V. 10. P. 3452–3456.
2. Kishore U. Target Pattern Recognition in Innate Immunity. Springer Science +Business Media, LLC Landes Bioscience, 2009. 202 p.
3. Hayden M.S., West A.P., Ghosh S. // Oncogene. 2006. V. 51. P. 6758–6780.
4. Carmody R.J., Chen Y.H. // Cell. Mol. Immunol. 2007. V. 1. P. 31–41.
5. Gill N., Davies E.J., Ashkar A.A. // Am. J. Reprod. Immunol. 2008. V. 59. P. 35–43.
6. Borsutzky S., Kretschmer K., Becker P.D., Mühlradt P.F., Kirschning C.J., Weiss S., Guzmán C.A. // J. Immunol. 2005. V. 174. P. 6308–6313.
7. Weeratna R.D., Makinen S.R., McCluskie M.J., Davis H.L. // Vaccine. 2005. V. 45. P. 5263–5270.
8. Warren S.E., Mao D.P., Rodriguez A.E., Miao E.A., Aderem A. // J. Immunol. 2008. V. 180. P. 7558–7564.
9. Burdelya L.G., Krivokrysenko V.I., Tallant T.C., Strom E., Gleiberman A.S., Gupta D., Kurnasov O.V., Fort F.L., Osterman A.L., Didonato J.A., et al. // Science. 2008. V. 5873. P. 226–230.
10. Girardin S.E., Boneca I.G., Carneiro L.A., Antignac A., Jéhanno M., Viala J., Tedin K., Taha M.K., Labigne A., Zähringer U., et al. // Science. 2003. V. 5625. P. 1584–1587.
11. Zhao L., Kwon M.J., Huang S., Lee J.Y., Fukase K., Inohara N., Hwang D.H. // J. Biol. Chem. 2007. V. 282. P. 11618–11628.
12. Alexander G., Carlsen H., Blomhoff R. // Invest. Ophthalmol. Vis. Sci. 2003. V. 44. P. 2683–2688.
13. Carlsen H., Moskaug J.O., Fromm S.H., Blomhoff R. // J. Immunol. 2002. V. 168. P. 1441–1446.
14. Ho T.Y., Chen Y.S., Hsiang C.Y. // Biomaterials. 2007. V. 30. P. 4370–4377.
15. Austenaa L.M., Carlsen H., Hollung K., Blomhoff H.K., Blomhoff R. //J. Nutr. Biochem. 2009. V. 20. P. 726–734.
16. Pruett S.B., Fan R. // BMC Immunol. 2009. Doi 10.1186/1471-2172-10-49.

Family Analysis of Linkage and Association of HLA-*DRB1*, *CTLA4*, *TGFB1*, *IL4*, *CCR5*, *RANTES*, *MMP9* and *TIMP1* Gene Polymorphisms with Multiple Sclerosis

O.Yu. Makarycheva[1], E.Yu. Tsareva[1,2], M.A. Sudomoina[1,2], O.G. Kulakova[1,2], B.V. Titov[1,2], O.V. Bykova[3], N.V. Gol'tsova[3], L.M. Kuzenkova[3], A.N. Boiko[2], O.O. Favorova[1,2*]
[1]Russian Cardiology Scientific and Production Center
[2]Russian State Medical University
[3]Scientific Center of Children Health, Russian Academy of Medical Sciences
*E-mail: olga_favorova@mail.ru
Received 14.02.2011

ABSTRACT **Multiple sclerosis (MS) is a chronic inflammatory autoimmune disease of the central nervous system (CNS). Proteins of the immune system, as well as proteins that are involved in the infiltration of activated immune cells in the CNS, play an important role in the pathogenesis of MS. We investigated the association and linkage with MS of the following immune-system genes polymorphisms: HLA-*DRB1*, *CTLA4*, *TGFB1*, *IL4*, *CCR5* and *RANTES*, as well as of the matrix metalloproteinase 9 (*MMP9*) and tissue inhibitor of metalloproteinase 1 (*TIMP1*) genes polymorphisms. For this purpose we used the transmission disequilibrium test (TDT). The group investigated was comprised of 100 nuclear families of Russian ethnicity, each consisting of an affected offspring and his nonaffected parents. It was found that HLA-*DRB1**15 allele and *MMP9**-1562C allele were transmitted from healthy heterozygous parents to affected children more frequently than alternative alleles ($p = 0.02$ and $p = 0.04$, respectively). Another family-based method, AFBAC (affected family-based control), showed MS association with HLA-*DRB1**15, but not with the *MMP9**-1562C allele.**

KEYWORDS **functional genomics, human, multiple sclerosis, genotyping, *CCR5* gene, *CTLA4* gene, HLA-*DRB1* gene, *IL4* gene, *MMP9* gene, *RANTES* gene, *TGFB1* gene, *TIMP1* gene, allelic polymorphism, TDT, AFBAC.**

ABBEVIATIONS **MS – multiple sclerosis; PCR – polymerase chain reaction; CNS – central nervous system; AFBAC (affected family-based control) – the method of family analysis, in which the control group consists of the alleles, that were not transmitted from parents to affected children; CCR5 (*CCR5*) – CC chemokine receptor 5 (its gene); CTLA4 (*CTLA4*) – cytotoxic T lymphocyte antigen-4 (its gene); HLA-DRB (HLA-*DRB1*) – β chain of human HLA-DR antigen (its gene 1); IL-4 (*IL4*) – interleukin-4 (its gene); MMP (*MMP*) – matrix metalloproteinase (its gene); RANTES (*RANTES*) – chemokine regulated on activation, normal T cell expressed and secreted (its gene); SNP – single-nucleotide polymorphism; TDT – transmission disequilibrium test; TGFβ1 (*TGFB1*) – transforming growth factor β1 (its gene); TIMP (*TIMP*) – tissue inhibitor of matrix metalloproteinases (its gene).**

INTRODUCTION

Multiple sclerosis (MS) is a severe inflammatory disease of the central nervous system (CNS) which typically develops in the young adults and subsequently leads to disability. This disease has a complex etiology with both genetic and environmental factors [1]. The ways MS is inherited are typical for polygenic diseases; their development is conditioned by the joint contribution of a number of polymorphic genes [2]. The elicitation of the genetic risk factors for MS may help shed light on the mechanisms underlying the pathogenesis of this disease and open new possibilities for its prevention and treatment. In spite of the large number of studies that have investigated the genetics of MS, the search for MS-associated genes remains a challenge. This is due to the nature of the disease, for which genetic heterogeneity is typical, particularly in different ethnic groups, as well as the absence of a main gene. On the other hand, the search for the risk factors for MS is made more difficult by the limitations of the major analysis approaches. The MS genome linkage analysis has yielded little information because of its

low sensitivity [3]. When analyzing genetic associations with MS using the case–control method, there is a low reproducibility of the results: a factor related to the ethnic heterogeneity of the healthy and affected groups under consideration and the influence of environmental factors [4].

The methods that use a family analysis of associations allow to eliminate or to minimize the influence of the ethnic heterogeneity of groups of patients and unrelated healthy controls, as well as the effect of environmental factors [5]. One such method is the transmission disequilibrium test, TDT [6], which is based on the analysis of marker allele or haplotype transmission from heterozygous parents to affected children. The TDT method has already been used to analyze the linkage and association of the alleles of a number of candidate genes with MS among various ethnicities [7–10], including Russians (our studies [11, 12]). This method is now being used not only to analyze the contribution of individual genes to the MS development, but also as a tool in a full genome search [13–15]. Family data have also been used to carry out the association analysis using the affected family-based control (AFBAC) method. According to this data, the control group is composed of a set of alleles from healthy parents which were not transmitted to affected children (one allele from each parent) [16]. This method was used to analyze MS susceptibility in Italy [17, 18], Great Britain [19], Belgium [20], and France [21]. Each of these methods of family analysis has advantages and drawbacks. Thus, AFBAC is a more powerful method as compared with TDT, while TDT makes it possible to completely eliminate the population stratification effects [22].

In this study, we analyzed MS linkage and association of HLA-*DRB1, CTLA4, TGFB1, IL4, CCR5, RANTES, MMP9,* and *TIMP1* genes in ethnic Russians on the basis of family data using the TDT and AFBAC methods.

Numerous data suggest the involvment of these genes in the immunopathogenesis of MS as an autoimmune disease [2]. A repeatedly confirmed fact is that particular alleles (depending on the population ethnicity) of the HLA-*DRB1* gene class II are involved in the development of MS. This gene encodes the β-chain of the heterodimer, which presents the antigen to CD4+ T-lymphocytes. Our study also includes the *CTLA4* gene encoding the cytotoxic T-lymphocyte antigen 4 (CTLA4 or CD152) – the T-lymphocytes costimulation receptor, which is an important negative regulator of the T cells activity and participates in the maintenance of the peripheral T cell tolerance [23].

Cytokines are believed to play the key role in the development and regulation of the autoimmune inflammatory process that is typical of MS. In addition to the data obtained by the analysis of MS linkage and association with alleles of proinflammatory cytokine genes [12], the genes of anti-inflammatory cytokines TGFβ1 and IL-4 – were also considered in this study. Cytokine TGFβ1 is secreted by numerous cell types, including regulatory T- lymphocytes, astrocytes, and endothelial cells; while cytokine IL-4 is secreted mainly by activated Th2 -cells. These cytokines can be detected in the brain tissues at the remission stage; their level being reduced upon active progressive multiple sclerosis [24].

The key stage in the development of the immunopathological process upon MS is the disturbance of the hematoencephalic barrier and T and B cells penetration into the CNS. The stimulation and direction of migration of different cell classes is to a large extent determined by chemokines. Our study includes genes of RANTES (Regulated on Activation Normal T cells Expressed and Secreted) chemokine, which is an attractant for lymphocytes and monocytes, and of its receptor CCR5. The levels of RANTES and CCR5 sharply increase on lymphocytes, macrophages, and microglias in the demyelination lesions upon MS acute attack [25].

The penetration of immune cells into the CNS is accompanied by the type IV collagen degradation, which is the extracellular matrix major constituent. The matrix metalloproteinases (MMPs) play the key role in this barrier penetration. The MMPs are involved in various stages of MS pathogenesis: they participate in the local damaging of the hematoencephalic barrier and perivascular lymphocytes infiltration, in the damaging of myelin sheath and in the formation of the demyelination lesions and axonal death [26]. One of the major metalloproteinases, MMP9, is expressed by perivascular mononuclear cells of white matter and, together with other MMPs, is associated with monocytes and astrocytes in the demyelination lesions.

MMP activity is controlled by tissue inhibitors of matrix metalloproteinases (TIMPs), while the TIMP1 level in the cerebrospinal fluid of MS patients was found to be decreased [26]. Considering these data, the *MMP9* and *TIMP1* genes were included in our study.

The genomic typing of 18 allelic groups of the HLA-*DRB1* gene and the following single-nucleotide polymorphisms (SNPs) 49A>G of the *CTLA4* gene; −509C>T of the *TGFB1* gene; −590C>T of *IL4* gene; −403G>A of the *RANTES* gene; −1562C>T of the *MMP9* gene; 372C>T of the *TIMP1* gene; as well as of the deletion-insertion polymorphism *CCR5* (w→d) ("wild type" → deletion of 32 bp), was carried out for Russian MS patients and their healthy parents, followed by the analysis of genetic predisposition to MS using the TDT and AFBAC methods. Selection of the

polymorphic regions for the analysis proceeded from the data on their influence on the level and/or activity of the encoded proteins Thus, the functional roles of the *DRB1* gene alleles in antigen presentation and the consequences of deletion in the *CCR5* gene resulting in the production of the CCR5 inactive protein are well known. With regard to the SNPs analysis, rare alleles of the *TGFB1*, *IL4*, *RANTES*, and *MMP9* genes are associated with the enhanced production of the protein [27–30], whereas the expression of the encoded protein on the cell surface is increased in the carriers of the allele A of the *CTLA4* gene [31]. SNP 372C>T of the *TIMP1* gene is the only exception with no data available.

EXPERIMENTAL

The object of investigation

The study was performed using peripheral blood samples obtained from members of 104 nuclear families, each of them comprising MS patients and their healthy parents. The blood samples were collected at the Research Center of Children Health, Russian Academy of Medical Sciences, and at the Multiple Sclerosis Moscow City Center . The MS diagnosis was done according to McDonald's criteria [32]. There were 46 male patients and 58 female ones; all patients experienced the onset of MS before the age of 35. The mean MS onset age was 18 ± 8 years. The disease had a relapsing–remitting course in 102 patients and a primary progressive course in two patients. All patients and their healthy relatives were residents of the Moscow region and belonged to Russian ethnicity. All families provided their informed consent for participation in the study.

DNA extraction and genotyping

Genomic DNA was extracted from mononuclear blood cells using a phenol–chloroform mixture according to the standard procedure [33].

Table 1 lists the polymorphic regions of the analyzed genes, PCR-based genotyping methods, and the primers used. Typing of the HLA-*DRB1* gene was carried out by allele-specific PCR, in accordance with the recommendations of the manufacturer of the kit (AO DNA Technology, Russia) used to identify the allele groups corresponding to serological specificities from DR1 to DR18.

Statistical analysis

Linkage and association of the genes with MS was studied using TDT [6] with χ^2 criterion. Haploview 3.32 free software was used for analysis of bi-allelic polymorphism, and FBAT [35] was used for analysis of multi-allelic polymorphism of the HLA-*DRB1* gene and polymorphism of the *TIMP1* gene located on the *X*-chromosome. We analyzed the transmission of gene alleles from parents to affected children in families with at least one heterozygous parent. The difference between the frequencies of transmitted and non-transmitted alleles was considered significant at $\chi^2 > 3.8$ ($p < 0.05$). In order to analyze MS association with alleles of the studied genes using the AFBAC method, the control group was made up of the alleles of both parents which were not transmitted to the affected children. The probability value (p) was assessed with the two-sided Fischer's exact test using GraphPAD InStat 1.12a software.

The discrepancy in the observed distribution of genotype frequencies in the groups of patients and their healthy parents from the Hardy–Weinberg equilibrium was analyzed by the expectation maximization algorithm, using Haploview 3.32.

RESULTS AND DISCUSSION

All the members of the 104 nuclear families were genotyped for the polymorphisms shown in *Table 1*. Four families, for which the paternity was not confirmed by the results of genotyping, were excluded from further analysis. Using Haploview 3.32, we showed that the genotype frequency distributions in MS patients and their parents were in Hardy–Weinberg equilibrium ($p < 0.05$).

TDT was used to obtain the χ^2 values characterizing the difference between the observed frequencies of inheritance of alleles of the HLA-*DRB1, CTLA4, TGFB1, IL4, CCR5, RANTES, MMP9,* and *TIMP1* genes by affected children from 100 nuclear families from the frequencies expected in the absence of association between the allele and the disease. The χ^2 value was used to calculate the p value (*Table 2*). We detected a significant linkage/association between MS and the HLA-*DRB1**15 ($\chi^2 = 5.7$, $p = 0.02$) and *MMP9**(−1562) C ($\chi^2 = 4.1$, $p = 0.04$) alleles. For the remaining polymorphic regions, no significant results were obtained ($\chi^2 < 3.8$, $p > 0.05$). TDT did not detect the linkage/association of any studied polymorphism with MS in male and female groups separately.

Table 3 lists the results of the AFBAC analysis of MS association with the examined polymofphic alleles. By comparing the allele frequency in affected children with that in the control group consisting of the alleles belonging to their mothers and fathers and not transmitted to their children, we detected a significant MS association only with the HLA-*DRB1**15 allele ($p = 0.02$), but not with the alleles of other genes.

Despite the fact that the family-based association analysis has a number of advantages over the population-based analysis, such investigations remain rela-

Table 1. Polymorphisms of the analyzed genes, genotyping methods, and primers used

Gene	Polymorphism	SNP ID	Analysis method (reference)	PCR primers (restrictase used)
HLA-*DRB1*	Allele 01–18 groups, corresponding to DR1–DR18 specificities	–	SSP-PCR	From the kit for amplification of HLA-*DRB1* (AO DNA Technology, Russia)
CTLA4	SNP 49A>G (17Thr → Ala)	rs231775	PCR RFLP [34]**	5'-AAGGCTCAGCTGAACCTGGT and 5'-CTGCTGAAACAAATGAAACCC[BstEII]
TGFB1	SNP -509C>T	rs1800469	SSP-PCR	5'-GGGCAACAGGACACCTGAA-3'(SSP T),5'-GGGCAACAGGACACCTGAG-3' (SSP C), and 5'-AAGGCATGGCACCGCTTCTG-3' (common forward primer)
IL4	SNP -590C>T	rs2243250	SSP-PCR	5'-CTAAACTTGGGAGAACATTGTC-3' (SSP C), 5'-CTAAACTTGGGAGAACATTGTT 3' (SSP T), and 5'-AGTACAGGTGGCATCTTGGAAA-3' (common reverse primer)
CCR5	(w → d) ("wild type" → deletion of 32 bp)	–	PCR	5'-AGGTCTTCATTACACCTGCAGC-3' and 5'-CTTCTCATTTCGACACCGAAGC-3'
RANTES	SNP -403G>A	rs2107538	SSP-PCR	5'-CCATGGATGAGGGAAAGGAGG-3' (SSP G), 5'-CCATGGATGAGGGAAAGGAGA-3' (SSP A), and 5'-AGGGAAGGGGTCCTCCTCAG-3' (common reverse primer)
MMP9	SNP -1562C>T C	rs3918242	PCR RFLP	5'-GCCTGGCACATAGTAGGCCC-3' and 5'-CTTCCTAGCCAGCCGGCATC-3' [SphI]
TIMP1	SNP 372C>T	rs4898	SSP-PCR	5'-CTGTTCAGGGAGCCACG-3' (ASP SSP C), 5'-CTGTTCAGGGAGCCACA-3' (SSP T), and 5'-AGCGAGGAGTTCTCATTGCT-3' (common forward primer)

* All SNP positions are presented relative to transcription start sites, with the exception of CTLA4 49A>G, where 49 is the position relative to the translation start site.
** The reference is given for the case when the technique described was used.
Note. SSP–site-specific primer; RFLP–restriction fragment length polymorphism.

tively rare around the world. This is particularly true for Russia due to the complexity of collecting nuclear family data. Along with the issue of incomplete families, cases of false paternity are of considerable quantity. Thus, we had to exclude four families out of the initial 104 families in the study.

The genes whose participation in the development of MS was studied in this work can be divided into two groups, with respect to the extent they were previously investigated in Russians. The HLA-*DRB1*, *CTLA4*, *TGFB1*, and *CCR5* genes can be referred to the first group; we had previously analyzed MS association with the polymorphism of the above genes using the case–control method with unrelated individuals as controls. The second group included the *IL4*, *RANTES*, *MMP9*, and *TIMP1* genes, which had not previously been studied in details.

The replication (validation) of the data on the association of a particular gene with the disease on independent samples is now considered as a necessary condition for the results to be accepted by the scientific community. This requirement was thoroughly satisfied in our study for the genes from the first group. The MS association with *DRB1**15 HLA class II allele in Russians, which was revealed by TDT and AFBAC, had been shown earlier in population-based studies [36, 37]. On the other hand, we observed no MS association with alleles of the *CTLA4*, *TGFB1*, and *CCR5* genes neither while carrying out the family-based analysis in this study nor while carrying out the case-control analysis on independent groups of unrelated individuals [37–39].

We had previously used the TDT method to show the MS linkage/association of *DRB1**15 HLA class II allele in children and adolescents (so-called juvenile MS, with onset below the age of 15) [11]. Since only DNA samples obtained from 39 nuclear families were available, we simulated the analysis of the bi-allelic locus and compared the carriers of the *DRB1**15 allele with allele non-carriers: i.e., the carriers of all other alleles of the *DRB1* gene. In the present study, we first analyzed the MS linkage and association with all the alleles of multi-allele polymorphism of the HLA-*DRB1* gene in Russians and confirmed MS association and linkage

Table 2. Transmission of polymorphous alleles of HLA-*DRB1*,*CTLA4*, *TGFB1*, *IL4*, *CCR5*, *RANTES*, *MMP9*, and *TIMP1* genes from healthy heterozygous parents to children with multiple sclerosis in100 nuclear families (analysis by TDT)*

Gene	Allele	Number of heterozygous parents	Transmitted, cases	Non-transmitted, cases	χ^2	p
DRB1	01	35	22	13	2.3	> 0.05
	04	34	16	18	0.2	> 0.05
	07	36	18	18	0.0	> 0.05
	08	12	4	8	1.3	> 0.05
	11	53	24	29	0.5	> 0.05
	13	37	18	19	0.1	> 0.05
	15	70	45	25	5.7	0.02
	16	11	3	8	2.3	> 0.05
	17	46	20	26	0.8	> 0.05
CTLA4	A	104	51	53	0.04	> 0.05
	G		53	51		
TGFB1	C	101	48	53	0.3	> 0.05
	T		53	48		
IL4	C	69	32	37	0.4	> 0.05
	T		37	32		
CCR5	w	39	20	19	0.03	> 0.05
	d		19	20		
RANTES	G	63	31	32	0.1	> 0.05
	A		32	31		
MMP9	C	48	31	17	4.1	0.04
	T		17	31		
*TIMP1***	C	49	28	21	0.5	> 0.05
	T		21	28		

* Data for the *DRB1**09, *10, *12, and *14 alleles, the number of carriers of which among healthy parents is ≤ 5 (2.5%), are insignificant and are not listed in *Tables 2* and *3*.
** Since the TIMP1 gene is located on the *X*-chromosome, we considered the transmission of alleles to affected children only from heterozygous mothers.

with the *DRB1**15 allele, regardless of the age of onset.

The data on MS association with polymorphism of *CCR5* (w→d) [40–42] and SNP 49A>G of *CTLA4* in other Caucasians are controversial [43–45], whereas no MS association with SNP –509C>T of *TGFB1* has been observed [46–48]. As for the *DRB1* gene, it appears to be the major genetic risk factor for MS in all Caucasians, although MS associations with other allelotypes, rather than *DRB1**15, have been detected in some populations in the Mediterranean [2].

The absence of individual MS association with polymorphisms in the *CTLA4*, *TGFB1*, and *CCR5* genes does not exclude their possible role as genetic risk factors for the disease, in combination with several other alleles/genotypes. Indeed, the alleles *CTLA4**49G, *TGFB1**(–509)C, and *CCR5**d are the parts of MS-predisposing bi- and tri-allelic combinations with alleles of other genes found using the APSampler algorithm [37]. Combinations of alleles including the *CTLA4* and *TGFB1* genes that are associated with MS were detected in other studies [2]. The question of whether the association of allelic combinations with polygenic diseases can be determined either by the additive contribution of separate genes or by gene-gene interactions remains open.

Among the genes first time investigated using the TDT method in Russian MS patients, nonrandom transmission of the *MMP9*(–1562)*C allele from healthy parents to the affected child was shown. The results obtained for other Slavic populations (in Serbia [49] and the Czech Republic [50]) showed a significant decrease in T-allele frequency in MS patients as compared with healthy individuals and are in agreement with our data that allele C participates in the development of MS. However, these results were not confirmed with the AFBAC method in our study, whereas T allele in Poles

Table 3. Family-based analysis of MS association with alleles of HLA-*DRB1*, *CTLA4*, *TGFB1*, *IL4*, *CCR5*, *RANTES*, *MMP9*, and *TIMP1* genes in 100 nuclear families carried out using the AFBAC method

Gene	Allele	Number (%) of alleles in MS patients (n = 200)	Number (%) of alleles that were not transmitted to affected children by parents (n = 200)	p
DRB1	01	25 (12.5)	6 (8)	> 0.05
	04	22 (11.0)	25 (12.5)	> 0.05
	07	22 (11.0)	22 (11.0)	> 0.05
	08	5 (2.5)	9 (4.5)	> 0.05
	11	25 (12.5)	30 (15)	> 0.05
	13	21 (10.5)	22 (11)	> 0.05
	15	50 (25)	30 (15)	0.02
	16	3 (1.5)	8 (4)	> 0.05
	17	22 (11)	28 (14)	> 0.05
CTLA4	A	113 (57)	103 (52)	> 0.05
	G	87 (43)	97 (48)	
TGFB1	C	132 (66)	137 (69)	> 0.05
	T	68 (34)	63 (31)	
IL4	C	158 (79)	165 (83)	> 0.05
	T	42 (21)	35 (17)	
CCR5	w	179 (90)	178 (89)	> 0.05
	d	21 (10)	22 (11)	
RANTES	G	163 (82)	164 (82)	> 0.05
	A	37 (18)	36 (18)	
MMP9	C	120 (60)	105 (53)	> 0.05
	T	80 (40)	95 (47)	
TIMP1	C	88 (56)	80 (55)	> 0.05
	T	68 (44)	65 (45)	

[51] acts as a MS predisposing allele. Thus, the issue of the participation of the *MMP9* gene in the appearance of MS predisposition requires additional studies.

We did not reveal MS association with polymorphisms of the *IL4*, *RANTES*, and *TIMP1* genes with the two methods of family-based analysis. According to published data SNP −590C>T of the *IL4* gene is associated with MS in Germans, particularly in females [52]. In Spaniards, SNP 33C>T of the *IL4* gene is associated with MS, demonstrating a total linkage disequilibrium with SNP -590C>T of this gene [53]. The results of a study carried out in Iranians are in agreement with our data on the absence of MS linkage/association with the 33C>T region of the *IL4* gene [54]. Association of *RANTES* SNP −403G>A with MS remains insufficiently studied; however, association of this polymorphism with MS was observed in Caucasians in the single study found, [55]. Data concerning the analysis of the 372C>T region of the *TIMP1* gene has not been published.

CONCLUSIONS

In this study, we used the methods of family-based analysis of linkage and/or association, which allow to eliminate or minimize the effects of a possible ethnic heterogeneity of the studied sample in the obtained results. The role of the HLA-*DRB1*, *CTLA4*, *TGFB1*, *IL4*, *CCR5*, *RANTES*, *MMP9*, and *TIMP1* genes polymorphisms in MS development in ethnic Russians was analyzed. The data obtained by TDT are evidence of MS linkage/association with the *DRB1**15 and *MMP9**(−1562)C alleles; association of *DRB1**15 with the disease was confirmed by the AFBAC method. The present study shows the efficiency of the family-based approach in the study of polygenic diseases. ●

This work was supported by the Russian Foundation for Basic Research (grants № 05-04-48982 and 08-04-01834).

REFERENCES

1. Dyment D.A., Ebers G.C., Sadovnick A.D. // Lancet Neurol. 2004. V. 3. № 2. P. 104–110.
2. Favorova O.O., Kulakova O.G., Boiko A.N. // Genetika. 2010. V. 46. № 3. P. 302–313.
3. Risch N.J. // Nature. 2000. V. 405. № 6788. P. 847–856.
4. Hattersley A.T., McCarthy M.I. // Lancet. 2005. V. 366. № 9493. P. 1315–1323.
5. Spielman R.S., McGinnis R.E., Ewens W.J. // Am. J. Hum. Genet. 1993. V. 52. № 3. P. 506–516.
6. Spielman R.S., Ewens W.J. // Am. J. Hum. Genet. 1996. V. 59. № 5. P. 983–989.
7. Marrosu M.G., Murru R., Costa G., Melis M.C., Rolesu M., Schirru L., Solla E., Cuccu S., Secci M.A., Whalen M.B., et al. // BMC Genet. 2007. V. 8. P. 25.
8. Cuturier N., Gourraud P.A., Cournu-Rebeix I., Gout C., Bucciarelli F., Edan G., Babron M.C., Clerget-Darpoux F., Clanet M., Fontaine B., Brassat D. // Eur. J. Hum. Genet. 2009. V. 17. № 6. P. 844–847.
9. D'Alfonso S., Bolognesi E., Guerini F.R., Barizzone N., Bocca S., Ferrante D., Castelli L., Bergamaschi L., Agliardi C., Ferrante P., et al. // Genes Immun. 2008. V. 9. № 1. P. 7–15.
10. Chao M.J., Barnardo M.C., Lui G.Z., Lincoln M.R., Ramagopalan S.V., Herrera B.M., Dyment D.A., Sadovnick A.D., Ebers G.C. // Hum. Mol. Genet. 2007. V. 16. № 16. P. 1951–1958.
11. Boiko A.N., Gusev E.I., Sudomoina M.A., Alekseenkov A.D., Kulakova O.G., Bikova O.V., Maslova O.I., Guseva M.R., Boiko S.Y., Guseva M.E., Favorova O.O. // Neurology. 2002. V. 58. № 4. P. 658–660.
12. Makarycheva O.Yu., Tsareva E.Yu., Sudomoina M.A., Kulakova O.G., Bikova O.V., Gol'tsova N.V., Kuzenkova L.M., Boiko A.N., Favorova O.O. // Molekularnaya Biologia. 2010. V. 44. № 5. P. 824–830.
13. Hafler D.A., Compston A., Sawcer S., Lander E.S., Daly M.J., De Jager P.L., de Bakker P.I., Gabriel S.B., Mirel D.B., Ivinson A.J., et al. // N. Engl. J. Med. 2007. V. 357. № 9. P. 851–862.
14. Willer C.J., Dyment D.A., Cherny S., Ramagopalan S.V., Herrera B.M., Morrison K.M., Sadovnick A.D., Risch N.J., Ebers G.C. // J. Hum. Genet. 2007. V. 52. № 12. P. 955–962.
15. Giedraitis V., Modin H., Callander M., Landtblom A.M., Fossdal R., Stefansson K., Hillert J., Gulcher J. // Genes Immun. 2003. V. 4. № 8. P. 559–563.
16. Thomson G. // Am. J. Hum. Genet. 1995. V. 57. № 2. P. 487–498.
17. Liguori M., Sawcer S., Setakis E., Compston A., Giordano M., D'Alfonso S., Mellai M., Malferrari G., Trojano M., Livrea P., et al. // J. Neuroimmunol. 2003. V. 143. № 1–2. P. 97–100.
18. Lampis R., Morelli L., Congia M., Macis M.D., Mulargia A., Loddo M., De Virgiliis S., Marrosu M.G., Todd J.A., Cucca F. // Hum. Mol. Genet. 2000. V. 9. № 20. P. 2959–2965.
19. Yeo T.W., Roxburgh R., Maranian M., Singlehurst S., Gray J., Hensiek A., Setakis E., Compston A., Sawcer S. // J. Neuroimmunol. 2003. V. 143. № 1–2. P. 53–59.
20. Goris A., Sawcer S., Vandenbroeck K., Carton H., Billiau A., Setakis E., Compston A., Dubois B. // J. Neuroimmunol. 2003. V. 143. № 1–2. P. 65–69.
21. Alizadeh M., Genin E., Babron M.C., Birebent B., Cournu-Rebeix I., Yaouanq J., Dreano S., Sawcer S., Compston A., Clanet M., et al. // J. Neuroimmunol. 2003. V. 143. № 1–2. P. 74–78.
22. Schulze T.G., McMahon F.J. // Am. J. Med. Genet. 2002. V. 114. № 1. P. 1–11.
23. Racke M.K., Ratts R.B., Arredondo L., Perrin P.J., Lovett-Racke A. // J. Neuroimmunol. 2000. V. 107. № 2. P. 205–215.
24. Imitola J., Chitnis T., Khoury S.J. // Pharmacology and Therapeutics. 2005. V. 106. P. 163–177.
25. Szczuciński A., Losy J. // Acta Neurol. Scand. 2007. V. 115. № 3. P. 137–146.
26. Ram M., Sherer Y., Shoenfeld Y. // J. Clin. Immunol. 2006. V. 26. № 4. P. 299–307.
27. Grainger D.J., Heathcote K., Chiano M., Snieder H., Kemp P.R., Metcalfe J.C., Carter N.D., Spector T.D. // Hum. Mol. Genet. 1999. V. 8. P. 93–97.
28. Rosenwasser L.J., Klemm D.J., Dresback J.K., Inamura H., Mascali J.J., Klinnert M., Borish L. // Clin. Exp. Allergy. 1995. V. 25. № 2. Suppl. P. 74–78.
29. Nickel R.G., Casolaro V., Wahn U., Beyer K., Barnes K.C., Plunkett B.S., Freidhoff L.R., Sengler C., Plitt J.R., Schleimer R.P., et al. // J. Immunol. 2000. V. 164. P. 1612–1616.
30. Zhang B., Ye S., Herrmann S.M., Eriksson P., de Maat M., Evans A., Arveiler D., Luc G., Cambien F., Hamsten A., et al. // Circulation. 1999. V. 99. P. 1788–1794.
31. Ligers A., Teleshova N., Masterman T., Huang W.X., Hillert J. // Genes Immun. 2001. V. 2. P. 145–152.
32. McDonald W.I., Compston A., Edan G., Goodkin D., Hartung H.P., Lublin F.D., McFarland H.F., Paty D.W., Polman C.H., Reingold S.C., et al. // Ann. Neurol. 2001. V. 50. № 1. P. 121–127.
33. Sambrook J., Fritsch E.F., Maniatis T. // Molecular Cloning: A Laboratory Manual. Cold Spring Harbor, N.Y.: Cold Spring Harbor Lab. Press, 1989. 923 p.
34. Marron M.P., Raffel L.J., Garchon H.J., Jacob C.O., Serrano-Rios M., Martinez Larrad M.T., Teng W.P., Park Y., Zhang Z.X., Goldstein D.R., et al. // Hum. Mol. Genet. 1997. V. 6. № 8. P. 1275–1282.
35. Laird N.M., Horvath S., Xu X. // Genet. Epidemiol. 2000. V. 19. № 1. Suppl. P. S36–S42.
36. Sudomoina M.A., Boiko A.N., Demina T.L., Gusev E.I., Boldyreva M.N., Trofimov D. Yu., Alekseev L.P., Favorova O.O. // Molekulyarnaya Biologia. 1998. V. 32. P. 291–296.
37. Favorova O.O., Favorov A.V., Boiko A.N., Andreewski T.V., Sudomoina M.A., Alekseenkov A.D., Kulakova O.G., Gusev E.I., Parmigiani G., Ochs M.F. // BMC Med. Genet. 2006. V. 7. P. 63.
38. Favorova O.O., Andreewski T.V., Boiko A.N., Sudomoina M.A., Alekseenkov A.D., Kulakova O.G., Slanova A.V., Gusev E.I. // Neurology. 2002. V. 59. № 2. P. 1652–1655.
39. Andreewski T.V., Sudomoina M.A., Gusev E.I., Boiko A.N., Alekseenkov A.D., Favorova O.O. // Molekulyarnaya Biologia. 2002. V. 36. № 4. P. 643–648.
40. Ristic S., Lovrecic L., Starcevic-Cizmarevic N., Brajenovic-Milic B., Jazbec S.S., Barac-Latas V., Vejnovic D., Sepcic J., Kapovic M., Peterlin B. // Mult. Scler. 2006. V. 12. № 3. P. 360–362.
41. Silversides J.A., Heggarty S.V., McDonnell G.V., Hawkins S.A., Graham C.A. // Mult. Scler. 2004. V. 10. № 2. P. 149–152.
42. Pulkkinen K., Luomala M., Kuusisto H., Lehtimaki T., Saarela M., Jalonen T.O., Elovaara I. // Acta Neurol. Scand. 2004. V. 109. № 5. P. 342–347.
43. Malferrari G., Stella A., Monferini E., Saltini G., Proverbio M.C., Grimaldi L.M., Rossi-Bernardi L., Biunno I. // Exp. Mol. Pathol. 2005. V. 78. № 1. P. 55–57.
44. Rasmussen H.B., Kelly M.A., Francis D.A., Clausen J. // J. Neurol. Sci. 2001. V. 184. № 2. P. 143–147.

45. Fukazawa T., Yanagawa T., Kikuchi S., Yabe I., Sasaki H., Hamada T., Miyasaka K., Gomi K., Tashiro K. // J. Neurol. Sci. 1999. V. 171. № 1. P. 49–55.
46. Arthur A.T., Armati P.J., Bye C., Heard R.N., Stewart G.J., Pollard J.D., Booth D.R. // BMC Med. Genet. 2008. V. 9. P. 17.
47. Weinshenker B.G., Hebrink D., Kantarci O.H., Schaefer-Klein J., Atkinson E., Schaid D., McMurray C.M. // J. Neuroimmunol. 2001. V. 120. № 1–2. P. 138–145.
48. Green A.J., Barcellos L.F., Rimmler J.B., Garcia M.E., Caillier S., Lincoln R.R., Bucher P., Pericak-Vance M.A., Haines J.L., Hauser S.L., Oksenberg J.R. // J. Neuroimmunol. 2001. V. 116. № 1. P. 116–124.
49. Zivkovic M., Djuric T., Dincic E., Raicevic R., Alavantic D., Stankovic A. // J. Neuroimmunol. 2007. V. 189. № 1–2. P. 147–150.
50. Benesova Y., Vasku A., Stourac P., Hladikova M., Beranek M., Kadanka Z., Novotna H., Bednarik J. // J. Neuroimmunol. 2008. V. 205. № 1–2. P. 105–109.
51. Mirowska-Guzel D., Gromadzka G., Czlonkowski A., Czlonkowska A. // J. Neuroimmunol. 2009. V. 214. № 1–2. P. 113–117.
52. Akkad D.A., Arning L., Ibrahim S.M., Epplen J.T. // Genes Immun. 2007. V. 8. № 8. P. 703–706.
53. Urcelay E., Santiago J.L., Mas A., Martinez A., de Las Heras V., Arroyo R., de la Concha E.G. // J. Neuroimmunol. 2005. V. 168. № 1–2. P. 164–167.
54. Kamali-Sarvestani E., Nikseresht A., Aflaki E., Sarvari J., Gharesi-Fard B. // Acta Neurol. Scand. 2007. V. 115. № 3. P. 161–166.
55. Gade-Andavolu R., Comings D.E., MacMurray J., Vuthoori R.K., Tourtellotte W.W., Nagra R.M., Cone L.A. // Mult. Scler. 2004. V. 10. № 5. P. 536–539.

Comparative Bioinformatic Analysis of Active Site Structures in Evolutionarily Remote Homologues of α,β-Hydrolase Superfamily Enzymes

D. A. Suplatov[1,2], V. K. Arzhanik[1], V. K. Švedas[1,2*]
[1]Faculty of Bioengineering and Bioinformatics, Lomonosov Moscow State University
[2]Belozersky Institute of Physicochemical Biology, Lomonosov Moscow State University
E-mail: vytas@belozersky.msu.ru
Received 25.02.2011

ABSTRACT **Comparative bioinformatic analysis is the cornerstone of the study of enzymes' structure-function relationship. However, numerous enzymes that derive from a common ancestor and have undergone substantial functional alterations during natural selection appear not to have a sequence similarity acceptable for a statistically reliable comparative analysis. At the same time, their active site structures, in general, can be conserved, while other parts may largely differ. Therefore, it sounds both plausible and appealing to implement a comparative analysis of the most functionally important structural elements – the active site structures; that is, the amino acid residues involved in substrate binding and the catalytic mechanism. A computer algorithm has been developed to create a library of enzyme active site structures based on the use of the PDB database, together with programs of structural analysis and identification of functionally important amino acid residues and cavities in the enzyme structure. The proposed methodology has been used to compare some α,β-hydrolase superfamily enzymes. The insight has revealed a high structural similarity of catalytic site areas, including the conservative organization of a catalytic triad and oxyanion hole residues, despite the wide functional diversity among the remote homologues compared. The methodology can be used to compare the structural organization of the catalytic and substrate binding sites of various classes of enzymes, as well as study enzymes' evolution and to create of a databank of enzyme active site structures.**
KEYWORDS **bioinformatics, comparative analysis, active site, structural alignment, α,β-hydrolases**
ABBREVIATIONS **PDB - Protein Data Bank; CSA - Catalytic Site Atlas**

INTRODUCTION

Comparative bioinformatic analysis is the cornerstone in the study of enzymes' structure-function relationship. Multiple sequence comparisons have become a common tool in such an analysis. While a statistically significant sequence or tertiary structure similarity between proteins is justified as evidence of homology [1], some enzymes lose sequence similarity during natural selection and specialization from a common ancestor. Consequently, a bioinformatics analysis of remote homologues remains a bottleneck of existing methods for sequence comparison.

The protein's structure is better conserved throughout evolution as compared to sequence [2, 3]. There are numerous examples of proteins that show sequence similarity close to random (roughly 8-15% identity considering gaps) but still adopt similar structures, contain identical or related amino acid residues in their active sites, and have similar catalytic mechanisms [4]. In contrast to commonly known sequence alignments [5-7], a three-dimensional alignment is based on the comparison of the geometric orientation of amino acid residues in tertiary structures, rather than on the biochemical properties of these residues at corresponding positions of primary structures [8]. Currently, there are almost 70,000 structures in the Protein Data Bank (PDB), and this number is constantly growing [9]. Accessibility of this information provides new opportunities for a comparative bioinformatic analysis. For example, the 3D-alignment of crystal structures has allowed to identify the relationship between distant members of Ntn-hydrolases family enzymes with low sequence similarity [10, 11]. It is therefore hoped that studying the structure-function relationship in enzyme families consisting of evolutionarily remote homologues using three-dimensional alignment could provide more significant clues as to a protein's function, properties, and evolution than sequence alignment alone.

The experience gained in a comparative analysis allows to assume that the spatial organization of the ac-

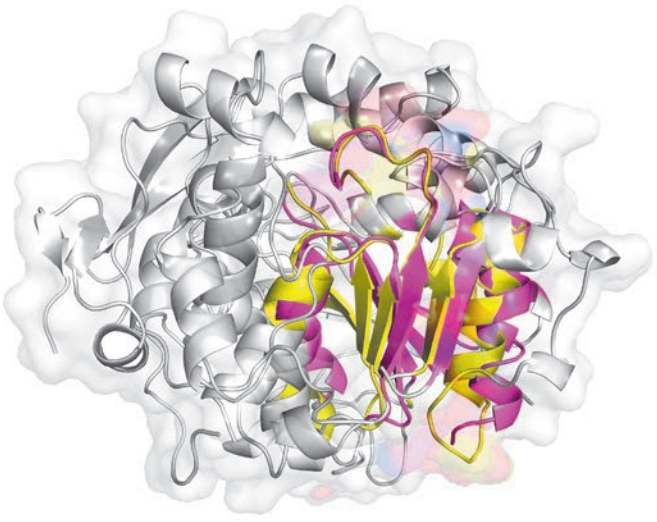

Fig. 1. Structure alignment of lipase B from *C. antarctica* (1TCB) and hydroxynitrile lyase from *H. brasiliensis* (1YB6). Conserved parts containing the active site residues of two enzymes are marked in different colors.

tive site area is the best conserved part of homologous enzymes, while the remaining structure may significantly differ (*Fig. 1*) [12-15]. It is widely believed that packing of the polypeptide chain and side chain orientation of the amino acid residues in the active site has a major impact on the ability of an enzyme to recognize, bind, and transform a substrate. Moreover, amino acid residues that impact substrate specificity and catalytic activity generally have been observed within 7-15Å from key catalytic residues [16]. Thus, while studying the relationship between remote homologues it is necessary to perform a bioinformatics analysis in three layers: on the amino acid sequences, three-dimensional structures, and structural organization of the active site areas. A comparative study of the most functionally significant parts of the enzyme structures - the active sites - is of particular interest.

A computer algorithm has been developed to create a library of enzyme active site structures based on the use of the PDB database, together with numerous programs of structural analysis and identification of functionally important amino acid residues and cavities in an enzyme's structure. The proposed methodology was used for a comparative bioinformatic analysis of some α,β-hydrolase superfamily members.

METHODS

Gathering homologues

A structure-based similarity to lipase B from *Candida antarctica* search in the PDB databank was performed using the SSM program [8]. Hits were dismissed by the amount of successfully fitted secondary structure elements (at least 30% SSEs should coincide in both the target structure and the query 1TCB). A sequence-based similarity search was performed with the PSI-BLAST program [7] via a nonredundant (nr) sequence dataset. Sequences were clustered at a 95% similarity threshold, and only one representative sequence from a cluster was retrieved.

Multiple alignment

Multiple sequence alignment of both the full-size structures and active site areas of enzymes was performed using the t-coffee [17] and Mustang [18] algorithms.

Visualization

The Pymol [19] program was used for structural analysis. The Jalview program [20] was used for the representation of primary structure alignments.

Multiple alignment statistical analysis

To assess the conservation score of a column I in a multiple alignment, the Valdar&Thornton formulation was used:

$$C_I = \gamma \sum_{i}^{N} \sum_{j>i}^{N} w_i w_j M(s_i, s_j),$$

where M is the amino acids substitution matrix; s_i and s_j – the amino acids in the sequences i and j of column I; and the coefficient γ is calculated as

$$\gamma = \left(\sum_{i}^{N} \sum_{j>i}^{N} w_i w_j \right)^{-1}.$$

The parameters w_i and w_j refer to the weights of the sequences i and j as in the Vingron&Argos formulation[22]:

$$w_i = \frac{1}{N-1} \sum_{j \neq i}^{N} d(s_i, s_j),$$

where d is the "genetic" distance between the sequences i and j calculated in terms of pairwise identities.

Finally, a Z-score of standard normal distribution was taken as a measure of a column's conservation:

$$Z_i = \frac{C_i - \langle C_i^{случ} \rangle}{\sigma(C_i^{случ})},$$

where C_I^{rnd} is the conservation score of a randomly assigned column.

A Bernoulli rank-order statistics (B-cutoff) was im-

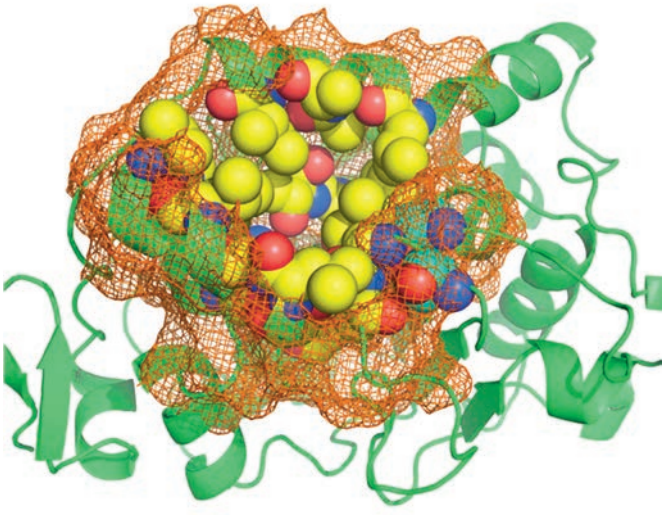

Fig. 2. Active site area – a substructure of an enzyme consisting of the amino acid residues involved in substrate delivery, binding, and orientation (yellow), as well as the amino acid residues of the catalytic machinery (blue) and some surrounding residues selected to benefit the integrity of the fragment (showed as dashes).

plemented [23, 24] to estimate the statistical significance of the acquired Z-scores. Previously obtained Z_i scores are ordered in decreasing order, and then a rank k is computed so that the first k scores comprise a set of hits that are the least probable to be observed by chance:

$$k = arg_k \min \mathrm{P}\,(\text{there are at least k Z-scores } Z \geq Z_k) = arg_k \min\left(1 - \sum_{i=n-k+1}^{n} C_n^i q^i p^{n-i}\right),$$

where n is the total number of computed Z-scores, C_n^i is the binomial coefficient, and

$$p = \mathrm{P}(Z \geq Z_k) = \int_{Z_k}^{\infty} \frac{1}{\sqrt{2\pi}} \exp(-Z^2)\, dZ, \quad q = 1 - p.$$

RESULTS AND DISCUSSION

A comparative analysis of the catalytic site organization, as opposed to a full-size structural comparison, could become a source of new crucial information concerning an enzyme's structure-function relationship. Here, the term "active site" refers to the amino acid residues involved in the catalysis, together with those forming the active site cavity and thus indirectly involved in the catalytic mechanism by interacting with the substrate or "catalytic" amino acid residues. To perform a comparison of enzymes' active sites, a library of corresponding structures should first be created. A computer algorithm is being proposed to localize and isolate the structure of an enzyme's active site (*Fig. 2*). It consists of three steps:

1. Identification of the active site residues involved in the catalytic mechanism. Amino acid residues are defined as catalytic if they meet any of the following criteria – direct involvement in the catalytic mechanism (for example, as a nucleophile), alteration of the acid-base properties of an active site residue or water molecule directly involved in the catalytic mechanism, and stabilization of the transition state or intermediate of an enzymatic reaction. The Catalytic Site Atlas database (CSA) [25] provides an annotation of the catalytic residues of the enzymes present in the PDB databank. CSA is available to the public at http://www.ebi.ac.uk/thornton-srv/databases/CSA and contains two types of annotated sites: an original hand-annotated set based on information gathered from the literature and an additional homologous set with transferred annotations produced by the PSI-BLAST program [7]. If an enzyme is not listed in the CSA, then catalytically important residues should be gathered manually in the literature or identified using different bioinformatics approaches [26-28].

2. Identification of the amino acid residues responsible for substrate delivery, binding and orientation in the active site. Substrate binding, as a rule, takes place in the so-called structural pockets and cavities on the protein's surface. Various amino acid residues forming the active site area are not involved directly into the catalytic machinery but interact with the substrate's functional groups, while diffusion and orientation ensure a productive binding and reactive conformation of the enzyme-substrate complex. The CASTp structural analysis algorithm [29] can be used to complete this step.

3. Finalizing enzyme active site structural data and the PDB coordinate file. Catalytic residues (determined in step 1) and amino acid residues forming the substrate binding site (determined in step 2) are joined together with surrounding residues, forming secondary-structure elements and intermediate loops.

Finally, a substructure of an enzyme is created containing the amino acid residues involved in substrate binding, together with the catalytic amino acid residues and some surrounding residues selected to benefit the integrity of the structural fragment. Technically, it is dumped into the hard drive as a PDB coordinate file with the possibility of including additional information from other databases concerning enzyme structure, function or the peculiarities of its catalytic mechanism.

Conserved amino acid residues in active site of lipase B from *Candida antarctica*, serine carboxypeptidase from *Triticum aestivum*, as well as hydroxynitrile lyase from *Hevea brasiliensis* and their homologues

Rank	Z-score	p-value	Position	Alignment column content
1	5.909034	1.496923E-07	224H	HHHHH HHHHH ... HHHHH HH
2	5.909034	1.107511E-14	187D	DDDDD DDDDD ... DDDDD DD
3	5.909034	5.399159E-22	105S	SSSSS SSSSS ... SSSSS SS
4	5.585937	4.061221E-26	39G	GGGGG GGGGG ... GNTTG GG
5	4.976042	1.329205E-25	108G	GGGGG GGGGG ... AAAAA GG
6	3.643481	2.960176E-15	103T	GGGGG GGTTS ... STTSS AG
7	3.077561	7.318560E-12	107G	AAAAA AAGGG ... GGGGG GG
8	2.282191	6.757472E-06	106Q	YYYYY YYQLQ ... YFFYY FF
9	2.097392	2.845755E-05	190V	CCCCC CCCCC ... VVVVL LL
10	1.970983	5.325320E-05	184S	GGGGG GGGGG ... SNNSS NN
11	1.833495	1.540646E-04	80T	AAAAA AAAAA ... GAAVA YY
12	1.525180	8.996767E-03	42T	GGGGG GGGGG ... TRVAG GG
13	1.238283	1.410807E-01	132A	NNNNN NNNNN ... AAAAD DD
14	1.203052	1.191297E-01	133P	GGGGG GGGGG ... PPPPP PG
15	1.173696	9.573976E-02	82Y	DDDDD NNDSN ... QEEQQ YY

Note. Results of bioinformatic analysis are presented in decreasing order of their statistical significance (Z-score). The P-value for a position rank *i* refers to the probability of a result from 1 to *i* to occur in a random sample. Reference position numbering as in 1TCB lipase. Statistical significance threshold is shown in red.

The suggested algorithm could be used to create a library of the active site structures of all enzymes included in the PDB databank.

The proposed methodology has been used for a comparative bioinformatic analysis of some α,β-hydrolase superfamily enzymes – lipase B from *Candida antarctica* (PDB code 1TCB) [12], serine carboxypeptidase from *Triticum aestivum* (1WHS) [30], and hydroxynitrile lyase from *Hevea brasiliensis* (1YB6) [13], as well as their homologues established via a combination of iterative sequence searches and structural comparisons (see Methods). The pairwise sequence identity between 1TCB and 1WHS is 7.8%; 1TCB and 1YB6 – 12.4%; and 1WHS and 1YB6 – 13.7%. Such a low sequence identity does not allow to compare distant homologues by sequence alignment. A 3D-Comparison also failed to reveal a significant similarity in the spatial organization of enzyme structures. For example, only catalytic triad residues can be aligned using the SMM program [8], while oxyanion hole residues remain unattended. Oppositely, the Mustang [18] program can align the oxyanion hole residues with catalytic serines but cannot fit other residues of the catalytic triad: histidines and aspartates. With this type of interposition, it remains hard to identify hidden and functionally important regions, while partial manual correction of the alignment does not seem to be a reliable means to improve its quality. The obvious discrepancies in the results obtained using various programs of structural alignment are due to the major differences between the full-size structures of enzymes catalyzing different reactions – only 161 out of 408 amino acid residues of the 1WHS serine carboxypeptidase structure could potentially fit the structure of 1TCB lipase from *Candida antarctica* and 1YB6 hydroxynitrile lyase from *Hevea brasiliensis*. Thus, the proposed procedure was used to prepare the corresponding active site structures for a comparative structural analysis of enzymes so distinct. The resulting files consisted of 170 amino acid residues for 1TCB (54% of the full-size structure), 287 for 1WHS (70%), and 159 for 1YB6 (62%). The analysis of the multiple structural alignment of enzyme active sites revealed a packing similarity between the polypeptide chains, while the organization of the catalytic triad residues was the best conserved – Ser105, His224 and Asp187 (as in 1TCB, see *Table*). Those positions not only contain the same type of amino acid residues amongst homologues, but they also have similar orientation in the structure (*Figs. 3, 4*). Moreover, a geometric comparison of the active sites of the enzymes that catalyze

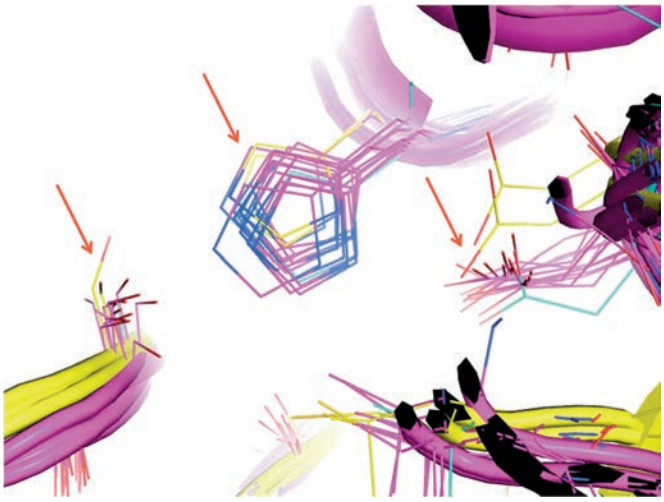

Fig. 3. Structural alignment of the active sites of α,β-hydrolase family enzymes: lipase B from *Candida antarctica*, serine carboxypeptidase from *Triticum aestivum* and hydroxynitrile lyase from *Hevea brasiliensis* and their homologues. Conserved residues of the catalytic triad and surrounding loops are indicated with red arrows.

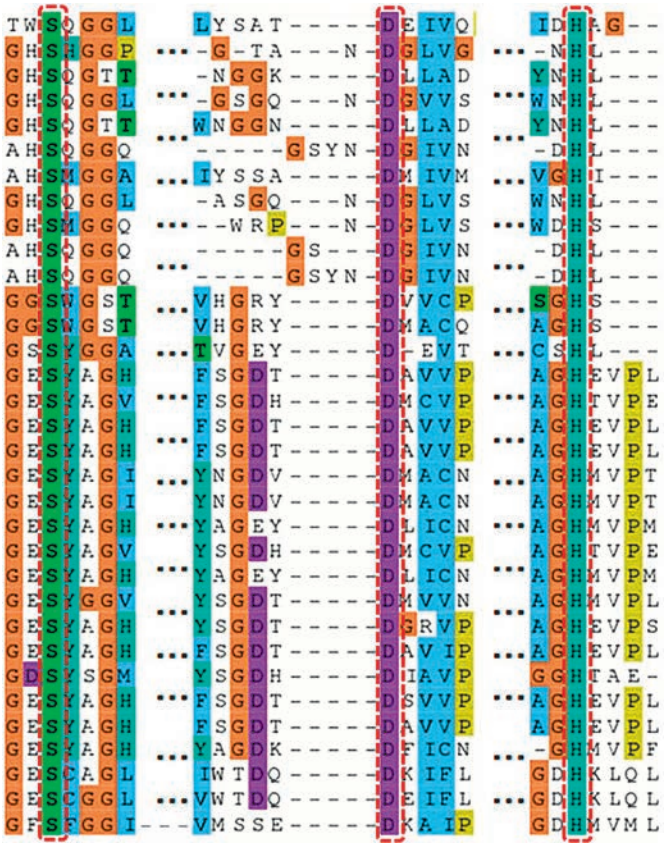

Fig. 4. Structural alignment (textual representation) of the active sites of α,β-hydrolase family enzymes: lipase B from *Candida antarctica*, serine carboxypeptidase from *Triticum aestivum* and hydroxynitrile lyase from *Hevea brasiliensis* and their homologues. The sequence is less conserved throughout evolution, compared to structures. Conserved residues of the catalytic triad are indicated with red dashes.

quite diverse chemical reactions revealed a similarity in the organization of the oxyanion hole residues and accompanying loops – part of the structure containing amino acid residue Thr40 in lipase B fits Ile12 in hydroxynitrile lyase and Gly53 in carboxypeptidase. Another oxyanion hole residue – Gln106 in lipase B – that follows the catalytic Ser105 also fits into homologous positions in other enzymes: Tyr147 in carboxypeptidase and Cys81 in hydroxynitrile lyase. The variability of amino acid types in those positions could be justified by taking into account the fact that the NH-group of the main chain peptide bond formed by these residues is involved in the stabilization of the tetrahedral intermediate [12, 13]. The observed structure conservation is especially interesting for hydroxynitrile lyases, since their catalytic mechanism does not involve the formation of a tetrahedral intermediate and its stabilization [31]. Thus, a comparative analysis has helped outline the structural conservation of functionally important active site areas for the evolutionarily remote homologues of α,β-hydrolase superfamily enzymes: lipase B from *Candida antarctica*, serine carboxypeptidase from *Triticum aestivum,* and hydroxynitrile lyase from *Hevea brasiliensis.*

CONCLUSIONS

A computer algorithm has been developed to create a library of enzyme active site structures based on the use of the PDB database, in combination with numerous programs for the structural analysis and identification of functionally important amino acid residues and cavities. The proposed methodology has been used for a comparative bioinformatic analysis of some α,β-hydrolase superfamily enzymes. The comparative analysis helped pinpoint a high similarity in the active site structures of evolutionarily remote homologues of α,β-hydrolase superfamily members – lipase B from *Candida antarctica*, serine carboxypeptidase from *Triticum aestivum* and hydroxynitrile lyase from *Hevea brasiliensis* – despite the low sequence and full-structure identity of these enzymes. A common structural organization of catalytic residues and oxyanion holes was observed between serine carboxypeptidase, lipase B, and hydroxynytrile lyase, despite a significant difference in their functional properties and ability to catalyze diverse chemical transformations. These results demonstrate that a bioinformatic analysis of enzymes and the study of the general principles of biocatalysis

should not be limited to sequence and full-structure alignments only. A comparative bioinformatic analysis of the most functionally significant parts of enzyme structures – their active sites – can help uncover resemblances even among remote homologues. This methodology can be used to study the structural organization of the catalytic and substrate-binding sites of various enzymes, as well as to create a database of enzyme active site structures. In addition, the proposed algorithm can be applied when comparing unrelated enzymes with no sequential or structural similarity but with an analogous function developed independently in the course of convergent evolution. ●

This work was supported by the Russian Ministry of Science and Innovation (contract № 02.740.11.0866)

REFERENCES

1. Koonin E.V., Galperin M.Y. Sequence-Evolution-Function: Computational approaches in comparative genomics. Boston: Kluwer Academic, 2003. 488 p.
2. Holm L., Sander C. // Science. 1996. V. 273. № 5275. P. 595–603.
3. Grishin N.V. // J. Mol. Evol. 1997. V. 45. № 4. P. 359–369.
4. Ollis D.L., Cheah E., Cygler M., Dijkstra B., Frolow F., Franken S.M., Harel M., Remington S.J., Silman I., Schrag J., Sussman J.L., Verschueren K.H.G., Goldman A. // Protein Engineering. 1992. V. 5. P. 197–211.
5. Smith T.F., Waterman M.S. // Adv. Appl. Math. 1981. V. 2. P. 482–489.
6. Altschul S.F., Gish W., Miller W., Myers E.W., Lipman D.J. // J. Mol. Biol. 1990. V. 215. № 3. P. 403–410.
7. Altschul S.F., Madden T.L., Schäffer A.A., Zhang J., Zhang Z., Miller W., Lipman D.J. // Nucl. Acids Res. 1997. V. 25. № 17. P. 3389–3402.
8. Krissinel E., Henrick K. // Acta Cryst. 2004. V. D60. P. 2256–2268.
9. Dutta S., Zardecki C., Goodsell D.S., Berman H.M. // J. Appl. Crystall. 2010. V. 43. № 5. P. 1224–1229.
10. Suresh C.G., Pundle A.V., SivaRaman H., Rao K.N., Brannigan J.A., McVey C.E., Verma C.S., Dauter Z., Dodson E.J., Dodson G.G. // Nat. Struct. Biol. 1999. V. 6. № 5. P. 414–416.
11. Carita O., Rouvinen J. // Protein Sci. 2000. V. 9. P. 2329–2337.
12. Uppenberg J., Hansen M.T., Patkar S., Jones T.A. // Curr. Biol. 1994. V. 2. P. 293–398.
13. Gartler G., Kratky C., Gruber K. // J. Biotechnol. 2007. V. 129. № 1. P. 87–97.
14. Wallace A.C., Laskowski R.A., Thornton J.M. // Protein Sci. 1996. V. 5. № 6. P. 1001–1013.
15. Varfolomeev S.D., Uporov I.V., Fedorov E.V. // Biochemistry (Moscow). 2002. V. 67. № 10. P. 1099-1108.
16. Morley K., Kazlauskas R.J. // TRENDS Biotechnol. 2005. V. 23. № 5. P. 231–237.
17. Notredame C., Higgins D., Heringa J. // J. Mol. Biol. 2000. V. 302. P. 205–217.
18. Konagurthu A., Whisstock J., Stuckey P., Lesk A. // Proteins. 2006. V. 64. P. 559–574.
19. The PyMOL Molecular Graphics System. Version 1.0r1. Schrödinger, LLC.
20. Waterhouse A., Procter J., Martin D., Clamp M., Barton G. // Bioinformatics. 2009. V. 25. P. 1189–1191.
21. Valdar W.S.J., Thornton J.M. // Proteins. 2001. V. 42. P. 108–124.
22. Vingron M., Argos P. // Comput. Appl. Biosci. 1989. V. 5. P. 115–121.
23. Vinogradov D.V., Mironov A.A. // Proc. 3rd Int. Conf. On Bioinformatics of Genome Regulation and Structure BGRS'2002, 2002. Novosibirsk, Russia, July 1. P. 28–30.
24. Kalinina O.V., Gelfand M.S., Russel R.B. // BMC Bioinformatics. 2009. V. 10. P. 174-198.
25. Porter C.T., Bartlett G.J., Thornton J.M. // Nucl. Acids. Res. 2004. V. 32. D129–D133.
26. Casari G., Sander C., Valencia A. // Nat. Struct. Biol. 1995. V. 2. P. 171–178.
27. Sankararaman S., Sha F., Kirsch J.F., Jordan M.I., Sjolander K. // Bioinformatics. 2010. V. 26. № 5. P. 617–624.
28. Pazos F., Bang J.-W. // Curr. Bioinformatics. 2006. V. 1. P. 15–23.
29. Dundas J., Ouyang Z., Tseng J., Binkowski A., Turpaz Y., Liang J. // Nucl. Acids Res. 2006. V. 34. W116–W118.
30. Liao D.-I., Breddam K., Sweet R.M., Bullock T., Remington S.J. // Biochemistry. 1992. V. 31. P. 9796–9812.
31. Gruber K., Garter G., Krammer B., Schwab H., Kratky C. // J. Biol. Chem. 2004. V. 279. № 19. P. 20501–20510.

Multi-walled Carbon Nanotubes Penetrate into Plant Cells and Affect the Growth of *Onobrychis arenaria* Seedlings

E.A. Smirnova*[1], A.A. Gusev[2], O.N. Zaitseva[2], E.M. Lazareva[1], G.E. Onishchenko[1], E.V. Kuznetsova[3], A.G. Tkachev[4], A.V. Feofanov[1,5], M.P. Kirpichnikov[1,5].
[1]Biology Faculty, Lomonosov Moscow State University
[2]Derzhavin Tambov State University
[3]Siberian Institute of Plant Physiology and Biochemistry, Siberian Branch, Russian Academy of Sciences
[4]NanoTechCenter Ltd.
[5]Shemyakin and Ovchinnikov Institute of Bioorganic Chemistry, Russian Academy of Sciences
*E-mail: kinggobi@yandex.ru
Received 21.02.2011

ABSTRACT **Engineered nanoparticles (ENPs) are now being used in many sectors of industry; however, the impact of ENPs on the environment still requires further study, since their use, recycling, and accidental spill can result in the accumulation of nanoparticles in the atmosphere, soil, and water. Plants are an integral part of ecosystems; hence their interaction with ENPs is inevitable. It is important to understand the consequences of this interaction and assess its potential effects. The present research is focused on studying the effects of the industrial material Taunit, containing multi-walled carbon nanotubes (MWNTs), on plants, and testing of its ability to penetrate into plant cells and tissues. Taunit has been found to stimulate the growth of roots and stems and cause an increase in peroxidase activity in *Onobrychis arenaria* seedlings. Peroxidase activity increases with decreasing concentration of Taunit from 1,000 to 100 mg/l. MWNTs from Taunit were detected in the cells and tissues of seedling roots and leaves, implying the ability of MWNTs to penetrate into roots and accumulate there, as well as their ability to be transported into seedling leaves. Thus, the changes in the physiological parameters of plants are associated not only with MWNT adsorption on the root surface, as previously believed, but also with their penetration, uptake and accumulation in the plant cells and tissues.**
KEYWORDS **multi-walled carbon nanotubes, light microscopy, electron microscopy, electron diffraction pattern, *O. arenaria* seedlings.**
ABBREVIATIONS **CNM – carbon nanomaterials; MWNT – multi-walled carbon nanotubes; SWNT – single-walled carbon nanotubes; TEM – transmission electron microscopy, SAED – selected area electron diffraction.**

INTRODUCTION

The great benefits of using nanomaterials in modern technologies are no longer questioned. However, the potential negative effects associated with the propagation and accumulation of nanomaterial components, such as nano-particles and nanofibers in the environment, require further study [1, 2]. Plants are the major components of ecosystems; subsequently, significant attention should be paid to the effects of various technogenical materials upon them [3–5]. Carbon nanomaterials (CNM), such as fullerenes, multi-walled carbon nanotubes (MWNTs), and single-walled carbon nanotubes (CWNTs), are a matter of special interest, as their industrial production is rapidly developing. Since nanotubes have a fibrillar form, they are compared with asbestos [6]. In light of such an analogy, potential adverse effects on living organisms can be anticipated [7]. Preliminary studies have provided evidence that MWNTs and SWNTs are pathogenic to animals [8], yet they have different effects on plants. MWNTs were shown to considerably increase the growth rate of tomato seedlings [9], have no effect on the growth parameters of wheat [10], and inhibit the growth of rice seedlings [11]. SWNTs have been shown to suppress the growth of tomato roots, but stimulate the root growth of onion and cucumber [12]. In contrast, MWNTs have a toxic effect on *Arabidopsis* cultured cells. [13]. High adsorption of MWNT/SWNT on the roots of seedlings was observed in all the experiments conducted. However, the penetration, uptake and accumulation of MWNTs/SWNTs in plant cells and tissues are not well documented . Furthermore, the mechanism of the development of the physiological changes caused by the exposure of plants to nanotubes also remains unclear. The present work was aimed at studying the effect of the industrial nanomaterial Taunit, containing MWNTs, on *O. arenaria*

seedlings, and the ability of MWNTs to penetrate and accumulate in plant cells and tissues.

EXPERIMENTAL PART

Object of the study

The object of the present study is industrial CNM Taunit (NanoTechCenter Ltd., Tambov, Russia). This material is a loose black powder, composed of grainy agglomerates with a size of several micrometers. Agglomerates mostly consist of entangled MWNT bundles. MWNTs have a hollow cylindrical structure; at least 2 μm long, with an external diameter of 20–70 nm and an internal diameter of 5–10 nm. Taunit is produced by chemical vapor deposition; its purity is above 98% [14].

Seed germination and morphometric assessment

The seeds of *Onobrychis arenaria* were germinated in a medium containing a colloidal aqueous solution of CNM Taunit with a concentration of 100 or 1,000 mg/l. Prior to use, CNM was dispersed in distilled water by ultrasonic treatment . Distilled water was used to prepare the control medium. The seeds (50 seeds per dish) were grown for 10 days on filter paper in glass Petri dishes (diameter of 90 mm) with 5 ml of a CNM suspension added. 200 seeds were used in each experiment. The growth conditions followed the requirements of the State Standard procedure GOST 12038-84 (Agricultural seeds. Methods for evaluation of germination). The effect of CNM on esparcet seedlings was estimated on the basis of the following parameters: the rate of seed germination (%), the energy of germination (%), and the length of the roots and stems . The energy of germination and the rate of germination were determined as the ratio between the number of germinated seeds and the number of plated seeds by day 5 and day 10, respectively (%, in accordance with the State Standard).

Extraction of soluble peroxidases and determination of their activity

The weighed samples (2 g) of *O. arenaria* seedlings tissues were placed into 5 ml of a cold phosphate/citrate buffer (1 M solution of citric acid + 1 M NaH_2PO_4, two solutions combined to achieve pH 5.5) and ground in a porcelain mortar at 4°C [15]. The homogenate was centrifugated at 3,000 g for 15 min. The cleared supernatant was used to determine the activity of soluble peroxidases on the basis of the change rate (time, s) of the optical density at a wavelength of 580 nm in the reaction mixture containing 0.5 ml of 0.1 M solution of the phosphate/citrate buffer (pH 5.5), 0.5 ml of 0.3% H_2O_2, 0.5 ml of 0.05% guaiacol (Sigma, USA), and 0.5 ml of the sample. Peroxidase activity was measured at 25°C immediately after the enzymes were extracted from the samples. Enzymatic activity was calculated by Boyarkin's method [16] and expressed in arbitrary units of activity per gram of fresh tissue weight per second, according to the following formula:

$$A = (\varepsilon \times \alpha \times \beta \times \gamma)/(d \times t),$$

where ε is the extinction coefficient,
α is the ratio between the amount of buffer taken for extract preparation (ml) to fresh tissue weight (g),
β is the degree of additional dilution of the extract in the reaction mixture,
γ is the degree of constant dilution of the extract in the reaction mixture,
d is the thickness of the absorbing layer (mm); and
t is the reaction time (s).

Light and electron microscopy

The bottom of a plastic box (approximate dimensions 40 × 40 × 7 cm) was covered with four gauze layers moistened with a CNM solution or water (in the control sample). 100 *O. arenaria* seeds were placed on the gauze and exposed either to the CNM solution at the concentration 300 mg/l or water without CNM.

After 5 and 10 days of exposure to CNM, the seedlings were fixed for light and electron microscopic studies . For light microscopy, the seedlings were fixed in a 3:1 mixture of 96% ethanol and acetic acid for 16 h. After fixation, the plant samples were put into 70% ethanol. The plant parts under study (roots, leaves, coleoptiles) were then placed onto a glass slide into a drop of 45% acetic acid. The preparations of whole mount plant parts were made according to the standard procedure [17]. The preparations were analyzed using a Leica DM1000 light microscope (objectives ×10, ×20, ×40, and ×100). The images were recorded with a Leica DFC 295 digital camera (sensor size 3×10^6 pixels).

For transmission electron microscopy (TEM), the seedlings were fixed with 2.5% glutaraldehyde on a 0.1 M Na-K-phosphate buffer (pH 7.2) supplemented with sucrose (15 mg/ml). The samples were then dehydrated in a series of solutions of increasing ethanol concentrations and embedded in Epon 812, according to the standard procedure. For optimization of MWNTs detection within plant tissues, we opted not to use additional fixation with OsO_4 and staining with uranyl acetate and lead citrate.

The sample of pure CNM was prepared for TEM as follows: 25 mg of Taunit was placed onto the surface of unpolymerized resin (Epon 812), poured into a tube. Then, the sample was centrifugated for 3 min at 6,000 g and polymerized, according to the standard procedure.

Ultrathin sections of the samples embedded into Epon were investigated by TEM and SAED (selected area electron diffraction) using transmission electron microscopes JEM-1011 (JEOL) equipped with a GATAN ES500W digital camera, and LEO 912AB (Carl Zeiss).

RESULTS AND DISCUSSION

Effect of Taunit on the morphometric and biochemical characteristics of *O. arenaria* seedlings

In order to characterize the phytotoxicity of CNM, we used seed germination tests, in which the germination energy, germination rate, length of roots and stems, and peroxidase activity were estimated [18]. The germination of *O. arenaria* seeds in the presence of the colloidal solution of CNM Taunit increased the germination energy by 14% as compared with the control sample. CNM with a concentration of 100 and 1,000 mg/l increased the seeds germination rate by 2 and 7%, respectively (*Fig. 1a*). Taunit also stimulated the growth of roots and stems of seedlings . At CNM concentrations of 100 and 1,000 mg/l, the root length increased by 55 and 73%, respectively; the length of seedling stems increased by 84 and 82%, as compared with the control sample (*Fig. 1b*). Thus, CNM Taunit slightly increased the germination rate and the germination energy of seeds and considerably increased the length of roots and stems of seedlings . Taunit at the concentrations of 100 and 1,000 mg/l also enhanced peroxidase activity in *O. arenaria* seedlings, respectively, to 0.31 ± 0.01 and 0.19 ± 0.02 au/g fresh weight, which is significantly higher than the control value (0.12 ± 0.01) (*Fig. 1c*). It is well-known that plants respond to mechanical stress and injury by changing their morphology or growth rate. This phenomenon has become known as thigmomorphogenesis. Thigmomorphogenetic changes are regarded as the adaptation process to stress in plants, and plant hormones play an important role in this process [19]. Under mechanical stress or after injury, the activity of the plants stress hormone, jasmonic acid, increases, whereas the activity of auxin , which controls the processes of morphogenesis and plant growth, decreases. These changes of plant hormone levels may be associated with the increase of peroxidase activity [20-22]. Peroxidases are involved in a number of biological processes, such as photosynthesis, respiration, and protein metabolism. It is an antioxidant enzyme with high sensitivity towards external factors, and this allows using peroxidase activitiy assay for testing of the physiological state of plants. In most cases, a high level of peroxidase activity demonstrates the initiation of the mechanism of a nonspecific response of the plant to stress [23]. It can be assumed that increase in peroxidase activity is associated with the oxidative stress caused by

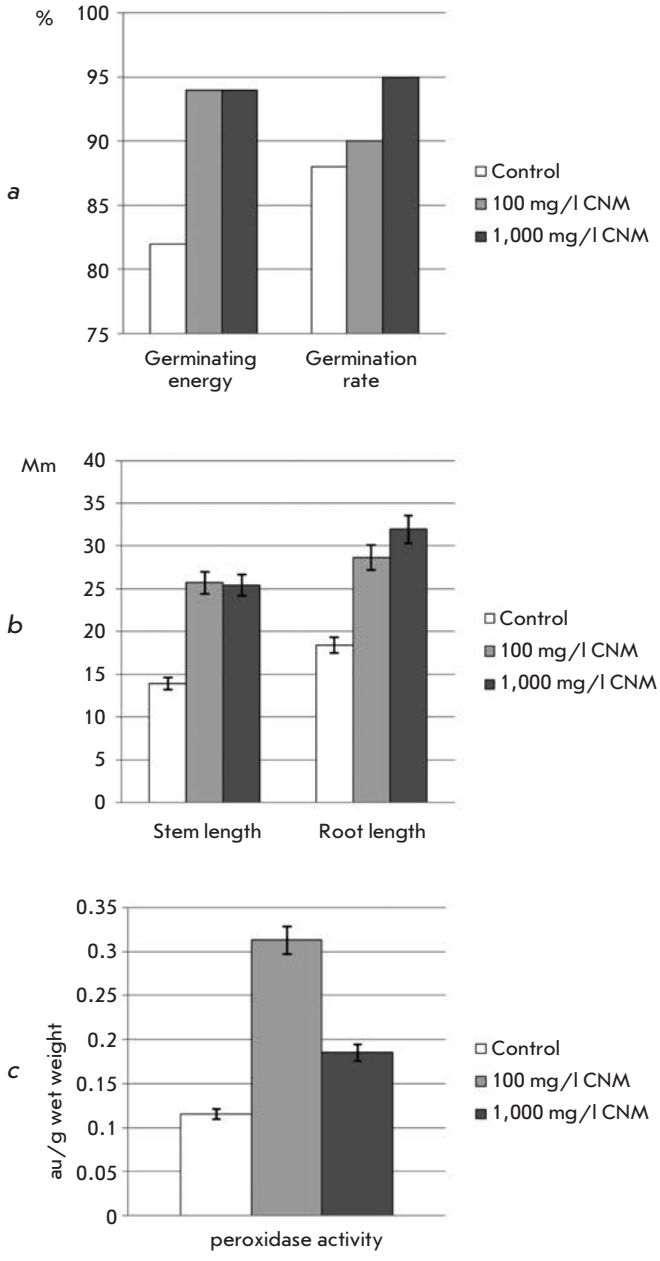

Fig. 1. The effect of different concentrations of CNM on the viability, morphological and biochemical parameters of *O. arenaria* seedlings.

CNM. It has been shown that MWNTs, accumulated at the root surface, often pierce cell walls of epidermal cells [10]. Such interaction can be considered as a mechanical injury and thus elevate the level of peroxidase activity. Our results confirmed that the level of peroxidase activity decreases with an increase in CNM concentration. This observation could be explained by the inactivation of peroxidase molecules by nanotubes due to sorption or

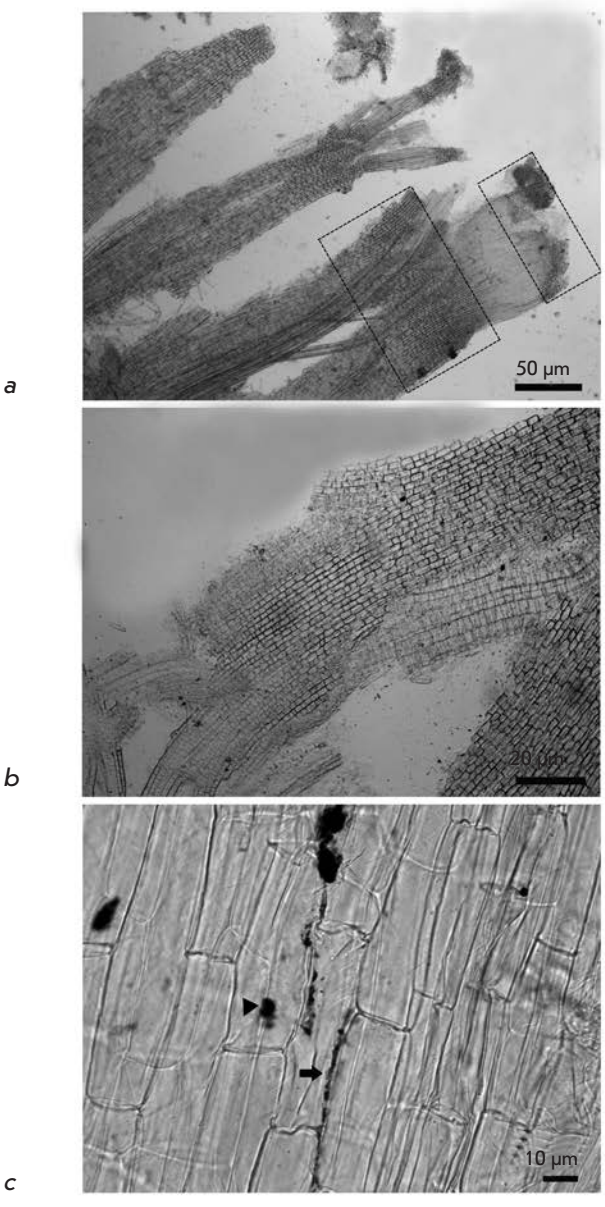

Fig. 2. Not stained and not contrasted preparation of a squashed esparcet root. *a* – areas of CNM accumulation in the root are shown by rectangles. CNM decorates root cap, region of maturation and vascular tissues. Scale 50 μm. *b* – inclusions of CNM located in the maturation region. Scale 20 μm. *c* – large accumulations of CNM in the apoplast (arrow) and in the cell (triangular arrow). Scale 10 μm.

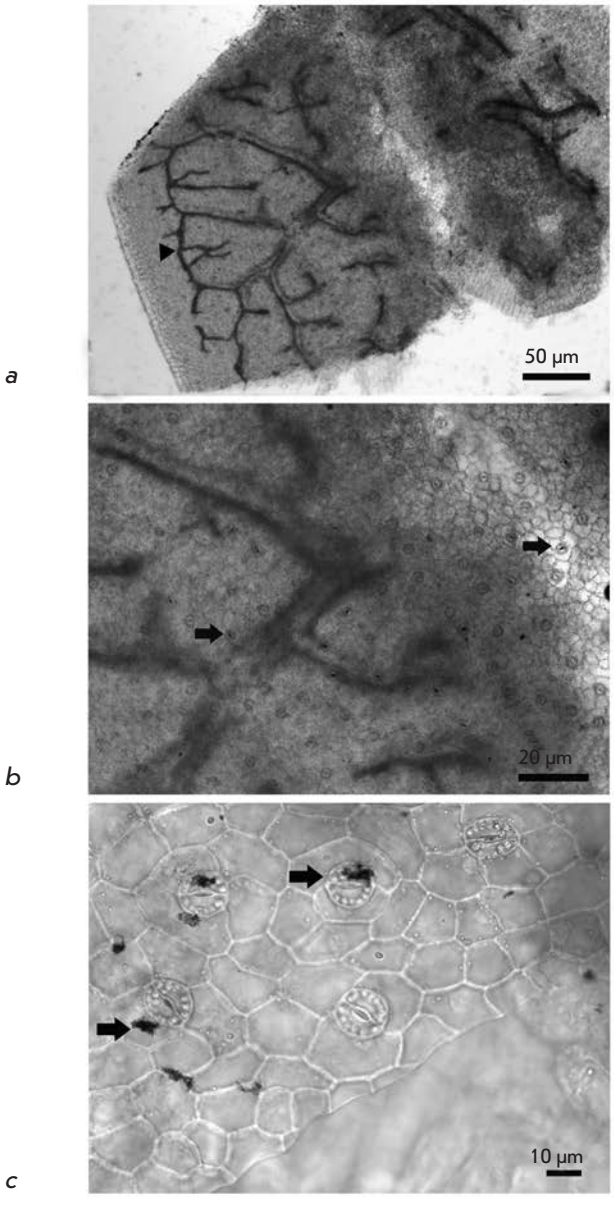

Fig. 3. Not stained and not contrasted preparation of a squashed esparcet leaf. *a* – CNM decorates vascular tissue (triangular arrow). Scale 50 μm. *b* – CNM stains vascular strands and localizes in stomata (arrows). Scale 20 μm. *c* – CNM in stomata guard cells and epidermal cells (arrows). Scale 10 μm.

other chemical interactions. Our studies demonstrated that, along with an increase in the level of peroxidase activity, exposure to CNM stimulated the growth of roots and stems of plants . Further research is needed to explain the mechanisms of the enhanced growth of plants in the presence of CNM.

Analysis of CNM Taunit in *O. arenaria* seedlings using light and electron microscopy

Upon germination of *O. arenaria* in the presence of CNM Taunit, the roots, stems, and leaves of seedlings acquire a characteristic dark gray color. Analysis of whole mount preparations showed that dark gray and

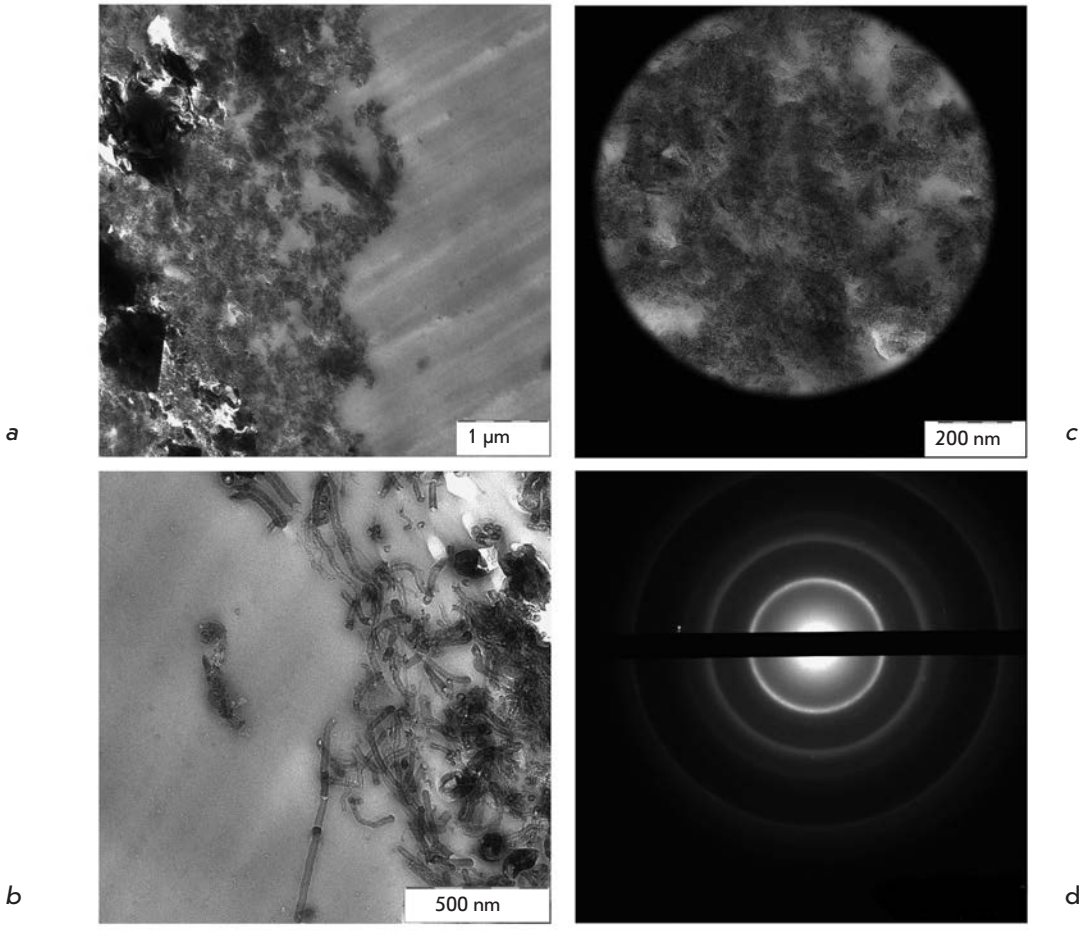

Fig. 4. TEM analysis of CNM Taunin sample. *a*, *b* – ultrathin section of CNM sample; *c* – accumulation of SNM analyzed with SAED; *d* – the diffraction pattern of CNM shown in *c*.

black agglomerates are localized on the surface of seedling roots and within particular tissues and cells of the roots, stems, and leaves (*Figs. 2a-c, 3a-c*). Ultrathin sections prepared from the plant organs containing aggregations of CNM were analyzed by TEM. Prior to studies of plant material, we had analyzed a pure CNM sample. TEM demonstrated that CNM Taunit (*Fig. 4a, b*) contains mostly agglomerates of MWNTs and some inclusions of a nanodispersed electron-dense material (presumably, graphitized carbon). The characteristic features of MWNTs are presented in *Fig. 4b*. The MWNTs without a small amount of inclusions (*Fig. 4c*) were characterized by the SAED method . As shown in *Fig. 4d*, due to the regular periodical packing of carbon atoms, MWNTs have an electron diffraction pattern typical for polycrystalline structures. This diffraction pattern was used as a reference sample for the identification of MWNTs in biological material.

The analysis of ultrathin sections of roots and leaves showed that CNM is present on the surface and inside the seedling organs. The adsorption of MWNTs on the root surface (*Fig. 5a*) has also been reported by other researchers [3, 10, 11]. Furthermore, agglomerates and single MWNT of different lengths are detected in root (*Figs. 5b,c*) and leaf cells (*Figs. 6a-c*). Thus the MWNTs are unmistakably identified by TEM. However, if MWNTs are located transversely or at some angle to the section plane, it is difficult to distinguish the MWNT fragments from different electron-dense endogenous inclusions. The method SAED can be used to identify MWNT in plant tissues (*Figs. 5d, 6d*). Superposition of electron diffraction patterns of MWNTs found in biological samples (*Fig. 5e, 6e*) with the reference electron diffraction pattern (*Fig. 4d*) confirms the presence of MWNTs in plant cells. Additional diffraction spots on the electron diffraction pattern are accounted for by the presence of endogenous crystalline inclusions in plant tissues.

The accumulation of MWNTs on the root surface was reported by many authors [3, 9–11] and it has been suggested that interaction of MWNTs with plant organs affects plant growth and development [13]. Adsorption

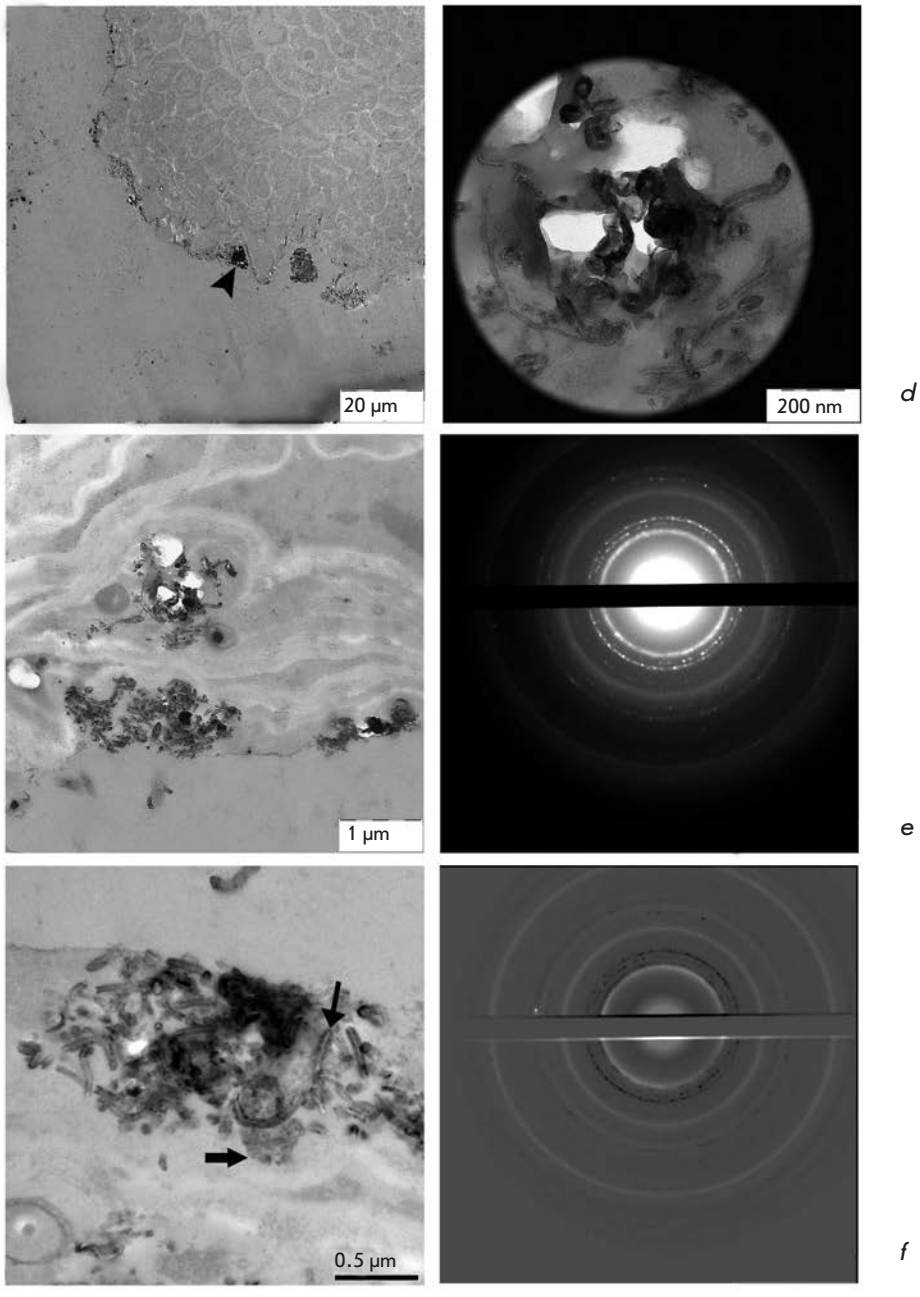

Fig. 5. *O. arenaria* seedling grown in the presence of CNM, ultrathin sections of root. *a* – accumulation of CNM on the root surface is shown with arrow; *b* – accumulations of CNM on the root surface and within the root cells; *c* – aggregates of CNM found in the cells containing nanotubes (thin arrow) and finely dispersed electron-dense material (thick arrow); *d* – the area of the root with CNM selected for analysis with SAED; *e* – diffraction pattern of the area shown in *d*; *f* – superimposed image of pure CNM diffraction pattern (*Fig. 4d*) and inverted image of the diffraction pattern of CNM found in the root cell (*Fig. 5e*). The overlapping diffraction spots are white; non-overlapping – black.

of a large amount of MWNTs on the root surface may suppress the water flux and uptake of nutrients, thus inhibiting plant growth [11]. Conversely, the stimulation of seed germination may be associated with the fact that nanotubes (SWNTs) pierce the seed cover and increase water uptake, facilitating seed germination and plant growth [9]. However, SWNTs not only pierce the cell wall , but also penetrate inside the cells; this phenomenon was demonstrated using FITC-labeled SWNTs (SWNT/FITC) [24]. Insertion of MWNT into the wall of epidermal cells and root hairs up to 4 μm was observed in wheat seedlings using two-photon excitation microscopy; however, penetration of whole MWNTs into the cytoplasm was not noted [10]. The authors assumed that penetration, uptake and accumulation of MWNTs are less evident due to the larger nanotube diameter as compared with that of SWNT [10].

CONCLUSIONS

We demonstrated that MWNTs penetrate cell walls, accumulate in the cells and tissues, and most likely are transported via a plant's vascular system from roots to

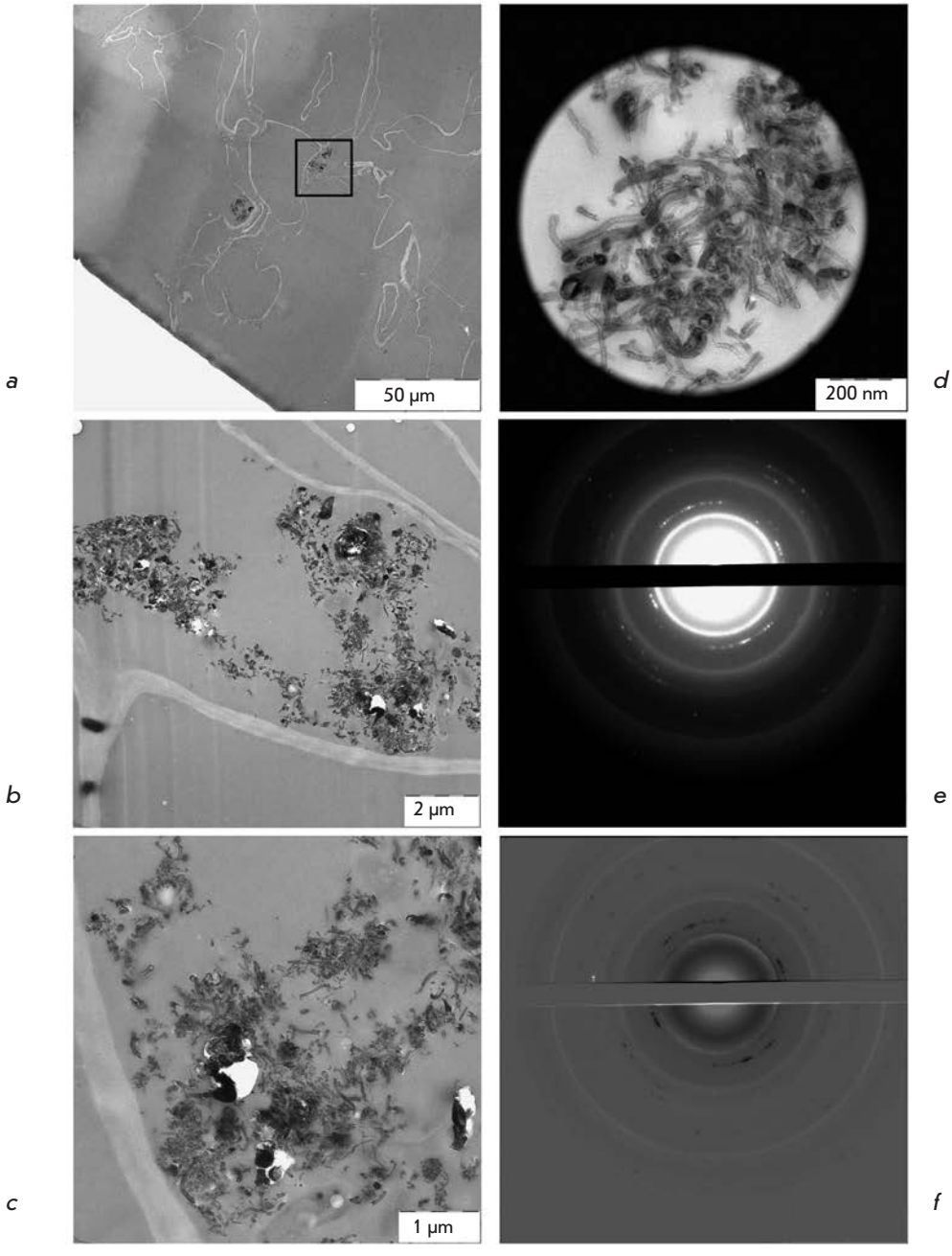

Fig. 6. *O. arenaria* seedling grown in the presence of CNM, ultrathin sections of leaf. *a* – the leaf area containing two aggregates of CNM. Framed area is magnified and shown in *b* and *c; b*, *c* – CNM contains nanotubes and finely dispersed electron dense inclusions; *d* – the area of the leaf with CNM selected for analysis with SAED; *e* – diffraction pattern of the area shown in *d*; *f* – superimposed image of the pure CNM diffraction pattern (*Fig. 4d*) and inverted image of the the diffraction pattern of CNM found in the leaf cell (*Fig. 6e*). The overlapping diffraction spots are white; nonoverlapping – black.

stems and the leaves of *O. arenaria* seedlings. We argue that the stimulation of *O. arenaria* roots and stems growth and the increase in peroxidase activity were induced by the oxidative stress which develops due to the accumulation of MWNTs in plant cells and tissues. ●

The authors are grateful to S.S. Abramchuk (Belozersky Institute of Physico-chemical Biology) for assistance with this study.

This work was supported by the Federal Program "Scientific and Scientific-Pedagogical Personnel of Innovative Russia" (Government contracts P 208 dated April 23, 2010 and 16.740.11.01-94 dated September 24, 2010) and Government contract №01.648.11.3003.

REFERENCES

1. Handy R.D., Owen R., Valsami-Jones E. // Ecotoxicology. 2008. V. 17. P. 315–325.
2. Moore M.N. // Environ. Internat. 2006. V. 32. P. 967–976.
3. Ma X., Geiser-Lee J., Deng Y., Kolmakov A. // Sci. Total Environ. 2010. V. 408. P. 3053–3061.
4. Navarro E., Baun A., Behra R., Hartmann N.I.B., Filser J., Miao A.-J., Quigg A., Santschi P.H., Sigg R. // Ecotoxicology. 2008. V. 17. P. 372–386.
5. Ruffini Castiglione M., Cremonini R. // Cariologia. 2009. V. 62. P. 161–165.
6. Berhanu D., Dybowska A., Misra S.K., Stanley C.J., Ruenraroengsak P., Boccaccini A.R., Tetley T.D., Luoma S.N., Plant J.A., Valsami-Jones E. // Environ. Hlth. 2009. V. 8 (Suppl 1). S3.
7. Yuliang Zh., Genmei Xi., Zhifang Ch. // Nat. Nanotechnol. 2008. V. 4. P. 191–192.
8. Poland C.A., Duffin R., Kinloch I., Maynard A., Wallace W. A., Seaton A., Stone V., Brown S., MacNee W., Donaldson K.// Nat. Nanotechnol. 2008. V. 3. P. 423–428.
9. Khodakovskaya M., Dervishi E., Mahmood M., Xu Y., Li Z., Watanabe F., Biris A.S. // ACS Nano. 2009. V. 3. P. 3221–3227.
10. Wild E., Jones K.C. // Environ. Sci. Technol. 2009. V. 43. P. 5290–5294.
11. Lin S., Reppert J., Hu Q., Hudson J.S., Reid M.L., Ratnikova T.A., Rao A.M., Luo H, Ke P.C. // Small. 2009. V. 5. P. 1128–1132.
12. Canas J.E., Long M., Nations S., Vadan R., Dai L., Luo M., Ambikapathi R., Lee E.H., Olszyk D. // Environ. Toxicol. Chem. 2008. V. 27. P. 1922–1931.
13. Lin C., Fugetsu B., Su Y., Watari F. // J. Hazardous Material. 2009. V. 170. P. 578–583.
14. Tkachev A.G., Zolotukhin I.V. Apparatura i metody sinteza tverdotelnih nanostructure (Instrumentation and Methods of Synthesis of Solid-state Nanomaterials). M.: Mashinostroenie-1, 2007. 316 p.
15. Padu E.H. // Fiziologiya rasteniy (Physiology of Plants). 1995. V. 42. №3. P. 408-415.
16. Boyarkin A.N. // Biokhimia. 1951. V. 16, №4. P. 352-355.
17. Pausheva Z.P. Praktikum po tsitologii rasteniy (Methods in Plant Cell Cytology). M.: Kolos, 1974. 288 p.
18. Barrena R., Casals E., Colón J., Font X., Sánchez A., Puntes V. // Chemosphere. 2009. V. 75. P. 850–857.
19. Chehab E.W., Eich E., Braam J. // J. Exp. Bot. 2009. V. 60. P. 43–56.
20. Hofinger M., Chapelle B., Boyer N., Gaspar T. // Plant Physiol. 1979. V. 63. S-52.
21. Ostin A., Kowalyczk M., Bhalerao R.P., Sandberg G. // Plant Physiol. 1998. V. 118. P. 285–296.
22. Woodward A.W., Bartel B. // Ann. Botany. 2005. V. 95. P. 707–735.
23. Andreeva V.A. Ferment peroksidaza: Uchastie v zaschitnom mekhanisme rasteniy (Peroxidase: the Role in Mechanism of Plant Defense). M.: Nauka, 1988. 128 p.
24. Liu Q., Chen B., Wang Q., Shi X., Xiao Z., Lin J. Fang X.// Nano Lett. 2009. V. 9. P. 1007–1010.

Modeling Myocardial Infarction in Mice: Methodology, Monitoring, Pathomorphology

A.A. Ovsepyan[4], D.N. Panchenkov[1,3], E.B. Prokhortchouk[1*], G.B. Telegin[4], N.A. Zhigalova[1], E.P. Golubev[2], T. E. Sviridova[5], S.T. Matskeplishvili[2], K.G. Skryabin[1], U.I. Buziashvili[1,2]

[1]Center "Bioengineering", Russian Academy of Sciences

[2]Bakoulev Center for Cardiovascular Surgery, Russian Academy of Medical Sciences

[3] Moscow State University of Medicine and Dentistry

[4]The Branch of the Shemyakin and Ovchinnikov Institute of Bioorganic Chemistry, Pushchino, Russian Academy of Sciences

[5]Semashko Railway Hospital

*E-mail: prokhortchouk@biengi.ac.ru

Received 12.11.2010

ABSTRACT **Myocardial infarction is one of the most serious and widespread diseases in the world. In this work, a minimally invasive method for simulating myocardial infarction in mice is described in the Russian Federation for the very first time; the procedure is carried out by ligation of the coronary heart artery or by controlled electrocoagulation. As a part of the methodology, a series of anesthetic, microsurgical and revival protocols are designed, owing to which a decrease in the postoperational mortality from the initial 94.6 to 13.6% is achieved. ECG confirms the development of large-focal or surface myocardial infarction. Postmortal histological examination confirms the presence of necrosis foci in the heart muscles of 87.5% of animals. Altogether, the medical data allow us to conclude that an adequate mouse model for myocardial infarction was generated. A further study is focused on the standardization of the experimental procedure and the use of genetically modified mouse strains, with the purpose of finding the most efficient therapeutic approaches for this disease.**

KEYWORDS **myocardial infarction, coronary artery, ligation, controlled electrocoagulation, ECG (electrocardiogram).**

INTRODUCTION

The simulation of myocardial infarction in animals is of great importance. First of all, there is a need to search for and develop optimal regimens for treating this disease using new approaches, including pharmacological and cell therapies. As a result of the heterogeneity of the concept 'myocardial infarction' in humans and its various clinical manifestations (which may occur with another, already present pathology, i.e. diabetes mellitus or an increased concentration of cholesterol in the blood-stream), the question arises as to how to create an animal model which adequately reflects the complex etiology of this disease. The general approach underlying the selection of objects for biomodeling should satisfy the following criteria: 1) convenience in performing open-heart surgeries on animals; 2) the possibility of using genetically modified or selectively bred animal strains with particular features of myocardial infarction simulated; and 3) the possibility of further standardization and certification in compliance with international standards, for both the technology and the laboratory in which the bio-model was obtained. It is reasonable to note that the first two conditions are in conflict with one another since the suitability of organisms for genetic studies is defined by their large population and small size (*Drosophila melanogaster* and *Danio rerio* are the classical genetic objects). This fact imposes an obvious restriction on carrying out surgical intervention. For to the third condition, it is necessary to obtain a quantity of model animals that will be sufficient in terms of statistical reliability to successfully carry out the first stage of the preclinical testing of new pharmaceutical preparations, or for the performance of cell therapy. From one perspective, the survival rate of animals is dependent upon the reliability of surgery and post-operation recovery protocols. In turn, this makes the process of bio-model development a larger scale one. On the other hand, the process depends on the availability of the certified facilities and hardware required for these procedures in the Russian Federation. Thus, a researcher has to compromise between the size of the animals and availability of their genetic strains, something that could affect the quality of preclinical testing.

In this work, laboratory mice were chosen for the simulation of myocardial infarction. Working with these animals is a well-established procedure at the internationally accredited Research and Production Division Nursery of Laboratory Animals branch of the Shemyakin and Ovchinnikov Institute of Bioorganic Chemistry. Thus, in the case of developing and certifying the technology in accordance with the requirements of the International Organization for Standardization (ISO), there appears to be a possibility of not only using these bio-models in fundamental research, but also supplying Russian and foreign pharmaceutical companies with them. The latter is particularly important, since preclinical testing should be carried out only on standard-model animals with a special health status (specific pathogen-free animals), which is maintained in the nursery at the branch of the Shemyakin and Ovchinnikov Institute of Bioorganic Chemistry. The main advantage provided by mice is that there is a developed network of their genetic resources, something that is in acute shortage in their relatives, rats. The genetic diversity of inbred mouse strains allows us to select animals that are suitable for the study of cardiovascular diseases. In particular, the A/J and C3H/HeJ strains are resistant to atherosclerotic lesions of the aorta occurring when the animals are kept on an atherogenic diet (1.25% cholesterol, 0.5% cholic acid, and 15% fat), while the C57BL/6J mouse strains are extremely sensitive to the atherogenic diet, and the CBA/J strains are partially resistant [1–3]. There are also inbred rat strains which are potentially suitable for infarction simulation (in this context, spontaneously hypertensive rats (SHR) with an increased blood pressure should be mentioned as a popular animal model) [4]. The main advantage of mouse models is the possibility of genetic manipulation of mouse embryonic stem cells, while this type of technology is still poorly developed for rat cells. Transgenesis, knock-out, and knock-in technologies, which are both tissue-specific and inducible, make it possible to remove and insert genes and sometimes to introduce point mutations into the mouse's genome.

A researcher can always select the desired genes, their diversity enabling the creation of any genetic anomalies. These anomalies can act as a background for the infarction model. Thus, the microsurgical simulation of infarction can be applied to any available genetic model. For instance, if the infarction has to be simulated against a background of an increased cholesterol level, mice carrying an apolipoprotein E4 gene (*apoE4*) should be chosen. Meanwhile, if the infarction has to be obtained against a background of cardiomyopathy, BALB/c or CD-1 mice should be used. The catalog of the Jackson Laboratory (USA) offers 373 strains for cardiovascular disease research; twenty of them are selectively bred inbred strains, while the rest of the strains were obtained by genetic manipulations involving more than 50 genes. Among genetic models of diseases to which the microsurgical simulation of infarction can be applied, the following models can be mentioned: hypo- and hypertension, atherosclerosis, cardiomyopathy, lesion of coronary vessels, various metabolic syndromes, ischemia, hypo- and hypercholesterolemia, and hypo- and hypertriglyceridemia. The combination of infarction simulated by means of microsurgical techniques with genetic models creates the prerequisites for reproducing various human heart diseases in mice and for further use of these animals in the clinical testing of drugs and in cell therapy. In the latter case, the observation of fluorescent-labeled (e.g., green fluorescent protein, GFP) or radioactively labeled (labeled with isotopes) cells injected into the heart (or vessels) is possible. The injected cell material is not rejected by homozygous animals, and the sites of its integration can be easily determined by multislice computed tomography, thereby performing the intra-vital monitoring of the efficiency of cell therapy. The obvious shortcomings in the case of mice include the small size of their viscera and the small volume of blood circulation. The use of current methods for developing mouse bio-models leads to a high mortality of laboratory animals [5–9], a phenomena that is due to surgical aggression and loss of blood [10–13]. Therefore, a whole complex of anesthetic, microsurgical, and revival protocols is needed in order to perform a successful surgical intervention. This complex involves tracheal intubation for pulmonary ventilation by means of a medical ventilator, inhalation narcosis, bloodless thoracotomy, ligation of the left-anterior descending coronary artery, procedures for the recovery of animals after surgical modification, and measurement of electrocardiograms (ECG).The methodology and technical equipment in these procedures are considerably different from those used in Russia for surgical operations in rats.

The purpose of the present work is to develop for the first time in Russia a minimally invasive method for simulating myocardial infarction in laboratory mice. This will be accompanied by a complex of postoperation procedures aimed at achieving successful rehabilitation of the animals operated upon, and monitoring their state during the postoperation period.

EXPERIMENTAL

Preoperation Period and Narcotization

In this work, we used 48 CD-1 mice of mixed sex, more than 8 weeks old, and weighing 3,236 g. Twenty-four

hours prior to the operation, the mice were put into a cage with clean litter and water. Food was completely removed from the feedboxes. Just prior to the operation, the animals were weighed, and the needed volume of anesthetic was calculated. For the anesthesia, the injection mixed zoletil/xylazine narcosis (40–50 mg zoletil (tiletamine + zolazepam) per 1 kg of body weight and 15–20 mg xylazine per 1 kg of body weight) was used. After surgical anesthesia and prior to tracheal intubation, the official drug, Vetranquil 1% inj. (Ceva Sante Animale, France), containing 1% acepromazine and 0.5% chlorobutanol, was used in a dose of 2–4 mg/kg acepromazine and 1–2 mg/kg chlorobutanol for neuromuscular relaxation when needed. In order to prevent drying of the cornea, a moisture-donating gel, Normlgel – 0.9% (Mölnlycke Health Care), was applied to the eyes of the anesthetized animals prior to the surgery. The preparation of the surgical site on the left side of the chest was performed according to the following procedure: the hair was shaved off, the skin was disinfected with a disinfectant, Decosept (BORER CHEMIE AG, Switzerland), and draped in a sterile transparent adhesive film, Opsite incise drape (Smith & Nephew, England) (*Fig. 1a*). Immediately after narcotization of the mice, ECG measurements were performed (the procedure is described below). In order to carry out the tracheal intubation, the mouse was fixed in a supine position on a heated surgical table. The tracheal intubation was carried out using an endotracheal tube with the following dimensions: the outer diameter was 1–1.2 mm, the inner diameter was 0.6–0.8 mm, and the length was 25–30 mm) (*Fig. 2b*). The endotracheal tube was connected to a MiniVent Ventilator for Mice (HSE Harvard, Germany) (*Fig. 1c*), the inspiratory oxygen concentration was equal to 30% (oxygen was generated using a NewLife oxygen concentrator (AirSep, USA). The calculated values of the volume and the ventilation rate are listed in *Table*.

Weight of a mouse, g	Stroke volume, µl	Ventilation rate, strokes/minute
22–27	175	130
28–35	200	120
≥35	225	110

Surgical Procedure

Using a Leica MZ7.5 high-performance stereomicroscope (the magnification range is from 10x to 25x, the working distance is 25–30 cm), an incision in the fourth left intercostal space was made and the muscles of the chest wall (the broadest muscle of the back, the serratus ventralis muscle, and the external abdominal oblique muscle) were prized apart with scissors. Ligatures (surgical silk 3-0) were applied to these groups of muscles, and the muscles were moved in opposite directions. Using an eye dressing, forceps with angled serrated tips (Fine Science Tools, USA) and scissors, the intercostal muscle and parietal pleura were cut. Then, a Mini-Goldstein 3x3 (Fine Science Tools) retractor was placed into the wound. Next, the pericardium was cut by careful blunt dissection, and the lung was moved to the edge of the wound, giving access to the front (lower) surface of the heart (*Fig. 1e*). By manipulation with forceps and the pericardium in the incision wound, the heart was brought to a position suitable for finding the left coronary artery. This artery has a vivid red color and pulsates. With the help of an atraumatic needle and a nonabsorbable suture Prolene 6/0 (Ethicon, USA), the coronary artery was ligated in the center of its descending branch (*Fig. 1f*). If the ligation is performed correctly, the tachycardia, arrhythmia, and myocardial anemia develop fast in the ligated site. Then, the pericardium and the lung were moved back.

Since the identification of the coronary artery and its ligation are rather complicated procedures from a technical point of view, we proposed another method for the simulation of myocardial infarction. This method involves producing a necrotic zone by means of an electro-coagulator. In this method for simulating infarction, an active electrode of the electro-coagulator acts directly on the myocardium after the front (lower) surface of the heart is reached.

After the surgical procedures were performed, the ribs and the pleura were sutured with two or three isolated, interrupted sutures using a VICRYL 5-0 (Ethicon) thread, and the incision wound in the chest wall was closed. Then, the dissected muscles were put together and tightly pressed against each other. The wound was irrigated with a sterile saline solution. After that, an uninterrupted glover's suture was placed using an atraumatic needle and a nonabsorbable suture VICRYL 4-0 (Ethicon). During this procedure, the chest in the area of the wound was compressed by forceps with the purpose of removing air and creating negative pressure in the thoracic cavity. In order to protect the surface of the surgical wound, the skin was treated with a special suspension of microporous aluminum AluSpray (Vetoquinol, France), which forms a thin layer of aluminum coating on the skin's surface (*Fig. 2*).

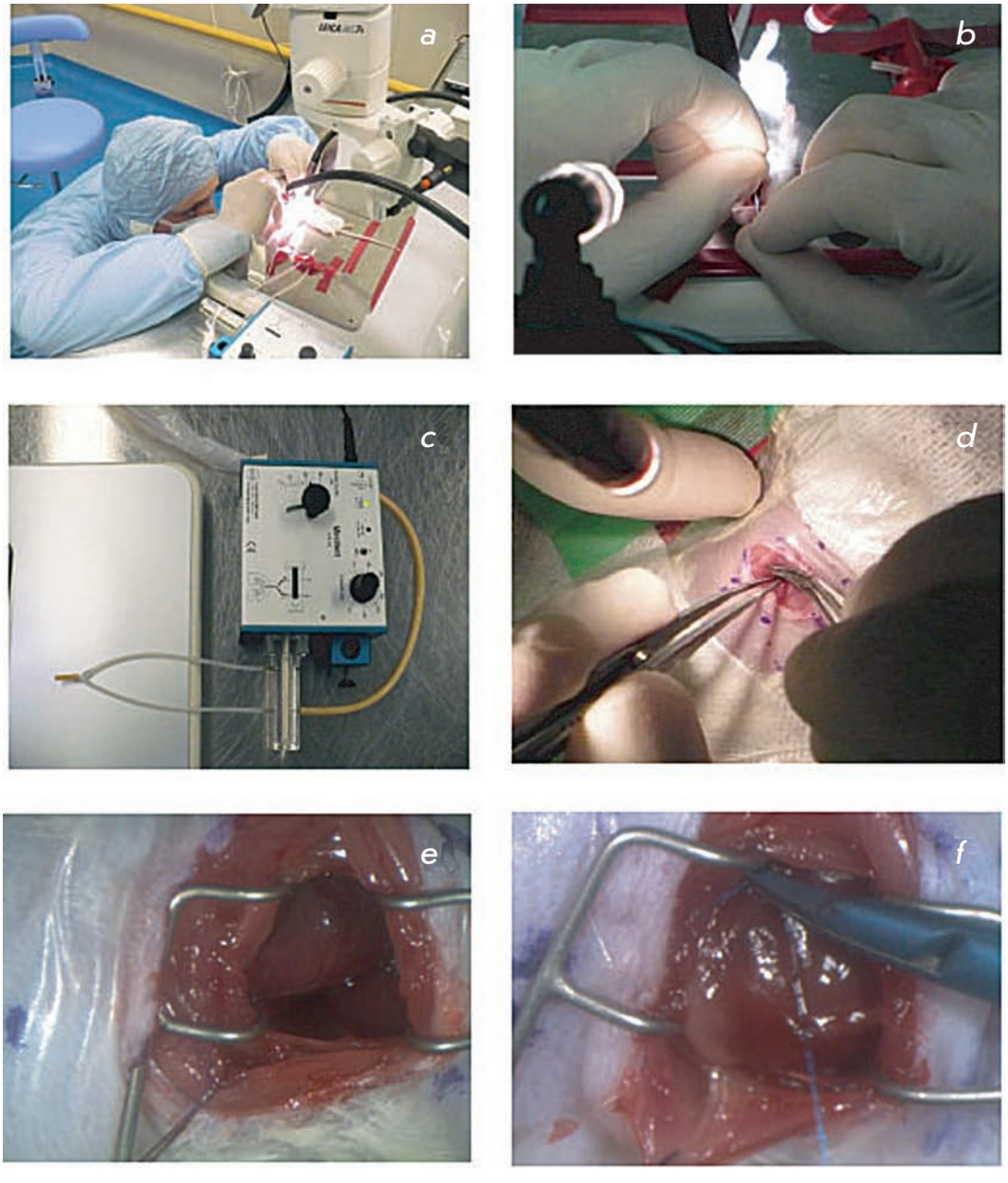

Fig. 1. Preoperation and operation procedures during simulation of myocardial infarction in mice: *a* – fixation of a mouse on a heated operation table; *b* – intubation of trachea; *c* – device for artificial pulmonary ventilation "MiniVent Ventilator for Mice"; *d* – incision in the 4-th left intercostal space; *e* – front (lower) surface of the heart can be seen in the incision wound; *f* – ligation of the descending branch of the coronary artery.

Temperature Conditions

In order to prevent the hypothermia that may result as a consequence of narcotization, the animal was placed on the heated surgical table with a heating temperature of 32–34°C. Immediately upon completion of the surgery, the animal was put into a recovery chamber Warm Air System (Vet Tech Solutions, England), supplied with heated (30–32°C) oxygen-enriched air.

Postoperation Period

Xylazine in a quantity of 10 mg xylozane per 1 kg of body weight was used for postoperation analgesia in the mice. When an animal emerged, it was put into an individual cage. Moist feed was given to the animal. Normally, there is no need for the removal of absorbable sutures.

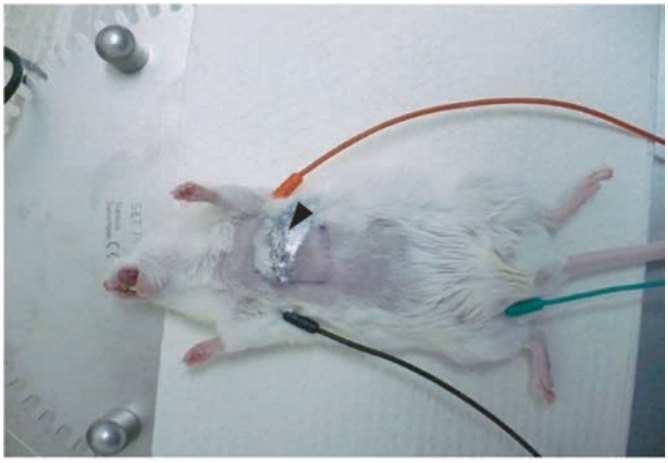

Fig. 2. Illustration of postsurgery ECG measurements. A mouse is placed on a heated operation table and connected to the ECG apparatus by three electrodes: one on the left foreleg (red), one on the right foreleg (black), and one on the right hind leg (black). The sutured wound is covered with an AluSpray suspension (shown with an arrow).

ECG Measurements

ECG plays an important role in the diagnostics of myocardial infarction. The changes observed in the ECG allow one to determine the infarction location, its extent and depth; i.e., whether it is large-focal, small-focal or intramural, sometimes the prescription (during the first few weeks), and a number of other features. Therefore, ECG measurements were performed in mice before and after the ligation of the coronary heart artery and coagulation in order to obtain an experimental myocardial infarction. Prior to ECG recording, a mouse was subjected to injection narcosis using a zoletil/xylazine solution (40–50 mg zoletil (tiletamine + zolazepam) per 1 kg of body weight and 15–20 mg xylazine per 1 kg of body weight). Then, the mouse was put in a supine position on a heated surgical table and connected to three electrodes: one on the left foreleg, one on the right foreleg, and one on the right hind leg (*Fig. 2*). The ECG was recorded on a PowerLabSupport apparatus (ECG Analysis Module) (ADINSTRUMENTS, Australia). The value of electrocardiographic waves, their duration and intervals were defined in accordance with the parameters proposed in the ECG Analysis software. The excitation and repolarisation width was 100 ms (Pre-P was 10 ms, PR was 50 mc, and RT was 40 ms). The ECG was recorded prior to the surgery, 5–10 min after the surgery, and on the 3rd, 10th, and the 30th days after the surgery.

Morphological Examination

A morphological examination was performed in 32 mouse hearts: in 21 hearts, myocardial infarction was simulated by ligating the left coronary artery; and in 11 hearts, by electrocoagulation of a myocardial site. After their removal, all organs were placed into 10% neutral formalin for 1 day, with the purpose of fixation. According to the macroscopic examination, the hearts had rather similar sizes and weights: the average weight of a mouse heart was 4 g, and the average size was 1.6 × 0.9 × 0.7 cm. In 11 cases, the necrosis was induced by controlled electro-coagulation; a spot trace from the electrode was detected on the epicardium of the left ventricle during macroscopic examination.

For histological examination, each heart was cut into two pieces along the interventricular and interatrial septa. These pieces were subsequently held in formalin at room temperature for 24 h with the purpose of further fixation. The pieces were then washed with running water for 1–2 h. The washed pieces dehydrated at room temperature using several portions of solutions with increasing concentrations: once with 70.96 ethanol and twice with 100% ethanol (for 2 h). The pieces were then prepared to be embedded in paraffin in accordance with the following procedure: the pieces were placed into an alcohol/xylene mixture (1 : 1) for 2 h at room temperature and held in a thermostat in a mixture of hot paraffin and xylene (1 : 1) for 2 h at 60°C. The pieces dehydrated and coated with paraffin were placed into metal frames with the dimensions 2 × 2 × 2 cm and embedded with a HISTOMIX paraffin medium (Biovitrum, Russia). After cooling, paraffin blocks containing pieces of the heart in bulk were obtained. Thus, for each heart, two paraffin blocks were obtained, each containing the right or left heart segments, and sections of the interventricular and interatrial septa.

The purpose of the histological examination was to detect the focus of myocardial necrosis, which required the performance of a series (layer-by-layer) of transmural histological sections with a thickness of 5 μm each throughout the entire thickness of the cardiac walls from each block. The sections were prepared using an ACCU-CUT SRM 200 rotatory microtome (ACCU-CUT, Japan) and placed on slides. On average, 30 histological sections were prepared from each block. Paraffin was then removed from the sections by holding them in a xylene solution for 15 min and treating with ethanol solutions with decreasing concentrations (twice with 100% ethanol (for 3 min each time), and twice with 96% ethanol). After the removal of paraffin, the sections were washed with distilled water and stained with Mayer's hematoxylin and eosin. The stained sections were covered with polystyrene and placed under a cover glass.

RESULTS AND DISCUSSION

Results of the Surgical Stage

During the first stage of the myocardial infraction simulation, 16 laboratory mice were operated upon. The ligation of the coronary artery was performed in 12 of them, and the controlled electro-coagulation procedure was carried out on four mice. The ECG was recorded on four mice. The mortality rate for this group was 94.5%. Further, the animals from this group were not included into the investigation and considered as a test group.

After the procedure was standardized, surgeries were carried out in 32 animals (the ligation of the coronary artery was performed in 21; and coagulation, in 11). Let us note the important details and peculiarities typical to the ligation procedure. At all stages of the surgery described above, it is extremely important to follow the topographic anatomic reference points. Otherwise, uncontrolled bleeding or damage to lung tissue could occur; this is inadmissible, since it leads to the death of laboratory animals. After opening the pericardium, the anterolateral wall of the myocardium with the left coronary artery in it should be identified. Since the coronary artery has a small diameter, its identification is complicated. The left descending branch of the coronary artery is characterized by an opalescent white band following a short oblique direction relative to the main direction of the operation procedure. When the artery was identified, a synthetic suture Prolene 6/0 in an autraumatic needle was brought under it. The artery was ligated, a microsurgical knot was formed, and the suture ends were cut using microsurgical scissors. During the ligation stage, it is extremely important to control the thickness of the tissue taken; if the needle is inserted too deeply, the probability of myocardial perforation is high; which leads to immediate death. The site the ligature is applied to should be determined correctly, since if it is applied not to the descending branch but to the main trunk of the left coronary artery, extensive myocardial infarction incompatible with life occurs. In order to determine which suture material is optimal for this operation, a comparative study of different types of suture material was performed. Synthetic monofilamental nonabsorbable material demonstrating no sawing effect was selected; Prolene 6/0 suture is an example of this kind of material.

The average surgery time for this group of animals was 57 min (39–75 min). Post-operation lethality decreased to 13.6% against the 94.6% observed in surgery in mice from the test group. These results are in agreement with the published data and in line with the task set.

ECG Data

In most mice with myocardium infarction simulated by ligating the coronary artery, rhythm disturbance, i.e. atrial fibrillation, was observed after the surgery. On the 10th day after the surgery, ECG typical for large-focal myocardial infarction was obtained; this type of infarction is characterized by the disappearance of the

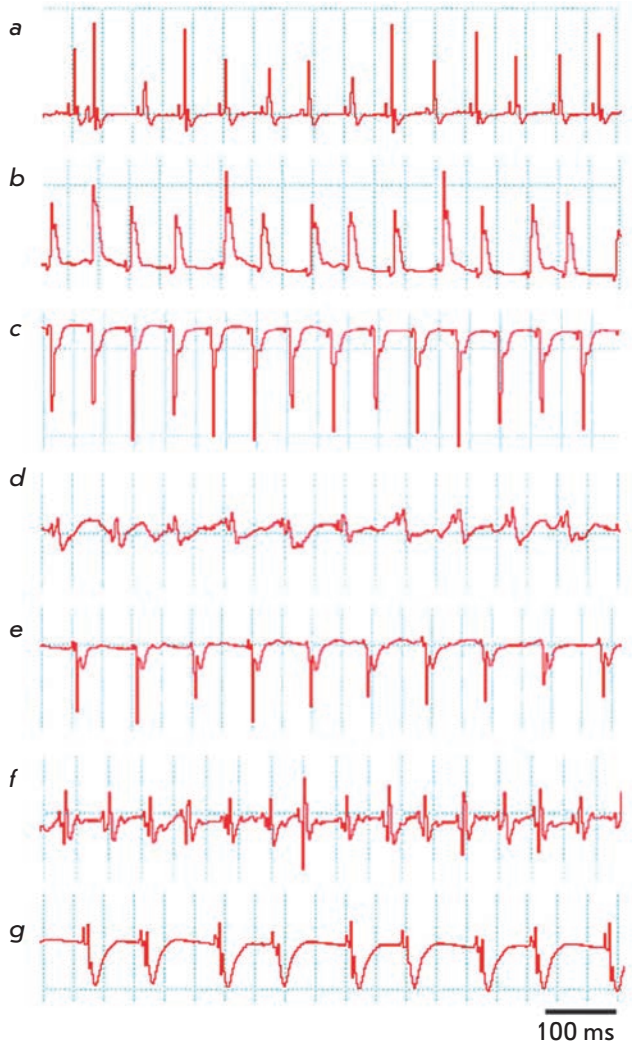

Fig. 3. ECG recorded in animals after surgery: *a* – ECG recorded prior to surgery; *b* – impaired heart rhythm in 5–10 minutes after ligation of the coronary artery; *c* – development of a large-focal infarction 10 days after the ligation of the coronary artery; *d* – heart rhythm measured 5 minutes after thermal coagulation of the coronary artery; *e* – development of surface infarction 10 days after thermal coagulation; *f* – tachycardia developed 5–10 minutes after the ligation of the coronary artery; *g* – brachycardia developed on day 3 after the ligation of the coronary artery. The excitation and repolarization width is 100 ms.

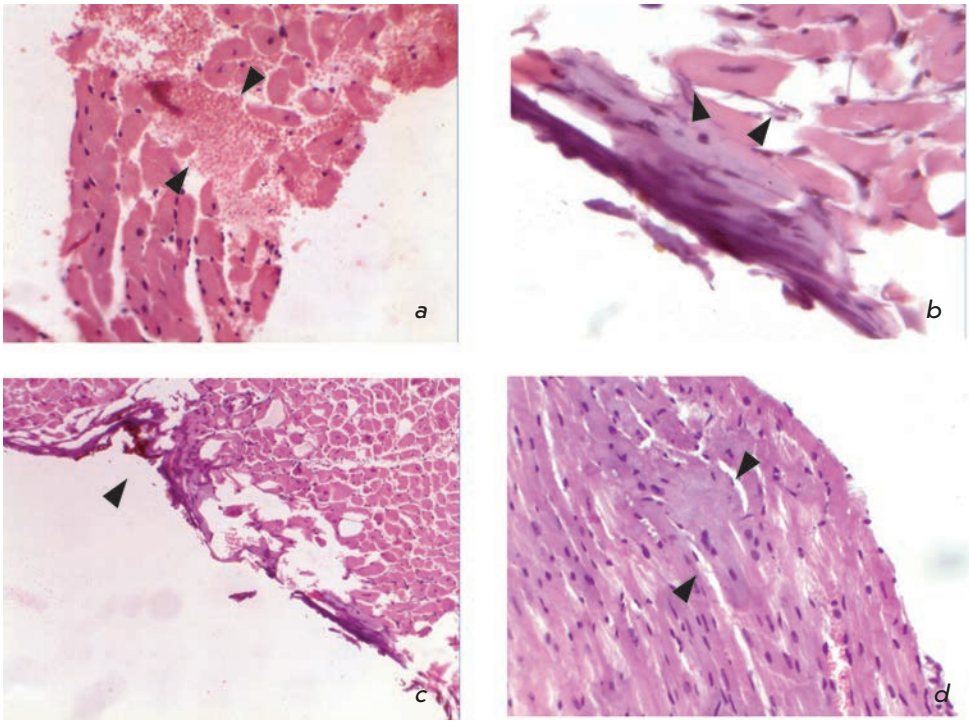

Fig. 4. Histopathology of the hearts in the case of infarction simulated in mice: *a* – beginning of coagulational necrosis and cardiomyocytes disorganization, stromal edema, and haemorrhage; hematoxylin and eosin staining; magnification of 20x; *b* – lack of cross striation within the sarcoplasm of cardiomyocytes; apoptotic patterns; hematoxylin and eosin staining; magnification of 60x; *c* – necrosis stripe of the epicardium and surface cardiomyocytes occurring under the impact of the electrode during coagulation; edema of the myocardial interstitium; hematoxylin and eosin staining; magnification of 10x; *d* – fragmentation of muscle fibers as a result of fibrillation; hematoxylin and eosin staining; magnification of 40x.

R wave, emergence of a broad and deep QS complex, and lifting of the ST segment above the isoelectric line (*Figs. 3a–3c*). The formation of a large-focal myocardial infarction was also observed in mice on the 3rd and 9th day after coagulation. In some cases, coagulation resulted in the formation of the surface myocardial infarction (*Figs. 3d, 3e*). In the case when the coronary artery was ligated, the emergence of tachycardia (pathological Q and a decrease in the R voltage) causing bradycardia against a background of myocardial infarction was revealed (*Figs. 3f, 3g*).

Results of Histological Examination

The histological examination revealed foci of necrosis in 28 mice (87.5%), whereas no necrosis was observed in 4 mice (12.5%). The mice with no necrosis belonged to the group of mice in which myocardial infarction was simulated by ligation of the coronary artery. This fact can in all likelihood be attributed either to the individual characteristics of heart blood supply with a well-developed collateral system or to an error in the method. A great number of types of heart blood supplies are known in humans, since the development of the coronary arteries varies widely. Consequently, the contribution of each to the blood supply of the left and right ventricles and atria may vary for each particular case, as well. In addition to the main left coronary and right coronary arteries, the relative weight of which is 15% (according to Smolyannikov and Naddachina [14]), a number of other forms of blood supply of the heart exist. Therefore, it can be assumed that similar features of blood supply are present in the mouse heart. Thus, the ligation of the coronary artery might have had no effect on the development of myocardial infarction in four cases.

When myocardial infarction was simulated by ligation of the coronary artery, the emergence of small scattered foci of coagulation necrosis in cardiomyocytes and their disorganization and the occurrence of stromal edema and hemorrhage without inflammatory reaction (*Fig. 4a*) were observed in the form of necrosis of individual cells. These changes manifested themselves in the disappearance of cross striation within the sarcoplasm of cardiomyocytes and the emergence of apoptosis. The changes were found in different parts of the left ventricle (*Fig.4b*).

In the case of controlled electro-coagulation, a direct coagulation necrosis of the epicardium and a layer of cardiomyocytes were observed in the site to which the electrode was applied (*Fig. 4c*). In deeper layers of the myocardium, fragmentation of muscle fibers was observed; a histological sign of the presence of intravital fibrillation of the left ventricle and edema of the myocardial interstitium (*Figs. 4c, 4d*). The fibrillation of ventricles is most likely associated with the direct impact of the electrode on the myocardium and with the

secondary ischemia induced by the damage to the local coronary blood flow. These sites can undergo necrotic changes with time, so that the necrotic zone can expand.

It should be taken into account that from the pathomorphological point of view, infarction is a form of necrosis that occurs as a result of the absolute or relative insufficiency of arterial blood circulation in organs that have no access to oxygen. Since in the case of electro-coagulation the necrotic changes emerge mostly due to the direct impact of the electrode, it is unreasonable to consider these changes as an actual myocardial infarction. Myocardial infarction is based on the coagulation (dry) necrosis of cardio-myoctes occurring upon hypoxia and developed tissue acidosis. Coagulation necrosis develops in tissues with a low fluid content, a high concentration of proteins, and a low activity of hydrolytic enzymes. Another form of cell death observed in the investigated material is apoptosis.

Apoptosis is genetically programmed cell death that is normally found in various organs and tissues, especially in those characterized by the constant renewal of cells. This process is a result of the activation of particular genes under the action of various stimuli. Apoptosis removes the unneeded cells that complete their cycle during the following processes: embryogenesis, homeostatic regulation of maintenance of the cell population in tissues, immune protection, aging, and removal of cells damaged by various pathologic factors. In particular, hypoxia may cause apoptosis if oxygen deficiency is not critical, whereas apparent oxygen starvation results in cell necrosis. Histologically, the nucleus undergoes the most significant changes during apoptosis. Chromatin condensates into compact aggregates of various shapes and sizes (karyopyknosis), which manifests itself under a light microscope as an irregular shape and hyperchromicity of a nucleus. A similar situation was observed when simulating myocardial infarction by ligating the coronary artery. Further, during apoptosis, the nucleus undergoes fragmentation (karyorrhexis) and cytoplasm disintegrates into several linked apoptotic bodies due to the formation of membrane bridges. Some fragments may contain no nuclear material at all. Finally, apoptotic bodies are phagocytized by surrounding healthy cells or tissue macrophages. Unlike necrosis, apoptotic bodies do not cause any inflammatory response, since the integrity of the cell's membrane persists until phagocytosis, which prevents the excretion of cell enzymes into surrounding tissues and does not result in chemotaxis for inflammatory cells.

Thus, the morphological patterns of changes in mice in which infarction was simulated by ligating the left coronary artery and that in the mice with infarction induced by controlled electro-coagulation are different. In the first group, they were characterized by the presence of small scattered foci of coagulation necrosis and foci of apoptosis in different sites of the left ventricle occurring due to a large area of tissues subjected to hypoxia. The insignificance of necrotic foci in the case when the coronary artery is ligated is most likely due to the well-developed network of blood supply and the absence of atherosclerotic lesions of arteries. In the second group of mice, local myocardial damage emerged mostly due to the direct damage done to the tissue. According to the conventional stages of myocardial infarction used in the morphology of this disease, the histological findings showing the incipient coagulation necrosis of cardiomyocytes, the edema and the hemorrhage without inflammatory reaction correspond to the prescription of a myocardial infarction of about 4–12 h. Irreversible changes in the myocardium at the occurrence of critical ischemia begin even after 0.5 h; however, they can be observed neither macroscopically nor histologically at this stage and can be detected only by electron microscopy. These changes are revealed during histological examination only after 4 h. Twelve hours after the occurrence of the infarction, necrotic changes involving karyorrhexis in the cell intensify and the first leukocytes emerge. After 24 h, an apparent necrosis of cardiomyocytes and interstitial infiltration of neutrophils emerge. On the fourth day, the phagocytosis of dead cardiomyocytes begins, and the granulation tissue appears at the margins of the infarction by the tenth day. Two weeks after the infarction, the infarction zone is completely replaced by granulation tissue and collagen appears. During the next six weeks, cicatrical tissue is formed. The changes observed in the first group of hearts correspond to the early stage of myocardial infarction.

CONCLUSIONS

The results obtained in this work allow to conclude that optimal anesthesia for surgery on simulating myocardial infarction is injecting zoletil/xylazine narcosis with muscle relaxants, accompanied by mechanical ventilation. Choosing the proper temperature conditions during pre-, intra- and post-operation periods allow to minimize the death rate of animals associated with nonsurgical causes. Accurate compliance with the specified anatomo-topographic landmarks during the stage of thoracotomy and pericardiotomy allows to minimize the intra-operative hemorrhage and the probability of lung tissue damage. Prolene 6/0 was chosen as an optimal suture material for ligating the descending branch of the left coronary artery. According to ECG data and postmortem histological examination, the

model proposed for simulating a myocardial infarction is adequate; however, it requires further investigation for the purpose of standardization, in line with international standards. ●

This work was supported by the program of the Ministry of Education and Science (Government Contract № 02.467.11.3010 and Agreement № 01.168.24.004).

REFERENCES

1. Burgueño A.L., Landa M.S., Schuman M.L., Alvarez A.L., Carabelli J., García S.I., Pirola C.J. // Metabolism. 2007. V. 56. № 10. P. 1439–1443.
2. Cascio W.E., Cozzi E., Hazarika S., Devlin R.B., Henriksen R.A., Lust R.M., van Scott M.R., Wingard C.J. // Inhal Toxicol. 2007. V. 19. P. 67–73.
Matsuzawa N., Takamura T., Kurita S., Misu H., Ota T., Ando H., Yokoyama M., Honda M., Zen Y., Nakanuma Y., et al. // Hepatology. 2007. V. 46. № 5. P. 1392–1403.
3. Cohen J.K., Cai L.Q., Zhu Y.S., La Perle K.M. // Comp. Med. 2007. V. 57. №4. P. 370-376.
4. Denvir M.A., Sharif I., Anderson T., Webb D.J., Gray G.A., McDicken W.N. // J. Am. Soc. Echocardiogr. 2005. V. 18. № 2. P. 155–162.
5. Lee S., Schwinger R.H., Brixius K. // Pflügers Arch. 2008. V. 455. № 5. P. 767–774.
6. Moura R., Tjwa M., Vandervoort P., Cludts K., Hoylaerts M.F. // Arterioscler. Thromb. Vasc. Biol. 2007. V. 27. № 10. P. 2163–2169.
7. Nogueira B.V., Peotta V.A., Meyrelles S.S., Vasquez E.C. // Arch. Med. Res. 2007. V. 38. № 8. P. 816–821.
8. Rajasingh J., Bord E., Hamada H., Lambers E., Qin G., Losordo D.W., Kishore R. // Vet. Res. Commun. 2007. V. 31. P. 35–41.
Simpson E.R., Jones M.E. // Ernst Schering Found. Symp. Proc. 2006. V. 1. P. 45–67.
Son N.H., Park T.S., Yamashita H., Yokoyama M., Huggins L.A., Okajima K., Homma S., Szabolcs M.J., Huang L.S., Goldberg I.J. // J. Clin. Invest. 2007. V. 117. № 10. P. 2791–2801.
9. Tang Y., Liu W., Yu S., Wang Y., Peng Q., Xiong Z., Wang Y., Wei T. // Plast. Reconstr. Surg. 2007. V. 120. № 4. P. 869–878.
10. Wang G.S., Kearney D.L., De Biasi M., Taffet G., Cooper T.A. // J. Clin. Invest. 2007. V. 117. № 10. P. 2802–2811.
11. Smolyannikov A. V., Naddachina T. A. Patologicheskaya anatomiya koronarnoi nedostatochnosti (Pathological Anatomy of Coronary Insufficiency). M.: Meditsina, 1963.

Association of Cytokine Gene Alleles with the Inflammation of Human Periodontal Tissue

A. V. Safonova[1]*, A.N. Petrin[1], S. D. Arutyunov[1], V. N. Tsarev[1], L. A. Akulenko[1], A. O. Zorina[2], D. V. Rebrikov[3,4], A. V. Rubanovich[4], S. A. Borinskaya[1,4], N. K. Yankovsky[4]

[1] Moscow State University of Medicine and Dentistry

[2] Central Research Institute of Dentistry and Oral Surgery, Federal Agency of Medical Technologies

[3] DNA-Technology JSC.

[4] Vavliov Institute of General Genetics, Russian Academy of Sciences

*E-mail: safnastia@yandex.ru

Received 29.10.2010

ABSTRACT **Gingivitis and periodontitis are chronic inflammatory diseases of the periodontal tissue in humans caused by both environmental and genetic factors. The human cytokine genes that regulate the immune response may play an important role in the development of these chronic inflammatory diseases. The aim of this study is to analyze the allele status of eight human cytokine genes and to associate it with the inflammation of periodontal tissue in humans. A total of 296 unrelated males of Russian origin were studied. A significant association of the *IL1B* and *IL6* minor alleles and gingivitis was found. In addition, we found a significant association of the OHI-S index with the *IL18* gene alleles. The influence of genetic factors on gingivitis may contribute to the understanding of the mechanisms of interaction between genetic and environmental factors in periodontal conditions, and to the identification of risk groups for effective prevention and treatment.**

KEYWORDS **gingivitis, periodontitis, cytokine genes, genetic polymorphism.**

INTRODUCTION

Gingivitis (inflammation of the gum tissue) and periodontitis (inflammation of tissues surrounding and supporting the teeth) are widespread oral diseases. Gingivitis can appear both in tandem with periodontitis and independently. Signs of periodontal tissue involvement might appear even in children 6—7 years old [1]; these indicators are found in more than 50% of 15-year-old adolescents, and the prevalence of periodontal diseases among adults in Moscow and other large cities reaches 98%. Moreover, symptoms of gingivitis are found in more than 80% of people [2].

The inflammation and the destruction of tissues in periodontal diseases occur due to a disequilibrium in the interaction between periodontal cells and bacteria found in the mouth, in particular in dental deposit. The pathogenic processes typical of gingivitis and periodontitis are caused by the immunopathological reaction, which, in turn, is initiated by bacteria present in dental deposit. This reaction leads to a progressing wavelike chronic inflammation, which is accompanied by the development of destructive processes.

The regulation of the inflammatory response is known to play an important role in the pathogenesis of gingivitis and perodontitis [3]. A study of transcriptome changes in the gingival biopsies during the development and treatment of experimental gingivitis showed that, during the development of the disease, there are changes in the expression level of tens of immune response genes, including interleukins *IL1A, IL1B, IL8* and a number of other genes[4]. In this instance, the transcription level of one gene increases, whilst the level of other genes decreases.

The role of an individual's genetic constitution in their predisposition to inflammatory diseases of the periodontal tissue and to the intensity of their progression has been inadequately studied thus far. Association studies reveal that carriers of certain cytokine gene alleles are more prone to develop gingivitis and/or periodontitis [5—9]. However, these data are rather contradictory [6, 10, 11].

The purpose of the present work is to study the association between the severity of the periodontal disease and the alleles affecting the transcription level of eight human cytokine genes, the level of which determines the severity of the inflammation and destructive processes in periodontal tissues. The results could allow to identify potential risk groups of inflammatory periodontal diseases and can later be used in preventive, personalized medicine.

EXPERIMENTAL

A group of 296 male soldiers from 20 to 52 years of age (the average age is 27.0 ± 6.3 years) was examined. The

Table 1. SNPs of cytokine genes checked in this work

Gene	Chromosome	SNP	dbSNP ID	Function	Ref.
IFNG	12q14	+874 T>A	rs2430561	Increasing the expression of HLA II by antigen-representing cells, increasing the level of intercellular adhesion molecules, increasing the level of proliferation of T-cells and production of Th1-cytokines	[14]
IL1A	2q14	-889 C>T	rs1800587	Anti-inflammation cytokine. Activation of osteoclasts, T-cells, and matrix metal proteases	[15, 16]
IL1B	2q14	-511 G>A	rs16944		
IL4	5q31.1	-590 C>T	rs2243250	Decreasing the level of anti-inflammation cytokine. Involvement in differentiation of B-cells and production of antibodies	[17]
IL6	7p21	-174 G>C	rs1800795	Activation of osteoclasts. Involvement in differentiation of B-cells and production of antibodies	[18]
IL10	1q31-q32	-592 C>A	rs1800872	Inhibiting replication of T-cells and inhibiting synthesis of anti-inflammation cytokine. Involvement in differentiation of B-cells and production of antibodies	[18]
IL18	11q22.2-q22.3	-607 G/T	rs1946518	Anti-inflammation cytokine. Increasing the level of producing IFN-γ by T-cells.	[19-21]
TNF	6p21.3	-308 G>A	rs1800629	Activation of osteoclasts and matrix metal proteases. Increasing the expression of HLA II by antigen-representing cells. Increasing the level of intercellular adhesion molecules	[19-21]

examination was performed during a routine medical examination; the procedure of informed consent was followed; the data were collected on the nationality and place of birth of the volunteers and two generations of their ancestors. The examined group included mainly Russian males (proportion of children from mixed marriages (the percentage of descendants from mixed marriages between Russians, Ukrainians, and Belarusians was 6.5%)). All patients underwent a standard external dental checkup and instrumental examination of the oral cavity. The description of the dental status contained the assessment of the intensity of inflammation and destructive processes and the index of oral hygiene.

For the assessment of the severity of gingivitis, the PMA (papillary-marginal-alveolar) index was used [12]. In order to determine this index, the condition of gum tissue for each tooth was assessed in points after it was stained with the purpose of revealing the inflamed areas; the value averaged over all teeth was calculated. PMA = 0 corresponds to the absence of gingivitis, PMA values of up to 30% inclusive correspond to mild gingivitis, the range from 31% to 60% corresponds to gingivitis of moderate severity, whereas PMA values of more than 60% correspond to severe gingivitis.

The examination of the probing pocket depth (PPD) was performed using a special periodontal probe. The highest value of the PPD (mm) was registered, and all values were then summarized and categorized by the number of teeth examined.

The hygiene condition of the oral cavity (the amount of dental calculus and dental deposit) was assessed in accordance with the OHI-S (oral hygiene indices – simplified) index [13].

Samples of venous blood were collected into evacuated tubes containing EDTA. DNA was extracted from the blood samples using the standard phenol-chloroform method. The alleles of the genes analyzed were genotyped twice using an "Immunogenetics" kit (DNA-technology, Moscow). PCR amplification and genotyping were carried out in 384 well plates using a DT-384 amplifier (DNA-technology, Moscow). Eight cytokine genes were investigated: γ-interferon (IFN-γ); α- and β-subunits of interleukin 1 (IL-1α and IL-1β); IL-4, IL-6, IL-10, IL-18 interleukins; and tumor necrosis factor α (TNFα) (*Table 1*). Polymorphic

Table 2. Mean values of the dental indices in carriers of some genotypes over eight cytokine genes

Genotype		N	Dental indices (±SE)*			Minor allele effect**
			PMA	PPD	OHI-S	
IFNG (+874)	A/A	67	0.25±0.02	1.61±0.10	1.85±0.09	$p > 0.2$ for all indices
	T/A	127	0.22±0.01	1.42±0.06	1.74±0.07	
	T/T	87	0.24±0.04	1.48±0.07	1.78±0.07	
IL1A (-889)	C/C	140	**0.22±0.01**	1.40±0.06	1.72±0.06	PMA↓ Recessive $p = 0.026$
	C/T	118	**0.26±0.02**	1.59±0.07	1.84±0.07	
	T/T	27	**0.20±0.02**	1.45±0.11	1.79±0.12	
IL1B (-511)	A/A	29	0.26±0.03	1.41±0.11	1.77±0.12	PMA↑ Recessive $p = 0.157$
	G/A	122	0.23±0.02	1.44±0.07	1.80±0.07	
	G/G	133	0.22±0.01	1.49±0.06	1.76±0.06	
IL4 (-590)	C/C	171	0.24±0.01	1.49±0.06	1.79±0.05	$p > 0.5$ for all indexes
	C/T	98	0.23±0.02	1.45±0.07	1.78±0.07	
	T/T	14	0.19±0.04	1.51±0.22	1.57±0.20	
IL6 (-174)	C/C	61	**0.25±0.02**	1.53±0.10	1.70±0.07	PMA↑ Dominant $p = 0.003$
	G/C	139	**0.24±0.01**	1.48±0.06	1.83±0.07	
	G/G	85	**0.21±0.02**	1.46±0.08	1.74±0.08	
IL10 (-592)	A/A	23	0.24±0.03	1.57±0.15	**1.66±0.16**	OHI-S↓ Dominant $p = 0.043$
	C/A	110	0.22±0.01	1.46±0.07	**1.72±0.06**	
	C/C	152	0.24±0.01	1.49±0.06	**1.84±0.06**	
IL18 (-607)	C/C	85	0.25±0.02	1.50±0.08	**1.69±0.07**	OHI-S↑ Recessive $p = 0.022$; PMA↑ recessive $p = 0.188$
	A/C	140	0.21±0.01	1.44±0.06	**1.75±0.06**	
	A/A	57	0.27±0.02	1.57±0.09	**1.96±0.09**	
TNF (-308)	A/A	4	0.17±0.04	1.45±0.22	1.83±0.25	$p > 0.2$ for all indexes
	G/A	68	0.25±0.02	1.50±0.08	1.84±0.09	
	G/G	212	0.23±0.03	1.48±0.05	1.76±0.05	

*The association level is significant.

**The arrow indicates an increased or decreased value of the character for the minor allele carriers (dominant effect) and for homozygous minor allele carriers (recessive effect). The minimum levels of significance are calculated in accordance with the permutation test.

SNPs predominantly from the promoter regions, affecting the expression of the indicated genes, were selected for analysis. The polymorphic SNPs are listed in *Table 2*.

A statistical analysis was carried out by the standard methods using the WinSTAT 2003.1 software integrated into the Excel software. For the intergroup comparison of the dental indices, the nonparametric Mann-Whitney criterion was used. We used WinPepi freeware, *http://www.brixtonhealth.com/pepi4windows.html* [22], to estimate the odds ratio (OR) and the significance of the differences between the frequencies in accordance with the Fisher's exact test. Corrections for multiple comparisons were introduced by the permutation test (100,000 stimulations) performed using the Mathematica 5.1 software.

RESULTS AND DISCUSSION

In only 1% (three patients) of the group examined (296 males), no sign of inflammation of gum tissue

(PMA = 0) was observed Mild gingivitis was found in 67.6% of males (205 patients), and 31.4% of males were suffering from gingivitis of moderate severity (93 patients) and severe gingivitis (12 patients) (PMA > 30%). The probing pocket depth varied from 0.6 to 4.5 mm. The mean value across the group examined was 1.50 ± 0.73 mm (±S.D.). The values of the OHI-S indices was in a range from 0 to 3.8 points, the mean value was 1.79 ± 0.73; it corresponds to an unsatisfactory hygiene level. The genotypes of all males examined were determined for each from eight loci. Due to technical difficulties, the genotypes of some SNPs were not determined for each individual; hence, the total number of genotypes for each gene is different.

The dental indices can be considered as quantitative characters; hence, in order to assess how genes influence the value of the characters, the mean values of the indices for the investigated genes were calculated in carriers of each genotype. The significant differences between the mean values of the indices for carriers of different genotypes indicate the possible influence of a gene on a given character. In this case, the differences between the carriers of the considered allele and the carriers not having this allele (homozygous alternative allele carriers) indicate the dominant effect of the considered allele and the recessive effect of the alternative allele. An increase in character, depending on the number of copies of the allele in the genotype (0, 1 or 2), corresponds to the additive model (the significance of the regression of the character value per number of allele copies is determined).

The mean values of dental indices were calculated in carriers of different genotypes over eight cytokine genes (*Table 2*). The significance levels of the effects of minor alleles calculated by the permutation test are contained in the right column of *Table 2*. The effects of minor alleles were estimated simultaneously in 100,000 permutations in accordance with the dominant, recessive, and additive models. The results of the significance were used in order to further verify the significance of associations. The additive model gave no added significance compared with the analysis results on the recessive/dominant effects; thus, the data for the additive model are not listed.

A significant increase in the mean PMA index value was revealed in carriers of the *IL6**(-174)C allele (*Table 2*). Since the PMA index value correlates with the age of patients ($r = 0.16$ at $p = 0.004$), the influence of the gene was checked in two age groups: 215 patients were up to 30 years old, and 70 patients were 30 years old and older). A significance association of the *IL6**(-174)C allele with an increased PMA index value according to the dominant model is revealed in each age cohort (*Fig. 1*). When splitting each age cohort into groups with

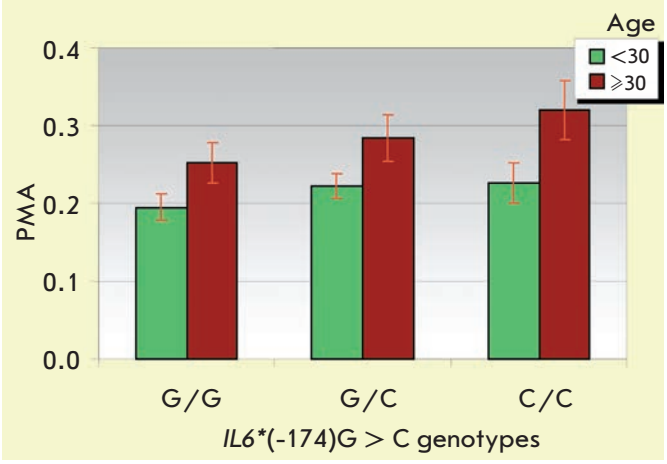

Fig. 1. Mean values (± SE) of the PMA index in carriers of different *IL6* (-174) genotypes from two groups: less than 30 years old, 215 individuals; and more than 30 years old, 70 individuals.

high PMA (>30% corresponds to moderate and severe gingivitis) and low (<30% corresponds to normal and mild gingivitis), the carriers of the IL6 * (-174) C allele showed a greater risk of being in the group of moderate and severe gingivitis. The corresponding odds ratios were $OR = 2.22$ at $p = 0.031$ in the group of patients younger than 30 and $OR = 3.78$ at $p = 0.052$ in the group of patients 30 years old and older. The uniformity of the effects in both age groups (the differences in the OR are negligible, $p = 0.496$ according to the χ^2 criterion) allows to estimate the odds ratio in the pooled sample: $OR = 2.56$ at $p = 0.002$ (95%CI = 1.32—5.21).

Analogous calculations carried out for the *IL1A**(-889) SNP revealed that the carriers of the major C allele are in greater risk of suffering from moderate and severe gingivitis (PMA > 30%) in comparison to the carriers of the T/T genotype: $OR = 3.86$ at $p = 0.026$ (95%CI = 1.14—13.10).

In addition to the assessment of the individual gene effects, their pairwise action was considered. The pairwise action of the minor alleles in the *IL6**(-174) SNP of the *IL6* gene and the *IL1B**(-511) SNP of the *IL1B* gene was found, while no significant effects of these genes were revealed in the previous stage of analysis. During consideration of the pairwise action of these two genes, their influence on the mean PMA value and on the association with moderate and severe gingivitis was analyzed as in the previous stage.

The lowest mean PMA value was typical of double homozygotes for both SNPs. Upon increase in the number of minor alleles in the *IL1B**(-511) and *IL6**(-174) SNPs, the mean PMA index value increases (*Fig.*

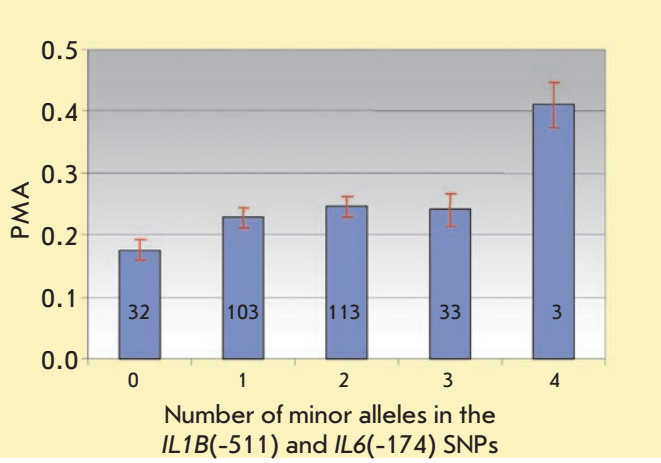

Fig. 2. Mean values (± SE) of the PMA index vs. the number of minor alleles in the *IL1B* (-511) and *IL6* (-174) SNPs. The number of individuals carrying each genotype is shown in histogram bars.

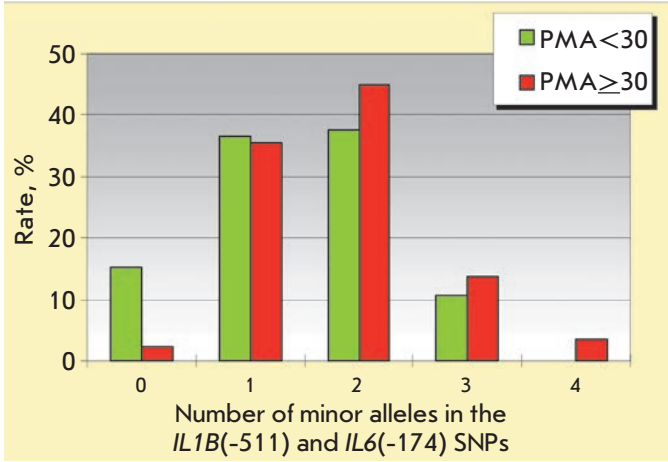

Fig. 3. Distribution of the total number of minor alleles copies found in the SNP *IL1B* (-511) and *IL6* (-174) SNPs vs. severity of gingivitis. The group of individuals with PMA index ≥ 30 (moderate and severe gingivitis) includes 87 individuals. The group of individuals with PMA index < 30 (no gingivitis and mild gingivitis) includes 197 individuals.

2). The difference in the PMA index values (by a factor of 2.3) found for two extreme cases (double homozygotes for the minor alleles and homozygotes for the major alleles) are significant according to the Mann-Whitney test ($p = 0.0067$).

The distributions of the total number of minor allele copies in the *IL1B**(-511) and *IL6**(-174) SNPs in the patients suffering from severe and moderate gingivitis (PMA ≥ 30%), from mild gingivitis (PMA < 30%), and the healthy patients are shown in Fig. 3. It can clearly be seen that the carriers of at least one minor allele of the *IL1B**(-511) and *IL6**(-174) genes are more likely to be found amongst patients with severe gingivitis. The risk of development of moderate and severe gingivitis (PMA ≥ 30%) is higher in the homozygous carriers of the minor *IL1B**(-511)A and *IL6**(-174)C alleles than in the homozygous carriers of the major *IL1B**(-511)G and *IL6**(-174)G alleles and is characterized by an odds ratio $OR = 7.63$ at $p = 0.0009$ (95%CI = 1.80—32.45). The percentage of homozygous carriers of minor alleles (individuals carrying the combination of the A/A genotype of the *IL1B**(-511) SNP and C/C genotype of *IL6**(-174) SNP associated with severe gingivitis) was 1.1%; the percentage of individuals carrying the "protective" combinations of the G/G and G/G genotypes of the same SNPs was 11.3% (32 patients). This effect has to be confirmed in larger samples, but an increase in the effect occurring upon an increase in the number of minor alleles argues for the nonarbitrariness of the association revealed (*Fig. 2*).

The prevention and treatment of periodontal diseases is a very pertinent issue within dentistry. Periodontal diseases are found even in infancy, and apparent clinical manifestations of this pathology are observed in more than half of people in their 30s. However, the problems of prevention and effective treatment of periodontal diseases remains unsolved [23]. The manifestations of the clinical signs of this disease depend on age, pernicious habits, general health status, and overall hygiene. In this context, it is reasonable to consider the phenomenon of the association between the OHI-S index and SNPs in the interleukin genes. The OHI-S index is increased in homozygous carriers of the *IL10**(-592)C allele (its value is 1.84 ± 0.06 against 1.71 ± 0.06 in carriers of the allele A; however the difference is insignificant, since $p = 0.092$ according to the Mann-Whitney test). Significant differences are observed in individuals carrying different genotypes of the *IL18**(-607) SNP, G > A. The value of the OHI-S index in carriers of the homozygous A/A genotype is 1.96 ± 0.09, while in carriers of the G allele, its value is 1.73 ± 0.05 (the difference is significant, $p = 0.018$ according to the Mann-Whitney test). It may be assumed that since hygiene hardly depends on the genotype, in homozygous carriers of the *IL18**(-607) A allele, the formation of plaques dental deposit is more intensive and pushes up the value of the OHI-S index.

No association of the PPD with the alleles of cytokine genes was found.

In this work, we established an association between the *IL1A**(-889)C and *IL6**(-174)C alleles and the severity of gingivitis and the increase in the effect of the

*IL6**(-174)C allele in the presence of the *IL1B**(-511)A allele. The 511 A/G polymorphism influences the expression of the *IL1B* gene under certain conditions and is associated with inflammatory and cancer diseases [11, 24]. Interleukin 1 is an anti-inflammatory cytokine secreted by monocytes, macrophages, and dendritic cells. The *IL1*gene is one of the first genes for which an association of single-nucleotide polymorphisms with inflammatory diseases of periodontal tissue was revealed in [5]. In the development of a periodontal disease, the role of interleukin 1 involves the induction of inflammation mediators. It has been demonstrated that in immortalized human gingival fibroblasts, the transcription level of the inflammatory genes of cytokines, chemokines, metalloproteases, cell adhesion molecules, and the transcription factor NF-kβ, which controls the expression of immune and anti-apoptotic response genes and cell cycle genes, increase. The activation of NF-kβ blocks apoptosis, thereby causing the stabilization of gingival fibroblasts *in vitro* [25]. An association of the polymorphic markers in the interleukin 1 gene cluster (*IL1A*, *IL1B* and *IL1RN*, IL1 receptor antagonist) with periodontitis and gingivitis has been established only in a few works [11].

Interleukin 6 is a multifunctional cytokine that plays an important role in the inflammatory response on infectious agents (especially gram-negative bacteria) [26]. The production of cytokine is decreased in carriers of the minor C allele at the -174 position of the regulatory site in the IL6 gene; this may cause a destruction of the immune protection [27]. While studying the associations of both genes with the inflammation of periodontal tissue, contradictory data were obtained. An analysis of the association between chronic periodontitis and the *IL6*(-174) SNP performed in six Caucasian populations reveal the presence of the association in three of them [11]. The interleukin genes may be involved in the regulation of the inflammatory response and could be responsible for the differences observed in the spectrum of oral pathogens for carriers of different genotypes. The *Aggregatibacter actinomycetemcomitans* and *Porphyromonas gingivalis* pathogenic bacteria were revealed to be more frequently found in sublingual biofilms for the carriers of a certain genotype in the *IL6*(-174) SNP [8]. The contradictions in the results obtained by different authors can be explained by changes in the correlation between the factors depending on age, ethnic homogeneity, and other peculiarities of the groups examined.

The formation of dental calculus and dental deposit is a complex process that depends on the quality of oral hygiene, microbiota, and local immunity. Genetically determined features of the immune response might also influence the formation of dental deposits and, consequently, the OHI-S index. Interleukin 18 is an anti-inflammatory cytokine, and in all probability it is one of the main cytokines involved in the development of pathological processes and destruction of periodontal tissues; it is secreted by macrophages/monocytes and epithelial cells of the oral cavity, stimulates cellular immunity and induces the production of IFN-γ. The level of interleukin 18 is increased in cases of various chronic inflammatory diseases. The content of interleukin 18 in gingival fluid increases proportionally to the severity of a periodontal inflammation and decreases to its initial level after the disease is cured [28, 29]. The -607 C/A SNP in the regulatory site of the *IL18* gene is localized in the CREB (cAMP response-element binding protein) site [30]. A significant increase in both the spontaneous and lipopolysaccharide-induced productions of interleukin 18 is observed in the cell culture of donors carrying the *A* allele [31]. The association of the OHI-S index with the interleukin gene alleles had not been described earlier. The associations revealed are significant for the ethnically homogeneous sample (Russians) examined. To date, the severity of the inflammation and destructive processes in periodontal diseases is known to be genetically dependent. These diseases should be considered as multifactor diseases [11]. However, the contribution of certain genes to the predisposition to and tolerance of inflammatory diseases of the periodontal tissue requires a more detailed study, especially with different genetic backgrounds, which could be ethnically dependent. Therefore, the practical significance of the association revealed here makes testing these results in independent samples of other ethnic groups especially interesting. ●

This work was supported by the Russian Academy of Sciences Presidium Program "Fundamental Sciences to Medicine."

REFERENCES

1. Grudianov A.I., Kirjukhina S.A., Vorobiev V.S. // Stomatologiia (Mosk). 1995. № 6. P. 16.
2. Artjushkevich A.S. Zabolevania peridonta (Periodontal Diseases). M.: Med. lit., 2006. 328 p.
3. Dmitrieva L.A., Romanov A.E., Tsarev V.N. Klinicheskie i mikrobiologicheskie aspekti primenenia restavratsionnih materialov I antiseptikov v kompleksnom lechenii zabolevaniy parodonta (Clinical and Microbiological Aspects of the Application of Restoration Materials and Antiseptics in Combined Treatment of Periodontal Diseases). M.: MED-press-inform, 2002. 96 p.
4. Offenbacher S., Barros S.P., Paquette D.W., Winston J.L., Biesbrock A.R., Thomason R.G., Gibb R.D., Fulmer A.W.,

Tiesman J.P., Juhlin K.D., Wang S.L., Reichling T.D., Chen K.S., Ho B. // J. Periodontol. 2009. V. 80 (1). P. 1963–1982.
5. Kornman K.S., Crane A., Wang H.Y., di Giovine F.S., Newman M.G., Pirk F.W., Wilson T.G., Higinbottom F.L., Duff G.W. // J. Clin. Periodontol. 1997. V. 24 (1). P. 72–77.
6. Kinane D.F., Shiba H., Hart T.C. // Periodontol. 2005. V. 39. P. 91–117.
7. Holla L.I., Musilova K., Vokurka J., Klapusová L., Pantuckova P., Kukletova M., Kukla L., Znojil V. // Acta Odontol. Scand. 2008. V. 66 (2). P. 105–112.
8. Nibali L., Tonetti M.S., Ready D.R., Parkar M., Brett P.M., Donos N., D'Aiuto F. // J. Periodontol. 2008. V. 79. P. 677–683.
9. Trombelli L., Scapoli C., Carrieri A., Giovannini G., Calura G., Farina R. // J. Clin. Periodontol. 2010. V. 37(8). P. 697–704.
10. Nibali L., Donos N., Henderson B. // J. Med. Microbiol. 2009. V. 58. P. 1269–1274.
11. Laine M.L., Loos B.G., Crielaard W. // Internat. J. Dentistry. 2010. Article ID 324719, 22 p.
12. Parma C. Parodontopathien. Leipzig: C Parma, 1960. 203 p.
13. Greene J.C., Vermillion J.R. // J. Am. Dent. Assoc. 1964. V. 68. P. 7–13.
14. Okamura H., Tsutsui H., Komatsu T., Yutsudo M., Hakura A., Tanimoto T., Torigoe K., Okura T., Nukada Y., Hattori K., et al. // Nature. 1995. V. 378. P. 88–91.
15. Micallef M.J., Ohtsuki T., Kohno K., Tanabe F., Ushio S., Namba M., Tanimoto T., Torigoe K., Fujii M., Ikeda M., et al. // Eur. J. Immunol. 1996. V. 26. P. 1647.
16. Gleichmann E., Pals S.T., Rolink A.G., Radaszkiewicz T., Gleichmann H. // Immunol. Today. 1984. V. 5. P. 324.
17. Romas E., Martin T.J. // Osteoporos Int. 1997. V. 7. P. 47–53.
18. Dayer J.M., Arend W.P. // Philadelphia: Saunders. 1997. V. 5. P. 267–286.
19. Schett G., Tohidast-Akrad M., Smolen J.S., Schmid B.J., Steiner C.W., Bitzan P., Zenz P., Redlich K., Xu Q., Steiner G. // Arthritis Rheum. 2000. V. 43. P. 2501–2512.
20. Kobayashi K., Takahashi N., Jimi E., Udagawa N., Takami M., Kotake S., Nakagawa N., Kinosaki M., Yamaguchi K., Shima N., et al. // J. Exp. Med. 2000. V. 191. P. 275–285.
21. Fuller K., Owens J.M., Jagger C.J., Wilson A., Moss R., Chambers T.J. // J. Exp. Med. 1993. V. 178. P. 1733–1744.
22. Abramson J.H. WINPEPI (PEPI-for-Windows): computer programs for epidemiologists. Epidemiologic Perspectives & Innovations. 2004. V. 1. P. 6.
23. Grudianov A.I., Ovchinnikov V.V. Profilaktika vospalitelnih zabolevaniy parodonta (Prevention of Periodontal Inflammatory Diseases). M.: Medical information agency, 2007. 80 p.
24. Rogus J., Beck J.D., Offenbacher S., Huttner K., Iacoviello L., Latella M.C., de Gaetano M., Wang H.Y., Kornman K.S., Duff G.W. //Hum. Genet. 2008. V. 123 (4). P. 387–398.
25. Vardar-Sengul S., Arora S., Baylas H., Mercola D. // J. Periodontol. 2009. V. 80 (5). P. 833–849.
26. Dalrymple S.A., Slattery R., Aud D.M., Krishna M., Lucian L.A., Murray R. // Infect. Immun. 1996. V. 64 (8). P. 3231–3235.
27. Fishman D., Faulds G., Jeffey R., Mohamed-Ali V., Yudkin J.S., Humphries S., Woo P. // J. Clin. Investigation. 1998. V. 102 (7). P. 1369–1376.
28. Pradeep A.R., Hadge P., Chowdhry S., Patel S., Happy D. // J. Oral Sci. 2009. V. 51. P. 261–266.
29. Orozco A., Gemmell E., Bickel M., Seymour G.J. // Oral Microbiol. Immunol. 2006. V. 21 (4). P. 256–260.
30. Giedraitis V., He B., Huang W.-X., Hillert J. // J. Neuroimmunol. 2001. V. 112 (1–2). P. 146–152.
31. Khripko O.P., Sennikova N.S., Lopatnikova J.A., Khripko J.I., Filipenko M.L., Khrapov E.A., Gelfgat E.L., Yakushenko E.V., Kozlov V.A., Sennikov S.V. // Mediators Inflamm. 2008. Article ID 309721. 6 p.

GENERAL RULES

Actae Naturae publishes experimental articles and reviews, as well as articles on topical issues, short reviews, and reports on the subjects of basic and applied life sciences and biotechnology.

The journal is published by the Park Media publishing house in both Russian and English.

The journal *Acta Naturae* is on the list of the leading periodicals of the Higher Attestation Commission of the Russian Ministry of Education and Science

The editors of *Actae Naturae* ask of the authors that they follow certain guidelines listed below. Articles which fail to conform to these guidelines will be rejected without review. The editors will not consider articles whose results have already been published or are being considered by other publications.

The maximum length of a review, together with tables and references, cannot exceed 60,000 symbols (approximately 40 pages, A4 format, 1.5 spacing, Times New Roman font, size 12) and cannot contain more than 16 figures.

Experimental articles should not exceed 30,000 symbols (20 pages in A4 format, including tables and references). They should contain no more than ten figures. Lengthier articles can only be accepted with the preliminary consent of the editors.

A short report must include the study's rationale, experimental material, and conclusions. A short report should not exceed 12,000 symbols (8 pages in A4 format including no more than 12 references). It should contain no more than four figures.

The manuscript should be sent to the editors in electronic form: the text should be in Windows Microsoft Word 2003 format, and the figures should be in TIFF format with each image in a separate file. In a separate file there should be a translation in English of: the article's title, the names and initials of the authors, the full name of the scientific organization and its departmental affiliation, the abstract, the references, and figure captions.

MANUSCRIPT FORMATTING

The manuscript should be formatted in the following manner:

- Article title. Bold font. The title should not be too long or too short and must be informative. The title should not exceed 100 characters. It should reflect the major result, the essence, and uniqueness of the work, names and initials of the authors.
- The corresponding author, who will also be working with the proofs, should be marked with a footnote *.
- Full name of the scientific organization and its departmental affiliation. If there are two or more scientific organizations involved, they should be linked by digital superscripts with the authors' names. Abstract. The structure of the abstract should be very clear and must reflect the following: it should introduce the reader to the main issue and describe the experimental approach, the possibility of practical use, and the possibility of further research in the field. The average length of an abstract is 20 lines (1,500 characters).
- Keywords (3 – 6). These should include the field of research, methods, experimental subject, and the specifics of the work. List of abbreviations.
- INTRODUCTION
- EXPERIMENTAL PROCEDURES
- RESULTS AND DISCUSSION
- CONCLUSION

  The organizations that funded the work should be listed at the end of this section with grant numbers in parenthesis.
- REFERENCES

  The in-text references should be in brackets, such as [1].

RECOMMENDATIONS ON THE TYPING AND FORMATTING OF THE TEXT

- We recommend the use of Microsoft Word 2003 for Windows text editing software.
- The Times New Roman font should be used. Standard font size is 12.
- The space between the lines is 1.5.
- Using more than one whole space between words is not recommended.
- We do not accept articles with automatic referencing; automatic word hyphenation; or automatic prohibition of hyphenation, listing, automatic indentation, etc.
- We recommend that tables be created using Word software options (Table → Insert Table) or MS Excel. Tables that were created manually (using lots of spaces without boxes) cannot be accepted.
- Initials and last names should always be separated by a whole space; for example, A. A. Ivanov.
- Throughout the text, all dates should appear in the "day.month.year" format, for example 02.05.1991, 26.12.1874, etc.
- There should be no periods after the title of the article, the authors' names, headings and subheadings, figure captions, units (s – second, g – gram, min – minute, h – hour, d – day, deg – degree).
- Periods should be used after footnotes (including those in tables), table comments, abstracts, and abbreviations (mon. – months, y. – years, m. temp. – melting temperature); however, they should not be used in subscripted indexes (T_m – melting temperature; $T_{p.t.}$ – temperature of phase transition). One exception is mln – million, which should be used without a period.
- Decimal numbers should always contain a period and not a comma (0.25 and not 0,25).
- The hyphen ("-") is surrounded by two whole spaces, while the "minus," "interval," or "chemical bond" symbols do not require a space.
- The only symbol used for multiplication is "×"; the "×" symbol can only be used if it has a number to its right. The "·" symbol is used for denoting complex compounds in chemical formulas and also noncovalent complexes (such as DNA·RNA, etc.).
- Formulas must use the letter of the Latin and Greek alphabets.

- Latin genera and species' names should be in italics, while the taxa of higher orders should be in regular font.
- Gene names (except for yeast genes) should be italicized, while names of proteins should be in regular font.
- Names of nucleotides (A, T, G, C, U), amino acids (Arg, Ile, Val, etc.), and phosphonucleotides (ATP, AMP, etc.) should be written with Latin letters in regular font.
- Numeration of bases in nucleic acids and amino acid residues should not be hyphenated (T34, Ala89).
- When choosing units of measurement, SI units are to be used.
- Molecular mass should be in Daltons (Da, KDa, MDa).
- The number of nucleotide pairs should be abbreviated (bp, kbp).
- The number of amino acids should be abbreviated to aa.
- Biochemical terms, such as the names of enzymes, should conform to IUPAC standards.
- The number of term and name abbreviations in the text should be kept to a minimum.
- Repeating the same data in the text, tables, and graphs is not allowed.

GUIDENESS FOR ILLUSTRATIONS

- Figures should be supplied in separate files. Only TIFF is accepted.
- Figures should have a resolution of no less than 300 dpi for color and half-tone images and no less than 500 dpi.
- Files should not have any additional layers.

REVIEW AND PREPARATION OF THE MANUSCRIPT FOR PRINT AND PUBLICATION

Articles are published on a first-come, first-served basis. The publication order is established by the date of acceptance of the article. The members of the editorial board have the right to recommend the expedited publishing of articles which are deemed to be a priority and have received good reviews.

Articles which have been received by the editorial board are assessed by the board members and then sent for external review, if needed. The choice of reviewers is up to the editorial board. The manuscript is sent on to reviewers who are experts in this field of research, and the editorial board makes its decisions based on the reviews of these experts. The article may be accepted as is, sent back for improvements, or rejected.

The editorial board can decide to reject an article if it does not conform to the guidelines set above.

A manuscript which has been sent back to the authors for improvements requested by the editors and/or reviewers is reviewed again, after which the editorial board makes another decision on whether the article can be accepted for publication. The published article has the submission and publication acceptance dates set at the beginning.

The return of an article to the authors for improvement does not mean that the article has been accepted for publication. After the revised text has been received, a decision is made by the editorial board. The author must return the improved text, together with the original text and responses to all comments. The date of acceptance is the day on which the final version of the article was received by the publisher.

A revised manuscript must be sent back to the publisher a week after the authors have received the comments; if not, the article is considered a resubmission.

E-mail is used at all the stages of communication between the author, editors, publishers, and reviewers, so it is of vital importance that the authors monitor the address that they list in the article and inform the publisher of any changes in due time.

After the layout for the relevant issue of the journal is ready, the publisher sends out PDF files to the authors for a final review.

Changes other than simple corrections in the text, figures, or tables are not allowed at the final review stage. If this is necessary, the issue is resolved by the editorial board.

FORMAT OF REFERENCES

The journal uses a numeric reference system, which means that references are denoted as numbers in the text (in brackets) which refer to the number in the reference list.

For books: the last name and initials of the author, full title of the book, location of publisher, publisher, year in which the work was published, and the volume or issue and the number of pages in the book.

For periodicals: the last name and initials of the author, title of the journal, year in which the work was published, volume, issue, first and last page of the article.

Bressanelli S., Tomei L., Roussel A., et al // Proc. Natl. Acad. Sci. USA. 1999. V. 96. P.13034–13039 (If there are more than five authors). If there are less than five authors, all the authors must be listed.

References to books which have Russian translations should be accompanied with references to the original material listing the required data.

References to doctoral thesis abstracts must include the last name and initials of the author, the title of the thesis, the location in which the work was performed, and the year of completion.

References to patents must include the last names and initials of the authors, the type of the patent document (the author's rights or patent), the patent number, the name of the country that issued the document, the international invention classification index, and the year of patent issue.

The list of references should be on a separate page. The tables should be on a separate page, and figure captions should also be on a separate page.

The following e-mail addresses can be used to contact the editorial staff: vera.knorre@gmail.com, actanaturae@gmail.com, tel.: (495) 727-38-60, (495) 930-80-05